INELASTIC DYNAMIC ANALYSIS OF FLAT SLAB-SHEAR WALL BUILDING

By

SUDHIR L. AMBEKAR

B. Tech. I.I.T., Bombay, India

A Thesis

Submitted to the School of Graduate Studies

in Partial Fulfilment of the Requirements

for the Degree

Master of Engineering

McMaster University

July 1978

MASTER OF ENGINEERING (1978) McMASTER UNIVERSITY
(Civil Engineering) Hamilton, Ontario

TITLE: Inelastic Dynamic Analysis of Flat-slab Shear Wall Building

AUTHOR: Sudhir L. Ambekar, B. Tech. (Indian Institute of Technology)

SUPERVISOR: Dr. W.K. Tso

NUMBER OF PAGES: xxiii, 274

ABSTRACT

An analytical technique for determining the inelastic responses of coupled shear wall structures is developed based on the transfer matrix technique in combination with the continuum method. It applies to nonuniform coupled shear walls resting on flexible foundations. The P-Δ effect, the possibilities of formation of the yield hinges at the ends of the connecting beams and at the bases of the walls, the effects of the rotational ductility factor of the connecting beams are also considered in this analysis.

Based on this technique, a study is made on a two interconnected coupled shear wall model to simulate the earthquake response of a typical coupled shear wall building with different exterior and interior walls. The dynamic responses of these coupled shear walls are then compared with those obtained by conventional analysis of a single coupled shear wall to evaluate the effect of load transfer between dissimilar coupled shear walls within a building during an earthquake.

SUMMARY

In high rise buildings the design consideration due to lateral loads becomes important. One of the alternatives in design to provide adequate lateral strength and stiffness is the use of reinforced concrete shear walls. These walls extend the entire height of the building and are coupled together by a system of horizontal spandrel beams or connecting slabs. The typical shear wall-flat slab building consists of set of such parallel coupled shear walls arranged in symmetric manner, such that, all interior coupled shear walls are identical and also the two end coupled shear walls are the same.

In such a case, the behaviour of the whole building can be studied from the two dimensional behaviour of an interior or an exterior coupled shear wall in turn. Each coupled shear wall in the building is assumed to take the lateral load in proportion to its elastic stiffness and this proportion of load is assumed to be constant throughout the elasto-plastic analysis. This assumption is realistic so long as the shear wall is in the elastic state, but when the plastic hinges start forming at the ends of the connecting beams, the stiffness ratio of the shear walls changes and hence there will be a redistribution of lateral load between the interior and exterior coupled shear walls. This phenomenon of transfer of loads may lead to different behaviour of the coupled shear walls building and is studied by considering a

mathematical model consisting of two coupled shear walls, one representing all the interior coupled shear walls and the other representing the two exterior coupled shear walls, connected together at the floor levels.

The purpose of the present analysis is to develop a technique for a complete time history analysis of shear wall-flat slab multi-storey building. The behaviour of typical coupled shear walls, interior and exterior, obtained by this two interconnected coupled shear walls formulation is compared with those obtained by the single coupled shear wall formulation.

The analytical method developed herein, in single and two interconnected coupled shear walls formulation, is based on the transfer matrix technique which is based on the continuum method and is suitable for a wide variety of non-uniform shear wall configurations, foundation conditions and loading conditions. The technique is to divide the wall into a number of segments, and each segment can be considered as a uniform coupled shear wall. The continuum method of analysis can therefore apply to each segment to relate the parameters of interest from one end of the segment to the other end. In the dynamic analysis, the lumped mass approach is used where the masses of the segments of all shear walls are lumped at the discrete floor levels along the height of the wall and this technique automatically takes care of the sharing of lateral loads between the interconnected shear walls. The damping matrix is obtained from the modal matrix, mass matrix, the natural frequencies and percentage critical damping for each mode. Newmark's

"β" method of step-by-step integraton is used as it is found to be the most stable and accurate method. P-Δ Effect is included and this analysis takes into account the plastic deformations at the ends of the connecting beams of coupled shear walls. The effect of the connecting beam ductility on the seismic response of the coupled shear walls is also considered. The possibility of complete collapse with the formation of plastic hinges at the base of the piers is considered in the single coupled shear wall formulation. The failure and damage patterns of the coupled shear walls are studied by considering the modified waveforms of earthquake record of El-Centro (1940) N-S component.

This analysis technique is found to be very efficient to obtain a full time history inelastic response of a single and two interconnected coupled shear walls subjected to any type of ground motion. P-Δ Effect appears to have a minor influence as long as the walls are in the elastic state. But when the formation of the plastic hinges at the base of the piers is considered, the P-Δ Effect is likely to become important. For the coupled shear walls of practical dimensions, it may be concluded that when the monotonously increasing load is applied, the second plastic hinge at the base forms almost immediately after the first hinge has been formed. Based on the present study, it may be concluded that the model structure will suffer light damage and may survive against collapse if it is exposed to moderate earthquake shaking. On the other hand, if it is exposed to a severe earthquake, then heavy damage may occur and the walls may even fail as a complete

mechanism with the formation of hinges at the bases develops. The behaviour of the coupled shear wall will be improved if the ductility of the connecting beams is increased. This improvement is more important for the survival against severe earthquakes. But it should be noted that the improvement in the member ductility of only one or some of the coupled shear walls will not be much advantageous for the behaviour of the other coupled shear walls of the same system and hence due importance should be given for designing the coupling system of the interior shear walls.

Based on the behaviour of the coupled shear walls observed in the present study, the following recommendations can be made for the design of coupled shear walls. It is desirable to design the walls to maintain an elastic behaviour throughout an earthquake response for minimum nonstructural damage, and to ensure the moderate ductility capacity as a second line of defense. A strong and ductile wall can be designed by concentrating the flexural reinforcement at the two extreme ends of the section and detailing the transverse reinforcement to confine the concrete effectively. The coupling beams should be designed so as to be moderately stiff enough in order to render an effective coupling system. These beams should be carefully detailed with the diagonal, transverse reinforcement for ductile behaviour without brittle shear failure under a large number of reversals so as to reduce the possibility of significant yielding in the walls.

ACKNOWLEDGEMENTS

The author wishes to express his sincere appreciation to Dr. W.K. Tso for his consistent guidance, assistance and encouragement throughout the research program. His invaluable suggestions and advice are gratefully acknowledged.

The author wishes to record his indebtedness to McMaster University and the National Research Council of Canada for providing financial support during this research work.

TABLE OF CONTENTS

TABLE OF CONTENTS (cont)

TABLE OF CONTENTS (cont)

TABLE OF CONTENTS (cont)

LIST OF FIGURES

LIST OF FIGURES (cont)

LIST OF FIGURES (cont)

LIST OF FIGURES (cont)

LIST OF TABLES

LIST OF SYMBOLS

A_{i1}, A_{i2} (or A_1, A_2)	cross-sectional area of left and right walls of segment i.
A_i (or A)	equivalent cross-sectional area of the coupled shear walls, such that $1/A_i = 1/A_{i1} + 1/A_{i2}$.
A_b^*	effective shear cross-sectional area of connecting beam.
a_i (or a)	distance between centroidal axes of left and right walls of segment i.
a_n	ground acceleration at time t_n.
c_i, c	clear span length of the connecting medium within segment i.
[C]	damping matrix.
{D}	damping forces vector at time t_n.
E	elastic modulus.
$[F]_i$	field transfer matrix for ith segment.
$[\bar{F}]$	total matrix of the structure.
G	shear modulus.
H_i (or H)	height of segment i.
HT	total height of the structure.
HTT_i (or HTT)	the height from the ith mass to the top, such that $HTT_i = HT - \sum_{k=1}^{i} H_k$.

h_i	storey height within segment i.
I_{i1}, I_{i2}	second moment of area of left and right walls of ith segment, respectively.
I_i (or I)	$I_{i1} + I_{i2}$.
I_{10}, I_{20}	moment of intertia of left and right walls at the base, respectively.
I_0	$I_{10} + I_{20}$.
I_{bi}	second moment of area of connecting beam within segment i.
$K_{\delta 1}$, $K_{\delta 2}$	vertical displacement stiffness of foundation under left and right walls, respectively.
K_δ	equivalent vertical displacement stiffness of the foundation, such that $1/K_\delta = 1/K_{\delta 1} + 1/K_{\delta 2}$.
$K_{\theta 1}$, $K_{\theta 2}$	rotational stiffness of foundation under left and right walls, respectively.
K_θ	equivalent rotational stiffness of foundation, such that $K_\theta = K_{\theta 1} + K_{\theta 2}$.
[K]	stiffness matrix before P-Δ effect.
$[K^*]$	combined stiffness matrix.
$\{L\}_i$	load vector for ith segment.
m_{xi}	bending moment per unit height at distance x from the bottom of the segment "i".

$M_i(x)$	walls bending moment at a distance x from the bottom of segment i.
$M_i^e(x)$	cantilever moment at a distance x from the bottom of segment i due to external loads only.
M_{iA}, M_{iB} (or M_A, M_B)	walls bending moment at the upper and lower surfaces, respectively, of station i.
M_{iu}	ultimate bending moment of the ith pier at the base.
M_{io}	bending moment at the base of ith pier
[M]	mass matrix.
NSEG	number of segments within the wall.
NMAS	number of masses considered;
NFR	NSEG/NMAS
P_i	concentrated lateral load at station i.
{P}	applied loads vector at time t_n.
$q_i(x)$	shear distribution per unit height along the connecting medium in segment i.
q_p	maximum shear distribution per unit length along the connecting medium in segment i.
$\{R\}_n$	resisting forces vector at time t_n.
$[S]_i$	station transfer matrix for ith station.
T_i	period of the ith mode.
$T_i(x)$	axial force in the piers within segment i.
T_o	axial force at base of walls.

u_{i1}, u_{i2}	axial deformation in the left and right walls, respectively, in segment i.
u_i	$u_{i1} + u_{i2}$.
$\{u\}_n$	displacement vector at time t_n.
$\{\dot{u}\}_n$	velocity vector at time t_n.
$\{\ddot{u}\}_n$	acceleration vector at time t_n.
V_{iA}, V_{iB} (or V_A, V_B)	inter-storey shear on upper and lower surfaces, respectively, of station i.
V^*_{iA}, V^*_{iB} (or V^*_A, A^*_B)	wall shear on upper and lower surfaces, respectively, of station i.
V_o	total shear at the base of the coupled shear wall.
$\{W\}_t$	inertia load acting on the structure at time t.
$y_i(x)$	lateral deflection at a distance x from the bottom of segment i.
$y_i^n(x)$	nth derivative of $y_i(x)$.

* Suffices iA (or A) and iB (or B) refer to the upper and lower surfaces, respectively, of station i.

* Suffices "I" and "II" refer to the first and second coupled shear wall respectively (in two interconnected coupled shear walls formulation).

α^2	$\frac{a\,\mu^2}{E\,I}\,(1+I/Aa^2)$.
β^2	$1 + \frac{12E\,I_b}{GA^*_b\,c^2}$.

β_o	curvature at the base.
γ^2	$\frac{\mu^2}{E^2 AIa}$.
Δ	relative displacement of the foundation due to axial force at base.
Δt	time interval for the numerial integration of the equations of motion.
Δ_i	relative end displacements of the laminae of the ith segment.
Δ_{yi}	yield deflection of the ith segment's laminae.
Δ_{ui}	ultimate deflection of the ith segment's laminae.
δt	time interval for calculating the straining actions due to the inertia load.
θ_o	rotation of foundation.
$\{\lambda\}_j$	the jth eigenvector.
μ^2	$\frac{12EI_b a}{hc^3\beta^2}$.
$\overline{\mu}$	ductility factor of connecting beams.
$\overline{\mu}_{overall}$	top deflection ratio (overall ductility demand).
ξ_i	critical damping ratio for mode i.
$[\Phi]$	modal matrix.
$\{\phi\}_{iA}$, $\{\phi\}_{iB}$	state vectors at the upper and lower surfaces, respectively, of station i.

$\{\phi\}_j$	the jth normalized eigenvector.
ω_i	the ith natural frequency in radians per second.

CHAPTER 1

INTRODUCTION

1.1 GENERAL

In high-rise buildings, the design consideration due to lateral loads becomes important. It is necessary to provide adequate lateral strength and stiffness to the structure. One of the alternatives in design is the use of reinforced concrete shear walls. The high stiffness of the shear walls in their planes is employed to resist the lateral loads. Usually, these walls extend the entire height of the building. In order to have windows, doors and service ducts, openings must be provided in the shear walls, and the resulting structure often consists of two or more shear walls coupled together by a system of horizontal spandrel beams or connecting slabs. Usually, the exterior walls have spandrel beams, relatively deep, while the interior walls are connected by slabs.

When the shear walls are arranged in a symmetric manner in the plan of the building, wind and seismic loads will cause translational displacements only. In such a case, the behaviour of the whole building can be studied from the two-dimensional behaviour of a typical pair of shear walls, coupled either through the floor slabs or floor beams. This class of problem is generally known as the plane coupled shear wall problem.

Coupled shear walls can be analysed as equivalent frames using standard matrix structural analysis techniques. The finite width of the shear wall is accounted for by assuming sets of infinitely rigid beams connected to the column of the equivalent frame. The length of the rigid beam is taken from the center line of the wall to the inner edge of the shear wall. This approach has the advantage of being versatile. Coupled shear walls can also be analysed using the continuous approach which replaces the connecting beams between the walls by a continuous distribution of laminae of equivalent stiffness. This approach has the advantage of being relatively simple and explicit solutions can be obtained for a wide range of coupled shear wall geometries.

When the wind load is the predominant lateral load on high-rise building, elastic analysis is extremely useful in assessing the behaviour of the structure. On the other hand, in seismic areas where the structure may be exposed to moderate or severe earthquake, the lateral load may be sufficiently large to cause plastic deformations in some elements of the structure, hence an elasto-plastic analysis becomes appropriate.

In the coupled shear walls of ordinary proportions, the most critical areas are the connecting beams between the walls. Observations of the earthquake damages have repeatedly indicated the failure by diagonal tension of the coupling beams containing insufficient web reinforcement. Clearly such failures, usually brittle, which result in a high rate of strength degradation under cyclic loading, must be suppressed if satisfactory seismic resistance is to be provided.

Irrespective of the design loads, the shear strength of a coupling beam must be equal to or larger than its flexural capacity. It is expected that even under a moderate intensity earthquake, the plastic hinges will develop at the ends of some, if not all, connecting beams. The behaviour of a coupled shear wall building during a moderate earthquake will therefore, depend on the extent plastic hinges formed. When subjected to a strong earthquake, the rotation demand at the plastic hinges may even exceed the member's rotational capacity, causing the connecting beams to fail under flexure. Therefore, the behaviour of a coupled shear wall building subjected to a strong earthquake will affect not only the extent of formation of the plastic hinges, but also the extent the proportions of the connecting beams that have failed completely.

Therefore, in order to study the behaviour of a coupled shear wall structure subjected to earthquake loadings, it is necessary to perform a dynamic analysis of the structure, allowing the possibility of plastic hinges or real hinges to be formed at the ends of the connecting beams. An understanding of the dynamic behaviour is an essential step to design coupled shear wall structures in seismic areas.

1.2 REVIEW OF PAST WORKS

It is useful to review the existing knowledge of the coupled shear walls by citing some of the studies carried out by different authors. These works may be divided into three basic categories, namely; elastic studies, elasto-plastic studies, ductility limited

elasto-plastic studies. Each of these categories may be again divided into two cases, namely; static analysis and dynamic analysis. Table 1.1 gives the overall view over these past works.

	STATIC ANALYSIS	DYNAMIC ANALYSIS
ELASTIC	Beck [3], Coull and Choudhury [6,7], Tso and Chan [31,33], Pisandy and Traum [24], Smith [28], MacLeod [14]	Jennings and Skattum [13], Tso and Chan [32]
ELASTO-PLASTIC	Gluck [10], Paulay [21], Winokur and Gluck [37], Robinson and Elkholy [25]	El-Shafee [9], Sozen and Ochoa [29], Takayanagi and Schnobrich [30], Srichatrapimuk [29a]
DUCTILITY LIMITED ELASTO-PLASTIC	Gluck [10]	El-Shafee [9]

Table 1.1: Review of Past Works on Shear Wall Analysis

Based on the continuum approach, sets of design curves for different static loads are produced by Coull and Choudhury [6,7]. The effect of flexibility of foundation is studied by Tso and Chan [33]. Based on the transfer matrix technique coupled with the continuous approach, a general method is presented for static analysis of non-uniform walls by Tso and Chan [31]. The flexibility of foundation can also be incorporated in this method. Based on the equivalent frame approach, a modified beam equivalent structure method is presented by Smith [28].

Elasto-plastic static analysis of the coupled shear wall based on the continuous approach has been presented by Gluck [10], Paulay [21], and Winokur and Gluck [37].

Ductility limited elasto-plastic analysis is done by Gluck [10] and he concluded that full plastification along the entire height is very rarely possible due to the limitations on the ductility factor.

Dynamic properties of planar, coupled shear walls are studied by Jennings and Skattum [13]. Planar coupled shear walls are analysed dynamically by Tso and Chan [32] by a generalized method of continuous approach i.e. the points of contraflexure are not assumed to be at the center of the connecting beams.

Dynamic elasto-plastic analysis for limited and unlimited rotational ductility is done by El-Shafee [9] by extending the transfer matrix approach. Takayanagi and Schnobrich [30] and Sozen-Ochoa [29] have done analytical and experimental work to study the inelastic dynamic behaviour of the coupled shear wall. Srichatrapimuk [29a] has studied the earthquake responses of coupled shear wall buildings by considering inelastic yielding at the ends of the connecting beams.

Further references on the shear walls can be obtained from the bibliography compiled by Schwaighofer and Singh [27].

Both El-Shafee [9] and Takayanagi-Schnobrich [30] have assumed in their analysis that the shear walls are fixed at the base. But the bending moment may exceed the ultimate capacity of the section forming the plastic hinges at the base of the walls. It is, therefore, important to consider this type of failure to understand the complete

elasto-plastic dynamic behaviour of the coupled shear wall under severe earthquake excitation.

El-Shafee [9] has studied the behaviour of the coupled shear wall-flat slab building subjected to an earthquake excitation. He has assumed that the building is symmetrical in plan and consists of a series of planar coupled shear walls such that all the interior coupled shear walls are identical and also the two end coupled shear walls are the same. Since the building is symmetrical, he has studied its overall behaviour by considering a typical interior coupled shear wall and a typical exterior coupled shear wall. In his analysis each coupled shear wall in the building is assumed to take the lateral load in proportion to its elastic stiffness and this proportion of load is assumed to be constant throughout the elasto-plastic analysis of the coupled shear walls. This assumption is realistic so long as the shear wall is in the elastic state, but when the plastic hinges start forming at the ends of the connecting beams, the stiffness ratio of shear walls changes and hence there will be a redistribution of lateral load between the interior and exterior coupled shear walls. This phenomenon of transfer of loads may lead to different behaviour of the coupled shear walls. This can be studied by considering a mathematical model consisting of two coupled shear walls, one representing all the interior coupled shear walls and other representing the two exterior coupled shear walls, connected together at the floor levels.

1.3 OBJECTIVE AND SCOPE

The purpose of the present analysis is to develop a method for a complete time history analysis of shear-wall flat slab multistorey building, taking into account the plastic deformations at the ends of the connecting beams of coupled shear walls and the P-Δ effect. With this proposed method, it is possible to study the effect of the connecting beam ductility on the seismic response of the coupled shear walls within a building.

The method used for the dynamic elastic analysis including the P-Δ effect is presented in the subsequent sections of this chapter. The modification to the proposed method for the elasto-plastic analysis is presented in Chapter 2. The formulation of the plastic hinges at the base of the coupled shear wall is presented in Chapter 3. The static analysis of the coupled shear wall taking into account wall hinge failure is also presented in that chapter. The elasto-plastic dynamic behaviour of the single coupled shear walls, with and without considering the plastic hinges at the base, is presented in Chapter 4. The modification to the proposed method considering a structural model consisting of two inter-connected coupled shear walls for elasto-plastic analysis is presented in Chapter 5. The responses of the interior and exterior coupled shear walls in a building of typical dimensions are presented in Chapter 6. In that chapter, these responses are also compared with those obtained in single coupled shear wall analysis. The calculations for the ultimate capacities of the piers are presented in Appendix A.

It is hoped that the present work will provide some insight to the inelastic dynamic behaviour of the multistorey flat-slab shear wall building and will give some confidence for the accuracy of the conventional method of single coupled shear wall analysis.

1.4 APPRAISAL OF EXISTING APPROACHES AND OUTLINE OF THE TRANSFER MATRIX TECHNIQUE

Generally, coupled shear walls can be studied by one of the two methods. These are the equivalent frame method and the continuum method. In the first method, the coupled shear wall is treated as a single bay frame. In the second method, the discrete system of the spandrel beams is replaced by an equivalent continuous medium capable of transmitting actions of the same type as the discrete spandrels. This method is particularly convenient if the walls are uniform.

For non-uniform walls, a transfer matrix technique is developed by Tso and Chan [31]. This method is based on the continuum method and is suitable for a wide variety of nonuniform shear wall configurations, foundation conditions and loading conditions. The technique is to divide the wall into a number of segments, and each segment can be considered as a uniform coupled shear wall. The continuum method of analysis can therefore apply to each segment to relate the parameters of interest from one end of the segment to the other end.

Figure (1.1) shows a nonuniform coupled shear wall on flexible foundation. The cross-sectional properties of the coupled wall change at a number of discrete stations along the height of the wall and

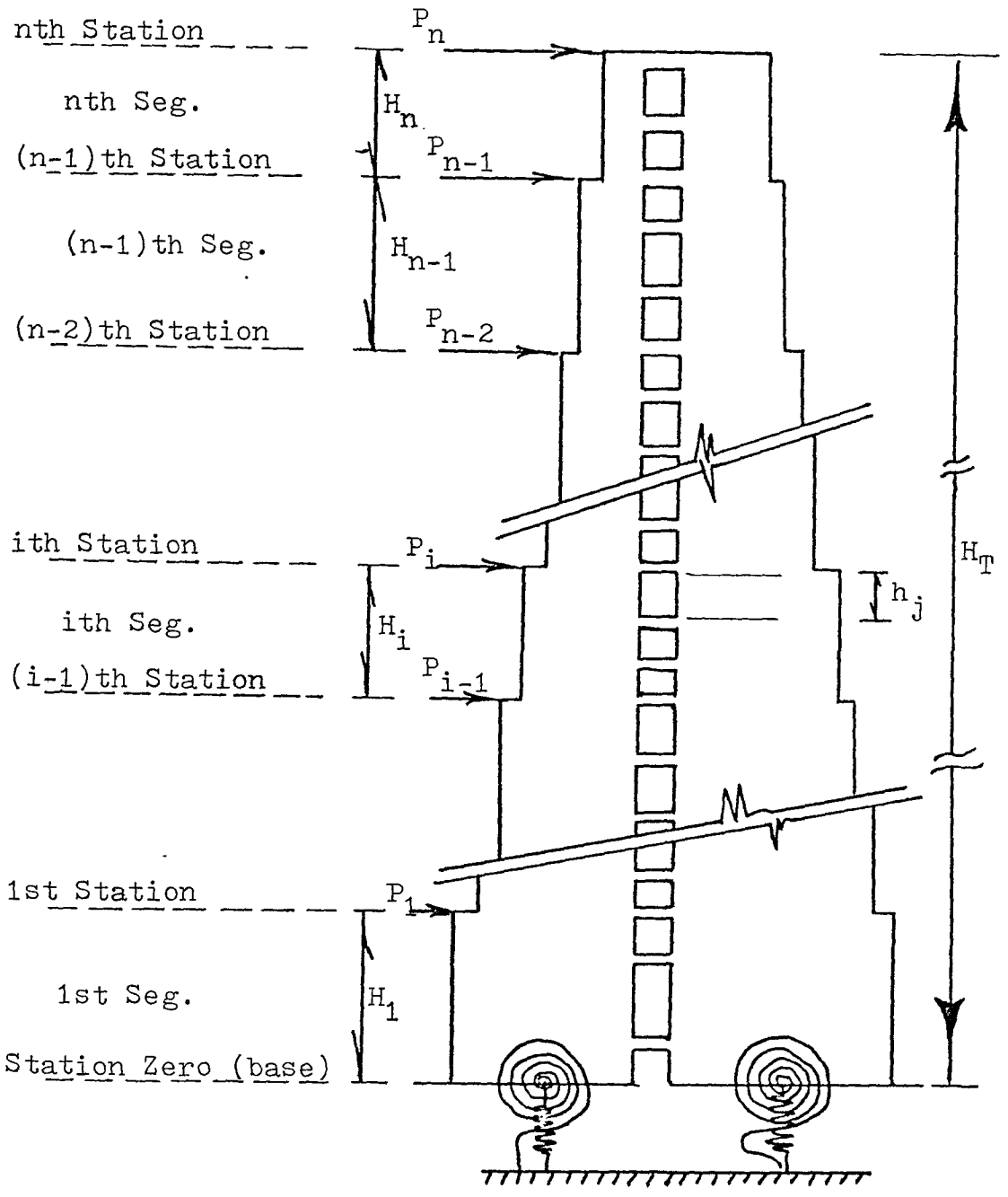

FIGURE 1-1 STEPPED COUPLED SHEAR WALL ON FLEXIBLE FOUNDATION

concentrated lateral loads are acting on these stations. So, the station is defined as the section at which the wall cross-section properties change or when there is a concentrated lateral load acting. The base is taken as station zero and the top as station n, where n is the number of segments into which the wall is divided. The ith segment lies between the (i-1)th station and the ith station. The force components on ith station and ith segment are shown in Fig. (1.2). A complete solution of the problem is obtained by determining the state vectors $\{\phi\}_{iA}$ and $\{\phi\}_{iB}$ above and below the ith station respectively. The state vectors are defined by,

$$\{\phi\}_{iA} = \text{column } \{y,\ y',\ y'',\ y''',\ T,\ q\}_{iA}$$
$$\{\phi\}_{iB} = \text{column } \{y,\ y',\ y'',\ y''',\ T,\ q\}_{iB} \qquad (1.1)$$

where

$y,\ y',\ y'',\ y'''$: deflection, slope, curvature and variation of curvature respectively

T: axial force

q: shear force intensity at the center of the connecting beams.

Station zero has one state vector $\{\phi\}_o$ and also station n has one state vector $\{\phi\}_{nB}$. These state vectors contain the boundary conditions of the coupled shear wall problem. By relating the state vector $\{\phi\}_o$ to the state vector $\{\phi\}_{nB}$ by means of the segment transfer matrices, $\{\phi\}_o$ and $\{\phi\}_{nB}$ can be determined. Then by back-substitution using the transfer matrices of the segments, other state vectors can be found.

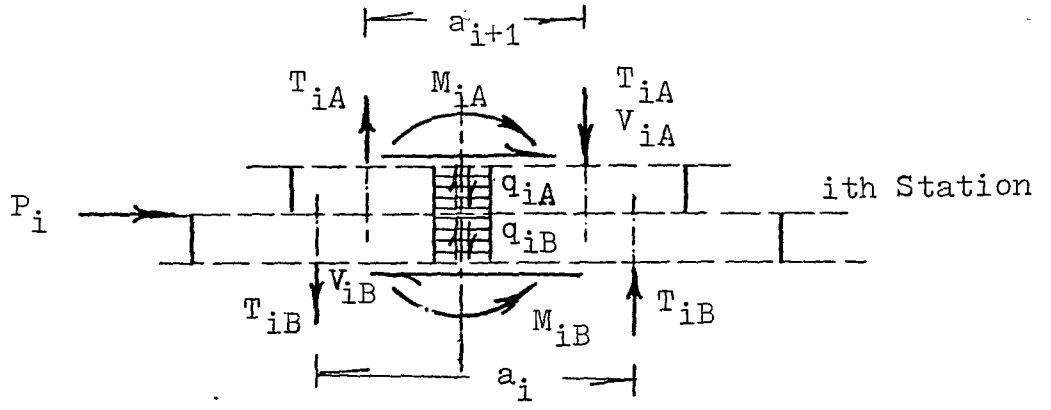

a. ith STATION

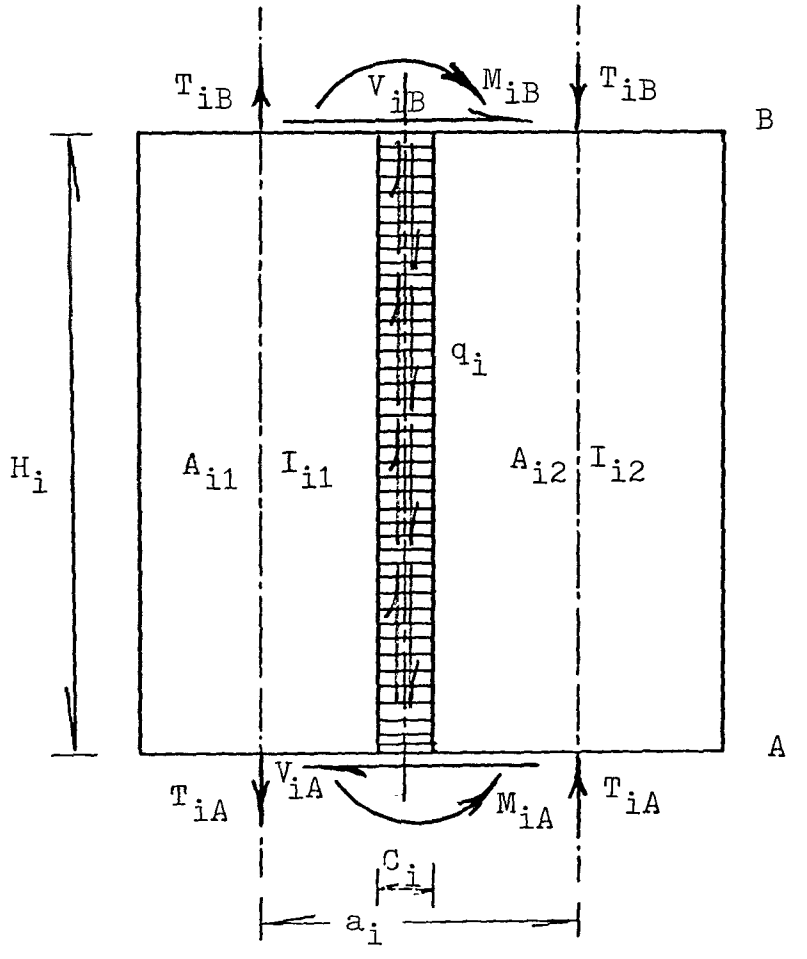

b. ith SEGMENT

FIGURE 1-2 FORCE COMPONENTS ACTING ON THE ith STATION AND SEGMENT

The transfer matrices necessary for the solution of the problem are defined as follows:

a) Field Transfer Matrix $[F]_i$

The matrix $[F]_i$ is the ith field matrix which relates the state vector at one end of the segment, $\{\phi\}_{(i-1)A}$, to the state vector at the other end of the segment, $\{\phi\}_{iB}$.

$$\{\phi\}_{(i-1)A} = [F]_i \{\phi\}_{iB} \tag{1.2}$$

b) Station Transfer Matrix $[S]_i$ and the Load Vector $\{L\}_i$

The matrix $[S]_i$ represents the station transfer matrix of the ith station. It relates the state vector at one side of the station to the state vector at the other side. The externally applied concentrated load P_i is included in the load vector $\{L\}_i$. The state vector $\{\phi\}_{iB}$ is related to the state vector $\{\phi\}_{iA}$ by the following equation.

$$\{\phi\}_{iB} = [S]_i \{\phi\}_{iA} + \{L\}_i \tag{1.3}$$

c) Total Transfer Matrix of the Structure $[\bar{F}]$

The matrix $[\bar{F}]$ is the product of all the field and station transfer matrices of the segments. The $[\bar{F}]$ matrix relates the state vectors at the base, $\{\phi\}_o$, to the state vector at the top, $\{\phi\}_{nB}$, and is given by the following equation [31].

$$[\bar{F}] = \left(\prod_{i=1}^{n} [F]_i [S]_i \right) \tag{1.4}$$

with $[S]_n$ = identity matrix.

d) Total Load Vector for the Structure $\{\bar{L}\}$

The externally applied concentrated loads are included in the total load vector for the structure. This load vector $\{\bar{L}\}$ is formed by the following equation [31].

$$\{\bar{L}\} = [F]_1 \{L\}_1 + \sum_{i=2}^{n-1} \left(\prod_{k=1}^{i-1} [F]_k [S]_k \right) [F]_i \{L\}_i \qquad (1.5)$$

The state vectors $\{\phi\}_o$ and $\{\phi\}_{nB}$ can be related by the above matrices $[\bar{F}]$ and $\{\bar{L}\}$ and is given by the following equation.

$$\{\phi\}_o = [\bar{F}] \{\phi\}_{nB} + \{\bar{L}\} \qquad (1.6)$$

There are six elements in each of the state vectors $\{\phi\}_o$ and $\{\phi\}_{nB}$. Out of these twelve elements, six are known as given by the boundary conditions at the top and bottom of the structure. The remaining six unknowns can be obtained from the set of six equations given by (1.6). Once this equation is solved, then every element in the state vector $\{\phi\}_o$ and $\{\phi\}_{nB}$ will be known.

By means of the transfer matrices of the segments other state vectors can be determined for all segments starting from the top and going down until segment 1 [31].

1.5 ASSUMPTIONS

Many assumptions are used for the present analysis. The assumptions which are listed below can be classified into two main groups. The first one is the general assumptions which have been verified by most investigators, and the second group of assumptions

concerns the present problem specifically.

1.5.1 General Assumptions

These assumptions are dealing with the stress-strain relationship and compatibility conditions of the lintel beam.

1. Moment-rotation relationship is considered linear up to the plastic moment followed by a horizontal plastic plateau.
2. Plane section perpendicular to the axis of the member before loading remains plane after application of load.
3. Shear deformation is neglected for the piers and axial deformation is neglected for connecting beams.
4. The midpoints of the connecting beams are points of contra-flexure.

1.5.2 Special Assumptions

These assumptions are made in order to simplify the analysis and to make it compatible with approach used. These assumptions are dealing with the modelling of the structure.

1. The wall remains elastic except at the base throughout the analysis.
2. Plastic hinge may form at the base of the wall depending on the base moment and axial force.
3. Uncracked, double reinforced concrete section for the wall is used in the calculation of wall stiffness and moment capacities.

4. The connecting beams are taken as a double reinforced concrete section and the cracked section is used for stiffness and moment capacity determination.
5. The masses are to be lumped at discrete points along the height of the wall. Therefore, the inertial forces of the wall are approximated by concentrated loads acting at different heights of the building.

1.6 DYNAMIC MODELLING

The lumped-mass approach is used in the dynamic analysis. The masses of the segments (of all walls) are lumped at discrete floors along the height of the wall. The locations of the masses are taken at the stations in the problem. These masses need not necessarily be located at the top of each segment. As shown in Fig. (1.3), the location of the masses may be at the top of one or more segments and the masses of all the segments between the two mass-stations can be lumped together at the upper mass-station. In the present study, the total number of segments in the wall is taken as an integer multiple of the total number of masses considered.

For dynamic analysis of coupled shear walls, only the first few modes are important and more accurate behaviour of the shear wall along the entire height can be achieved by increasing the number of segments. This compromise can be made in this modelling by considering the number of segments is larger than the number of lumped masses.

The mass matrix, stiffness matrix and damping matrix in the

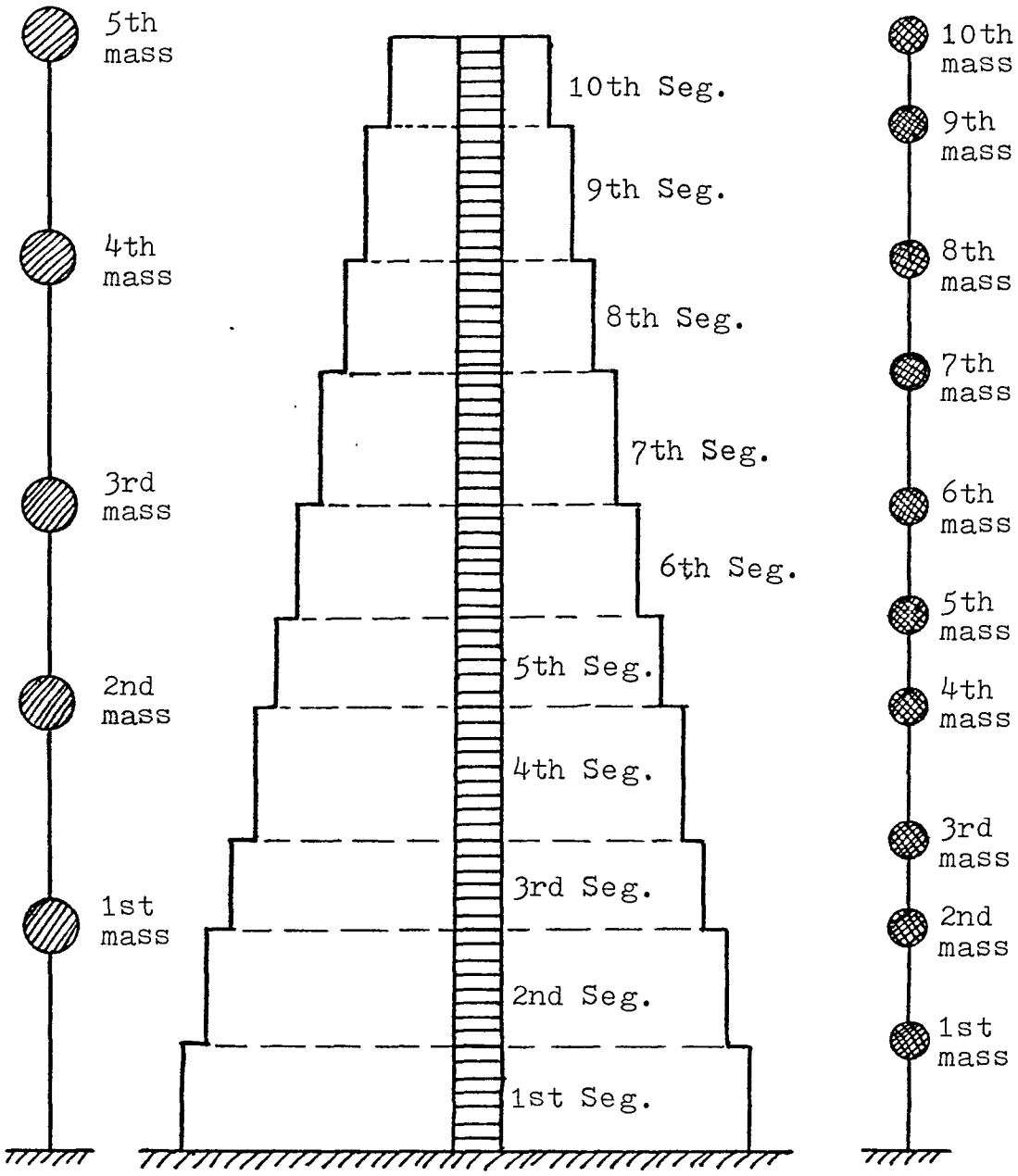

Lumped System	Shear Wall Structure	Lumped System
NMAS = 5	NSEG = 10	NMAS = NSEG = 10
NFR = NSEG/NMAS = 2		NFR = NSEG/NMAS = 1

NSEG : No. of Segments, NMASS : No. of lumped Masses

FIGURE 1-3 LUMPED MASS MODELLING

equations of motion for the system are m by m matrices, where m is the number of lumped masses.

1.6.1 Mass Matrix [M]

It is a diagonal matrix with the mass of the segments between ith mass-level and (i-1)th mass level to be the element $m_{(i,i)}$ on the main diagonal.

1.6.2 Stiffness Matrix [K^*]

The flexibility matrix [F'] can be obtained from static analysis. That is, the jth column is to be formed by calculating the lateral deflection y_i of the ith mass due to unit load acting on jth mass (i, j=1, m).

P-Δ effect can be introduced in this stage, i.e. before inverting the flexibility matrix [F'] to obtain the stiffness matrix. If P-Δ effect is to be neglected the inversion of [F'] will give the stiffness matrix [K]. The combined stiffness matrix [K^*] which includes the geometric stiffness, can be obtained by inverting the combined flexibility matrix [F^*]. The combined flexibility matrix [F^*] includes the P-Δ effect.

To introduce the P-Δ effect, the following iterative procedure is to be carried out:

1. From the resulting flexibility matrix [F'], the lumped weights at the stations will cause additional bending moment due to the eccentricity from the axis of the wall, Fig.

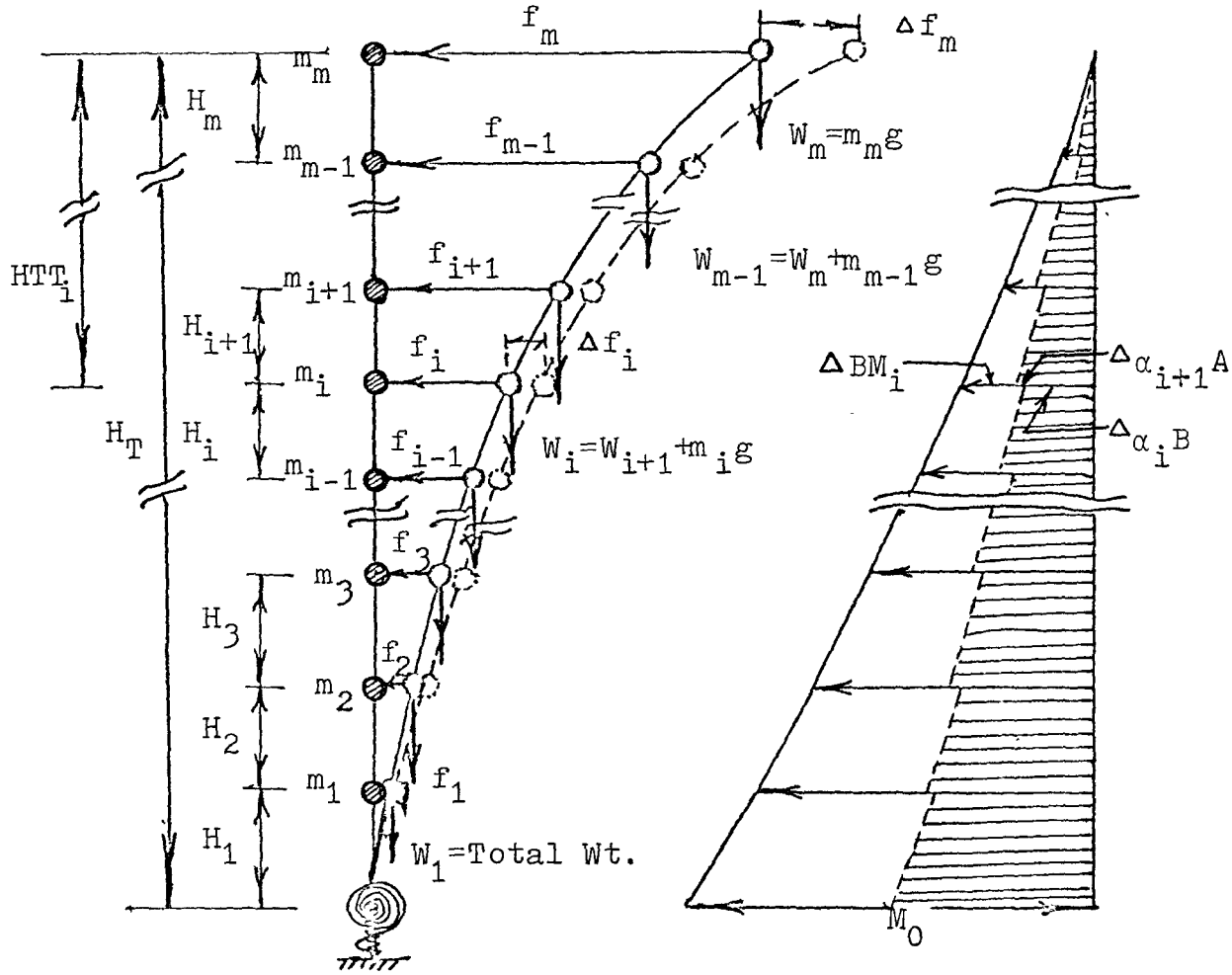

$$\Delta BM_i = \sum_{k=i+1}^{m} W_k(f_k - f_{k-1})$$

$$\Delta\alpha_{i+1}A = \Delta BM_i / EI_{i+1}$$

$$\Delta\alpha_i B = \Delta BM_i / EI_i$$

$$W_{i1} = \alpha_i H_i$$

$$W_{i2} = (\alpha_{iA} - \alpha_{iB}) H_i / 2$$

H_T = Total Height

$$HTT_i = H_T - \sum_{k=1}^{i} H_k$$

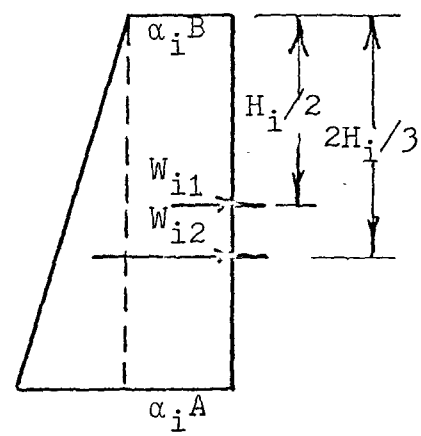

(mode j)

FIGURE 1-4 : P-Δ EFFECT

(1.4).

2. The additional lateral deflection Δf_i is calculated at each mass level i and is added to the flexibility coefficient f_i to get a modified coefficient f_i^*.
3. Step (1) is to be repeated using f_i^* and from which a new Δf_i can be calculated. This new Δf_i is to be added to the flexibility coefficient f_i to obtain a new f_i^{**}. Comparison is to be made between the resulting f_i^{**} and f_i^*. If the difference between two cycles is within certain allowable error, the resulting modified flexibility coefficient f_i^{**} is taken to be correct. Otherwise steps (1) to (3) have to be repeated again with f_i^{**} as f_i^*.

Figure (1.4) shows the eccentricities f_i for the lumped weights W_i, (i = 1, m), and the method of calculating the additional bending moment due to these eccentricities. Also the method of calculating the elastic weights α_i is shown in the same figure. The additional Δf_i can be calculated from the following equation:

$$\Delta f_i = \sum_{k=1}^{m} \{W_{i1}[(HTT_k - HTT_i) + H_k/2] + W_{i2}[(HTT_k - HTT_i) + \frac{2}{3} H_k]\} + \Delta\theta_i \qquad (1.7)$$

where $\Delta\theta_i$ is the additional deflection due to the additional rotation at the foundation level, which can be calculated as:

$$\Delta\theta_i = \frac{M_o}{K_\theta} (HT - HTT_i) \qquad (1.8)$$

It should be noted that in the above method the coupled action is neglected in calculating Δf and the coupled shear wall is considered as cantilever with equivalent moment of inertia $I_i = I_{i1} + I_{i2}$. (In case of two interconnected coupled shear walls formulation the coupled action in both coupled shear wall is neglected by considering $I_i = I_{i1} + I_{i2} + I_{i3} + I_{i4}$.)

By applying the above method for all the columns in the flexibility matrix (j = 1, m), a modified flexibility matrix $[F^*]$ is obtained. This matrix includes the gravity load effect.

The combined stiffness matrix $[K^*]$ is to be determined by inverting this combined flexibility matrix $[F^*]$

$$[K^*] = [F^*]^{-1} \tag{1.9}$$

1.6.3 Damping Matrix [C]

For the numerical integration the damping matrix must be introduced to the equations of motion with its original form. It is assumed that the damping matrix [C] will be diagonalized by the similar transformations that diagonalize the [M] and $[K^*]$ matrices. In other words,

$$[\Phi]^T [C] [\Phi] = \begin{bmatrix} \ddots & & 0 \\ & 2\xi_i\omega_i & \\ 0 & & \ddots \end{bmatrix} \tag{1.10}$$

where

$[\Phi]$: modal matrix

ξ_i: ith percentage damping ratio, and

ω_i: ith natural frequency in radians per second.

Therefore, to form [C] it is necessary to calculate the eigenvalues and the eigenvectors of the system. The periods and the normalized unit vectors can be determined from the eigenvalues and eigenvectors respectively.

$$\bar{T}_i = 2\pi/\omega_i \tag{1.11}$$

$$\{\phi\}_j = \left(\frac{1}{\sum_{i=1}^{m} m_{ii} \lambda_{ij}^2} \right)^{1/2} \{\lambda\}_j \tag{1.12}$$

where $\{\lambda\}_j$: Eigenvector for jth mode

If the percentage damping ratios ξ_1, ξ_2, ..., ξ_n are to be assigned, the damping matrix [C] can be determined from equation (1.10) as

$$[C] = [\Phi^T]^{-1} \begin{bmatrix} \ddots & & 0 \\ & 2\xi_i\omega_i & \\ 0 & & \ddots \end{bmatrix} [\Phi]^{-1} \tag{1.13}$$

from orthogonality condition

$$[\Phi]^T [M] [\Phi] = [I] \tag{1.14}$$

Premultiplying equation (1.14) by $[\Phi^T]^{-1}$ gives

$$[\Phi^T]^{-1} [\Phi^T] [M] [\Phi] = [\Phi^T]^{-1} [I]$$

therefore

$$[\Phi^T]^{-1} = [M] [\Phi] \tag{1.15}$$

Postmultiplying equation (1.14) by $[\Phi]^{-1}$ gives

$$[\Phi]^T [M] [\Phi] [\Phi]^{-1} = [I] [\Phi]^{-1}$$

therefore

$$[\Phi]^{-1} = [\Phi]^T [M] \tag{1.16}$$

Substituting for $[\Phi^T]^{-1}$ and $[\Phi]^{-1}$ from equation (1.15) and (1.16) in equation (1.13) gives

$$[C] = [M] [\Phi] \begin{bmatrix} \ddots & & 0 \\ & 2\xi_i\omega_i & \\ 0 & & \ddots \end{bmatrix} [\Phi]^T [M] \tag{1.17}$$

Above equation gives the damping matrix [C] by knowing the normalized eigenvector matric [Φ], the frequencies, the matrix [M], and after assuming the critical damping ratios ξ_i, (i = 1, m),for different modes.

1.7 NUMERICAL INTEGRATION

To obtain the seismic responses numerical integration needs to be carried out for any ground acceleration record input. The choice of the proper method for the step-by-step integration is governed by two factors.

a) Stability of the Integration Procedure

The rate of convergence is dependent upon the period of the highest mode of the system. Consequently, the time interval Δt used must be related to the shortest period of vibration, for lumped mass system. The method is unconditionally stable if the solution for any initial conditions does not grow without bound for any time step δt, in

particular when $\delta t/T_{min}$ is large. Unconditionally stable scheme is needed when we have very high frequencies. Alternatively, a numerical scheme can be conditionally stable, which requires an upper limit for $\delta t/T_{min}$, and is suitable for systems in which T_{min} is relatively large, so that fairly large integration step δt can be used. Among the different numerical schemes, such as Newmark method [18], Wilson θ method [2], and the direct step-by-step integration method [35], Newmark method is found to be the most stable method as stated by Wilson, Farhooh and Bathe [36].

b) The Accuracy of the Resulting Acceleration, Velocities and Displacements

The accuracy increases by decreasing δt, for large values of δt the errors in period are increased and the percentage amplitude decay also is increased. From Wilson and Bathe's analysis [36], Newmark method proved to be the only method which gives no errors either in the period or in amplitude alternation.

From the above discussion it can be seen that Newmark method is the best one to be used in integrating the equation of motion to ensure the stability of the integration. Given below is a summary of Newmark method [18], using "α" = 0.5, and "β" = 0.25.

1. Assume values of the acceleration of each mass at the end of the interval.
2. Compute the velocity and the displacement of each mass at the end of the interval from the following equations:

$$\dot{\{u\}}_{n+1} = \dot{\{u\}}_n + \frac{\Delta t}{2} \{\ddot{u}_{n+1} + \ddot{u}_n\} \tag{1.18}$$

$$\{u\}_{n+1} = \{u\}_n + \Delta t \dot{\{u\}}_n + \frac{(\Delta t)^2}{4} \{\ddot{u}_{n+1} + \ddot{u}_n\} \tag{1.19}$$

3. From the computed displacement $\{u\}_{n+1}$, compute the resistance forces $\{R\}$,

$$\{R\}_{n+1} = [K^*] \{u\}_{n+1} \tag{1.20}$$

4. From the computed velocity $\dot{\{u\}}_{n+1}$, compute damping forces $\{D\}$,

$$\{D\}_{n+1} = [C] \dot{\{u\}}_{n+1} \tag{1.21}$$

5. From the resisting forces $\{R\}_{n+1}$, the damping forces $\{D\}_{n+1}$ and the applied loads $\{P\}_{n+1}$, which is given by $-[M] \{\hat{1}\}a_{n+1}$, and a_{n+1} is the ground acceleration at t_{n+1}, the acceleration can take a new value for each mass at the end of the interval, as:

$$\ddot{\{u\}}_{n+1} = [M]^{-1} \{P - R - D\}_{n+1} \tag{1.22}$$

6. Compare the derived acceleration with the assumed acceleration at the end of the time interval. If these are the same, the calculation is completed and one can proceed to the next time interval. If these are different, repeat the calculation from step 1, with the derived value as the new acceleration for the end of the time interval.

1.8 EQUIVALENT STATIC LOAD

The output of the numerical integration process is the displacement, the velocity and the acceleration for each mass as a function of time. The product of mass times the corresponding acceleration will give the inertia load acting on the structure, namely:

$$\{W\}_t = - [M] \{\ddot{u}\}_t \qquad (1.23)$$

It should be noted that $\{\ddot{u}\}_t$ is total acceleration vector at time 't'.

Once the inertial loading is known, the stress state of the structure can be determined using the transfer matrix technique. In this manner, one can obtain a time history of the parameters of interest. The parameters of interest are the top deflection, base wall moment, the connecting beam end moments or shear intensity, and the axial force in the walls.

1.9 ELASTO-PLASTIC ANALYSIS

The main difference between an elasto-plastic analysis and the elastic analysis is that the inelastic behaviour of the connecting beams is taken into account. Depending on the shear intensity q(x,t) in the connecting beams, the beam may be in one of three states. It may remain elastic if q(x,t) is small. Plastic hinges may form at the ends of the connecting beams if the end moment exceeds the plastic moment of the beams [Fig. 1.5(b)]. Finally, if the deformation requirement on the connecting beam is sufficiently large then the beam may fail. No shear

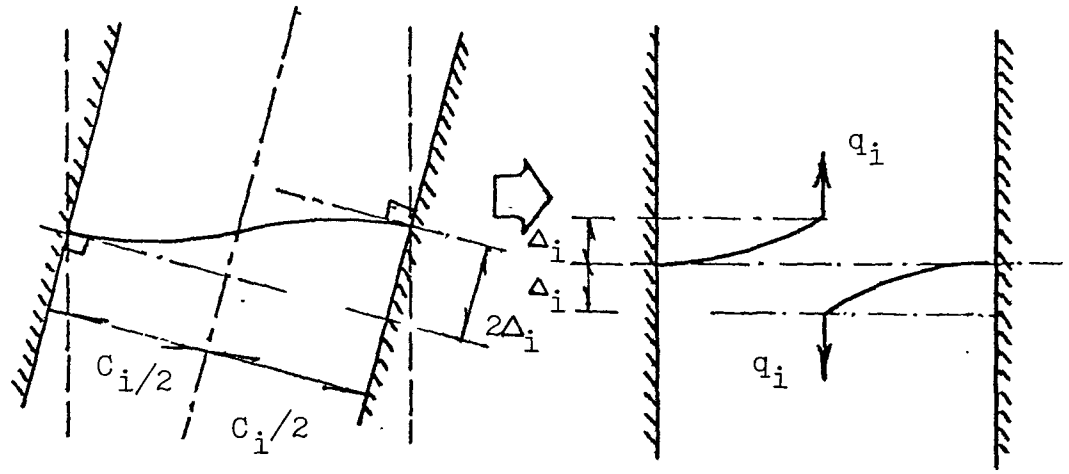

a. Segment Deflection (Δ_i)

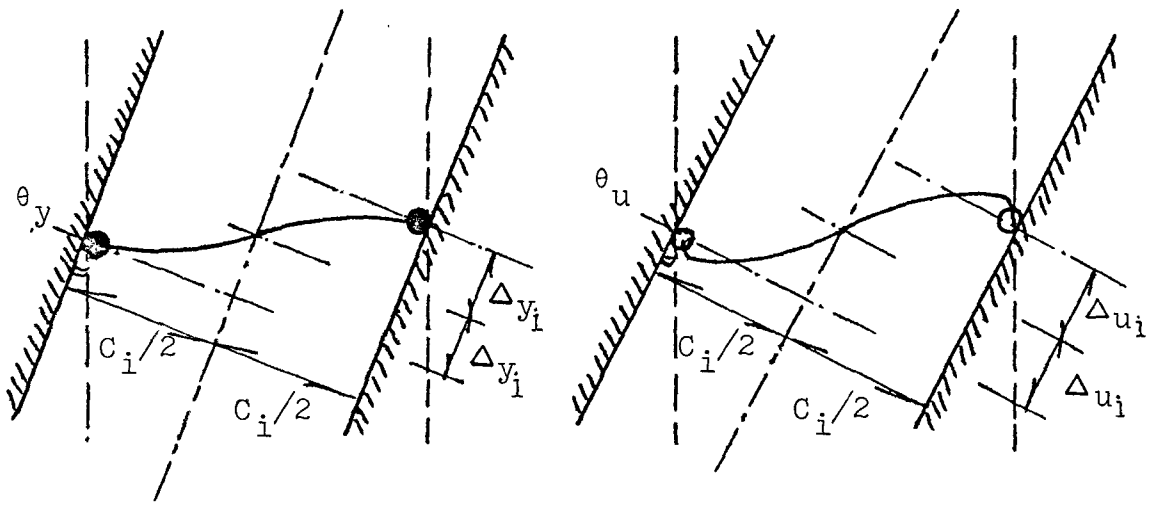

b. Plastic Hinges

c. Real Hinges

FIGURE 1.5 SHEARING FORCE INTENSITY (q_i) AND DEFLECTION (Δ_i)

or moment will be transmitted by connecting beams if this happens. Conceptually this is represented as the formation of two real hinges at the ends of the connecting beam [Fig. 1.5(c)].

In this section the segment states are defined and the overall scheme of analysis is described. The flow chart of the computer program to perform the computation is presented.

1.9.1 Assumptions for the Definition of Segment State

To decide what state a segment is in, the bending moment and the rotation at the ends of the connecting laminae are to be computed and related to the moment-rotation relationship of the connecting laminae. The relation between the bending moment at the ends of the connecting laminae and the shear intensity q_{xi} is as follows:

$$q_{xi} = \frac{2\, m_{xi}}{c_i} \tag{1.24}$$

where: m_{xi} = Bending moment per unit height at distance "x" from the bottom of the segment "i".

As c_i the length of the connecting laminae within the segment "i" is constant, q_{xi} can be used instead of the end moments to check the conditions of the connecting laminae. Also, the rotation of the laminae can be expressed in terms of the relative end displacements "Δ_i" of the laminae.

In the present analysis, the shearing force q_i per unit height of the ith segment is taken to be the average value in the ith segment's laminae q_i can be calculated from the following equation:

$$q_i = \frac{1}{2} (q_{i0} + q_{iH_i}) \tag{1.25}$$

where:

q_{i0} = shearing force intensity at the bottom of the ith segment,

q_{iH_i} = shearing force intensity at the top of the ith segment.

The deflection Δ_i of the connecting laminae of the ith segment is taken to be one half of the average value of the relative end displacements of the ith segments laminae at the faces of the walls [see Fig. (1.5a)]. Δ_i can be calculated from the following equation.

$$\Delta_i = \frac{1}{2} (\Delta_{i0} + \Delta_{iH_i}) \tag{1.26}$$

where:

Δ_{i0} = half the relative end displacements of the ith segment's laminae at the faces of the walls.

Δ_{iH_i} = half the relative end displacements of the ith segment's laminae at the faces of the walls.

1.9.2 Resistance Function

Instead of using the moment-rotation relationship, the resistance function of the ith segment's laminae will be expressed in terms of q_i and Δ_i defined previously. The resistance function used as shown in Fig. (1.6) is a bilinear hysteretic resistance function. As the deflection Δ_i increases from zero, the resistance q_i increases linearly

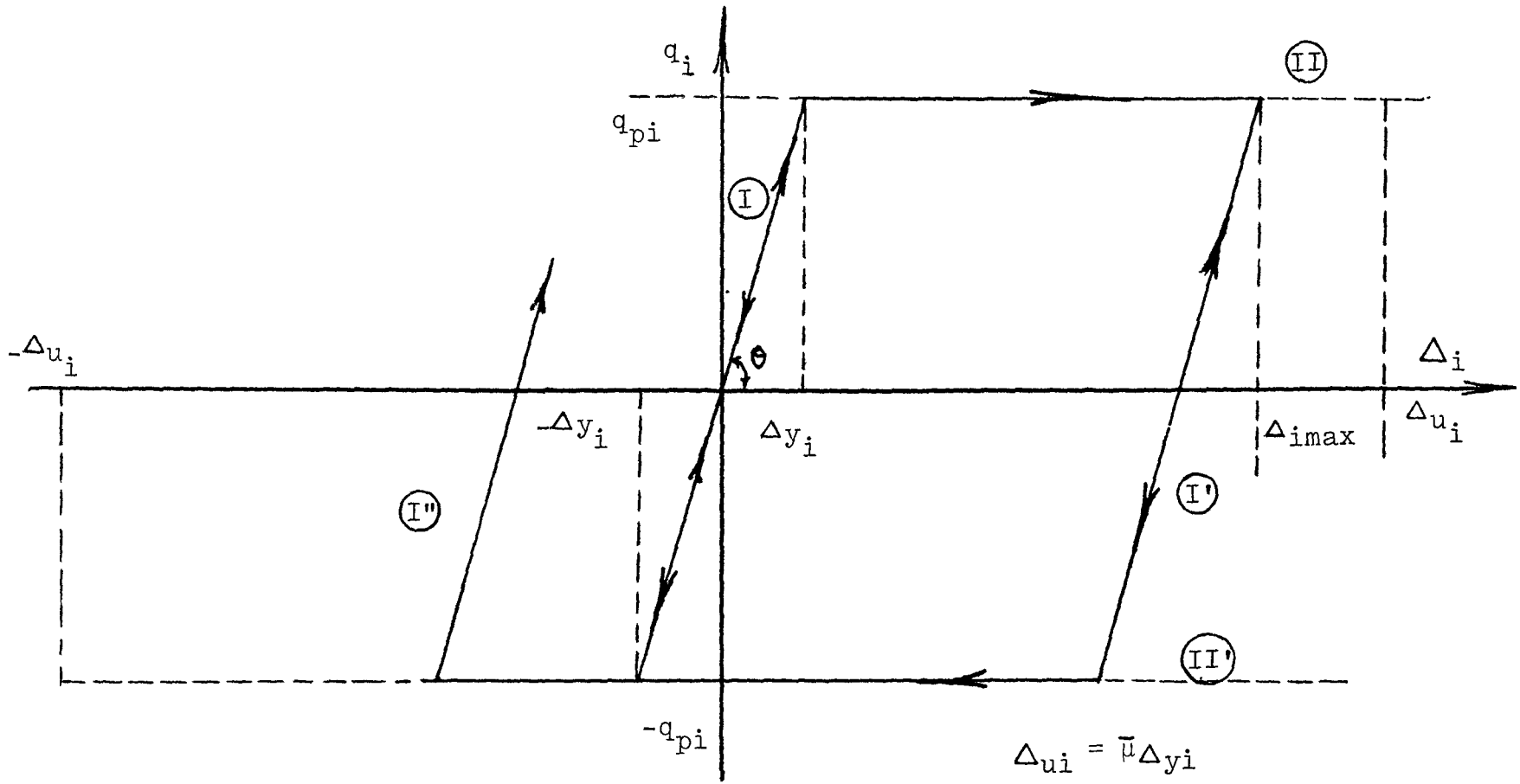

FIGURE 1-6 RESISTANCE FUNCTION

with the slope of $(2\mu_i^2/a_i)$. The linearity continues until the yielding deflection Δ_{yi} is reached. As the deflection Δ_i increases further, the resistance q_i is assumed to remain constant at q_{pi}. The latter value will be maintained until the ductility limit of the member is reached. However, if the deflection Δ_i reaches a maximum before the ductility limit and then decreases, the resistance q_i is assumed to decrease along the line parallelled to the initial elastic shape. This decrease will continue with decreasing the deflection Δ_i until a shearing intensity $-q_{pi}$ is attained.

1.9.3 Segment State

Shown in Fig. (1.6) is the resistance function of the connecting laminae in the ith segment. The ductility limit is denoted by Δ_{ui} which is the product of the yield displacement Δ_{yi} and the ductility coefficient $\bar{\mu}$. This figure contains two sets of lines, namely: Set I and set II.

The segment state can be defined as follows:

- If the average shear intensity q_i in the segment is such that $q_i \geq q_{pi}$ and average laminae deflection $\Delta_{i(t)} \geq \Delta_{i(t-\delta t)}$, i.e. along line II; or if $q_i \leq -q_{pi}$ and $\Delta_{i(t)} \leq \Delta_{i(t-\delta t)}$, i.e. along line II' and in both cases, $|\Delta_i| < |\Delta_{ui}|$, then the segment is in plastic hinged state
- If $\Delta_{i(t)} < \Delta_{i(t-\delta t)}$ and $q_i \geq q_{pi}$ i.e. along line I', or if $\Delta_{it} > \Delta_{i(t-\delta t)}$ and $q_i \leq -q_{pi}$, i.e. along line I", the segment is in the elastic state. Also the segment is in the elastic state if

$-q_{pi} < q_i < q_{pi}$.

- If the laminae displacement exceeds the ductility limit i.e. $|\Delta i| \geq |\Delta_{ui}|$, then the segment is in the real hinged state.

Once the segment is in the real hinged state, it will remain in the real hinged state until the end of the analysis. However when the segment is in the plastic hinged state, it will return to the elastic state upon unloading.

1.9.4 Scheme of Computation

The scheme of computation for response calculations is as follows. The segments are taken to be elastic initially. Step-by-step integration is performed to obtain the displacement, velocity and acceleration at every time interval Δt. The P-Δ effect is introduced here to consider the effect of the dead loads on the deflection pattern. The dead loads at the deflected mass-level will cause additional deflection due to the secondary moments and this additional displacement Δf_i at the ith level (equation (1.7), (1.8)) is calculated to get the modified deflection at each level. If these modified deflections at each level and corresponding deflections at the beginning of the cycle are within the allowable error, then the iteration procedure for P-Δ effect is stopped. Otherwise these modified deflections are taken as the values at the beginning of the cycle and next iteration cycle is carried out.

The stress states of the wall are checked not at every time step but at the intervals of K_{max} times δt. The value of K_{max} is to be

entered as an input to the computaton, and δt is the time interval of calculating the straining actions of the structure. This arrangement allows the user to obtain a compromise between the accuracy of solution and economy in computation time. If any segment changes its state, the overall stiffness matrix of the coupled shear wall is reevaluated before the next time step integration takes place. This procedure carries on until the end of the earthquake or when the time of integration reaches a prescribed limit or the complete failure of the shear wall, whichever occurs first.

The time history responses for top deflection, base wall moments, base axial force and shear intensity at the different segments are calculated and plotted out by the subroutine attached to the main computer program.

1.9.5 Flow Chart for the Elasto-Plastic Dynamic Analysis of Planar Coupled Shear Walls

For the purpose of saving the computer time the following steps are taken in computer program:

1. The response is printed out after every K_{max} cycles of integration, which is entered as input to the computation.
2. A factor K_{max} is introduced for the check of segment stress state, so that the segments state is to be checked at time interval = K_{max} δt second, and the segments state is assumed to be constant in the interval between checking.
3. The cracked moment of inertia of the connecting beams, is computed manually beforehand and then introduced to the

program as input data and kept constant in the analysis.

The flow chart of the computer program is shown in Fig. (1.7). Some controlling integer and real parameters are presented in the flow chart to control the operation. The controlling parameters are K_{max}, J, t_{max}, NSEG, NWHNG, NMAS, q_{pi}, Δ_{yi}, and Δ_{ui}. The following definitions may help in understanding the flow chart.

NSEG — number of segments considered.

NMAS — number of masses considered.

NWHNG — controlling parameter for wall hinge failure consideration if it is zero, then wall hinge failure is not considered if it is one, then wall hinge failure is considered.

K_{max} — segments check parameter, i.e. the segments state, are to be checked every $K_{max}\delta t$, where δt is the time interval for computing the stress state of the structure.

J — number of segments which change their states. If J = 0, no correction of the dynamic properties needs to be made.

t_{max} — time limit of the analysis

q_{pi} — plastic shearing force intensity of the ith segment's laminae.

Δy_i — yield displacement of the ith segment's laminae.

Δ_{ui} — ultimate displacement of the ith segment's laminae. Δ_{ui} is the product of the yield deflection Δy_i and the ductility coefficient $\overline{\mu}$.

NGEE — counter for iteration at wall hinge formation. If it is zero, then either wall hinge failure is not considered or

it is before hinge formation, hence next time step is considered. If it is non-zero; then an iteration procedure is to be started and hence next time step is not considered.

NHG(L) if it is equal to L, then hinge is formed at base of Lth pier. If it is zero, then hinge is not formed at base of Lth pier.

$BMM)_L$ max^m B.M. permissible at base of pier L for given A.F.

NPIER no of piers; = 2 for single coupled shear wall problem
= 4 for two interconnected coupled shear wall problem

NLC counter for iteration to check the segment states. If it is zero, then go for next time step i.e. the iteration procedure is completed. If it is non-zero, then go for an iteration procedure in the same time step.

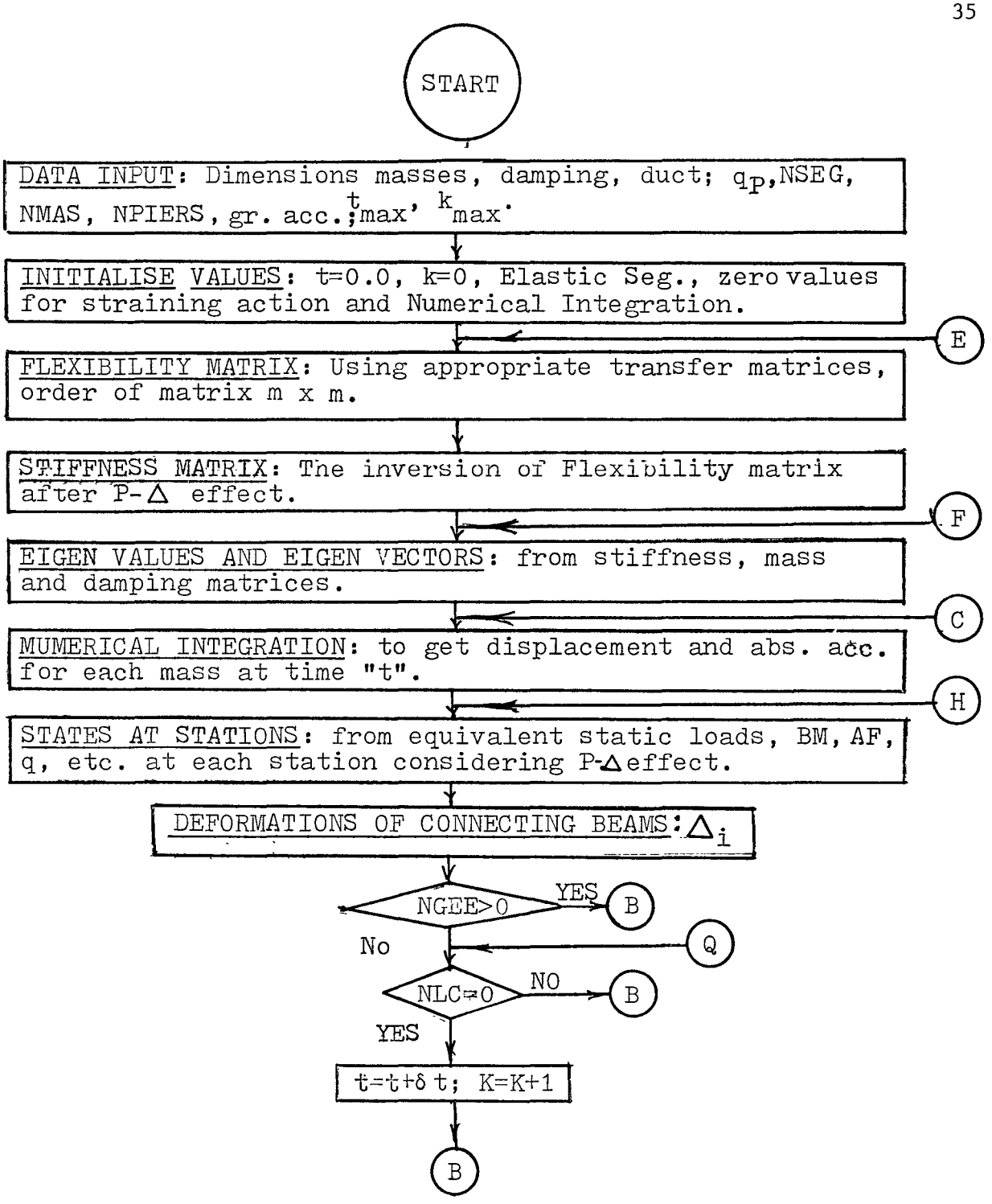

FIGURE 1-7 FLOW CHART FOR ELASTO-PLASTIC DYNAMIC ANALYSIS OF COUPLED SHEAR WALLS

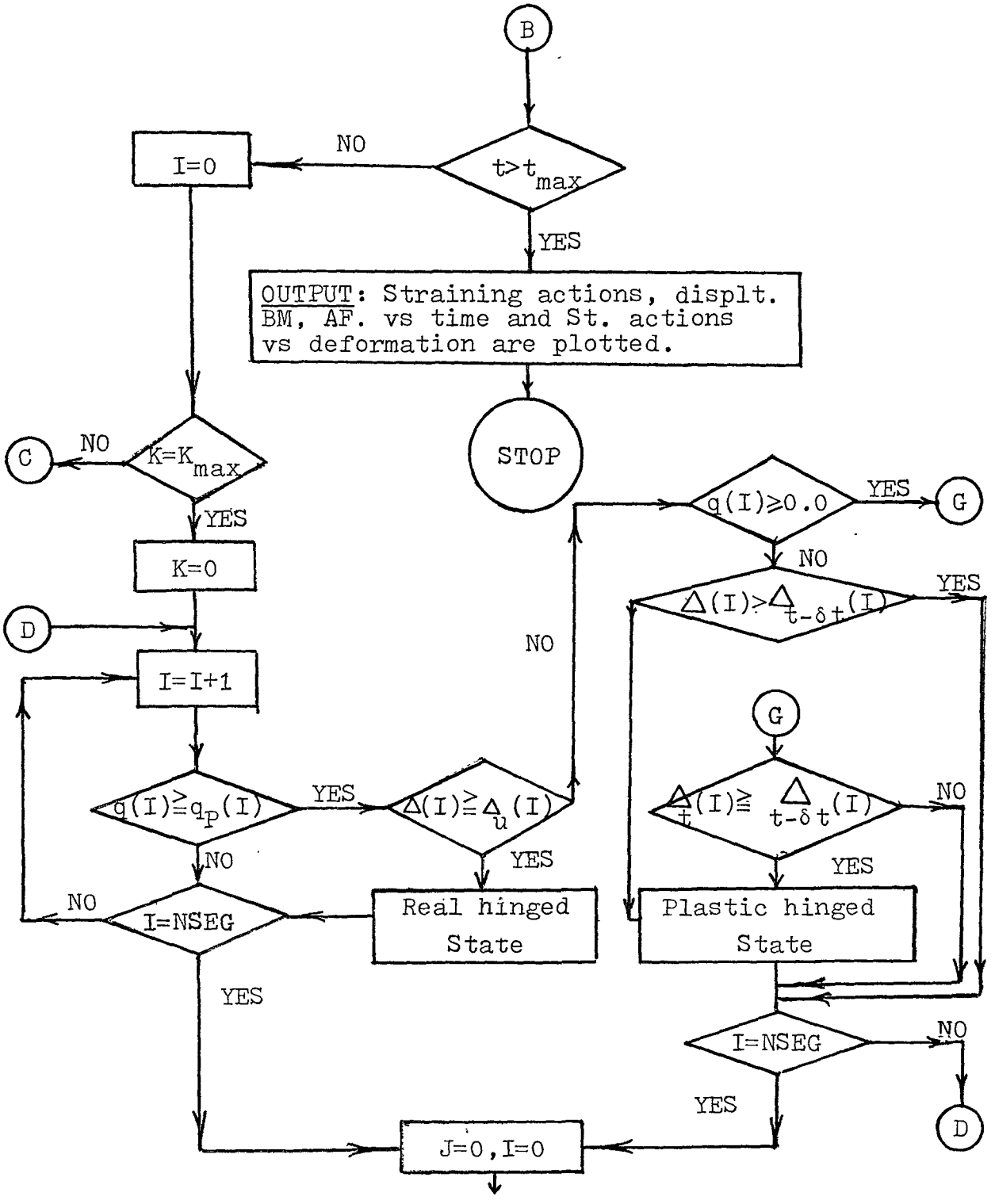

FIGURE 1-7 FLOW CHART FOR ELASTO-PLASTIC DYNAMIC ANALYSIS OF COUPLED SHEAR WALLS

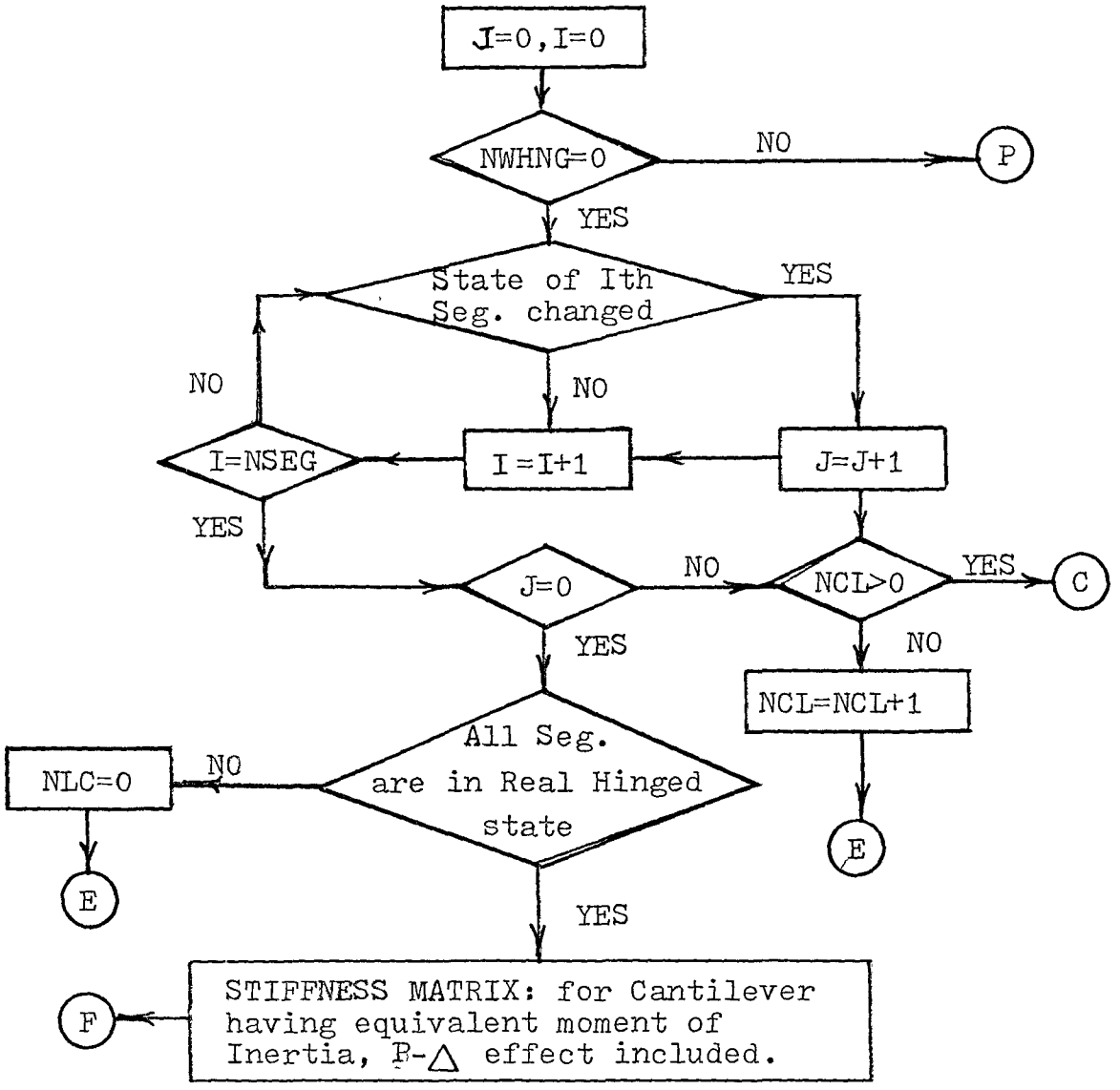

FIGURE 1-7 FLOW CHART FOR ELASTO-PLASTIC DYNAMIC ANALYSIS OF COUPLED SHEAR WALLS

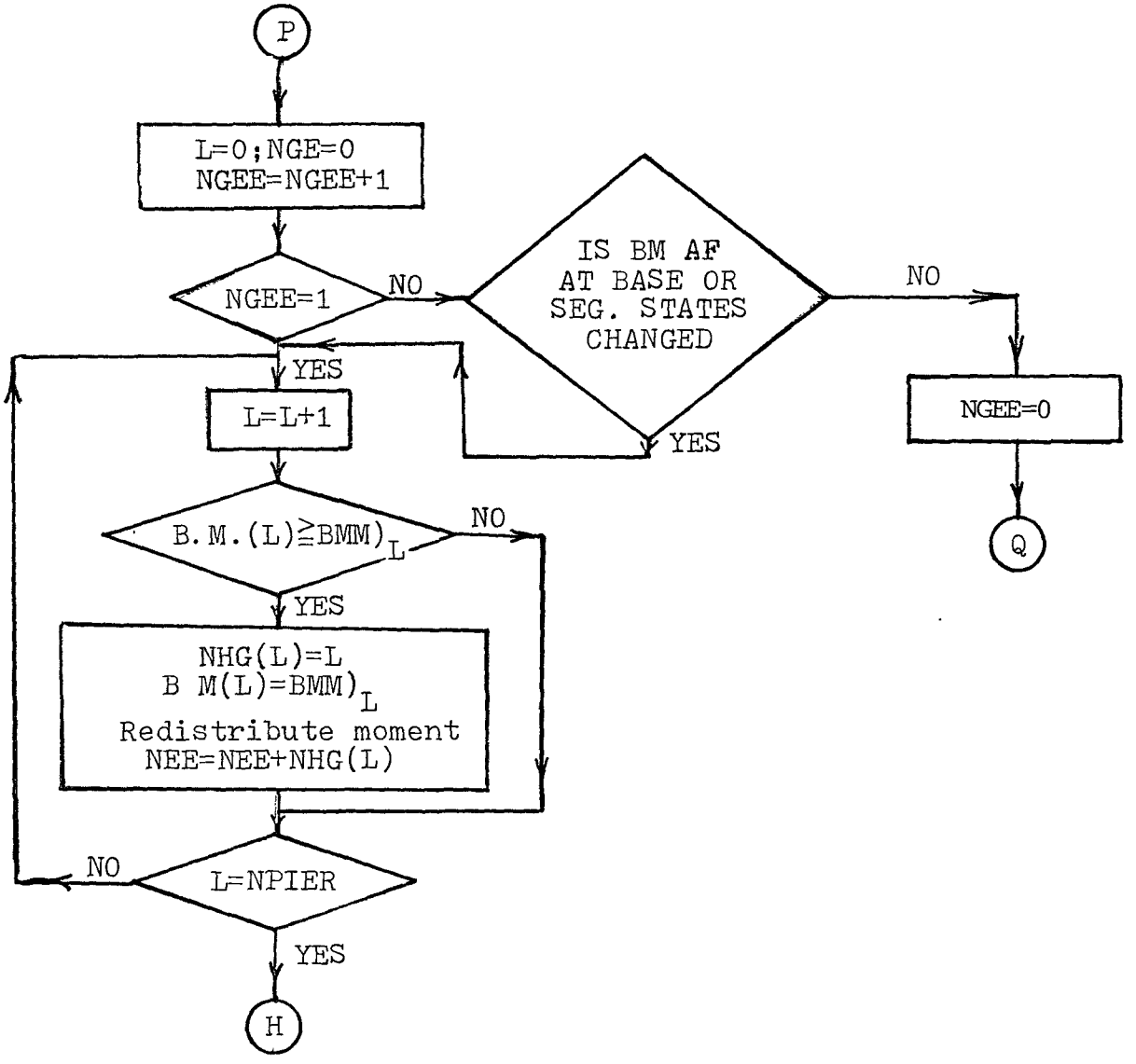

FIGURE 1-7 FLOW CHART FOR ELASTO-PLASTIC DYNAMIC ANALYSIS OF COUPLED SHEAR WALLS

CHAPTER 2

ELASTO-PLASTIC ANALYSIS OF SINGLE COUPLED SHEAR WALL

2.1 INTRODUCTION

An elasto-plastic analysis for one planar coupled shear wall is presented in this chapter. The analysis is based on the transfer matrix technique in combination with the continuum method as explained in the previous chapter.

Depending on the shear intensity $q(x,t)$ in the connecting beam, the beam may be in one of the three states, namely, the Elastic, Plastic-hinged or Real-hinged state. At any given time, the shear intensity varies along the height of the structure. Therefore, portions of the connecting beams along the height may be elastic, part of them may have plastic hinges formed at the ends and part of them may have failed and therefore represented by connecting beams with real hinges at the ends. A segment of a coupled shear wall containing only elastic connecting beams is called an elastic segment. Similarly, a segment containing beams with plastic hinges or real hinges are called plastic hinged segment or real hinged segment respectively.

The properties of a plastic hinged segment or real hinged segment will be different from an elastic segment. Hence it is necessary to

derive appropriate field transfer matrices for plastic and real hinged segments in addition to elastic segments. Furthermore, the station transfer matrix relating a state vector in an elastic segment to a state vector in a plastic hinged segment is different from the one which relates two state vectors both in either elastic segment or plastic segment. Since each segment can take the form of an elastic segment, a plastic hinged segment or a real hinged segment, it is necessary to deevelop nine station transfer matrices to cover all combinations of segment variations as shown in Figure (2-1).

2.2 DEVELOPMENT OF TRANSFER MATRICES

In this section the field transfer matrices for an elastic segment, a plastic hinged segment and a real hinged segment respectively. are presented. In addition, nine station transfer matrices are developed to cover all combinations of segment variations.

2.2.1 Field Transfer Matrices

Listed below are the three field transfer matrices with their derivations.

2.2.2.1 Field Transfer Matrix for Elastic Segment

By definition, this is the segment in which the connecting beams are in the elastic state (Fig. 2.1a(1)). It has been considered by Tso and Chan [31], and is given in the following form:

$$[F]_i = [\psi]_i \, [\lambda]_i^{-1} \tag{2.1}$$

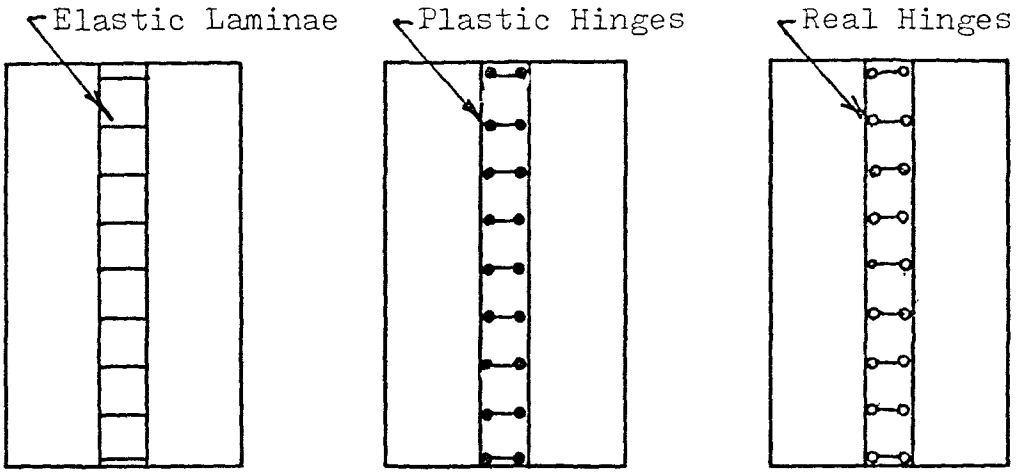

1. Elastic Segment 2. Plastic Segment 3. Real Hinged Segment

FIGURE 2-1(a) SEGMENT STATES

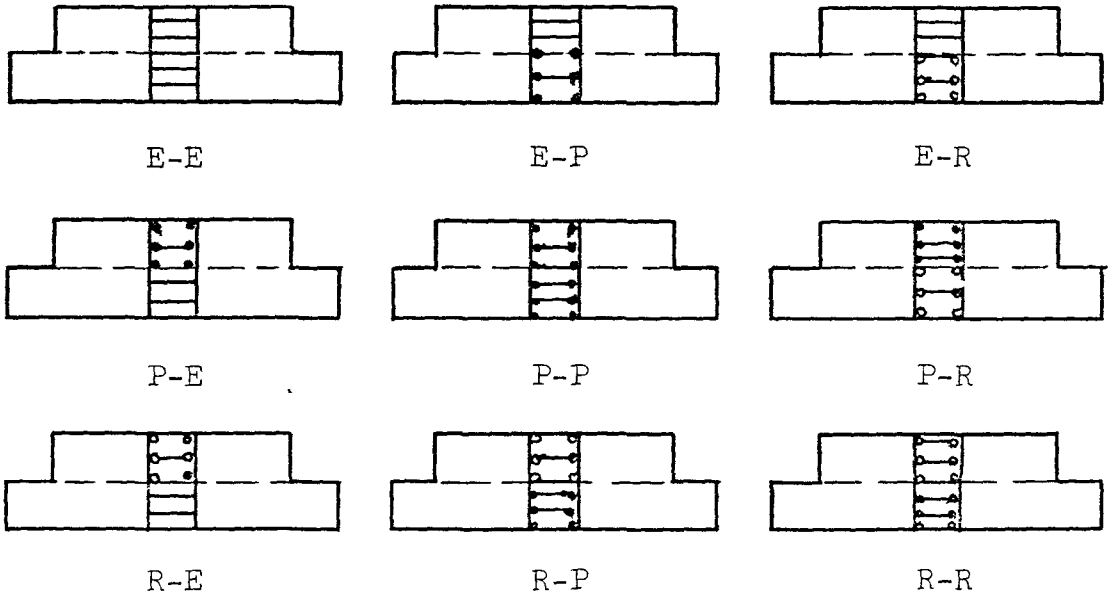

FIGURE 2-1(b) STATION COMBINATIONS

where $[F]_i$ is the field transfer matrix for the ith segment.

$$[\psi]_i = \begin{bmatrix} 1 & 0 & 1 & 0 & 0 & 0 \\ 0 & 1 & 0 & \alpha & 0 & 0 \\ 0 & 0 & \alpha^2 & 0 & \gamma^2/\alpha^2 & \gamma^2 H/\alpha^2 \\ 0 & 0 & 0 & \alpha^3 & 0 & -\gamma^2/\alpha^2 \\ 0 & 0 & 0 & 0 & 1 & H \\ 0 & 0 & 0 & 0 & 0 & 1 \end{bmatrix}_i ; \qquad (2.2)$$

and

$$[\lambda]_i^{-1} = \begin{bmatrix} 1 & -H & \frac{-1}{\alpha^2} & \frac{H}{\alpha^2} & \frac{\gamma^2}{\alpha^2}\left(\frac{H^2}{2} + \frac{1}{\alpha^2}\right) & \frac{\gamma^2}{\alpha^2} H\left(\frac{H^2}{6} + \frac{1}{\alpha^2}\right) \\ 0 & 1 & 0 & \frac{-1}{\alpha^2} & \frac{-\gamma^2 H}{\alpha^2} & \frac{-\gamma^2}{\alpha^2}\left(\frac{H^2}{2} + \frac{1}{\alpha^2}\right) \\ 0 & 0 & \frac{Ch\alpha H}{\alpha^2} & \frac{-Sh\alpha H}{\alpha^3} & \frac{-\gamma^2 Ch\alpha H}{\alpha^4} & \frac{-\gamma^2 Sh\alpha H}{\alpha^5} \\ 0 & 0 & \frac{-Sh\alpha H}{\alpha^2} & \frac{Ch\alpha H}{\alpha^3} & \frac{\gamma^2 Sh\alpha H}{\alpha^4} & \frac{\gamma^2 Ch\alpha H}{\alpha^5} \\ 0 & 0 & 0 & 0 & 1 & 0 \\ 0 & 0 & 0 & 0 & 0 & 1 \end{bmatrix}_i ; \qquad (2.3)$$

Where, the parameters of the ith segment are

$$Sh\alpha H = \sinh(\alpha H) \quad Ch\alpha H = \cosh(\alpha H)$$

and $$\alpha^2 = \frac{a\mu^2}{EI}\left(1 + \frac{I}{Aa^2}\right)$$

$$\gamma^2 = \frac{\mu^2}{E^2 AIa}$$

$$\mu^2 = \frac{12EI_b a}{hC^3\beta^2}$$

$$\beta^2 = 1 + \frac{12EI_b}{GA_b^* C^2}$$

$$\frac{1}{A} = \frac{1}{A_1} + \frac{1}{A_2}$$

$$I = I_1 + I_2$$

But this field transfer matrix is formulated to relate the state vector which are in terms of y, y', y", y"', M^e, V, i.e.

$$\{\phi\}_{(i-1)} = [\bar{F}]_i \{\phi\}_{iB} \tag{2.4}$$

where $\{\phi\}_{(i-1)A} = \{y\ y'\ y"\ y"'\ M^e\ V\}^{-1}_{(i-1)A}$

and $\{\phi\}_{iB} = \{y\ y'\ y"\ y"'\ M^e\ V\}^{-1}_{iB}$

M^e and V are functions of y" and y"' given by

$$M^e = EIy" + Ta \tag{2.5}$$

$$V = -EIy"' + qa \tag{2.6}$$

For coupled shear walls, it is considered more convenient to use the state vector {y, y' y" y"' T q}.

Reformulating this to relate the states which are in terms of y, y', y', y", y"', T, q.

multiplying $[\psi]_i$ and $[\lambda]_i^{-1}$ and as the field transfer matrix $[F]_i$ for an elastic segment is given in equation (2.7)

$$
\begin{Bmatrix} y \\ y' \\ y'' \\ y''' \\ T \\ q \end{Bmatrix}_{(i-1)} = \begin{bmatrix}
1 & -H & \frac{C-1}{\alpha^2}+\frac{K\gamma^2}{\alpha^4}\left(\frac{\eta^2}{2}+1-C\right) & \frac{\eta-s}{\alpha^3}-\frac{K\gamma^2}{\alpha^5}\left(\frac{\eta^3}{6}+\eta-S\right) & \frac{a\gamma^2}{\alpha^4}\left(\frac{\eta^2}{2}+1-C\right) & \frac{a\gamma^2}{\alpha^5}\left(\frac{\eta^3}{6}+\eta-S\right) \\
0 & 0 & \frac{-S}{\alpha}+\frac{K\gamma^2}{\alpha^3}(S-\eta) & \frac{C-1}{\alpha^2}-\frac{K\gamma^2}{\alpha^4}\left(C-\frac{\eta^2}{2}-1\right) & \frac{a\gamma^2}{\alpha^3}(S-\eta) & \frac{a\gamma^2}{\alpha^4}\left(C-\frac{\eta^2}{2}-1\right) \\
0 & 0 & C+\frac{K\gamma^2}{\alpha^2}(1-C) & \frac{\gamma^2}{\alpha^2}(1-C)-\frac{K\gamma^2}{\alpha^3}(\eta-S) & \frac{a\gamma^2}{\alpha^2}(1-C) & \frac{\gamma^2}{\alpha^3}(\eta-S) \\
0 & 0 & -\alpha S+\frac{K\gamma^2}{\alpha}S & C-\frac{K\gamma^2}{\alpha^2}(C-1) & \frac{a\gamma^2}{\alpha}S & \frac{\gamma^2}{\alpha^2}(C-1) \\
0 & 0 & \frac{K}{a}\left[1-C-\frac{K\gamma^2}{\alpha^2}(1-C)\right. & \frac{-K}{a}\left[H-\frac{S}{\alpha}-\frac{K\gamma^2}{\alpha^3}(\eta-S)\right] & 1-\frac{K\gamma^2}{\alpha^2}(1-C) & H-\frac{K\gamma^2}{\alpha^3}(\eta-S) \\
0 & 0 & \frac{K}{a}\left[-\alpha S+\frac{K\gamma^2}{\alpha}S\right] & \frac{K}{a}\left[C-\frac{K\gamma^2}{\alpha^2}(C-1)-1\right] & \frac{K\gamma^2}{\alpha}S & 1+\frac{K\gamma^2}{\alpha^2}(C-1)
\end{bmatrix} \begin{Bmatrix} y \\ y' \\ y'' \\ y''' \\ T \\ q \end{Bmatrix}_{iB}
$$

$$C = \cosh(\alpha H) \qquad (2.7)$$

$$S = \sinh(\alpha H)$$

$$K = EI$$

$$\eta = \alpha H$$

2.2.1.2 Field Transfer Matrix for Plastic Hinged Segment

A plastic hinged segment has all its connecting beams with plastic hinges formed at both ends. Consider the segment as shown in Fig. (2.2) subjected to uniform shearing force per unit height "q_p" in the connecting beams.

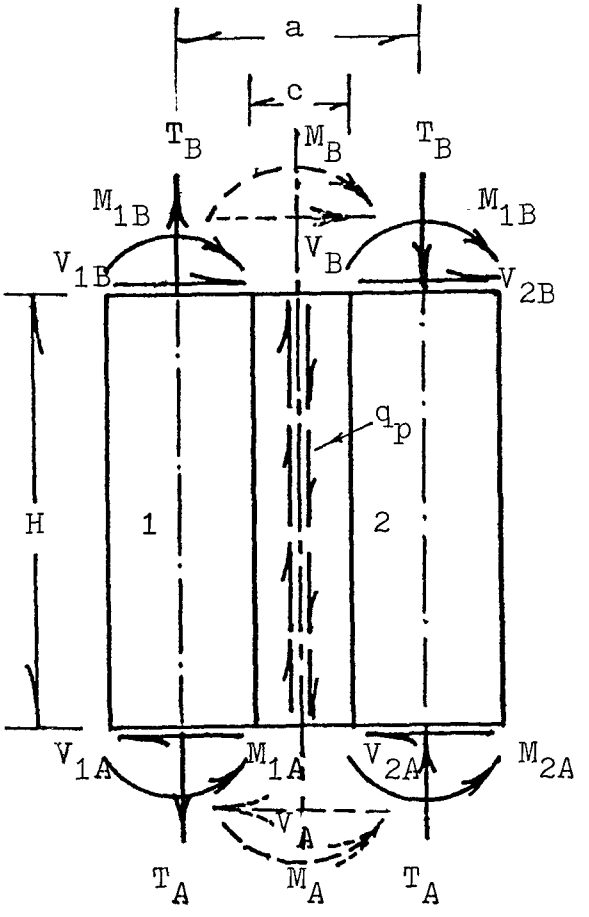

FIGURE 2-2 FORCES ACTING ON ith PLASTIC SEGMENT

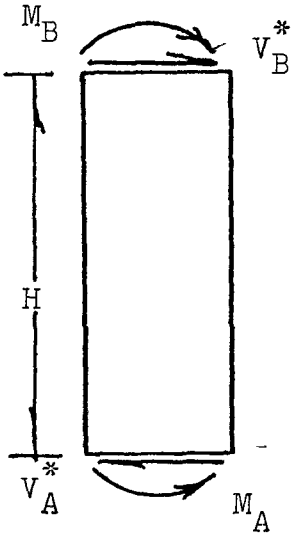

FIGURE 2-3 EQUIVALENT BEAM

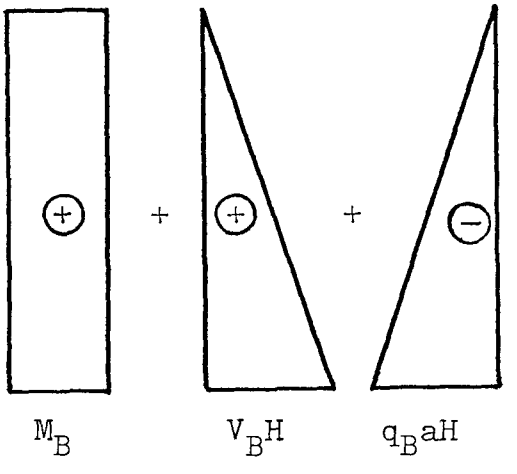

FIGURE 2-4 BENDING MOMENT DIAGRAMS FOR EQUIVALENT BEAM

where $$q_p = 2Mu/ch \quad (2.8)$$

Mu: ultimate moment of the connecting beams considered as double reinfored concrete cross-section

c: clear span of connecting beams

h: storey height in the ith segment

Here since q_p is known, this problem is essentially like a beam segment with modified "shear force" and "moment".

Equation of Axial forces gives

$$\frac{dT}{dx} = -q_p .$$

And as wall moment 'M' is given by

$$M = M^e - Ta$$

where M^e: overturning moment

$$\frac{dM}{dx} = \frac{dM^e}{dx} - \frac{dT}{dx} a$$

$$V^* = V - q_p a$$

where: V^*: wall shear

V : interstorey shear

To obtain the field transfer matrix for plastic hinged segment, it is necessary to obtain the relationship between y, y', y", y"', T and q at the top and bottom of the plastic hinged segment. The deflection, slope and curvature relationship can be obtained by considering a plastic hinged segment under the wall moment "M" and interstorey shear "V" to be the same as the beam with moment of inertia $I = I_1 + I_2$ under the action of beam moment "M" and beam shear "V^*" Fig. (2.3).

Consider a beam of length H under action of wall moment "M_B" and wall shear "V_B^*" at the top of the beam as shown in Fig. (2.3). The deflection and slope at the top relative to the beam are given by, (see Fig. (2.5))

$$y_A = y_B - H\,(y_B' - \theta_B) - y^* \tag{2.9}$$

$$y_A' = y_B' - \theta_B \tag{2.10}$$

To obtain a relationship between y_A, y_A' and y_B, y_B' respectively, from the bending-moment-diagram shown in Fig. (2.4) we get [Note: here the effect of change in axial force i.e. of the shear intensity is considered in the third bending-moment-diagram due to q_{pi} hence satisfying the equilibrium]

$$y^* = \frac{M_B H^2}{2EI} + \frac{V_B H^3}{3EI} - \frac{q_B a H^3}{3EI} \tag{2.11}$$

$$\theta_B = \frac{M_B H}{EI} + \frac{V_B H^2}{2EI} - \frac{q_B a H^2}{2EI} \tag{2.12}$$

Substituting these equations in (2.9) and (2.10) and as,

$$M_B = E\,I\,y_B'' \tag{2.13}$$

$$V_B = -E\,I\,y_B''' + a\,q_B \tag{2.14}$$

we get

$$y_A = y_B - H\,y_B' + (H^2/2)y_B'' - (H^3/6)y_B''' \tag{2.15}$$

$$y_A' = y_B' + H\,y_B'' + (H^2/2)y_B''' \tag{2.16}$$

from the moment equilibrium

$$M_A = M_B + V_B\,H - q_B\,a\,H$$

$$\therefore\ y_A'' = y_B'' - H\,y_B''' \tag{2.17}$$

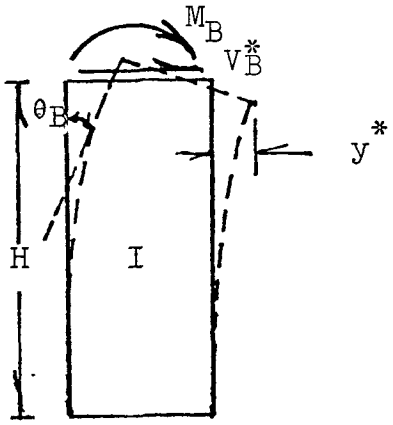

FIGURE 2-5 EQUIVALENT BEAM WITH RELATIVE DISPLACEMENT

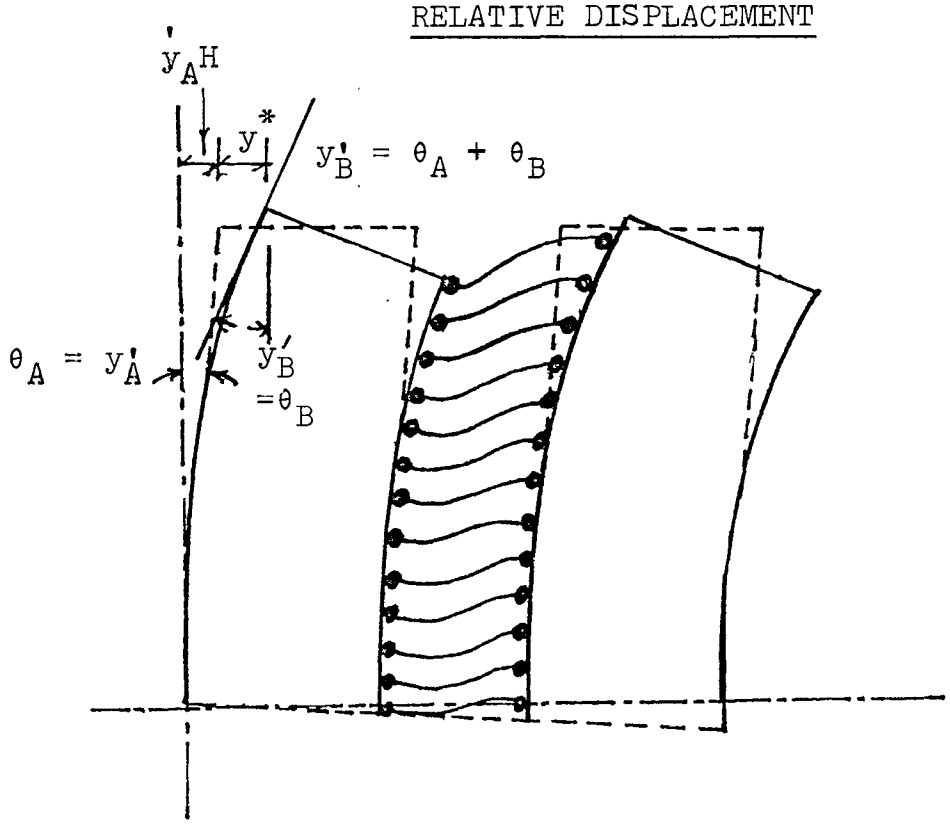

FIGURE 2-6 DEFLECTION PATTERN OF ith SEGMENT

from shear equilibrium

$$V^*_A = V^*_B$$

$$\therefore \quad y'''_A = y'''_B \tag{2.18}$$

from vertical force equilibrium

$$T_A = T_B + q_p H$$

$$T_A = T_B + H\, q_B \tag{2.19}$$

and as

$$q_A = q_B \; (= q_p) \tag{2.20}$$

Hence the field transfer matrix $[F]_i$ for a plastic hinged segment is given by equation (2.21)

$$\begin{Bmatrix} y \\ y' \\ y'' \\ y''' \\ T \\ q=q_p \end{Bmatrix}_{(i-1)_A} = \begin{bmatrix} 1 & -H & H^2/2 & -H^3/6 & 0 & 0 \\ 0 & 1 & -H & H^2/2 & 0 & 0 \\ 0 & 0 & 1 & -H & 0 & 0 \\ 0 & 0 & 0 & 1 & 0 & 0 \\ 0 & 0 & 0 & 0 & 1 & H \\ 0 & 0 & 0 & 0 & 0 & 1 \end{bmatrix} \begin{Bmatrix} y \\ y' \\ y'' \\ y''' \\ T \\ q=q_p \end{Bmatrix}_{i_B} \tag{2.21}$$

2.2.1.3 Field Transfer Matrix for a Real Hinged Segment

The field transfer matrix for a real hinged segment can be obtained from a plastic hinged segment assuming the connecting beams have lost their moment transmission capacities, i.e. when $q_A = q_B = 0$.

Therefore, by substituting the above value in place of q_B in equation (2.19)

$$T_A = T_B \tag{2.22}$$

and setting

$$q_A = q_B = 0 \tag{2.23}$$

The field transfer matrix $[F]_i$ for the real hinged segment becomes

$$\begin{Bmatrix} y \\ y' \\ y'' \\ y''' \\ T \\ q=0 \end{Bmatrix}_{(i-1)_A} = \begin{bmatrix} 1 & -H & H^2/2 & -H^3/6 & 0 & 0 \\ 0 & 1 & -H & H^2/2 & 0 & 0 \\ 0 & 0 & 1 & -H_i & 0 & 0 \\ 0 & 0 & 0 & 1 & 0 & 0 \\ 0 & 0 & 0 & 0 & 1 & 0 \\ 0 & 0 & 0 & 0 & 0 & 1 \end{bmatrix} \begin{Bmatrix} y \\ y' \\ y'' \\ y''' \\ T \\ q=0 \end{Bmatrix}_{i_B} \tag{2.24}$$

2.2.2 Station Transfer Matrices

Listed below are nine station transfer matrices, necessary to complete the solution of the problem.

2.2.2.1 Station Transfer Matrix Relating a State Vector in an Elastic Segment to a State Vector in an Elastic Segment [Elastic--Elastic S.T.M.]

The station transfer matrix for Elastic-Elastic Station as shown in Fig. (2.7a) has been formulated by Tso and Chan [31] in the following form

$$\{\phi\}_{iB} = [S]_i \{\phi\}_{iA} + \{L\}_i \tag{2.25}$$

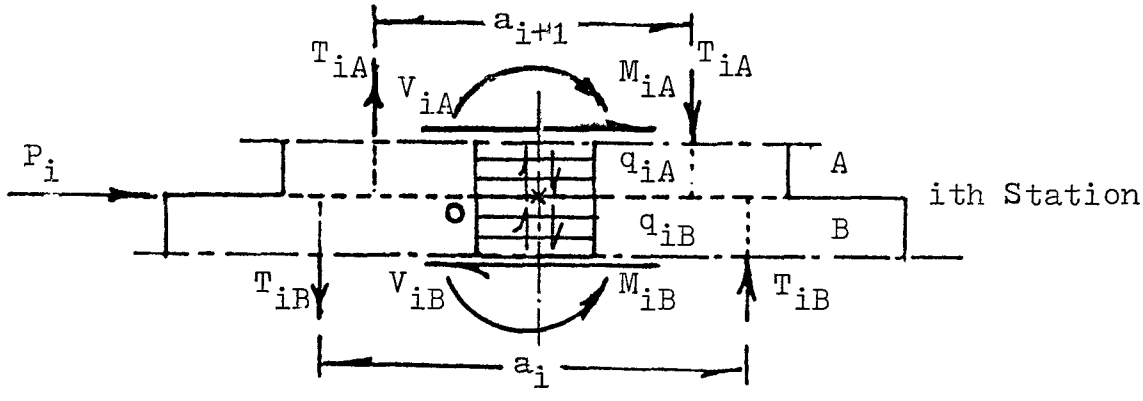

FIGURE 2.7(a) ELASTIC-ELASTIC STATION

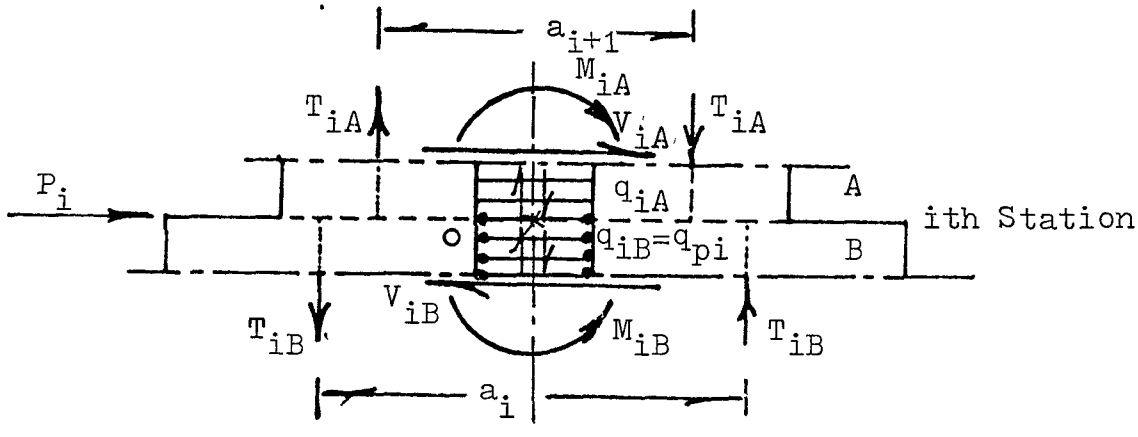

FIGURE 2.7(b) ELASTIC-PLASTIC STATION

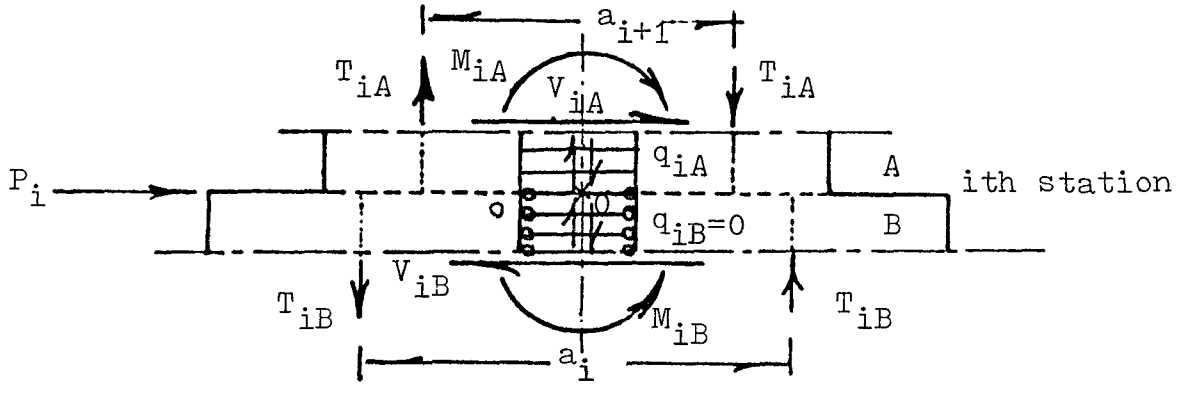

FIGURE 2.7(c) ELASTIC-REAL STATION

FIGURE 2.7 FORCE COMPONENTS ACTING ON ith STATION

where

$[S]_i$ = station transfer matrix for ith Station

$$= \begin{bmatrix} 1 & 0 & 0 & 0 & 0 & 0 \\ 0 & 1 & 0 & 0 & 0 & 0 \\ 0 & 0 & \frac{I_A a_B}{I_B a_A} & 0 & \frac{a_A - a_B}{EI_B a_A} & 0 \\ 0 & 0 & 0 & \frac{I_A \mu_B^2}{I_B \mu_A^2} & 0 & \frac{\mu_B^2 - \mu_A^2}{EI_B \mu_A^2} \\ 0 & 0 & 0 & 0 & 1 & 0 \\ 0 & 0 & 0 & 0 & 0 & 1 \end{bmatrix}$$

$\{L\}_i$ = load vector for ith station.

= Column $\{0 \quad 0 \quad 0 \quad -P/EI \quad 0 \quad P\}_i$

$\{\phi\}_{iB}$ = state vector giving the state i.e.

y, y', y", y"', M^e and V, at base of ith station

$\{\phi\}_{iA}$ = state vector giving above states at top of ith station

and $\mu_i^2 = \left(\frac{12EI_b a}{hC^3\beta^2} \right)_i$; $\beta_i^2 = 1 + \left(\frac{12EI_b}{GA_b^* C^2} \right)_i$

Reformulating this to relate the states y, y', y", y"', T and q from equations (2.5) and (2.6), the station transfer matrix for Elastic-Elastic station becomes

$$\begin{Bmatrix} y \\ y' \\ y'' \\ y''' \\ T \\ q \end{Bmatrix}_{iB} = \begin{bmatrix} 1 & 0 & 0 & 0 & 0 & 0 \\ 0 & 1 & 0 & 0 & 0 & 0 \\ 0 & 0 & \frac{I_A}{I_B} & 0 & \frac{a_A - a_B}{EI_B} & 0 \\ 0 & 0 & 0 & \frac{I_A}{I_B} & 0 & \frac{-a_A}{EI_B}\left(\frac{\mu_A^2 - \mu_B^2}{\mu_A^2}\right) \\ 0 & 0 & 0 & 0 & 1 & 0 \\ 0 & 0 & 0 & 0 & 0 & \frac{a_A \mu_B^2}{a_B \mu_A^2} \end{bmatrix} \begin{Bmatrix} y \\ y' \\ y'' \\ y''' \\ T \\ q \end{Bmatrix}_{iA} + \begin{Bmatrix} 0 \\ 0 \\ 0 \\ -\frac{P}{EI_B} \\ 0 \\ 0 \end{Bmatrix}_{i} \tag{2.26}$$

2.2.2.2 Station Transfer Matrix Relating a State Vector in an Elastic Segment to a State Vector in a Plastic Segment [Plastic-Elastic S.T.M.]

From the continuity of the wall, as lateral deflection, slope and axial force above and below the stations are to be same,

$$y_B = y_A \tag{2.27}$$

$$y'_B = y'_A \tag{2.28}$$

$$T_B = T_A \tag{2.29}$$

Equilibrium of moments about the central point "0" [Ref. Fig. 2.7.d] gives

$$M_A + T_A a_A - M_B - T_B a_B = 0$$

substituting from eqn. (2.13) and (2.29), above equation becomes

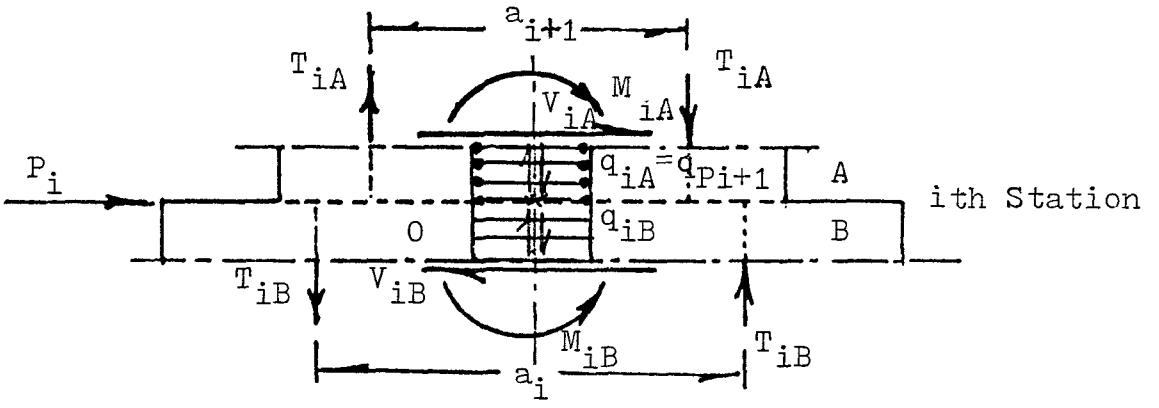

FIGURE 2-7(d) Plastic-Elastic Station

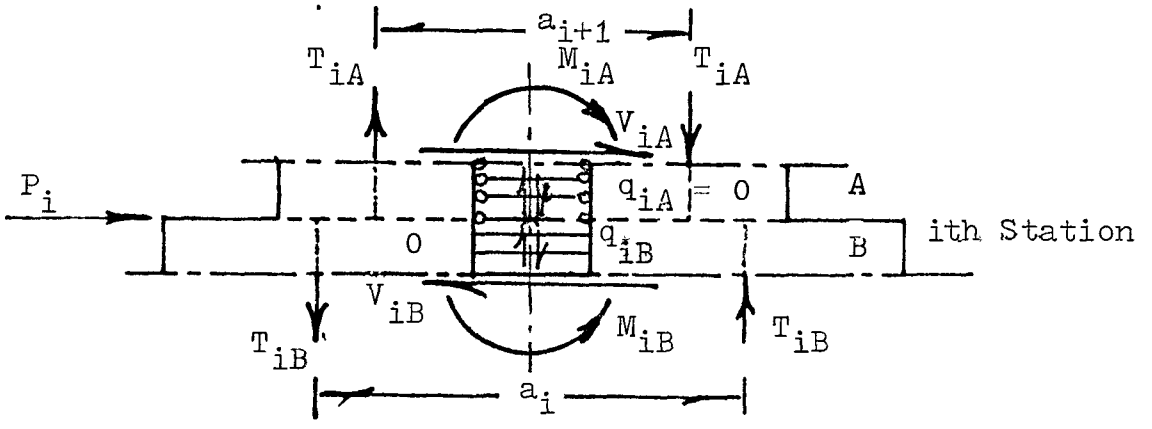

FIGURE 2-7(e) Real - Elastic Station

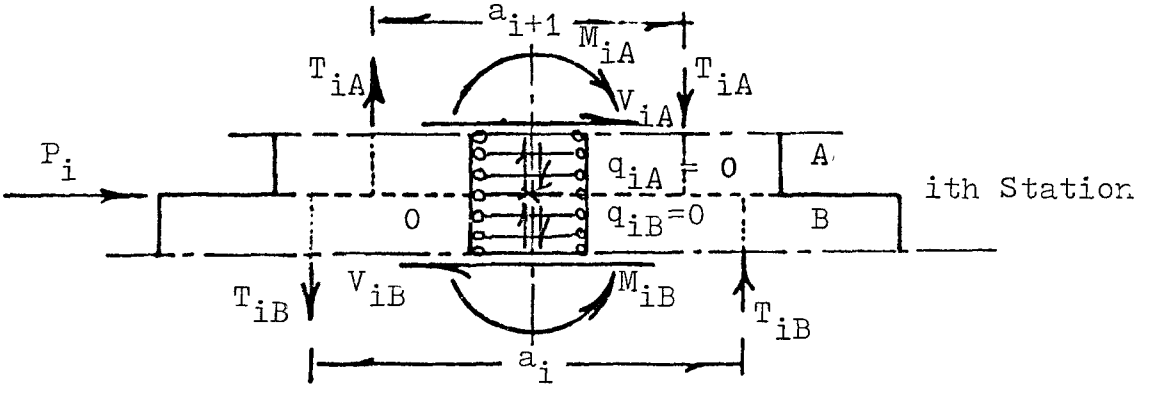

FIGURE 2-7(f) Real - Real Station

FIGURE 2-7 FORCE COMPONENTS ACTING ON ith STATION

$$y''_B = \frac{I_A}{I_B} y''_A + \frac{a_A - a_B}{EI_B} T_A \tag{2.30}$$

Equilibrium of lateral forces gives

$$V_A + P_i = V_B$$

$$-EI_A y'''_A + q_A a_A + P_i = -EI_B y'''_B + q_B a_B \tag{2.31}$$

as from Tso and Chan [31], the shear-intensity at the bottom and top of station "i" are related by

$$q_B = \frac{a_A \mu_B^2}{a_B \mu_A^2} q_A \tag{2.32}$$

But as the segment above the station is in plastic state

$$q_A = q_{PA}$$

$$q_B = \frac{a_A \mu_B^2}{a_B \mu_A^2} q_{PA} \tag{2.33}$$

therefore, from eqn. (2.33) and simplifying eqn. (2.31) becomes

$$y'''_B = \frac{I_A}{I_B} y'''_A - \frac{[P_i + a_A q_{PA}(1 - \frac{\mu_B^2}{\mu_A^2})]}{EI_B} \tag{2.34}$$

Hence the station transfer matrix for a Plastic-Elastic staton becomes

$$\begin{Bmatrix} y \\ y' \\ y'' \\ y''' \\ T \\ q \end{Bmatrix}_{i_B} = \begin{bmatrix} 1 & 0 & 0 & 0 & 0 & 0 \\ 0 & 1 & 0 & 0 & 0 & 0 \\ 0 & 0 & \frac{I_A}{I_B} & 0 & \frac{a_A - a_B}{EI_B} & 0 \\ 0 & 0 & 0 & \frac{I_A}{I_B} & 0 & 0 \\ 0 & 0 & 0 & 0 & 1 & 0 \\ 0 & 0 & 0 & 0 & 0 & 1 \end{bmatrix} \begin{Bmatrix} y \\ y' \\ y'' \\ y''' \\ T \\ q = q_P \end{Bmatrix}_{i_A} + \begin{Bmatrix} 0 \\ 0 \\ 0 \\ \frac{-[P_i + a_A q_{PA}(1 - \frac{\mu_B^2}{\mu_A^2})]}{EI_B} \\ 0 \\ (\frac{a_A \mu_B^2}{a_B \mu_A^2}) q_{PA} \end{Bmatrix} \tag{2.35}$$

2.2.2.3 Station Transfer Matrix Relating a State Vector in Plastic Segment to a State Vector in an Elastic Segment [Elastic-Plastic S.T.M.]

The continuity eqns. (2.27), (2.28), (2.29) holds good. Also the eqm. of moment gives the same relationship between curvature as given in eqn. (2.30).

Equilibrium of lateral forces gives

$$V_A + P_i = V_B$$

or $$-EI_A\, y'''_A + q_A a_A + P_i = -EI_B\, y'''_B + q_B a_B$$

from eqn. (2.32), after simplification,

$$y_B''' = \frac{I_A}{I_B} y_{iA}''' - \frac{a_A}{EI_B} q_A - \frac{(P_i - q_{PB} a_B)}{EI_B} \tag{2.36}$$

As the segment below the station is already in the plastic state (Fig. 2.7.b)

$$q_B = q_{PB} \tag{2.37}$$

Hence the station transfer matrix for Elastic-Plastic station becomes

$$\begin{Bmatrix} y \\ y' \\ y'' \\ y''' \\ T \\ q=q_P \end{Bmatrix}_{iB} = \begin{bmatrix} 1 & 0 & 0 & 0 & 0 & 0 \\ 0 & 1 & 0 & 0 & 0 & 0 \\ 0 & 0 & \frac{I_A}{I_B} & 0 & \frac{a_A - a_B}{EI_B} & 0 \\ 0 & 0 & 0 & \frac{I_A}{I_B} & 0 & -\frac{a_A}{EI_B} \\ 0 & 0 & 0 & 0 & 1 & 0 \\ 0 & 0 & 0 & 0 & 0 & \frac{a_A \mu_B^2}{a_B \mu_A^2} \end{bmatrix} \begin{Bmatrix} y \\ y' \\ y'' \\ y''' \\ T \\ q \end{Bmatrix}_{iA} + \begin{Bmatrix} 0 \\ 0 \\ 0 \\ \frac{-(P_i - q_{PB} a_B)}{EI_B} \\ 0 \\ 0 \end{Bmatrix} \tag{2.38}$$

2.2.2.4 Station Transfer Matrix Relating a State Vector in a Plastic Segment to a State Vector in a Plastic Segment [Plastic-Plastic S.T.M.]

Eqns. (2.27), (2.28), (2.29), (2.30) remain valid for this station also.

Equilibrium of lateral forces gives

$$V_B = V_A + P_i$$

or $$-EIy_B''' + q_B a_B = -EI_A y_A''' + q_A a_A + P_i \tag{2.39}$$

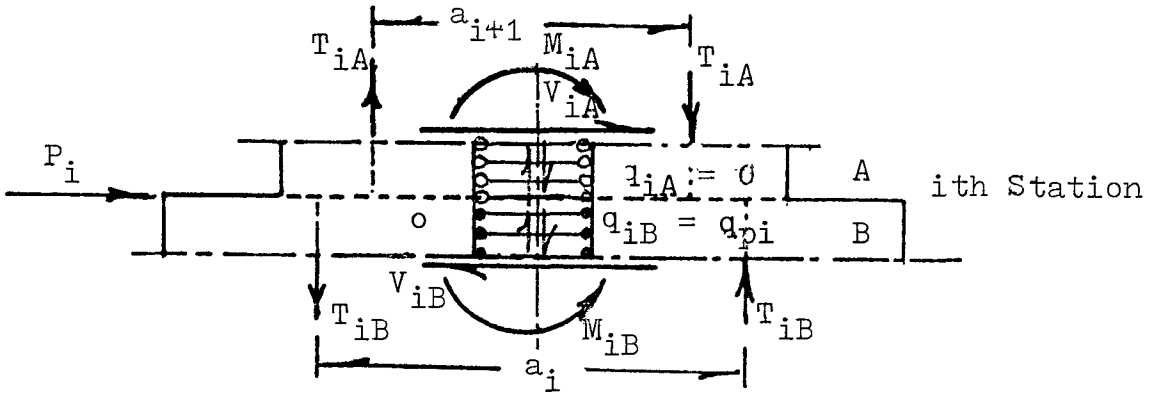

FIGURE 2-7(g) Real - Plastic Station

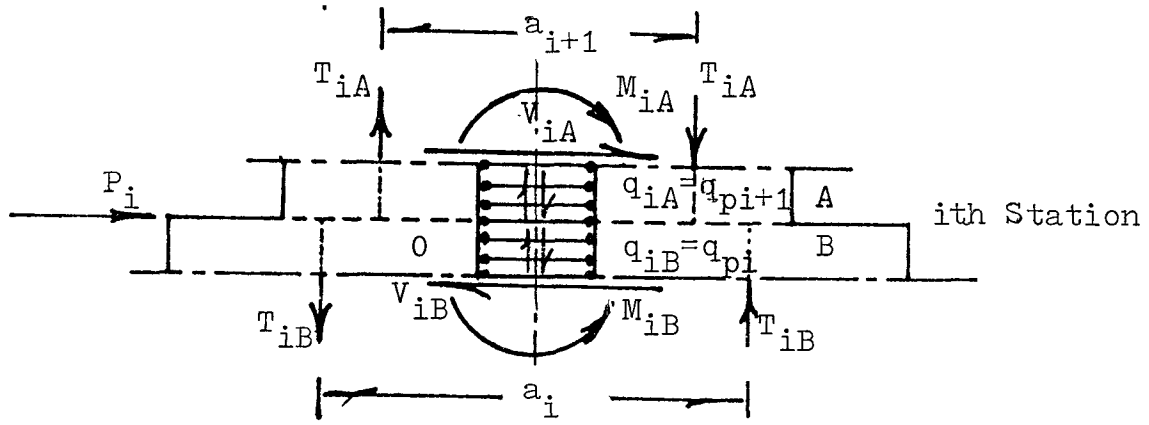

FIGURE 2-7(h) Plastic-Plastic Station

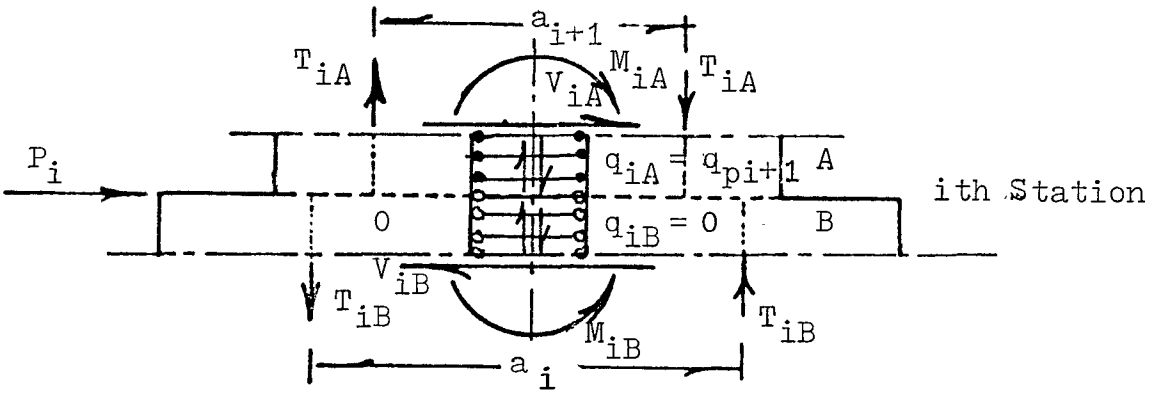

FIGURE 2-7(i) Plastic-Real Station

FIGURE 2-7 FORCE COMPONENTS ACTING ON ith STATION

As both the segments above and below the ith station are in plastic station [Fig. 2.7(h)]

$$q_B = q_{PB}$$
$$q_A = q_{PA} \tag{2.40}$$

therefore, after simplification eqn. (2.39) becomes

$$y_B''' = \frac{I_A}{I_B} y_A''' - \frac{(P_i - q_{PB}a_B + q_{PA}a_A)}{EI_B} \tag{2.41}$$

Hence the station transfer matrix for Plastic-Plastic station becomes

$$\begin{Bmatrix} y \\ y' \\ y'' \\ y''' \\ T \\ q=q_P \end{Bmatrix}_{iB} = \begin{bmatrix} 1 & 0 & 0 & 0 & 0 & 0 \\ 0 & 1 & 0 & 0 & 0 & 0 \\ 0 & 0 & \frac{I_A}{I_B} & 0 & \frac{a_A - a_B}{EI_B} & 0 \\ 0 & 0 & 0 & \frac{I_A}{I_B} & 0 & 0 \\ 0 & 0 & 0 & 0 & 1 & 0 \\ 0 & 0 & 0 & 0 & 0 & 0 \end{bmatrix} \begin{Bmatrix} y \\ y' \\ y'' \\ y''' \\ T \\ q=q_P \end{Bmatrix}_{iA} + \begin{bmatrix} 0 \\ 0 \\ 0 \\ \frac{-(P_i - q_{PB}a_B + q_{PA}a_A)}{EI_B} \\ 0 \\ q_{PB} \end{bmatrix} \tag{2.42}$$

2.2.2.5 Station Transfer Matrix Relating a State Vector in an Elastic Segment to a State Vector in a Real Hinged Segment [Real Hinged-Elastic S.T.M.]

This is a special case of the plastic-elastic station. If we substitute zero for q_{PA} in the load vector in equation (2.35) the load vector for the real hinged-elastic station will be obtained. The

station transfer matrix $[S]_i$; will be the same as it is independent of the lateral force in the connecting beams of the segment above ith station.

$$\begin{Bmatrix} y \\ y' \\ y'' \\ y''' \\ T \\ q \end{Bmatrix}_{iB} = \begin{bmatrix} 1 & 0 & 0 & 0 & 0 & 0 \\ 0 & 1 & 0 & 0 & 0 & 0 \\ 0 & 0 & \frac{I_A}{I_B} & 0 & \frac{a_A - a_B}{EI_B} & 0 \\ 0 & 0 & 0 & \frac{I_A}{I_B} & 0 & 0 \\ 0 & 0 & 0 & 0 & 1 & 0 \\ 0 & 0 & 0 & 0 & 0 & \left(\frac{a_A \mu_B^2}{a_B \mu_A^2}\right) \end{bmatrix} \begin{Bmatrix} y \\ y' \\ y'' \\ y''' \\ T \\ q=0 \end{Bmatrix}_{iA} + \begin{Bmatrix} 0 \\ 0 \\ 0 \\ \frac{-P_i}{EI_B} \\ 0 \\ 0 \end{Bmatrix} \tag{2.43}$$

2.2.2.6 Station Transfer Matrix Relating a State Vector in a Plastic Segment to a State Vector in a Real Hinged Segment [Real Hinged-Plastic S.T.M.]

By substituting in equation (2.41) for q_{PA} by zero we get

$$y_B''' = \frac{I_A}{I_B} y_A''' - \frac{(P_i - q_{PB} a_B)}{EI_B} \tag{2.44}$$

Equations (2.27), (2.28), (2.29), (2.30) and (2.40) are valid. Hence, the station transfer matrix becomes

$$\begin{Bmatrix} y \\ y' \\ y'' \\ y''' \\ T \\ q=0 \end{Bmatrix}_{iB} = \begin{bmatrix} 1 & 0 & 0 & 0 & 0 & 0 \\ 0 & 1 & 0 & 0 & 0 & 0 \\ 0 & 0 & \frac{I_A}{I_B} & 0 & \frac{a_A-a_B}{EI_B} & 0 \\ 0 & 0 & 0 & \frac{I_A}{I_B} & 0 & 0 \\ 0 & 0 & 0 & 0 & 1 & 0 \\ 0 & 0 & 0 & 0 & 0 & 0 \end{bmatrix} \begin{Bmatrix} y \\ y' \\ y'' \\ y''' \\ T \\ q=q_A \end{Bmatrix}_{iA} + \begin{Bmatrix} 0 \\ 0 \\ 0 \\ \frac{-(P_i-q_{PB}a_B)}{EI_B} \\ 0 \\ q_{PB} \end{Bmatrix} \tag{2.45}$$

2.2.2.7 Station Transfer Matrix Relating a State Vector in a Real Hinged Segment to a State Vector in an Elastic Segment [Elastic-Real Hinged S.T.M.]

Equations (2.27), (2.28), (2.29) are valid in this case. The change will be in the terms relating the lateral force in the connecting beams below the station.

The equation (2.36) of eqn. of lateral force gives

$$y_B''' = \frac{I_A}{I_B} y_A''' - \frac{a_A}{EI_B} q_A - \frac{P_i}{EI_B} \tag{2.46}$$

Hence the station transfer matrix becomes

$$\begin{Bmatrix} y \\ y' \\ y'' \\ y''' \\ T \\ q=0 \end{Bmatrix}_{iB} = \begin{bmatrix} 1 & 0 & 0 & 0 & 0 & 0 \\ 0 & 1 & 0 & 0 & 0 & 0 \\ 0 & 0 & \frac{I_A}{I_B} & 0 & \frac{a_A - a_B}{EI_B} & 0 \\ 0 & 0 & 0 & \frac{I_A}{I_B} & 0 & \frac{-a_A}{EI_B} \\ 0 & 0 & 0 & 0 & 1 & 0 \\ 0 & 0 & 0 & 0 & 0 & \frac{a_A \mu_B^2}{a_B \mu_A^2} \end{bmatrix} \begin{Bmatrix} y \\ y' \\ y'' \\ y''' \\ T \\ q \end{Bmatrix}_{iA} + \begin{Bmatrix} 0 \\ 0 \\ 0 \\ \frac{-P_i}{EI_B} \\ 0 \\ 0 \end{Bmatrix} \tag{2.47}$$

2.2.2.8 Station Transfer Matrix Relating a State Vector in a Real Hinged Segment to a State Vector in a Plastic Hinged Segment [Plastic-Real Hinged S.T.M.]

Besides eqns. (2.27), (2.28), (2.29), the following equations are obtained from eqn. (2.39)

$$y_B''' = \frac{I_A}{I_B} y_A''' - \frac{(P_i - q_{PA} a_A)}{EI_B} \tag{2.48}$$

as

$$q_B = 0 \tag{2.49}$$

Therefore station transfer matrix becomes

$$\begin{Bmatrix} y \\ y' \\ y'' \\ y''' \\ T \\ q=0 \end{Bmatrix}_{iB} = \begin{bmatrix} 1 & 0 & 0 & 0 & 0 & 0 \\ 0 & 1 & 0 & 0 & 0 & 0 \\ 0 & 0 & \frac{I_A}{I_B} & 0 & \frac{a_A - a_B}{EI_B} & 0 \\ 0 & 0 & 0 & \frac{I_A}{I_B} & 0 & 0 \\ 0 & 0 & 0 & 0 & 1 & 0 \\ 0 & 0 & 0 & 0 & 0 & \frac{a_A \mu_B^2}{a_B \mu_A^2} \end{bmatrix} \begin{Bmatrix} y \\ y' \\ y'' \\ y''' \\ T \\ q=q_P \end{Bmatrix}_{iA} + \begin{Bmatrix} 0 \\ 0 \\ 0 \\ \frac{-(P_i + q_{PA} a_A)}{EI_B} \\ 0 \\ 0 \end{Bmatrix} \quad (2.50)$$

2.2.2.9 Station Transfer Matrix Relating a State Vector in a Real Hinged Segment to a State Vector in a Real Hinged Segment [Real Hinged-Real Hinged S.T.M.]

Eqns. (2.27), (2.28), (2.29), (2.30) remain valid for this station also. By setting q_{PB} and q_{PA} equal to zero we get eqns. (2.39) and (2.40) as

$$y_B''' = \frac{I_A}{I_B} y_A''' - \frac{P_i}{EI} \quad (2.51)$$

$$q_{PB} = q_{PA} = 0 \quad (2.52)$$

Hence the station transfer matrix for this station becomes

$$\begin{Bmatrix} y \\ y' \\ y'' \\ y''' \\ T \\ q=0 \end{Bmatrix}_{iB} = \begin{bmatrix} 1 & 0 & 0 & 0 & 0 & 0 \\ 0 & 1 & 0 & 0 & 0 & 0 \\ 0 & 0 & \frac{I_A}{I_B} & 0 & \frac{(a_A-a_B)}{EI_B} & 0 \\ 0 & 0 & 0 & \frac{I_A}{I_B} & 0 & 0 \\ 0 & 0 & 0 & 0 & 1 & 0 \\ 0 & 0 & 0 & 0 & 0 & \frac{a_A \mu_B^2}{a_B \mu_A^2} \end{bmatrix} \begin{Bmatrix} y \\ y' \\ y'' \\ y''' \\ T \\ q=0 \end{Bmatrix}_{iA} + \begin{Bmatrix} 0 \\ 0 \\ 0 \\ \frac{-P_i}{EI_B} \\ 0 \\ 0 \end{Bmatrix} \tag{2.53}$$

2.3 FORMULATION OF MIXED BOUNDARY VALUE PROBLEM

The transfer matrix technique gives a relation between the state vector at the base and the state vector at the top as,

$$\{\phi\}_o = [\bar{F}]\ \{\phi\}_{nB} + \{\bar{L}\} \tag{2.54}$$

There are six elements in each of the state vectors $\{\phi\}_o$ and $\{\phi\}_{nB}$. Out of these twelve elements, six of them are known by the boundary conditions at the top and bottom of the structure, i.e. for a wall resting on flexible foundation it is shown that

At the base, (Ref. Tso and Chan [31])

$$y_o = 0 \tag{2.55a}$$

$$y_o' = \frac{EI_o}{K_\theta} y_o'' \tag{2.55b}$$

$$\text{as} \quad q_o = \frac{EI_o y_o''' + V_o}{a_1}$$

$$\text{and} \quad q_o = \mu_1^2 \left(\frac{EI_o}{K_\theta} y_o'' - \frac{T_o}{a_1 K_\delta} \right)$$

where K_θ = equivalent rotational stiffness of foundation

K_δ = equivalent vertical displacement stiffness of the foundation

adding these two and simplyfing for y_o'''

$$y_o''' = -\frac{a_1 \mu_1^2}{K_\theta} y_o'' + \frac{\mu_1^2}{K_\delta EI_1} T_o + \frac{2a_1}{EI_1} q_o - \frac{V_o}{EI_1}$$

$$= -F_r y_o'' + F_s T_o + F_a q_o - \frac{V_o}{EI_o} \qquad (2.55c)$$

<u>At the top</u>,

$$y_{nB}'' = 0 \qquad (2.55d)$$

$$T_{nB} = 0 \qquad (2.55e)$$

$$\text{as} \quad q_{nB} = \frac{EI_n y_{nB}''' + V_n}{a_n}$$

$$= \frac{EI_n}{a_n} y_{nB}''' + \frac{P_n}{a_n} \qquad (2.55f)$$

Hence the mixed boundary value problem becomes

$$\begin{Bmatrix} 0 \\ EI_o y_o''/K_\theta \\ y_o'' \\ -F_r y_o'' + F_s T_o + F_a q_o - V_o/EI_o \\ T_o \\ q_o \end{Bmatrix} = \begin{bmatrix} & & \\ & \bar{F} & \\ & & \end{bmatrix} \begin{Bmatrix} y_{nB} \\ y_{nB}' \\ 0 \\ y_{nB}''' \\ 0 \\ \frac{EI_n}{a_n} y_{nB}''' + \frac{P_n}{a_n} \end{Bmatrix} + \begin{Bmatrix} \\ \bar{L} \\ \end{Bmatrix} \tag{2.56}$$

Expanding above six equations and eliminating the three unknowns y_o'', T_o, q_o at the left hand side by Gauss Elimination Method, we get three independent equations in terms of three independent unknowns as

$$\begin{bmatrix} \bar{F}_{11} & \bar{F}_{12} & \bar{F}_{14}+e\bar{F}_{16} \\ \bar{F}_{21}-b\bar{F}_{31} & \bar{F}_{22}-b\bar{F}_{32} & (\bar{F}_{24}-b\bar{F}_{34})+(\bar{F}_{26}-b\bar{F}_{36})e \\ \bar{F}_{41}+F_r\bar{F}_{31}-F_s\bar{F}_{51}-F_a\bar{F}_{61} & \bar{F}_{42}+F_r\bar{F}_{32}-F_s\bar{F}_{52}-F_a\bar{F}_{62} & (\bar{F}_{44}+F_r\bar{F}_{34}-F_s\bar{F}_{54}-F_a\bar{F}_{64})+ \\ & & e(\bar{F}_{46}+F_r\bar{F}_{36}-F_s\bar{F}_{56}-F_a\bar{F}_{66}) \end{bmatrix} \begin{Bmatrix} y_{nB} \\ y_{nB}' \\ y_{nB}''' \end{Bmatrix} = \begin{Bmatrix} -\bar{L}_1-\bar{F}_{16}P_n/a_n \\ -\bar{L}_2+b\bar{L}_3-(\bar{F}_{26}-b\bar{F}_{36})P_n/a_n \\ -(\bar{L}_4+F_r\bar{L}_3-F_s\bar{L}_5-F_a\bar{L}_6) - (\bar{F}_{46}+F_r\bar{F}_{36}-F_5\bar{F}_{56}-F_a\bar{F}_{66})\frac{P_n}{a} - \frac{V_o}{EI_o} \end{Bmatrix} \tag{2.57}$$

where $e = \dfrac{EI_n}{a_n}$ $\qquad F_r = \dfrac{a_1\mu_1^2}{K_\theta}$

$b = \dfrac{EI_o}{K_\theta}$ $\qquad F_s = \dfrac{\mu_1^2}{EI_o K_\delta}$

$F_a = \dfrac{2a_1}{EI_o}$

For fixed base, as $b = F_r = F_s = 0$, and eqn. (2.57) simplifies to

$$\begin{bmatrix} \bar{F}_{11} & \bar{F}_{12} & \bar{F}_{14}+e\bar{F}_{16} \\ \bar{F}_{21} & \bar{F}_{22} & \bar{F}_{24}+e\bar{F}_{26} \\ \bar{F}_{41}-F_a\bar{F}_{61} & \bar{F}_{42}-F_a\bar{F}_{62} & \bar{F}_{44}-F_a\bar{F}_{64}+(\bar{F}_{46}-F_a\bar{F}_{66})e \end{bmatrix} \begin{Bmatrix} y_{nB} \\ y'_{nB} \\ y''_{nB} \end{Bmatrix} = \begin{Bmatrix} -\bar{L}_1-\bar{F}_{16}P_n/a_n \\ -\bar{L}_2-\bar{F}_{26}P_n/a_n \\ -\bar{L}_4+F_a\bar{L}_6-V_o/EIo \\ -(\bar{F}_{46}-F_a\bar{F}_{66})P_n/a_n \end{Bmatrix} \tag{2.58}$$

CHAPTER 3

WALL HINGE FAILURE FORMULATION

3.1 INTRODUCTION

In the previous chapter, the formulation of plastic hinges at both ends of the connecting beams is the only source of inelastic action considered. But in practice, when the wall-moment at the base of each pier reaches its ultimate value, plastic hinges should also be formed at its base. When a severe earthquake shakes a coupled shear wall of practical proportion, plastic hinges start to form at the ends of connecting beams before the hinges are formed at the base of the piers. The final collapse mechanism of a typical coupled shear wall under the action of severe earthquakes is the full plastification of the connecting beams and the formation of hinges at the base of both piers. The order and extent of formation of these hinges and hence, the final nature of collapse mechanism depends on strength of lintel (connecting) beams, strength of both piers, other dimensions of coupled shear wall, and the distribution of gravity loading. This formulation of plastic hinges at the base of the piers is considered in this chapter. The analysis is based on the same transfer matrix technique used, but with different boundary conditions at the base to denote the formation of the plastic hinges.

3.2 INTERACTION CURVE

In a typical coupled shear wall the bending moment and the axial force caused by gravity loads and lateral loads will be acting at the base of each pier as shown in Fig. (3.1). Under the combined action of these forces, the cross-section at the base of each pier will have the stress distribution pattern as shown in Fig. (3.1). This section can take the combined action of these forces until it reaches the ultimate state of stresses [Fig. (3.1)]. The corresponding bending moment at the formation of plastic hinge state is known as the ultimate bending moment (M_u). The locus of these values of axial force and bending moment causing the ultimate state, and hence the plastic hinge, leads to a curve known as the "Interaction Curve". Theoretically, the Interaction Curve is a smooth curve, but in the present work it is approximated by the set of two straight lines as shown in Fig. (3.2).

3.3 BOUNDARY VALUE PROBLEM FORMULATION

When the hinges are formed at the base of the piers, the boundary conditions of the problem become as follows.

At the base

$$y_o = 0 \tag{3.1a}$$

$$y_o' = \frac{EI_o}{K_\theta} y_o'' + \beta = b \quad \beta_o + \beta \tag{3.1b}$$

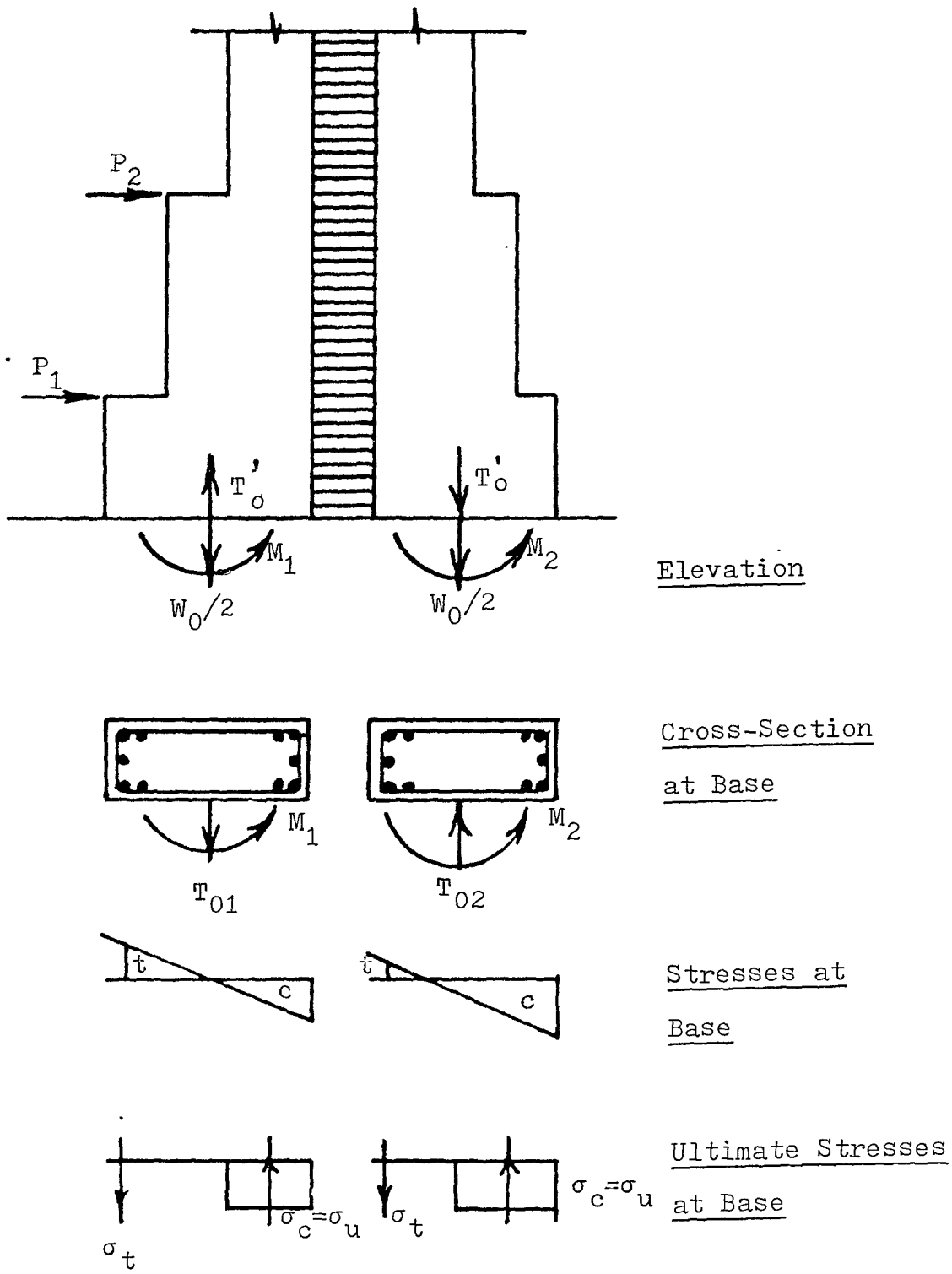

FIGURE 3-1 FORCES AND STRESSES ACTING AT THE BASE OF COUPLED SHEAR WALL

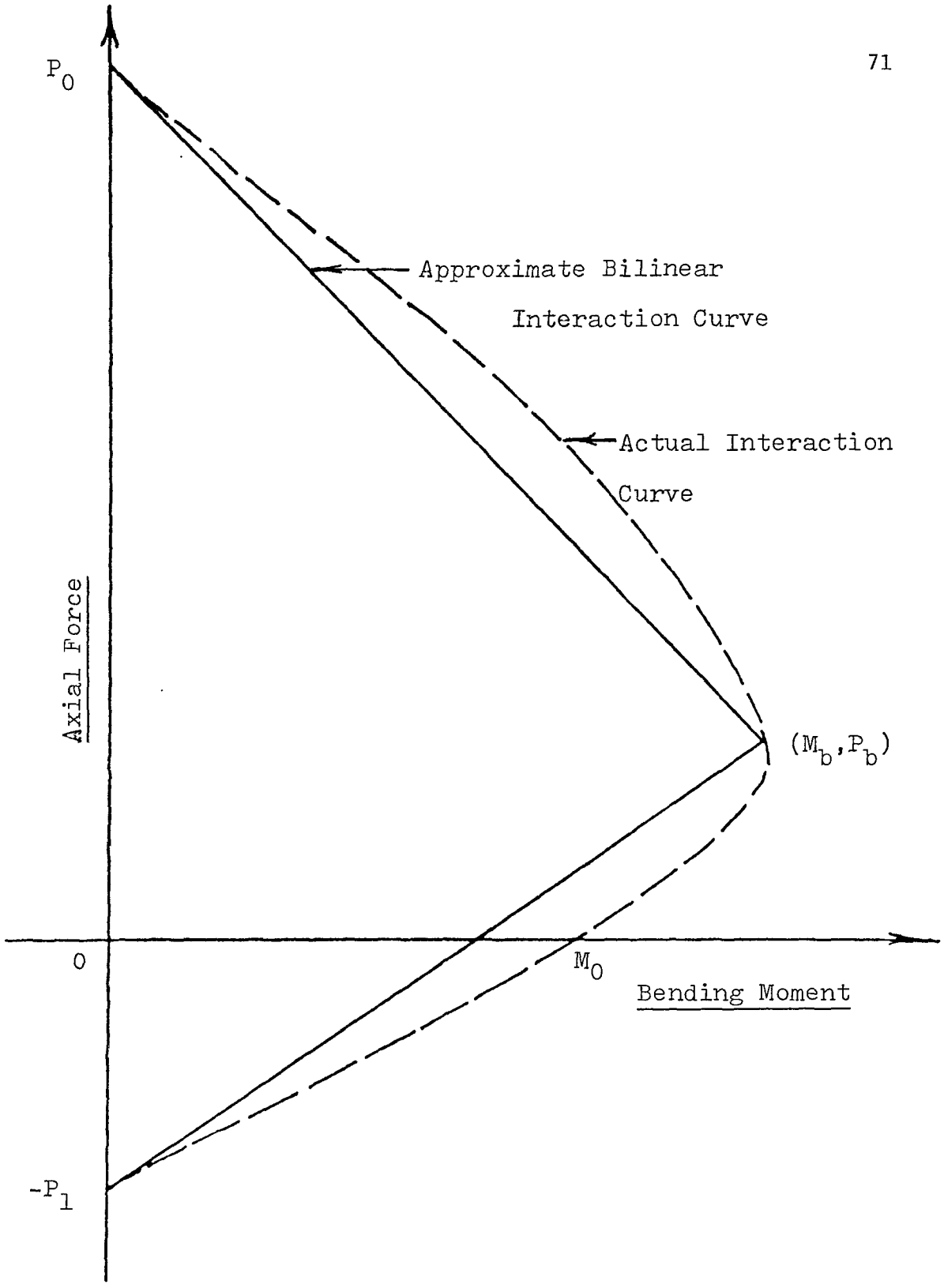

FIGURE 3-2 INTERACTION CURVE

where

β : slope at base due to the formation of hinge (unknown)

β_o: curvature at base (known); $b = EI_o/K_\theta$

and as

$$q_o = \frac{EI_o\, y_o''' + V_o}{a_1}$$

and $$q_o = \mu_1^2 \frac{EI_o}{K_\theta} y_o'' + \beta - \frac{T_o}{a_1 K_\delta}$$

adding these two and simplifying for y_o'''.

$$y_o''' = -\frac{a_1\mu_1^2}{K_\theta} y_o'' - \frac{a_1\mu_1^2}{K_\theta}\beta + \frac{\mu_1^2}{K_\theta EI_o} T_o + \frac{2a_1}{EI_o} q_o - \frac{V_o}{EI_o}$$

$$= -F_r y_o'' - F_r\beta + F_s T_o + F_a q_o - \frac{V_o}{EI_o} \qquad (3.1d)$$

where

K_θ = equivalent rotational stiffness of foundation

K_δ = equivalent vertical displacement stiffness of the foundation

$$F_r = \frac{a_1\mu_1^2}{K_\theta}$$

$$F_s = \frac{\mu_1^2}{K_\delta EI_o}$$

$$F_a = \frac{2a_1}{EI_o}$$

At the Top

$$y''_{nB} = 0 \tag{3.2a}$$

$$T_{nB} = 0 \tag{3.2b}$$

$$q_{nB} = \frac{EI_n y'''_{nB} + V_n}{a_n}$$

$$= ey'''_{nB} + \frac{P_n}{a_n} \tag{3.2c}$$

where

$$e = EI_n/a_n$$

Hence the mixed boundary value problem becomes

$$\begin{Bmatrix} 0 \\ b\beta_o+\beta \\ \beta_o \\ -F_r\beta_o-F_r\beta+F_aq_o+F_sT_o-V_o/EI_o \\ T_o \\ q_o \end{Bmatrix} = \begin{bmatrix} & & \\ & \bar{F} & \\ & & \end{bmatrix} \begin{Bmatrix} y_{nB} \\ y'_{nB} \\ 0 \\ y'''_{nB} \\ 0 \\ ey'''_{nB}+P_n/a_n \end{Bmatrix} + \begin{Bmatrix} \\ \bar{L} \\ \\ \end{Bmatrix} \tag{3.3}$$

Expanding above six equations and eliminating the three unknowns β, T_o, q_o at left hand side by Gauss-Elimination Method, we get the three independent equations in terms of three unknowns, y_{nB}, y'_{nB}, y'''_{nB}.

Rearranging it in matrix form we get

$$\begin{bmatrix} \overline{F}_{11} & \overline{F}_{12} & \overline{F}_{14}+e\overline{F}_{16} \\ \overline{F}_{31} & \overline{F}_{32} & \overline{F}_{34}+e\overline{F}_{36} \\ \overline{F}_{41}-F_a\overline{F}_{61}+F_f\overline{F}_{21}-F_s\overline{F}_{51} & \overline{F}_{42}-F_a\overline{F}_{62}+F_f\overline{F}_{22}-F_s\overline{F}_{52} & (\overline{F}_{44}-F_a\overline{F}_{64}+F_f\overline{F}_{24}-F_s\overline{F}_{54}) \\ & & +(\overline{F}_{46}-F_a\overline{F}_{66}+F_f\overline{F}_{26}-F_s\overline{F}_{56})e \end{bmatrix} \begin{Bmatrix} y_{nB} \\ y'_{nB} \\ y'''_{nB} \end{Bmatrix}$$

$$= \begin{Bmatrix} -\overline{L}_1-\overline{F}_{16}P_n/a_n \\ -\overline{L}_3-\overline{F}_{36}P_n/a_n+\beta_o \\ -\overline{L}_4+F_a\overline{L}_6-F_f\overline{L}_2+F_s\overline{L}_5-(\overline{F}_{46}-F_a\overline{F}_{66}+F_f\overline{F}_{26}+F_s\overline{F}_{56})P_n/a_n - V_o/EI_o + (F_fb-F_r)\beta_o \end{Bmatrix} \quad (3.4)$$

If the shear wall is fixed at the base initially,

$$b = F_r = F_s = 0;$$ and eqn. (3.4) simplifies to,

$$\begin{bmatrix} \overline{F}_{11} & \overline{F}_{12} & \overline{F}_{14}+e\overline{F}_{16} \\ \overline{F}_{31} & \overline{F}_{32} & \overline{F}_{34}+e\overline{F}_{36} \\ \overline{F}_{41}-F_a\overline{F}_{61}+F_f\overline{F}_{21} & \overline{F}_{42}-F_a\overline{F}_{62}+F_f\overline{F}_{22} & \overline{F}_{44}-F_a\overline{F}_{64}+F_f\overline{F}_{24}+(\overline{F}_{46}-F_a\overline{F}_{66}+F_f\overline{F}_{26})e \end{bmatrix} \begin{Bmatrix} y_{nB} \\ y'_{nB} \\ y'''_{nB} \end{Bmatrix}$$

$$= \begin{Bmatrix} -\overline{L}_1-\overline{F}_{16}P_n/a_n \\ -\overline{L}_2-\overline{F}_{36}P_n/a_n+\beta_o \\ -\overline{L}_4+F_a\overline{L}_6-F_f\overline{L}_2- V_o/EI_o - (\overline{F}_{46}+F_f\overline{F}_{26}-F_a\overline{F}_{66})\ P_n/a_n \end{Bmatrix}$$

where $$F_f = \frac{a_1\mu_1^2}{EI_o} \quad (3.5)$$

3.4 DETERMINATION OF CURVATURE AT BASE

To solve the above mixed boundary value problem, the curvature at the base ($y''_o = \beta_o$) should be known and this section explains a method to determine its value.

It should be noted that the piers of coupled shear wall are subjected to different axial forces, and the ultimate bending moment (M_u) is not a constant value, but depends on the axial force, hence the plastic hinges do not form simultaneously in the walls.

Consider the case of a fixed base coupled shear wall. From the initial fixed-fixed condition as shown in Fig. (3.3a), first only one hinge forms at the base of one pier [Fig. (3.3b)] with the base of other pier fixed. Both piers will have the bending moments and axial forces as shown in Fig. 3.3(b'). Let us consider the pier number 1 as the pier where the plastic hinge is formed first and T_o as the axial force, due to lateral loads, at the base. Then

$$\text{Total Wall Moment} = \text{Overturning Moment} - T_o\, a_o$$

$$EI_o\, y''_o = M^e - T_o\, a_o$$

$$\text{therefore} \quad (EI_{10} + EI_{20})\, y''_o = M^e - T_o\, a_o \tag{3.6}$$

As the plastic hinge is formed at the base of first pier, the above equation (3.6) becomes

$$M_{1u} + EI_{20}\, y''_o = M^e - T_o\, a_o$$

$$\text{therefore} \quad M_{20} = EI_{20}\, y''_o = M^e - T_o\, a_o - M_{1u} \tag{3.7}$$

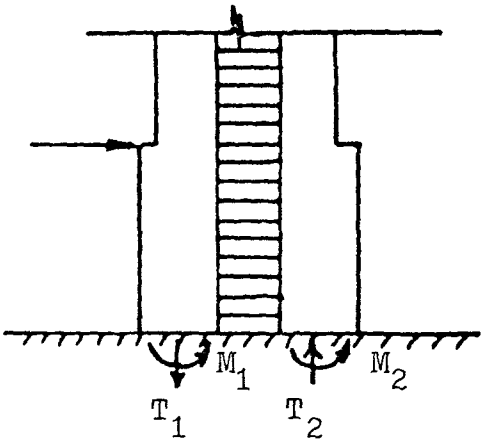

a. No Hinge State

(Fix - Fix)

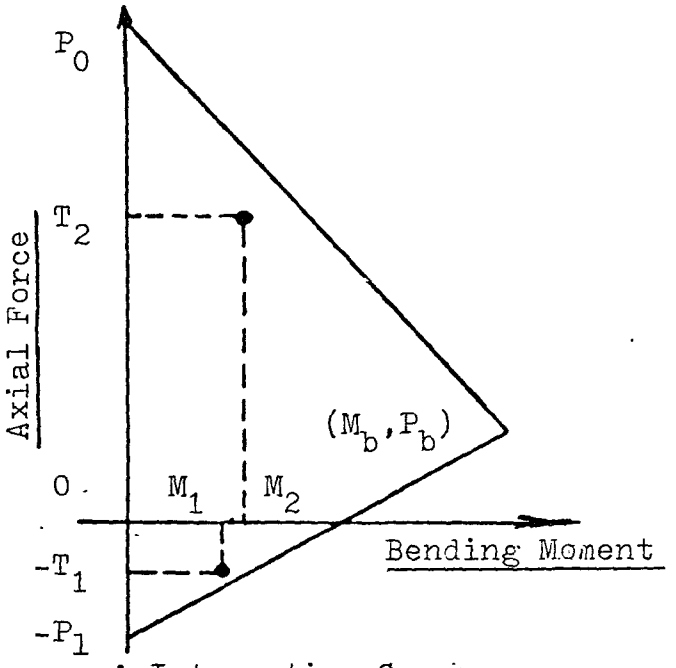

a' Interaction Curve

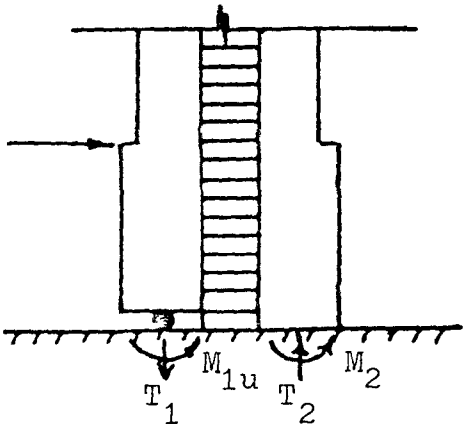

b. One Hinge State

(Hinge-Fix)

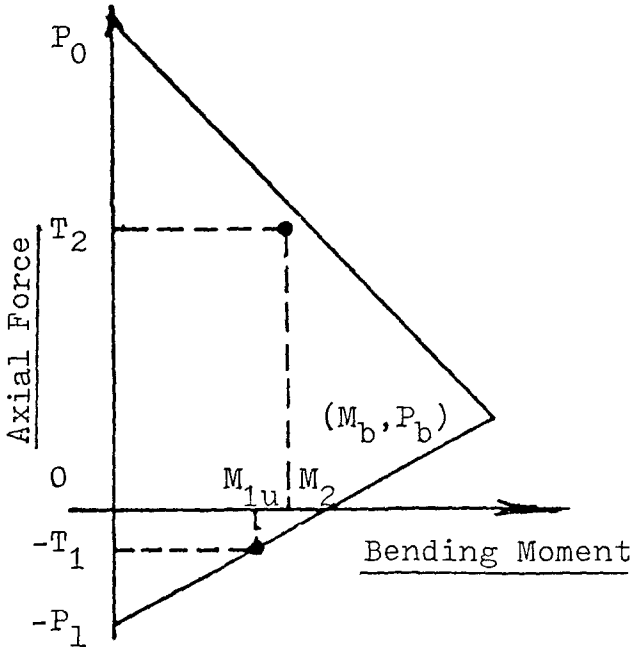

b' Interaction Curve

FIGURE 3.3 STATES AT THE BASE OF COUPLED SHEAR WALL

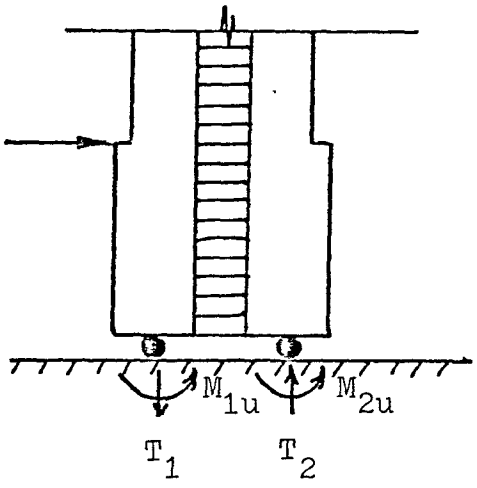

c. Two Hinge State

(Hinge-Hinge)

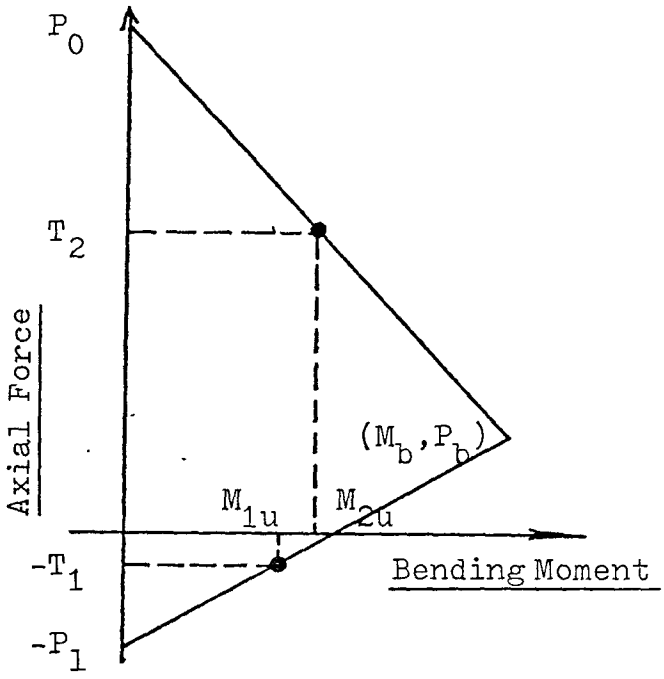

c' Interaction Curve

FIGURE 3-3 STATES AT THE BASE OF COUPLED SHEAR WALL

$$\beta_o = y''_o = \frac{M^e - T_o a_o - M_{1u}}{EI_{20}} \qquad (3.8)$$

where,

M^e : Total overturning moment at the base

T_o : axial force due to lateral loads at the base

a_o : c/c distance between the axes of both piers at the base

I_{10}: base moment of inertia of first pier

I_{20}: base moment of inertia of second pier

I_o : $I_{10} + I_{20}$

M_{1u}: ultimate bending moment (capacity) of the first pier (with combined effect due to axial force)

M_{20}: bending moment at the base of second pier

β_o : curvature at the base.

Then as the load increases continuously, all the extra additional wall moment at the base goes to the second pier as the first pier has already attained its capacity. This second pier can take the moment at the base until it also reaches its bending moment capacity, causing plastic hinges at the bases of both piers as shown in Fig. 3.3(c). At this condition both piers will have bending moments and axial forces at the base as shown in Fig. 3.3(c').

This stage, when all the segments are in plasic hinged state and hinges are formed at the bases of both piers, is taken as the "Complete Collapse State".

3.5 SCHEME OF COMPUTATION

In the actual analysis of coupled shear wall under the static or earthquake loads, the loading steps are usually not small enough to cause the axial force and bending moment at the pier base to fall precisely on the interaction curve and some iteration scheme is necessary.

From the initial fixed-fixed state shown in Fig. 3.3(a), the next hinged-fixed state [Fig. 3.3(b)] will be obtained. Let us assume that in pier 1 the plastic hinge forms first. Here as shown in Fig. 3.4(a) (step-II) the bending moment at base of first pier may fall beyond the interaction curve. But as it cannot take more bending moment than the ultimate capacity, the extra moment should be transfered to the other pier according to the equation (3.7). At this stage an iteration procedure is necessary because the boundary conditions are changed at the base which may change the segment states and hinge conditions at the base.

The iteration steps to be followed are:

1. The boundary value problem is solved with the corresponding boundary conditions at the base.
2. Revised base conditions are determined.
3. If the base axial forces at the beginning and the end of the iteration are close enough within acceptable accuracy, and the segment state and base conditions are the same as assumed in the beginning, the iteration procedure stopped.

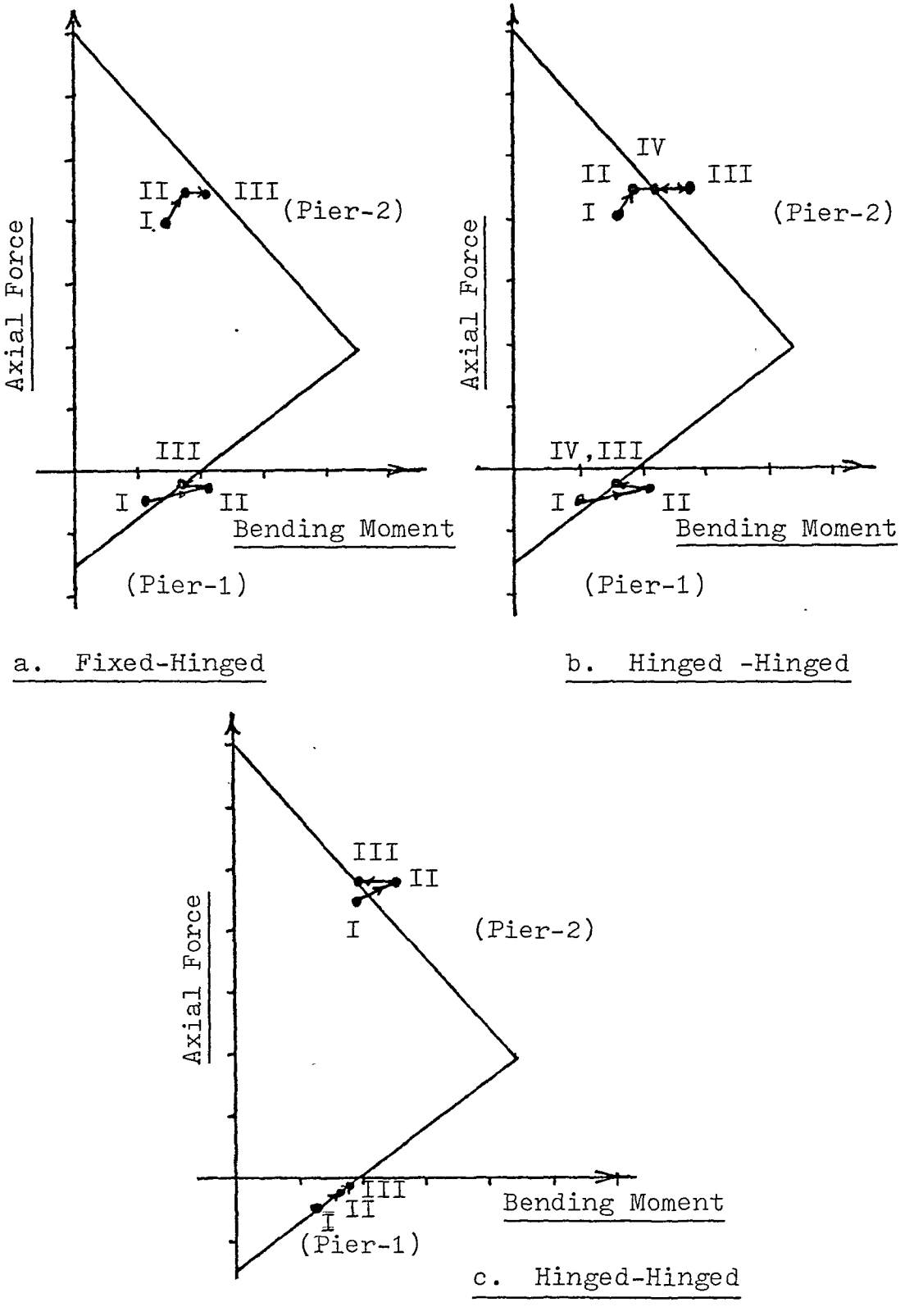

FIGURE 3-4 POSSIBLE ROUTS FOR FINAL BASE CONDITION

4. Otherwise the next iteration is carried out from step no. 1, using these new segment states and base boundary conditions.

It should be noted that, all these iteration steps are carried out at the same loading step.

Here this iteration procedure may lead to either of the two possibilities, namely: A) The final bending moment at the base of second pier may be less than its ultimate capacity, resulting the same Hinged-fixed condition at the base Fig. 3.4(a) (final part III).; B) The final bending moment at the base of second pier may reach its ultimate capacity, resulting the Hinged-Hinged condition at the base and hence a "collapse mechanism" at the same loading step [Fig. 3.4(b)].

3.6 STATIC ANALYSIS OF A COUPLED SHEAR WALL FOR WALL HINGE FAILURE

This phenomenon of formation of hinges at the base of piers is studied by applying a monotonously increasing static triangular loading. Two extreme cases are considered.

Case 1: All segments are in the plastic state i.e. all lintels between the piers have plastic hinges at their ends [Fig. 3.5(a)].

Case 2: All segments are in elastic state i.e. all lintels are elastic.

In the first case the loading is increased from W_1, a loading at which all segments become plastic. And in the second case the maximum allowable shear intensity for connecting beam is assumed to be very large so that the lintel is always elastic.

Two loading values W_2 and W_3 are compared for both of these cases.

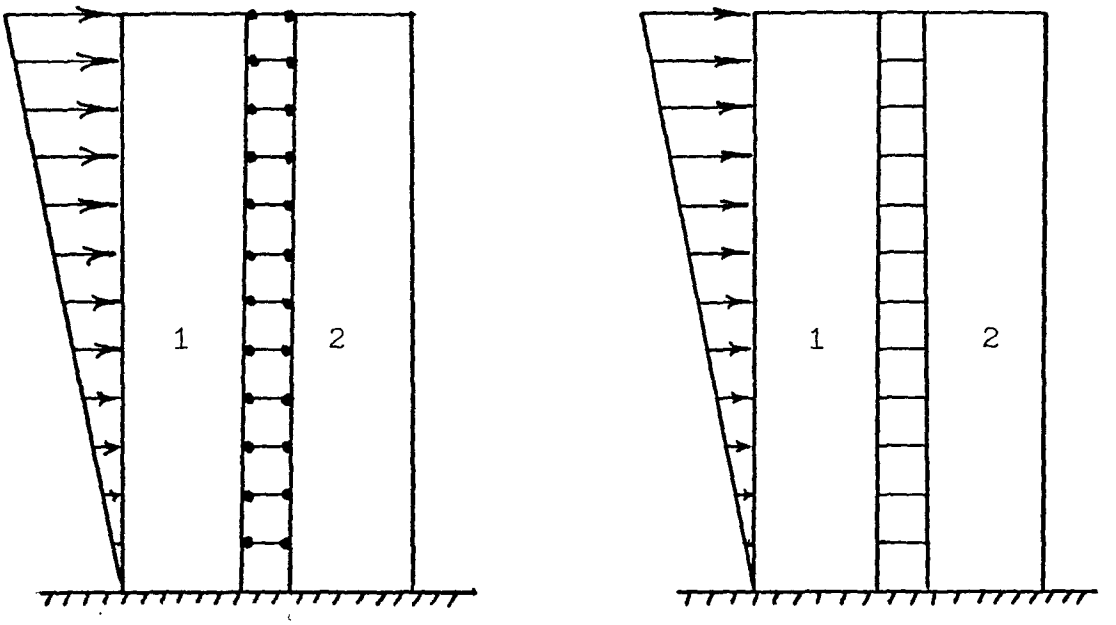

a. All-Plastic

b. All Elastic

FIGURE 3-5 STATIC CASES CONSIDERED FOR WALL HINGE FORMATION

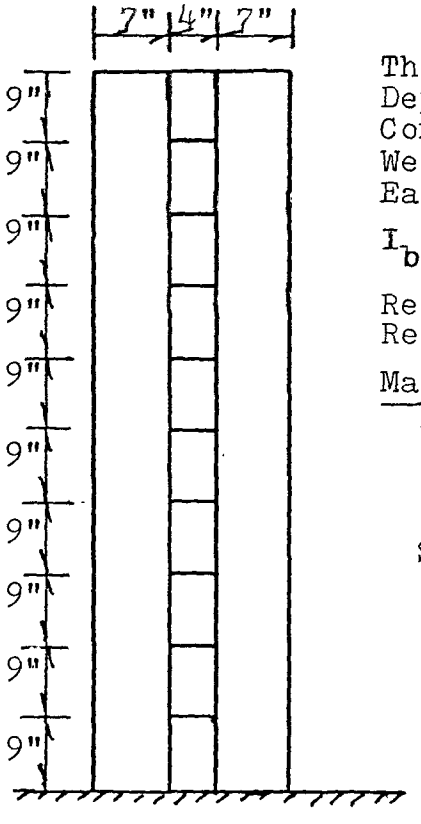

Thickness : 1"
Depth of Connecting Beams : 1.5"
Weight on Each Floor : 0.50 kips
I_b (cracked) : 0.169 in^4

Reinf. in Beams : 2#8 gage wire } Doubly
Reinf. in Piers : 8#8 gage wire } reinforced

Material Properties

Young's Modulus of
Concrete : 3000 $kips/in^2$
Steel : 29000 $kips/in^2$
Strength of
Concrete f'_c : 4.5 ksi
Steel f_y : 72.0 ksi

FIGURE 3-6 SHEAR WALL CONSIDERED FOR ABOVE CASES

W_2 is defined as the load at which the hinge forms at the base of one pier.

and W_3 is defined as the load at which hinges form at bases of both piers.

The coupled shear wall under study is the same as considered by Takayanagi and Schnobrich [30]. The properties and dimensions of this shear wall are given in Fig. (3.6). The observed behaviour of shear wall in both cases is shown in Fig. 3.7(a) and Fig. 3.7(b).

It is observed that once the first hinge forms at the base of one pier, the second hinge will form shortly after a small increment of loads. This is because, after one hinge formation in one pier, all the additional wall moment has to be absorbed by the other pier, causing it to reach the ultimate value more quickly.

This rate of formation of the second hinge, assuming all other properties of shear wall to be same, depends on the state of segments. In the case of plastic segments (case 1), the base axial forces remain the same for any additional loading. Therefore all the additional moment has to go to the second pier. In the second case of elastic lintels, the base axial force increases at higher load which acts as a reliever to the base wall moments. Hence not all the additional moments goes to the second pier. Therefore, the ratio of W_3 and W_2 in case 2 is more than that in case 1, i.e. the rate of formation of the second hinge reduces if all the segments are not in the plastic state.

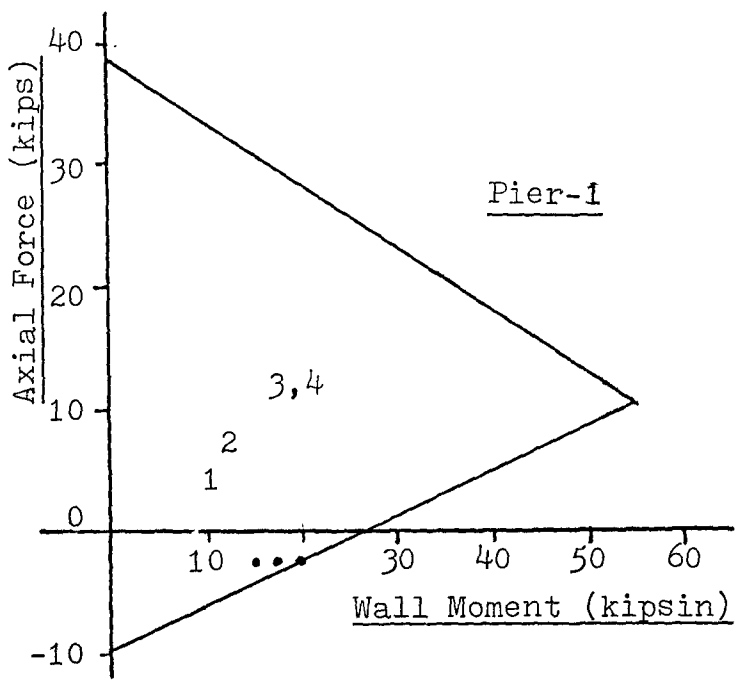

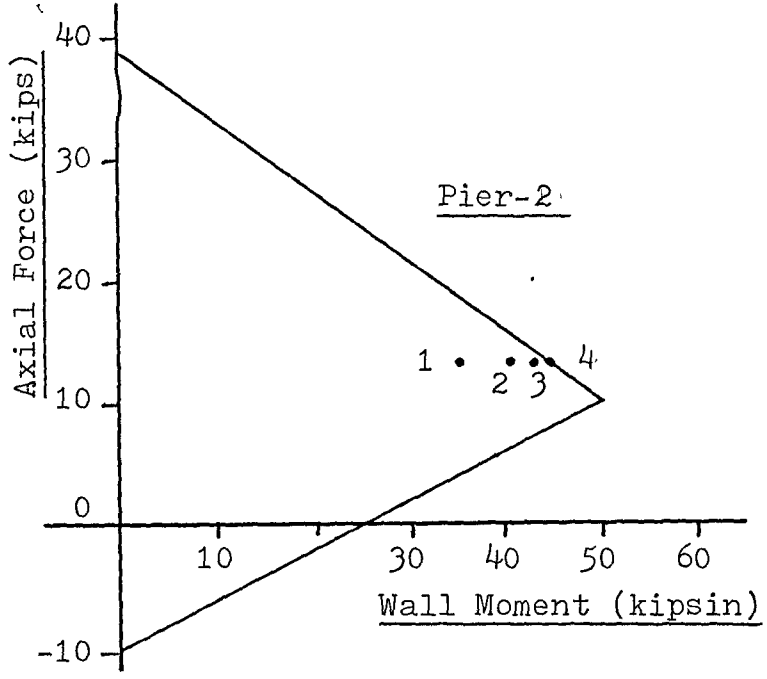

1. Plastification Starts W_0 = 2.925 kips
2. All Segments Plastic W_1 = 3.150 kips
3. Hinge Forms at the Base of Pier I W_2 = 3.375 kips
4. Hinges Form at the Bases of Both Piers W_3 = 3.600 kips

W_3/W_2 = 1.0666

FIGURE 3-7(a) CASE-1, ALL SEGMENTS PLASTIC (STRUCTURE-1)

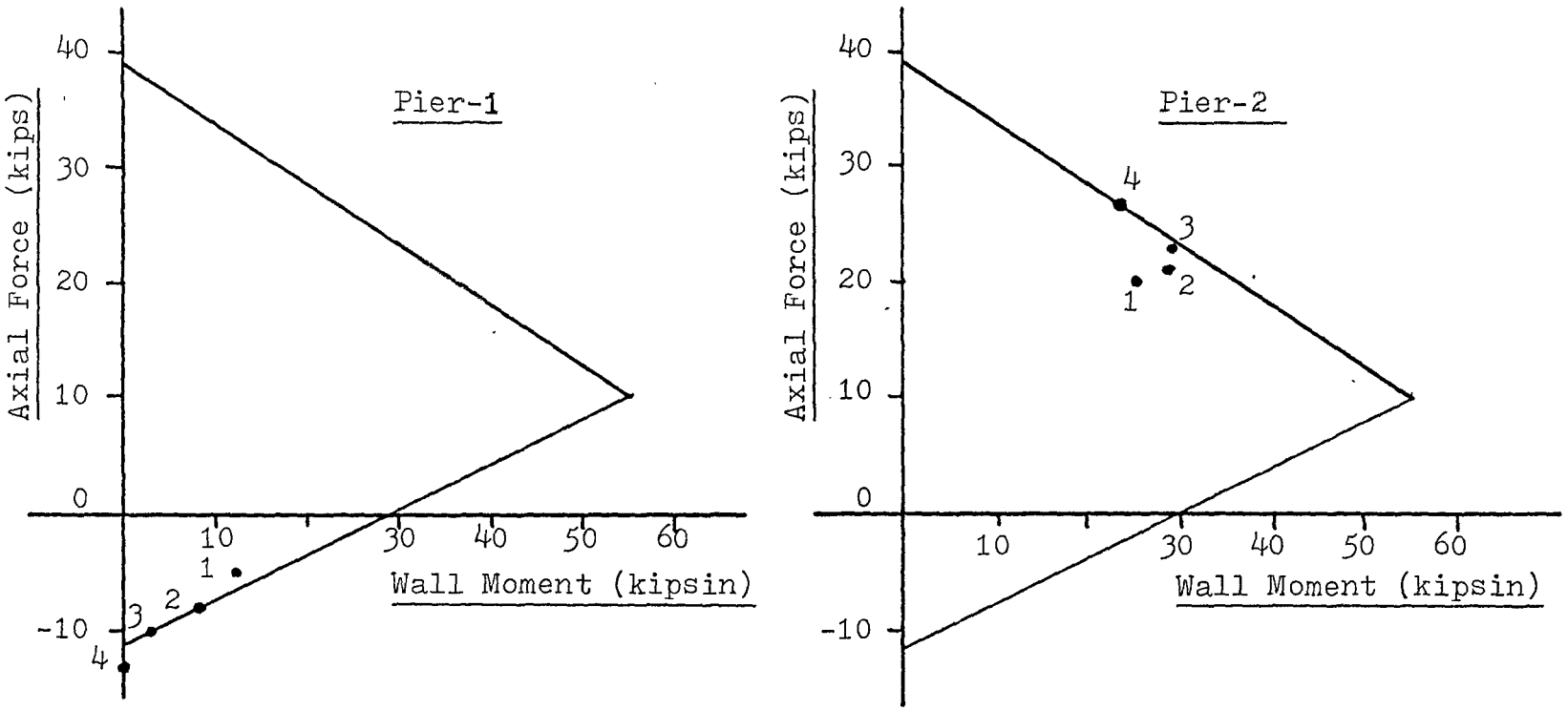

1. Just Before First Hinge	W_1' =	3.375 kips
2. Hinge Forms at the Base of Pier-I	W_2' =	3.600 kips
3. Hinge at the Base of One Pier	W =	3.825 kips
4. Hinges Form at the Bases of Both Piers	W_3' =	4.050 kips
	W_2'/W_3' =	1.125

FIGURE 3-7(b) CASE-2 : ALL SEGMENTS ELASTIC (STRUCTURE-1)

These are the two extreme cases of the coupled shear walls and in practice, the actual shear wall will have a behaviour within these two limits. Hence for the coupled shear wall of practical dimensions, it may be concluded that the second hinge at the base forms almost immediately after the first hinge has been formed.

Another important approximation worth mentioning is about the point of contraflexure in the connecting beams. It is assumed to be at the center of connecting beams and is maintained throughout the analysis. This is quite accurate as far as both piers are fixed at the base or rotate equally, but it is not true at the base, after one hinge forms at the base of one pier. Since the load intensity which causes one hinge to form is very close to that causes both hinges to form, it is believed that the inaccuracy introduced due to this assumption on the location of the point of contraflexure at center of connecting beams will not introduce substantial error in the analysis. In other words, if one hinge has formed at the base of one pier, the margin of safety of the coupled wall against total collapse is so low at this stage that one can treat that as a collapse load.

CHAPTER 4

DYNAMIC ANALYSIS OF SINGLE COUPLED SHEAR WALL

4.1 INTRODUCTION

In this chapter, the behaviour of typical coupled shear walls, representative of the coupled shear wall building, subjected to earthquake excitations is studied. Before using this computer program for the dynamic analysis of these coupled shear walls, the analytical technique is checked by performing a dynamic analysis on the coupled shear walls which have been studied by Sozen-Ochoa and Takayanagi-Schnobrich [29,30] and comparing the computed results with the corresponding results obtained by them.

Takayanagi and Schnobrich [30] in their analytical procedure, have considered the inelastic properties such as cracking and crushing of the concrete, yielding and bond slip of reinforcing steel, and inelastic behaviour of wall by dividing it into the subelements. In their beam-column model of shear wall, the constituent member stiffnesses are evaluated based upon the force-deformation relationships of the rotational springs of the beams and the subelements of the walls. Lumped mass concept is used by concentrating the masses at each floor level. The damping matrix is evaluated as the sum of a part proportional to the mass matrix and a part proportional to the structural stiffness matrix. The response under dynamic base motions is

calculated numerically by Newmark's method of step-by-step integration. The effect of load history in each constituent element is taken care of by using a set of hysteresis rule of Takeda.

4.2 CHECKING FOR METHOD OF DYNAMIC ANALYSIS

4.2.1 Coupled Shear Walls

This section explains the properties and dimensions of the coupled shear walls. These are the same as considered by Takayanagi-Schnobrich [30].

Two types of models are considered here. These are a weak lintel beam model and a strong lintel beam model. In further discussion they are referred to as structure-1 and structure-2, respectively. The main difference between these two models is the amount of steel reinforcement used in the connecting beams. The dimensions of these walls are shown in Fig. (4.1). A weight of 0.5 kips is placed at each floor level to represent the loadings at each floor level. The dimensions, reinforcement and capacities are given in Table 4.1. The material properties for these models are listed in Table 4.2.

WALL	Wall Thickness (in)	Conn. Beam Depth (in)	Conn. Beam Reinf. A_{sb}	Wall Reinf. A_{sw}	Shear Capacity q_p(kip/in)	I_b in^4
Structure-1	1	1.5	2#8*	8#8*	0.08667	0.169
Structure-2	1	1.5	4#8*	8#8*	0.1611	0.268

* Flexural Reinforcement: No. 8 gage wire

Table 4.1 Dimensions, Reinforcement and Capacities of Structure-1 and Structure-2

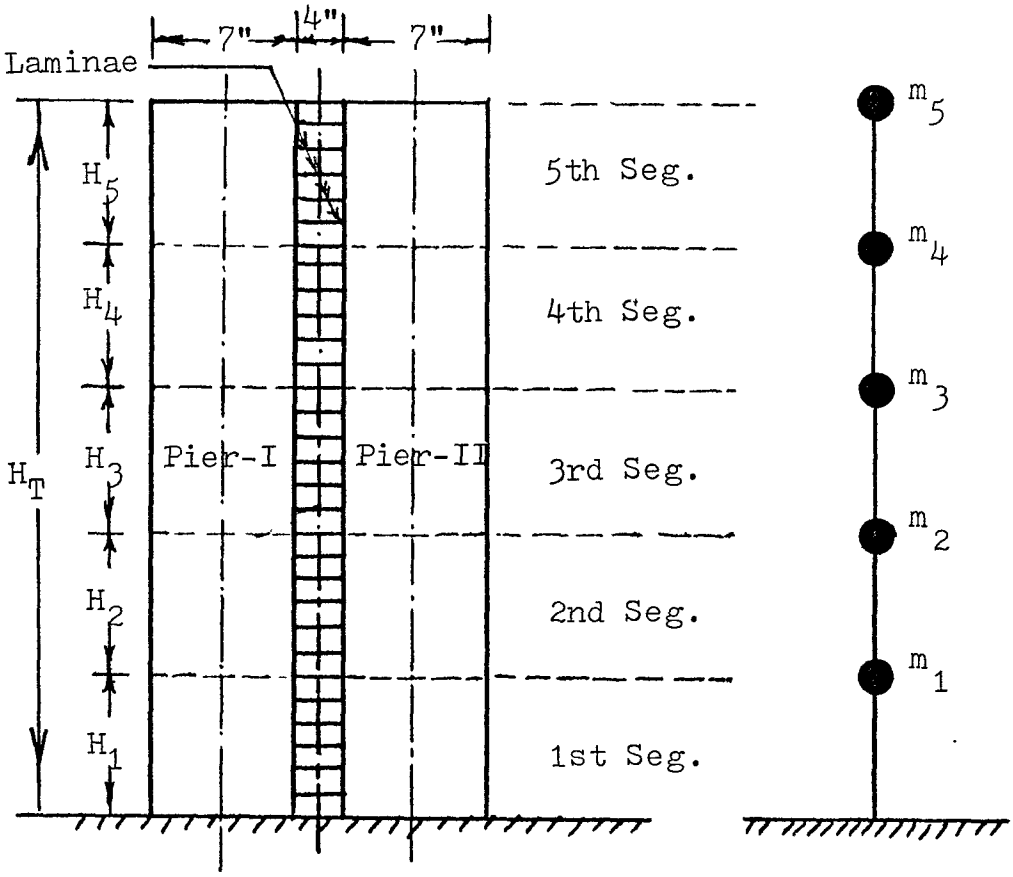

$H_1 = H_2 = H_3 = H_4 = H_5 = 18"$; $H_T = 90"$;

Thickness = 1"

Walls	$m_1=m_2=m_3=m_4=m_5$, MASS (kips.sec^2/in)	
	For Mass Matrix	For P-Δ Effect
Structure-1	0.002645	0.002645
Structure-2	0.002645	0.002645

FIGURE 4.1 DYNAMIC MODEL OF STRUCTURE-1 AND STRUCTURE-2.

Concrete	Compressive Strength (f_c')	4.50 ksi
	Young's Modulus (E_c)	3000 ksi
	Strain at f_c' (ε_c)	0.003
Steel	Yield stress (f_y)	72.0 ksi
	Young's Modulus (E_s)	29000 ksi
	Yield Strain (ε_y)	0.00248

Table 4.2 Assumed Material Properties of Structure-1 and Structure-2

4.2.2 Dynamic Model and Method of Excitation

The dynamic model for structure-1 and structure-2 is given in Fig. (4.1).

The base motions for structure-1 and structure-2 are refered to as base motion-1 and base motion-2, respectively. The waveforms of these base motions are the acceleration signals of El-Centro (1940) N.S component. The original time axes are compressed by a factor of 2.5 and the amplitudes of acceleration are modified relative to the original record as appropriate to the analytical work of Takayanagi and Schnobrich [30]. Only the first 3 sec. of the recorded base motion are used in the calculations, because the maximum responses and most of the damages to the structures are observed to be taken place within this time interval. This compressed duration of 3 sec. corresponds to 7.5 sec. of the original record. The typical modified waveform is shown in Fig. (4.2). The maximum accelerations of the base motions are listed below.

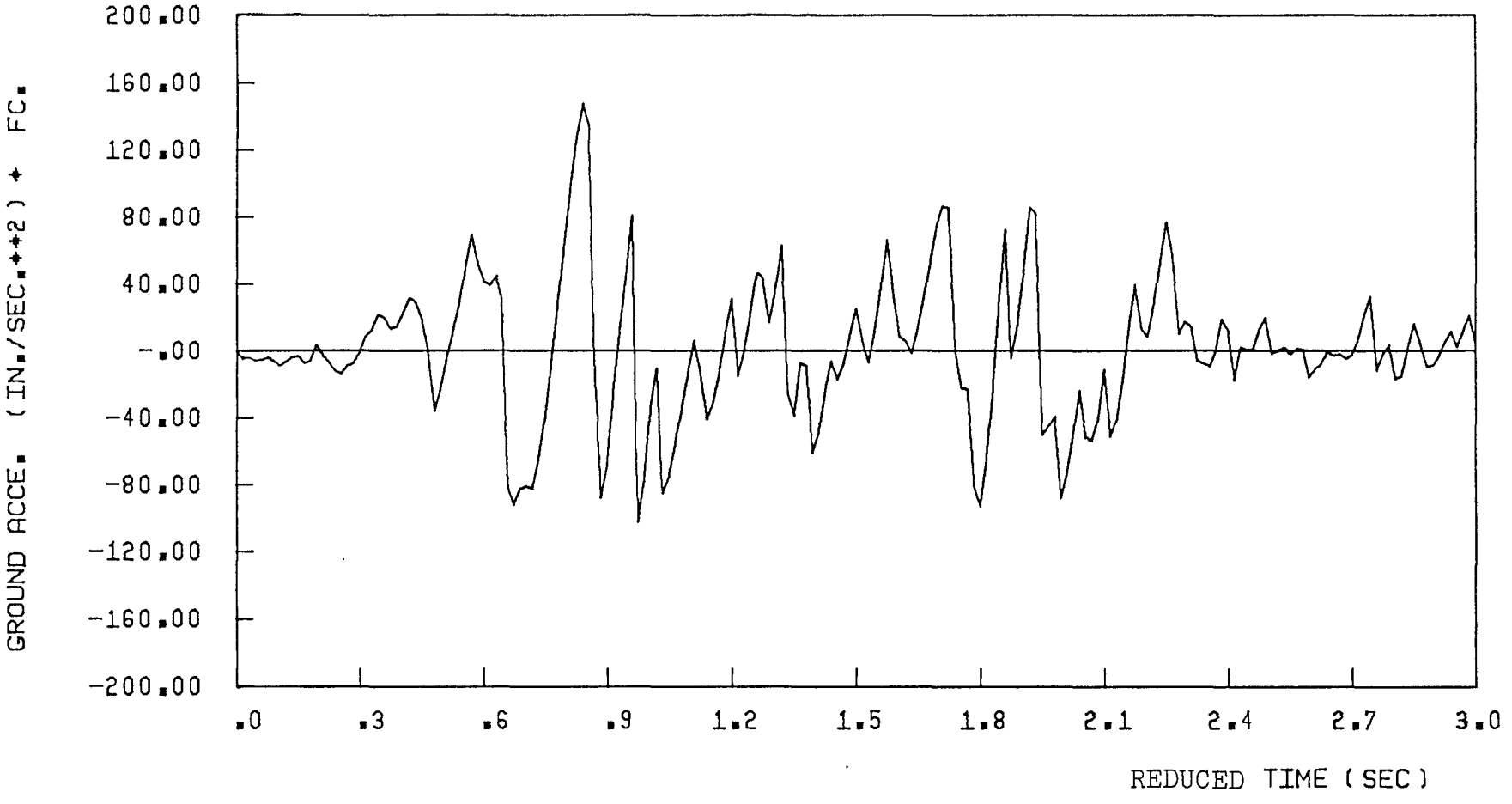

FIGURE 4-2 ELCENTRO COMP.NORTH 41 PERC. g

	Maximum Acceleration	Modified Duration Time
Base Motion-1	41% g	3.0 sec.
Base Motion-2	91% g	3.0 sec.

The time intervals used in the iteration procedure for the dynamic response calculation of structure-1 and structure-2 are 0.0005 and 0.0006 sec. The "β" factor in Newmark's method of step-by-step integration procedure is taken as 0.25.

4.2.3 Effect of the Percentage Critical Damping

Before we study the two cases posed above, it is necessary to study the effect of the modal critical damping ratios. This section presents a parametric study of the effect of the percentage critical damping on the total responses. Five sets of different modal critical damping ratios are considered and the behaviour of structure-1 under motion-1 is studied. A dynamic model of five segments and five masses is considered. Table 4.3 shows the range of the values of responses in each run.

From this table it is clear that the percentage of critical damping for the first mode is the most important. Also it is observed that the percentage change in the response is lesser than the percentage change in the damping. For the present analysis of structure-1 and structure-2, the percentage critical damping for five modes are taken as: $\xi_1 = 2\%$, $\xi_2 = 3\%$, $\xi_3 = 4\%$, $\xi_4 = 5\%$, $\xi_5 = 6\%$.

Percentage of Critical Damping for Mode (%)					Top Displacement Range (in)	Top Acceleration Range (%g)	Base Shear Range (kips)	Base Axial Force Range (kips)	Base Moment Range (kips./in)
1	2	3	4	5					
2	3	4	5	6	-0.64 to 0.50	-0.87 to 1.40	-1.3 to 1.4	-5.9 to 7.0	-125 to 144
2	2	2	2	2	-0.66 to 0.54	-0.87 to 1.40	-1.3 to 1.4	-5.9 to 7.0	-130 to 148
6	5	4	3	2	-0.51 to 0.36	-0.77 to 1.10	-1.3 to 1.4	-6.1 to 6.9	-118 to 131
6	6	6	6	6	-0.49 to 0.34	-0.80 to 1.10	-1.3 to 1.3	-6.1 to 6.9	-115 to 128
4	6	7	8	9	-0.53 to 0.39	-0.81 to 1.20	-1.4 to 1.4	-6.0 to 6.9	-120 to 135

Table 4.3 Comparison of Response Parameters; Structure-1, Motion-1

4.2.4 Dynamic Response of Structure-1

The initial mode shapes and the periods for those modes are computed for structure-1. The mode shapes agree with the previous analysis and the periods are compared in the Table 4.4.

MODE	1	2	3	4	5
(1) Present Work	0.208 sec	0.046 sec	0.0202 sec	0.0119 sec	0.0086 sec
(2) Takayagani et al	0.200 sec	0.047 sec	0.0208 sec	-	-
(1)/(2) X100	104%	97.9%	97.1%	-	-

Table 4.4 Comparison of Periods of Structure-1

The output time history responses of the top displacement, base overturning moment, base axial force and top acceleration are shown in Figs. (4.3) and (4.6). Figures (4.3), (4.4) and (4.6) also compare the computed responses with the responses obtained by Takayanagi and Schnobrich [30]. This shows that the nature of computed responses is similar to the nature of the responses obtaining by Takayanagi and Schnobrich. In case of top displacement, the first mode components are dominant throughout the time history of the motion. Also the dominance of the first mode components in the makeup of the response waveforms of the base moment with a slight second mode component contribution should be noted in Fig. (4.4). This means that each member behaves in the same way as the structural system does. The shearing force intensities of the segments are given in Figs. (4.7) through (4.11). Also the

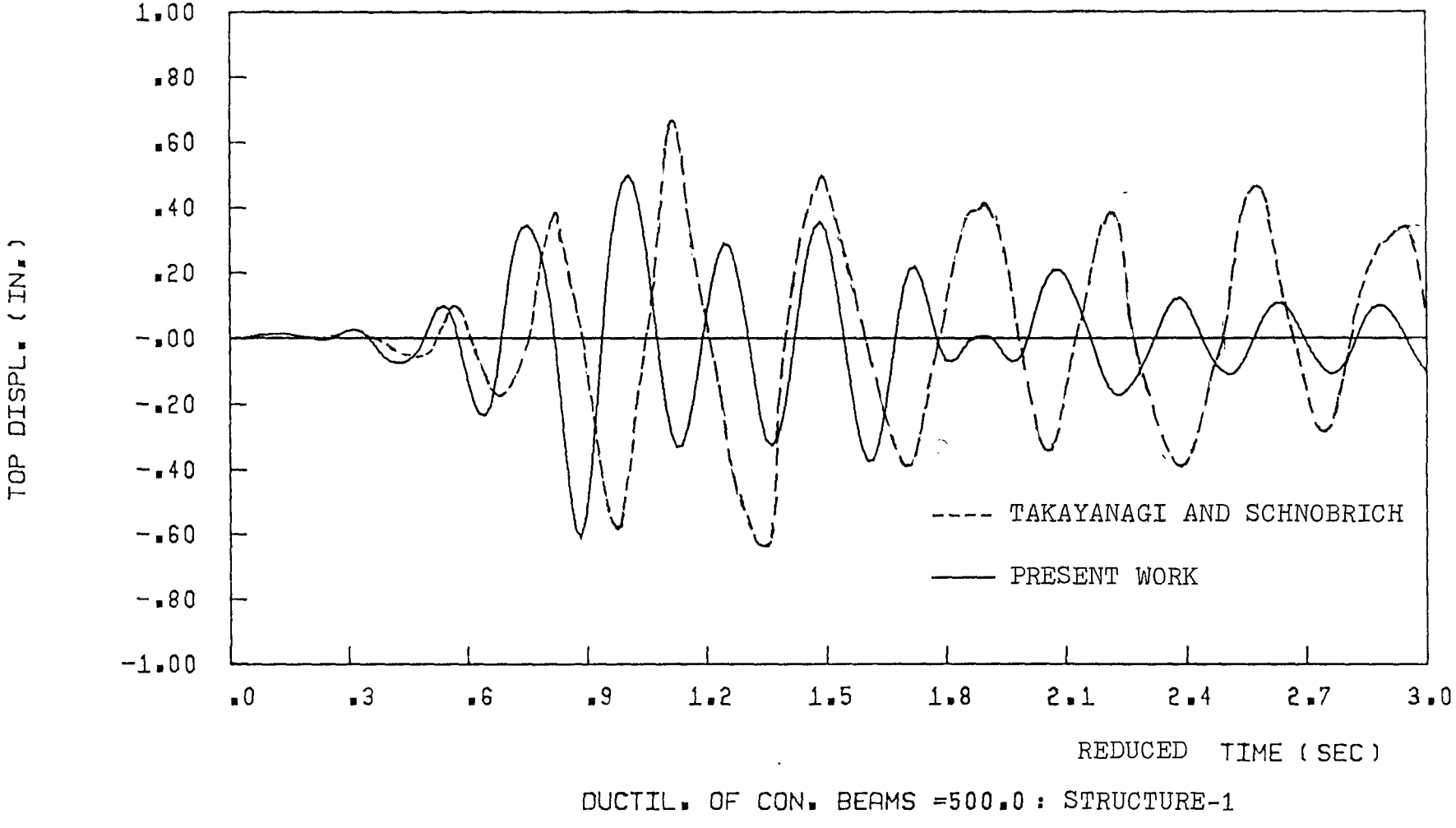

FIGURE 4-3 TOP DISPLACEMENT, ELCENTRO COMP. NORTH 41 PERC. g (MOTION-1)

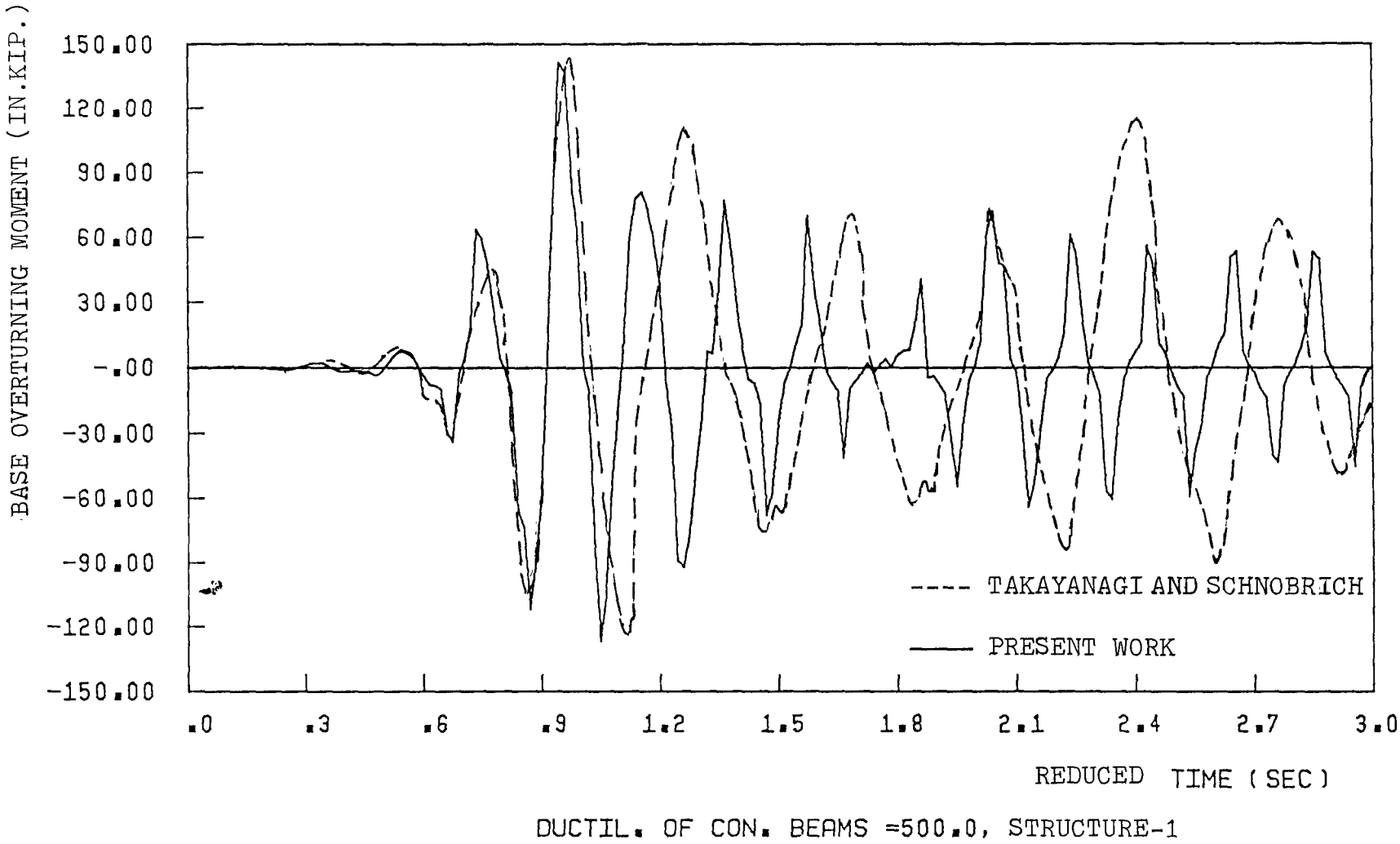

FIGURE 4-4 BASE O.T.M, ELCENTRO COMP.NORTH 41 PERC. g (MOTION-1)

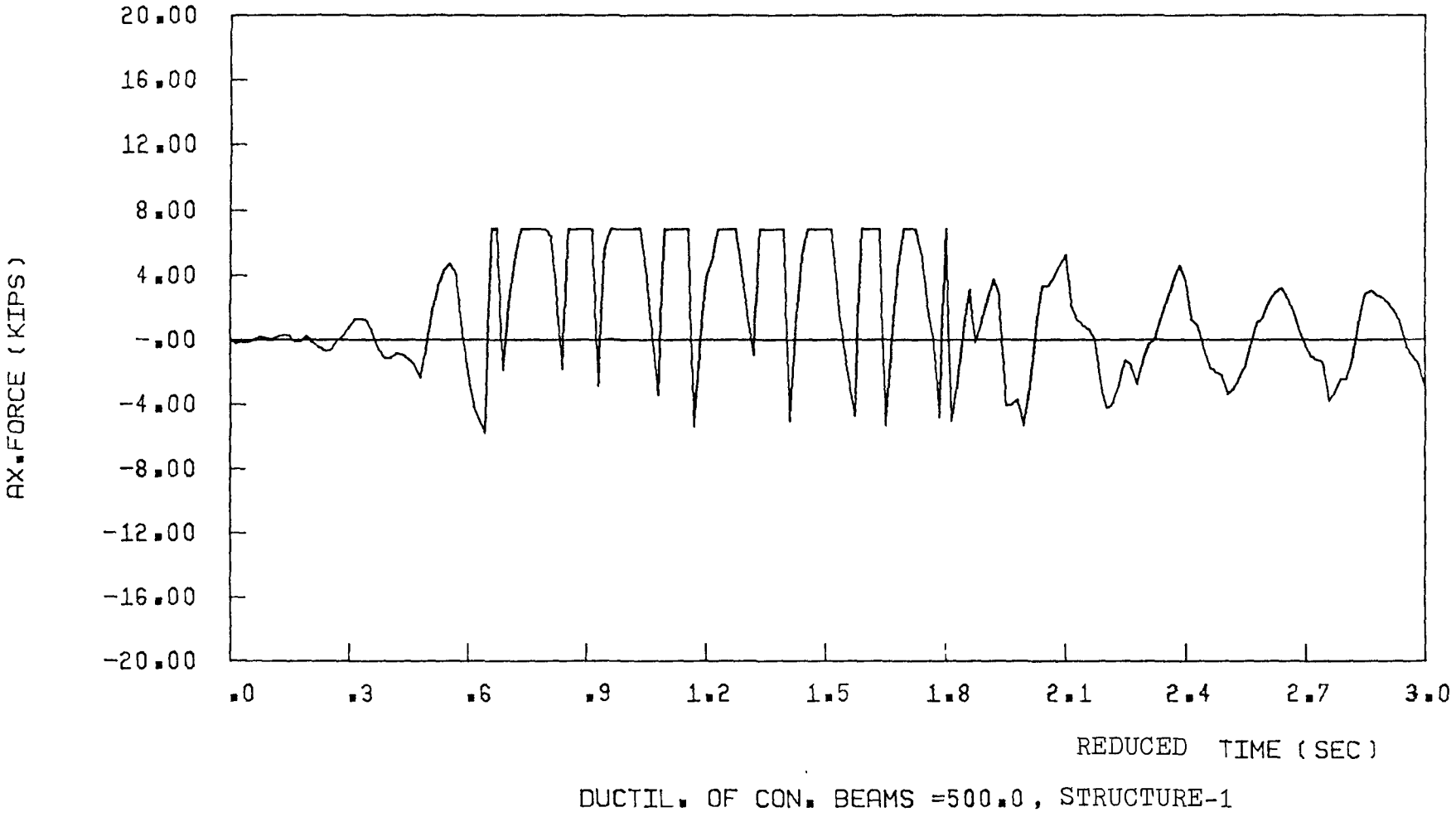

FIGURE 4-5 AX. FORCE, ELCENTRO COMP.NORTH 41 PERC. g

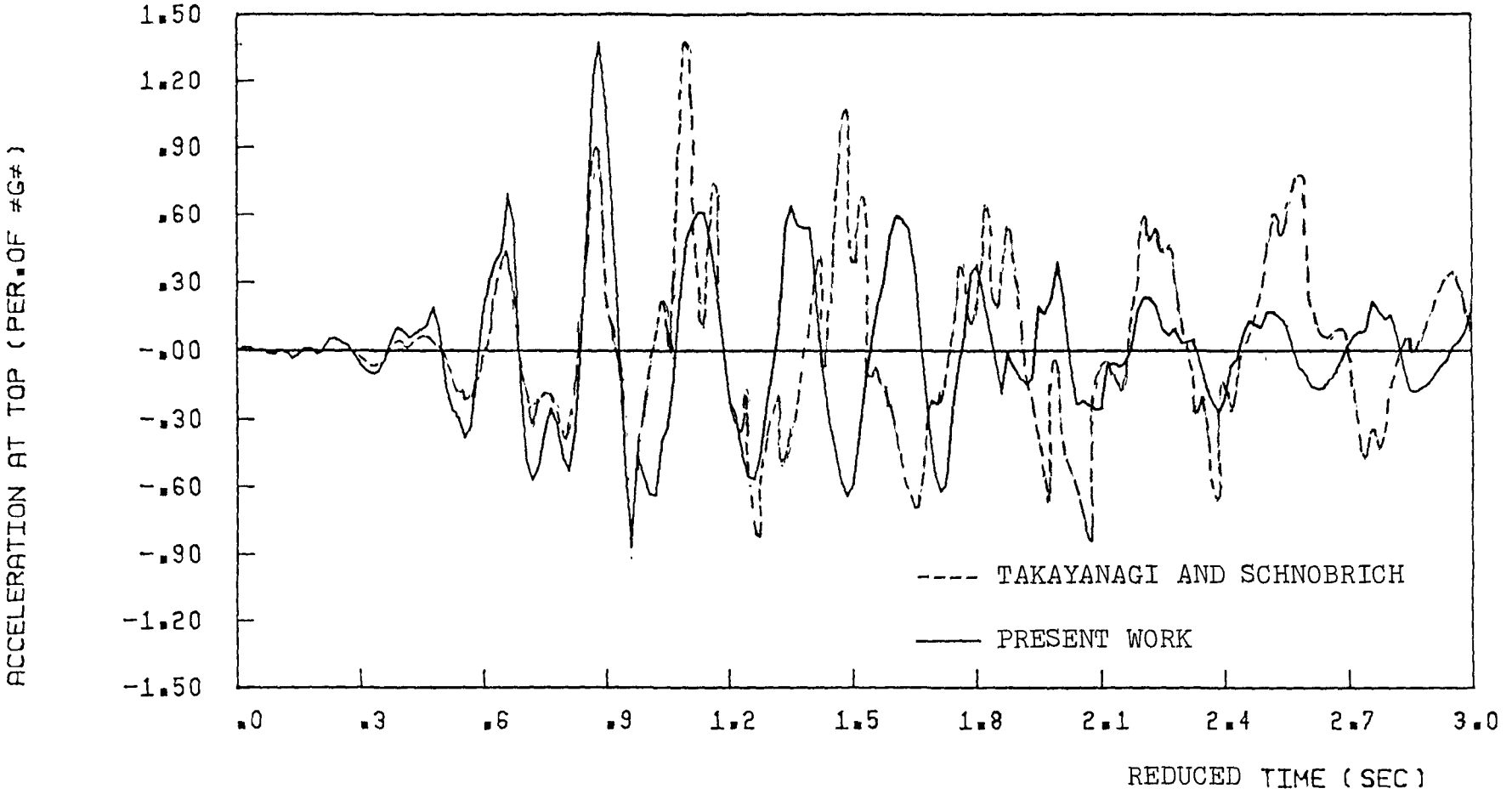

FIGURE 4-6 TOP ACCELERATION , ELCENTRO COMP.NORTH 41 PERC. g (MOTION-1)

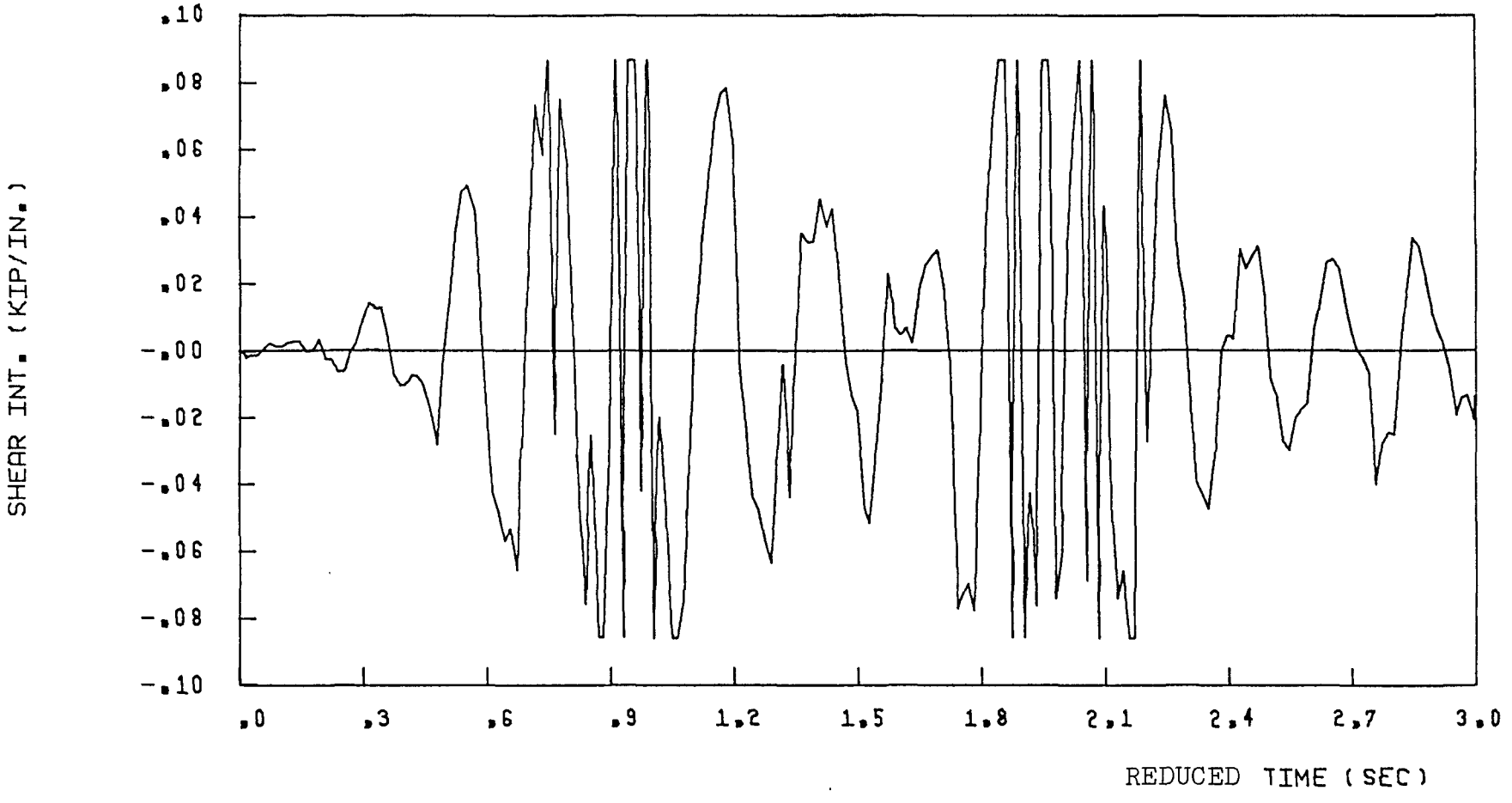

FIGURE 4-7 SHEAR INT., ELCENTRO COMP.NORTH 41 PERC. g

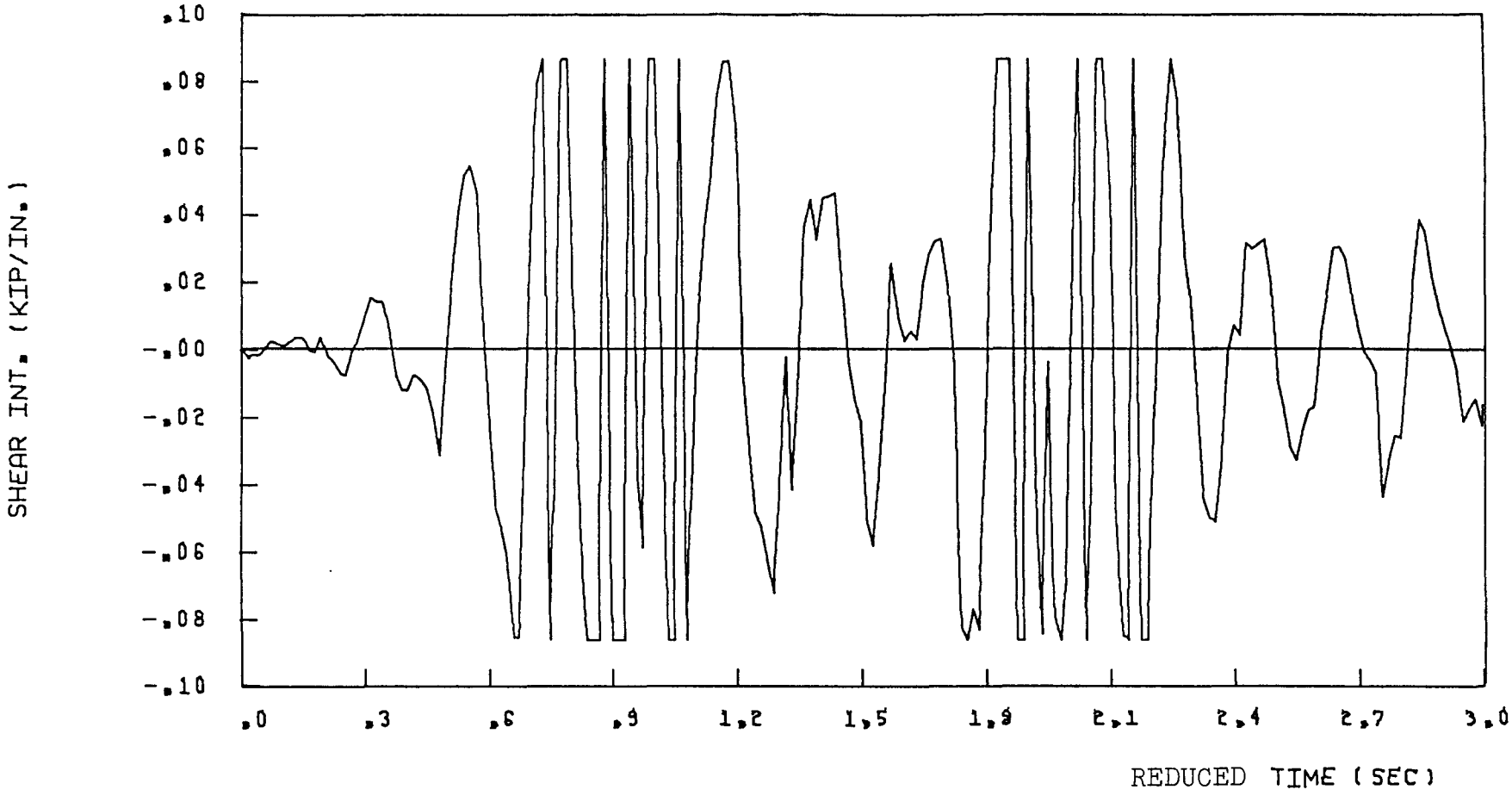

FIGURE 4.8 SHEAR INT., ELCENTRO COMP.NORTH 41 PERC. g

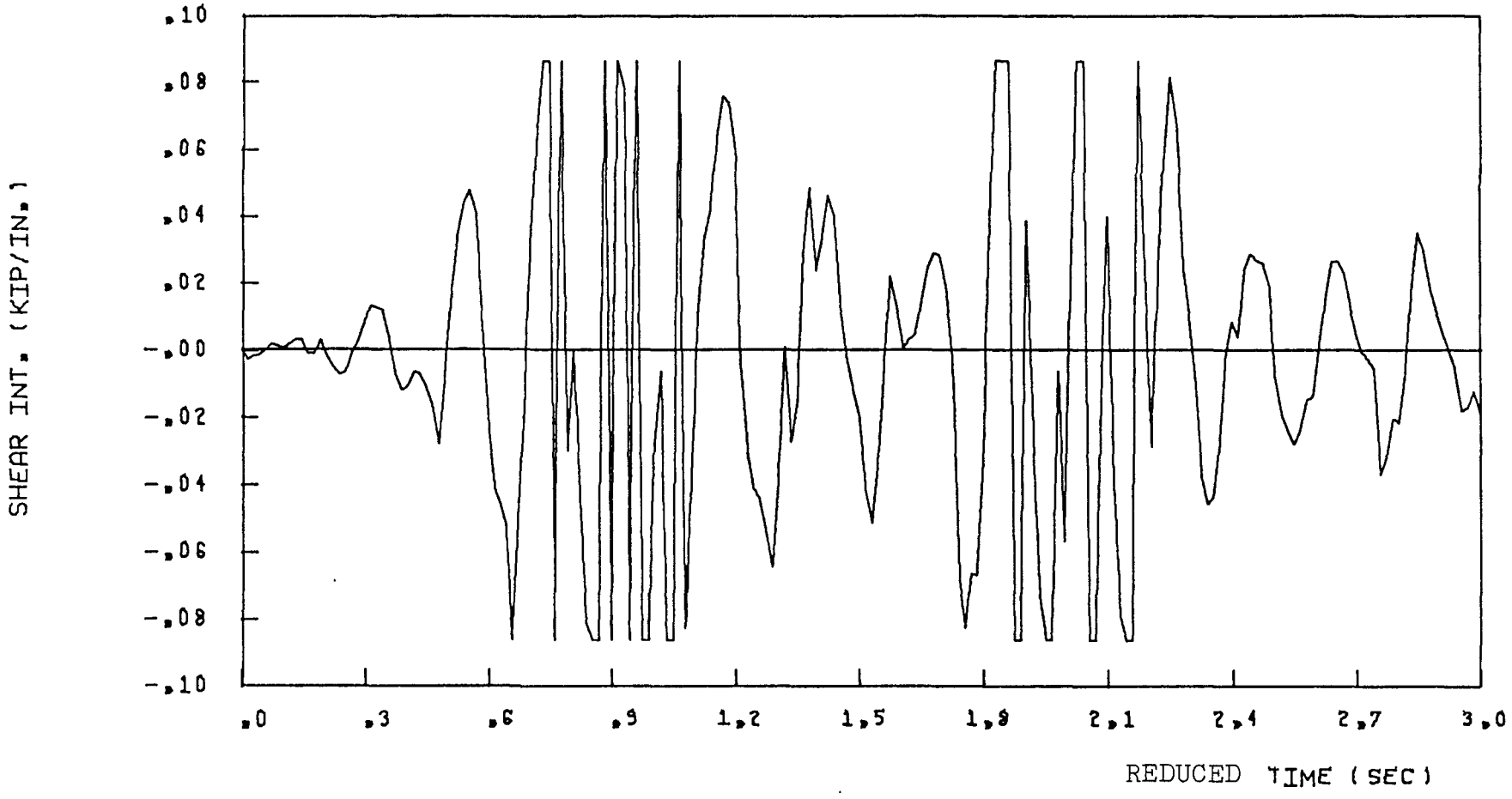

FIGURE 4-9 SHEAR INT., ELCENTRO COMP.NORTH 41 PERC. g

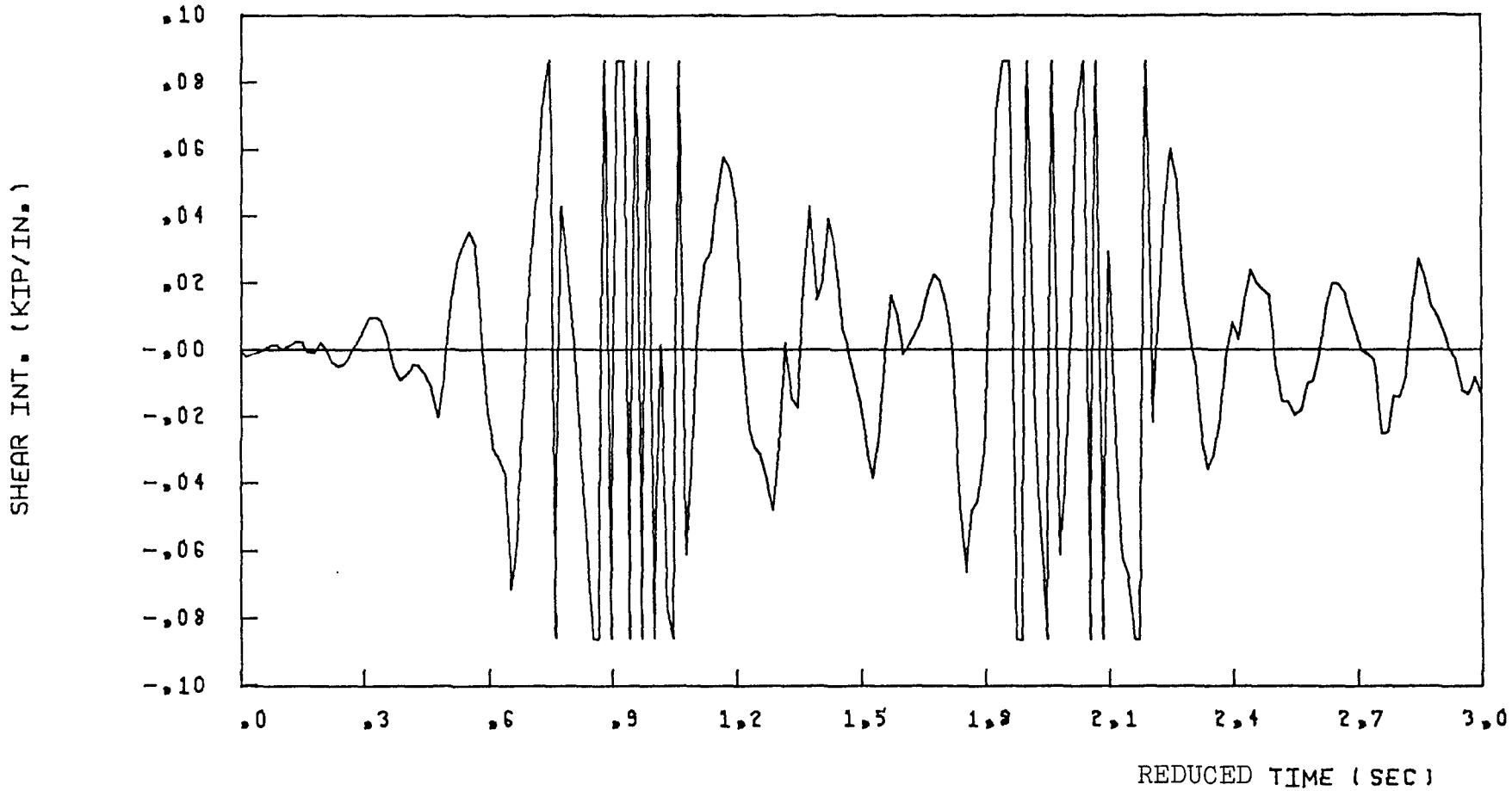

FIGURE 4.10 SHEAR INT., ELCENTRO COMP.NORTH 41 PERC. g

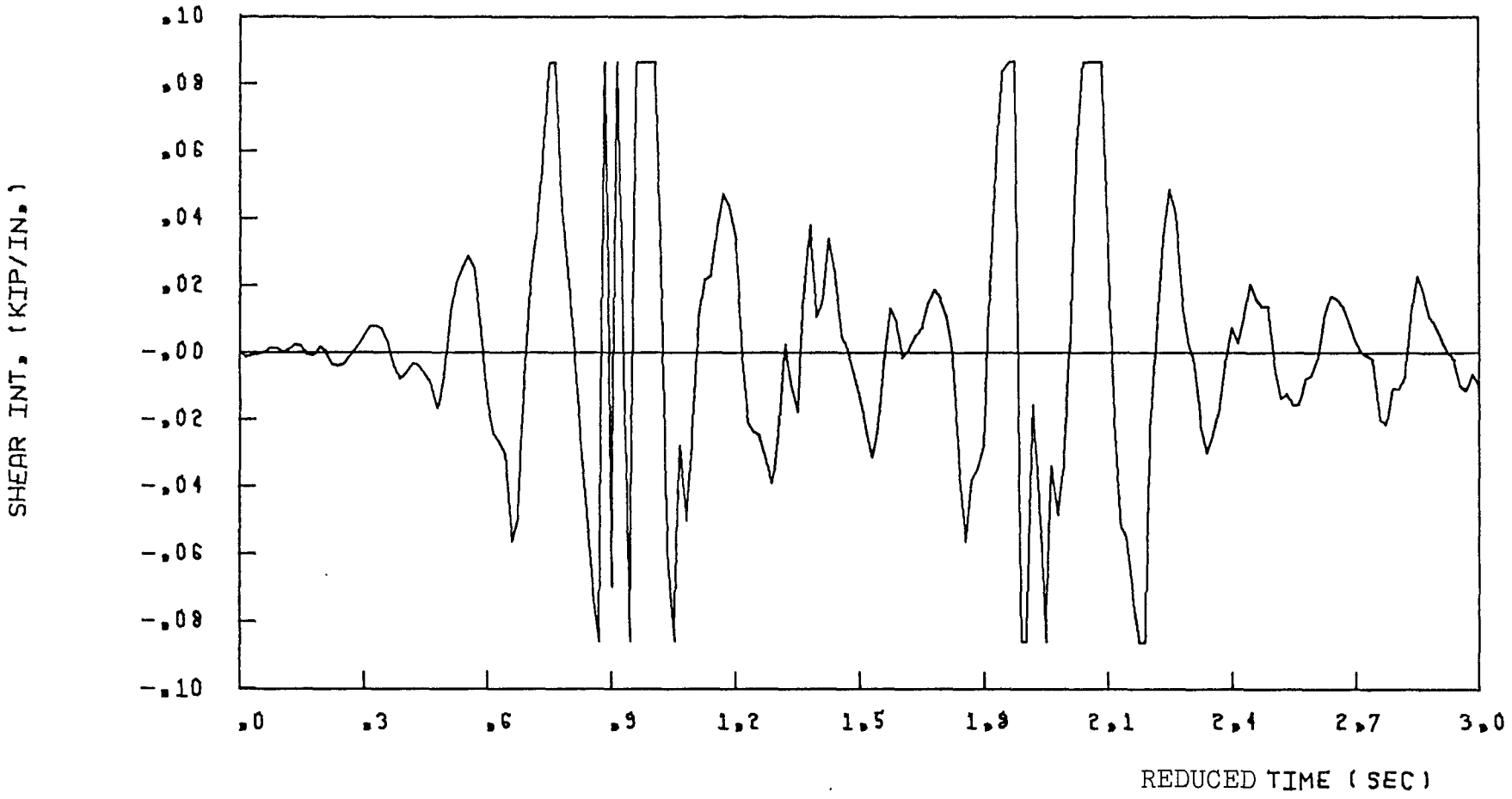

FIGURE 4-11 SHEAR INT., ELCENTRO COMP.NORTH 41 PERC. g

contribution of the higher modes is clear in these shearing force intensity responses, when the segments are in plastic state.

Listed below in Table 4.5 are the maximum values of the parameter of interest discussed above for the structure-1.

	Top Displacement (in)	Top acceleration (% g)	Base Shear (kips)	Base Axial Force (kips)	Base moment (kips-in)
Present work	0.64	1.40	1.40	7.0	144.0
Takayayani & Schnobrich	0.72	1.42	1.30	8.0	148.5

Table 4.5 Comparison of Maximum Responses of Structure-1 under Motion-1

4.2.5 Dynamic Response of Structure-2

The nonlinear response history of structure-2 subjected to base motion-2 is computed and discussed in this section. The calculated responses are compared with those of the analytical work of Takayanagi and Schnobrich [30].

The periods of different modes are computed before the ground excitation and are compared in Table 4.6.

MODE	1	2	3	4	5
(1) Present work	0.197 sec	0.041 sec	0.018 sec	0.0109 sec	0.008 sec
(2) Takayagani & Schnobrich	0.222 sec	0.048 sec	0.020 sec	-	-
$\frac{(1)}{(2)}$ X100	88.7%	85.4%	90%	-	-

Table 4.6 Comparison of Periods of Structure-2

The response waveforms of top displacement, base over-turning moment, axial force and top acceleration are shown in Figs. (4.12) through (4.15). Shown in Figs. (4.12), (4.13) and (4.15) are comparisons of the computed responses with the responses obtained in the analytical work of Takayanagi and Schnobrich [30].

Table 4.7 compares the maximum responses.

	Top Displacement (in)	Top acceleration (% g)	Base Shear (kips)	Base Axial force (kips)	Base moment (kips-in)
Present Work	1.20	2.85	4.8	14.0	255
Takayagani & Schnobrich	1.55	2.60	4.54	-	234

Table 4.7 Comparison of Maximum Responses of Structure-2 under Motion-2

The time history responses of both structures in present work show a reasonably good agreement with those obtained by Takayanagi and Schnobrich [30]. The maximum responses are also comparable. The top displacements in the present work are low, probably because this analysis does not consider the cracking and non-linear behaviour of walls pinching action and strength decay of the connecting beams. These characteristics are probably more important in case of strong beam model (structure-2) subjected to a strong earthquake excitation (motion-2) and hence causes more deviation in the responses. It also should be noted that the waveforms of motion-1 and motion-2 considered by Takayanagi and Schnobrich are not exactly the scaled waveforms of El-Centro (1940) N.S

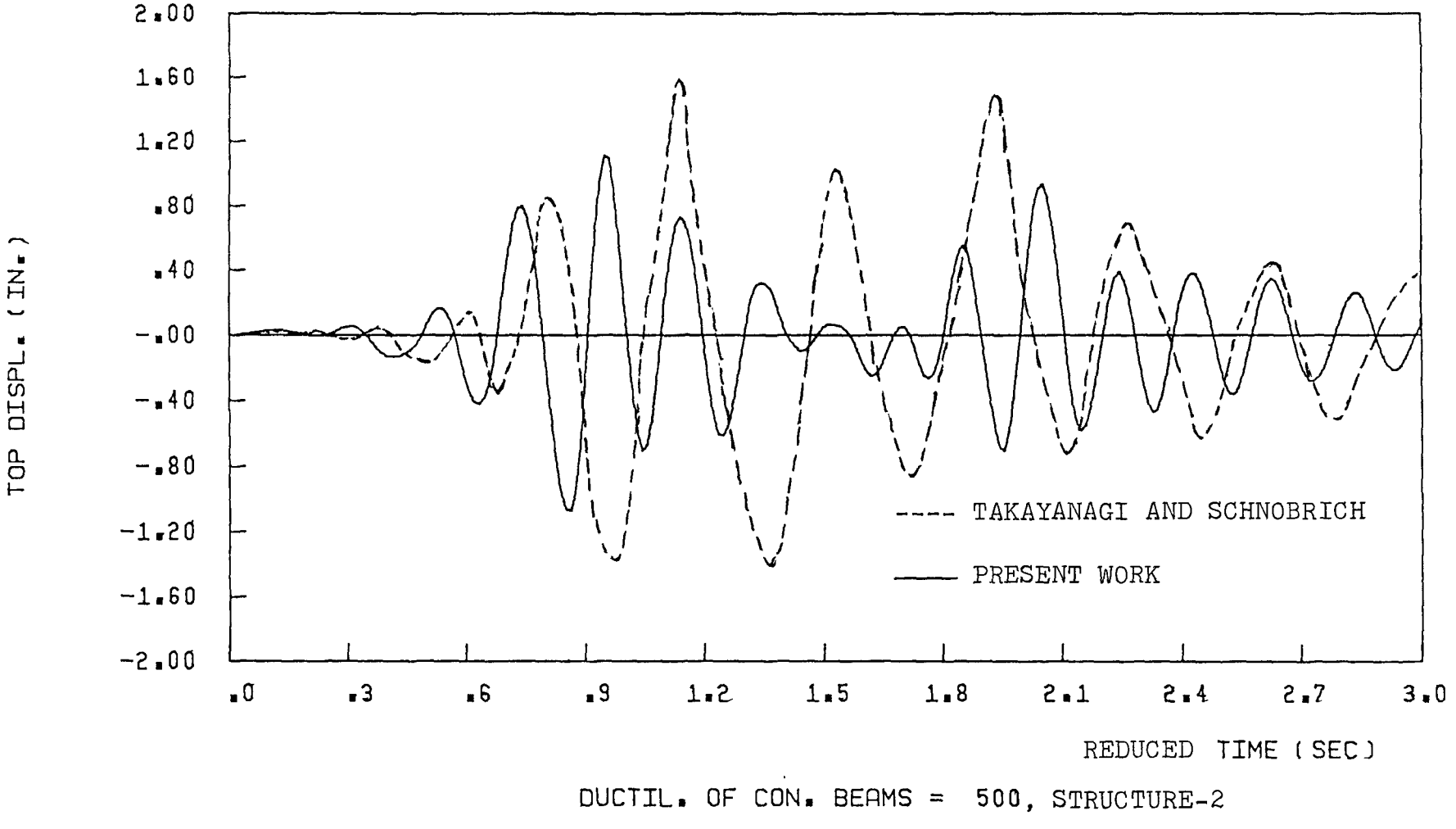

FIGURE 4-12 TOP DISPL., ELCENTRO COMP.NORTH 91 PERC. g (MOTION-2)

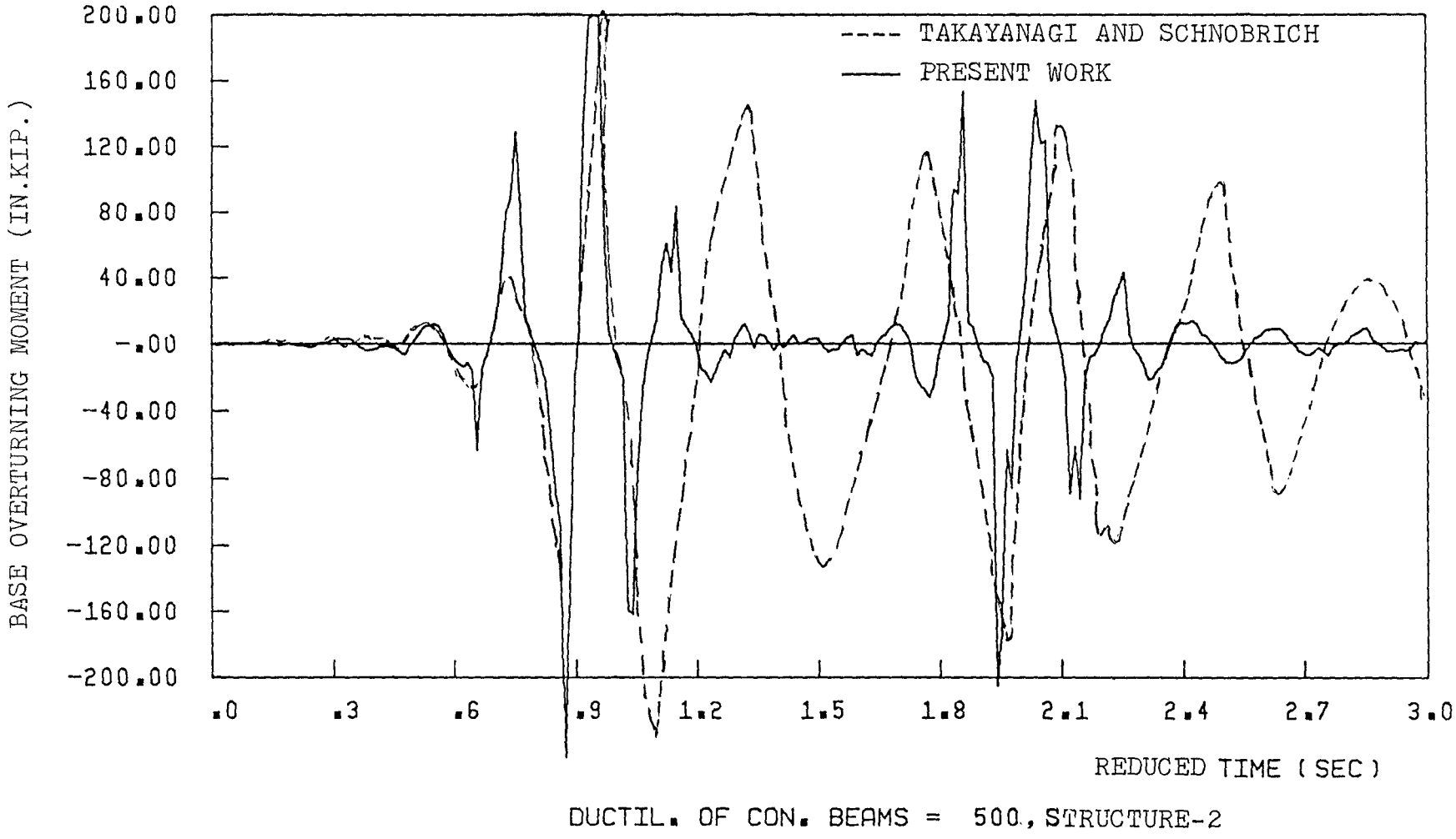

FIGURE 4-13 BASE O.T.M., ELCENTRO COMP.NORTH 91 PERC. g

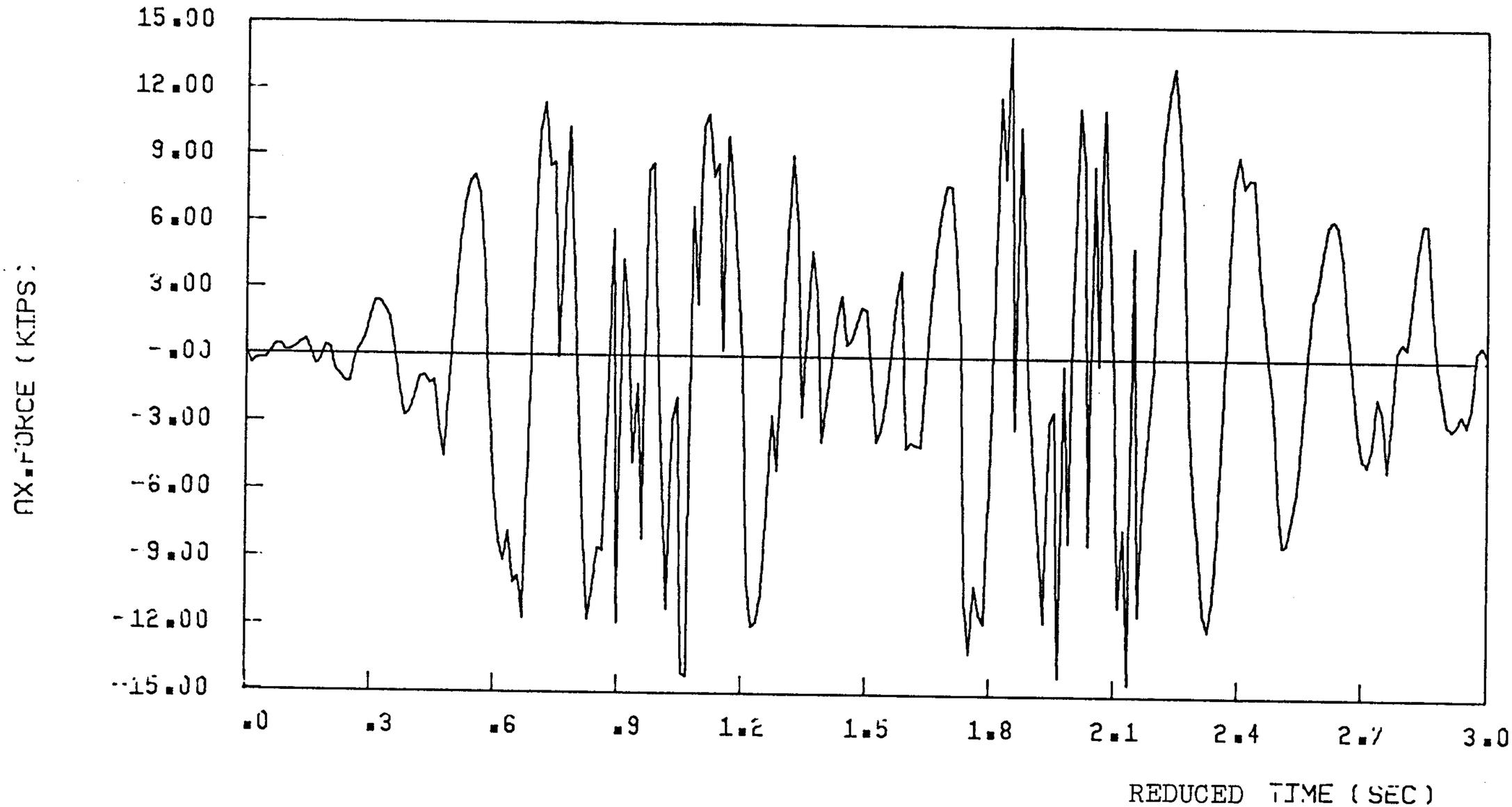

FIGURE 4-14 AX. FORCE, ELCENTRO COMP.NORTH 91 PERC. g (MOTION-2)

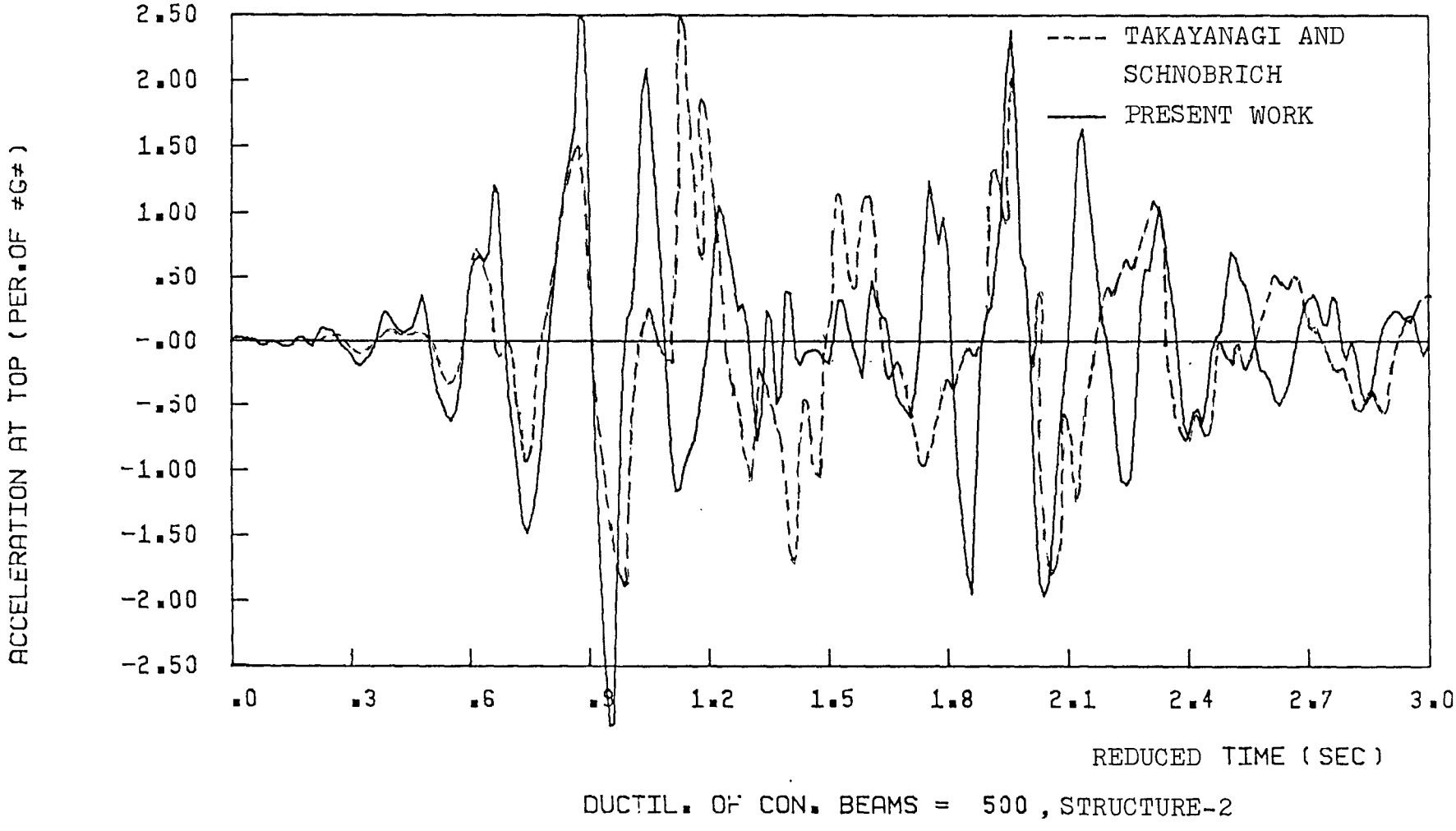

FIGURE 4-15 TOP ACCELERATION, ELCENTRO COMP.NORTH 91 PERC. g (MOTION-2)

component. But these waveforms are produced by the earthquake simulator at the University of Illinois using modified El-Centro (1940) N-S component as an input. Figure (4.16) shows the waveform of motion-1 used by Takayanagi and Schnobrich [30] and the modified waveform of El-Centro (1940) N.S component used in the present analysis. Both waveforms here are plotted with the same scale and it shows that these two responses are not exactly the same. This, probably, is the reason for the difference in the time-history responses obtained in present work and those obtained by Takayanagi and Schnobrich.

Considering the assumptions in the present analysis as against the overall complexity in the behaviour of the elements of the coupled shear wall, the material properties and the analytical procedure of Takayanagi and Schnobrich [30], it is felt that the present analytical procedure gives a reasonable description of the inelastic dynamic behaviour of the coupled shear walls. This comparison with the work of Takayanagi and Schnobrich provides a good check on the correctness and accuracy of the present method of analysis.

4.3 OBJECT OF INVESTIGATION

After checking the correctness of the present analytical method and the computer program, the behaviour of an interior and an exterior coupled shear wall, representative of those found in the coupled shear wall building, is studied in the following sections of this chapter.

The dynamic analysis of one coupled shear wall has been done previously by El-Shafee [9]. But in the present analysis a different

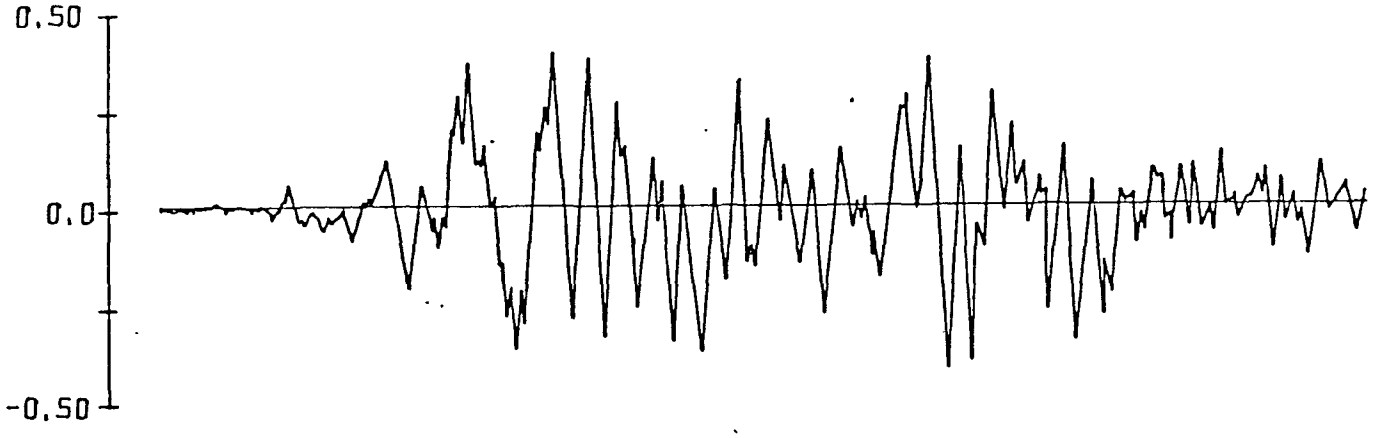

(a) BASE MOTION — 1

(TAKAYANAGI - SCHNOBRICH)

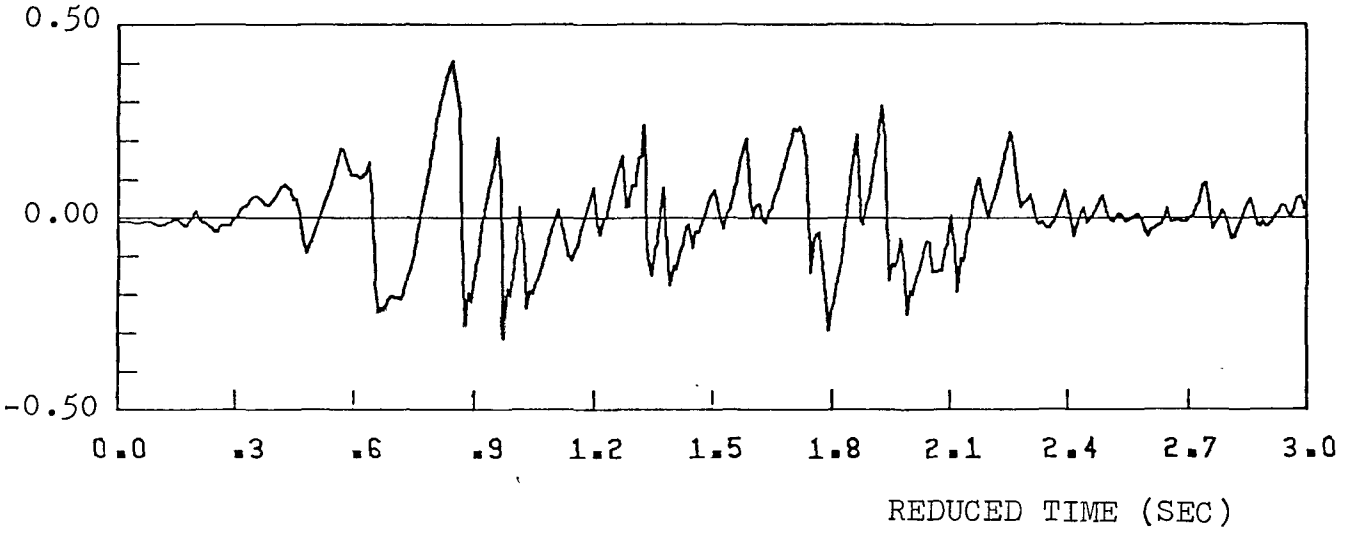

(b) BASE MOTION-1 (PRESENT WORK)

FIGURE 4-16 COMPARISON OF BASE MOTION-1

state vector is used. This state vector $\{y\ y'\ y''\ y'''\ T\ q\}$ gives a direct appreciation of the behaviour of the coupled shear wall as the parameters of the interest, namely, axial force (T) and shear force intensity (q), are given explicitly by this state vector. Also in the future formulation of two interconnected coupled shear wall problem this representation of the state vector is more convenient, as will be discussed in later chapters.

4.4 COUPLED SHEAR WALLS

Consider a multi-storey flat slab-shear wall building. It is assumed that the building is symmetrical in plan and consists of a series of planar coupled shear walls. It is assumed that all internal coupled shear walls are identical and also the two end coupled shear walls are the same. In addition, it is assumed that the internal walls are coupled by the floor slabs, while the exterior end walls are coupled by stiff connecting beams. The building is a twenty storey coupled shear wall-flat slab structure. The walls of the structure, the storey height and the connecting beam stiffnesses are constant throughout the height. The walls are assumed to rest on a rigid foundation. Figure (4.17) shows the plan and the wall dimensions of the building. The shear walls of this building under study are same as those considered and designed by El-Shafee [9]. The dimensions, reinforcement and capacities are given in Table 4.8 and Figs. (4.18) and (4.19). The walls are designed to resist an acceleration ratio A = 0.16 according to NBCC 1975 [16]. Since the building is symmetrical, its

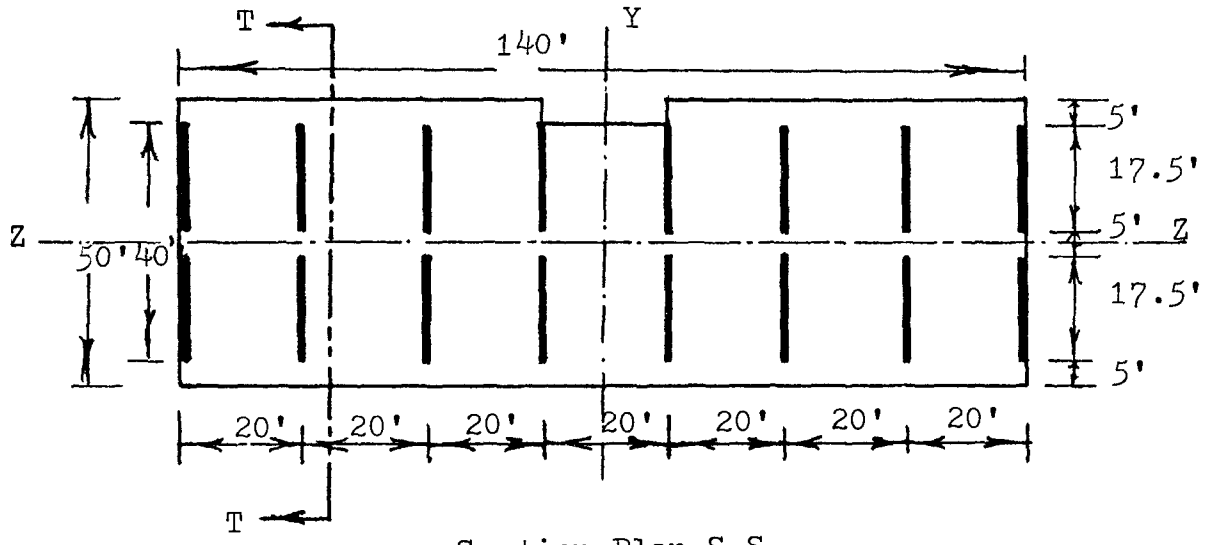

a. Section Plan S-S

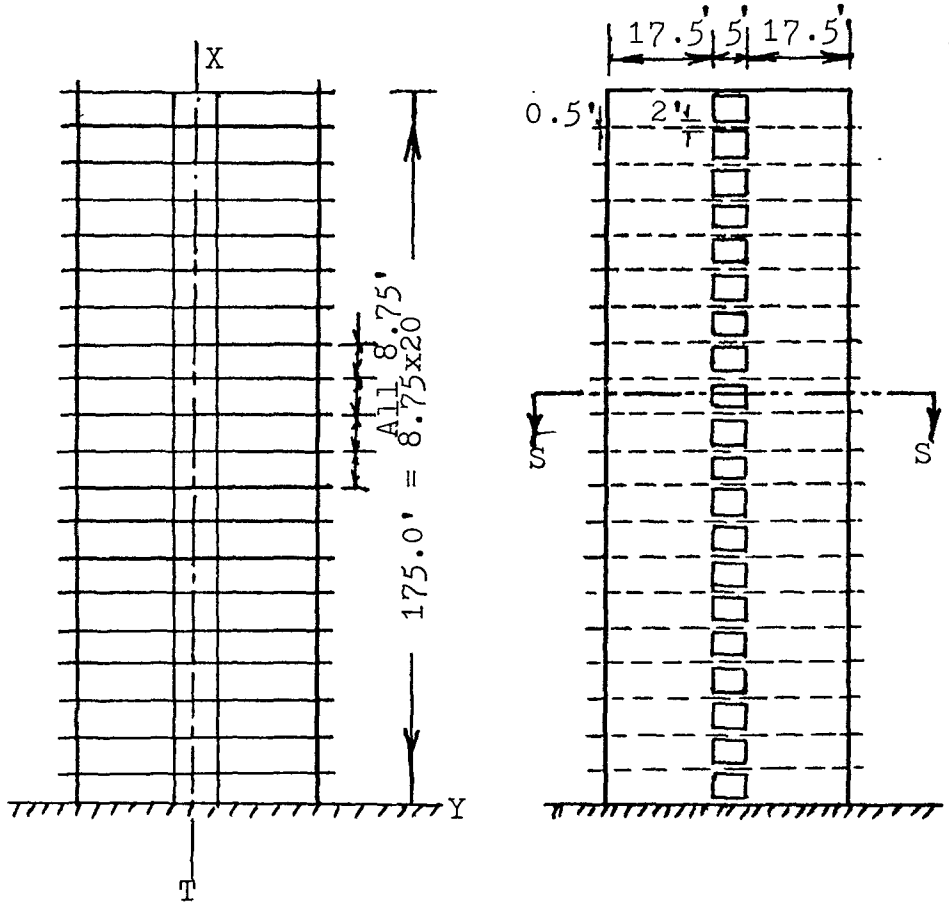

b. Section T-T

c. End View

FIGURE 4.17 OVERALL DIMENSIONS OF SHEAR WALL BUILDING

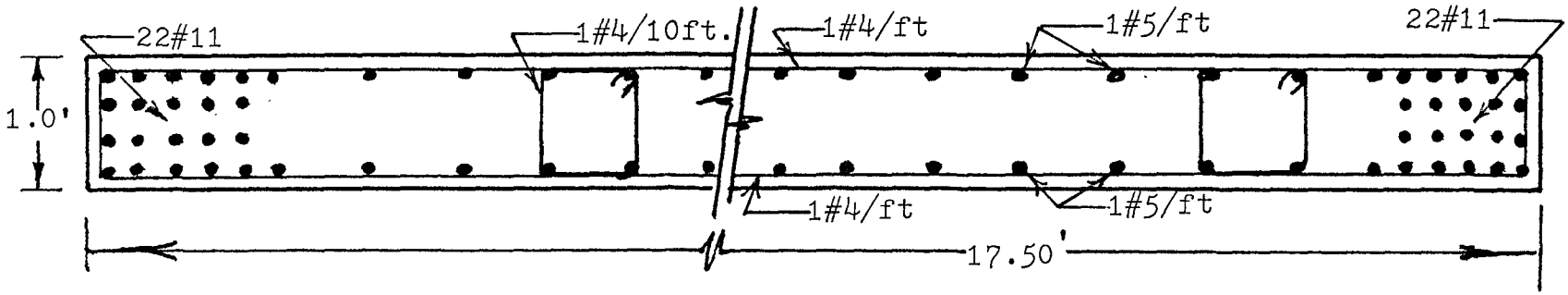

Detailing of Base Cross Section of Pier

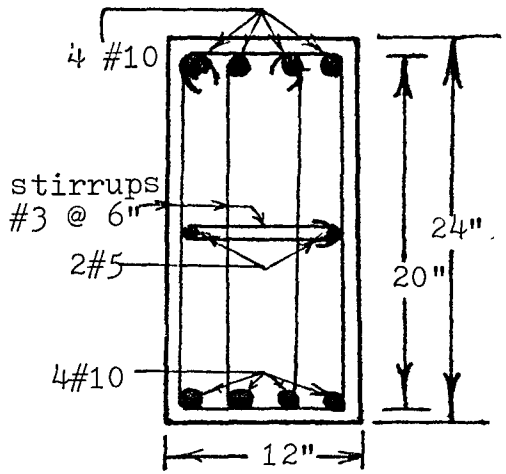

Conn. Beam Cross Section

FIGURE 4-18 REINFORCEMENT DETAILS, EXTERIOR SHEAR WALL (20 STOREY)

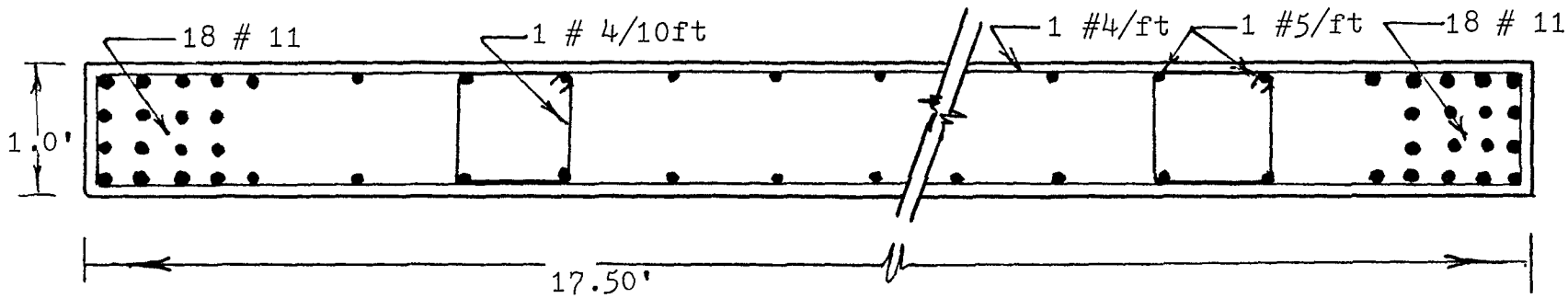

Detailing of Base Cross Section of Pier

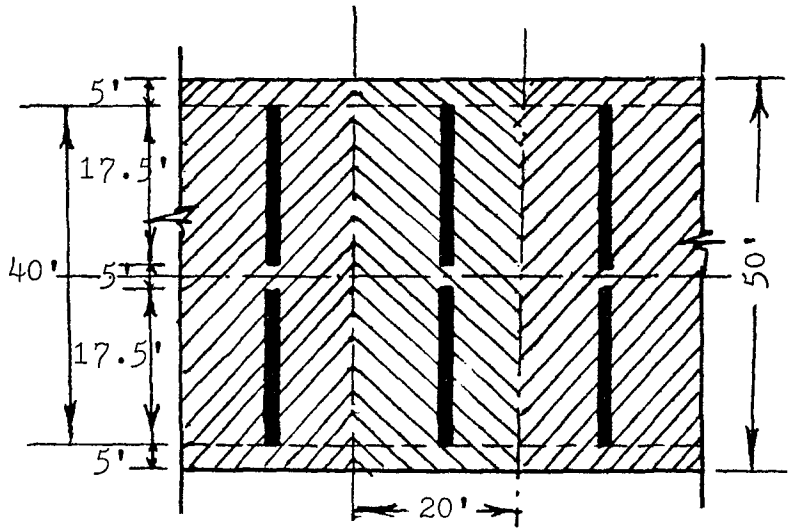

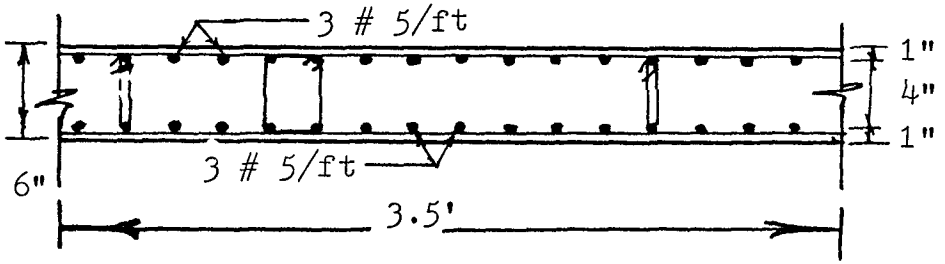

Conn. Slabs of Interior Walls

FIGURE 4-19 REINFORCEMENT DETAILS, INTERIOR SHEAR WALL (20 STOREY)

overall behaviour can be understood by studying the responses of a typical interior coupled shear wall and a typical exterior coupled shear wall.

WALL	Wall Thickness	Connecting Beam depth	Connecting Beam Reinf.		Wall Reinf.		Shear Capacity q_p	I_b / f_t^4
			Asb	Perc.	Asw	Perc.		
Exterior	12	24	4#10	1.70%	22#11	1.20%	20.0	0.56
Interior	12	6*	3#5/ft	1.27%	18#11	1.06%	2.68	0.0235

* Effective connecting slab width = 3.5 ft

Table 4.8 Dimensions, Reinforcement and Capacities of Exterior and Interior Walls of the Example Building

4.4.1 Dynamic Modeling of Interior and Exterior Coupled Shear Wall

The dynamic model for the exterior and interior wall is given in Fig. (4.20).

For buildings with rigid floor diagrams, the lateral loads caused by the ground acceleration are distributed according to the stiffness of the lateral force resisting elements. In order to have the building to vibrate as a unit, it is necessary to have the mass of the complete structure being distributed in proportion to the stiffness of the walls as shown in Fig. (4.20). Table 4.9 gives the periods of the exterior and interior walls of the twenty storey building. The masses of the walls are assumed to be distributed uniformly throughout the height in accordance with the wall stiffnesses, and then lumped into five masses.

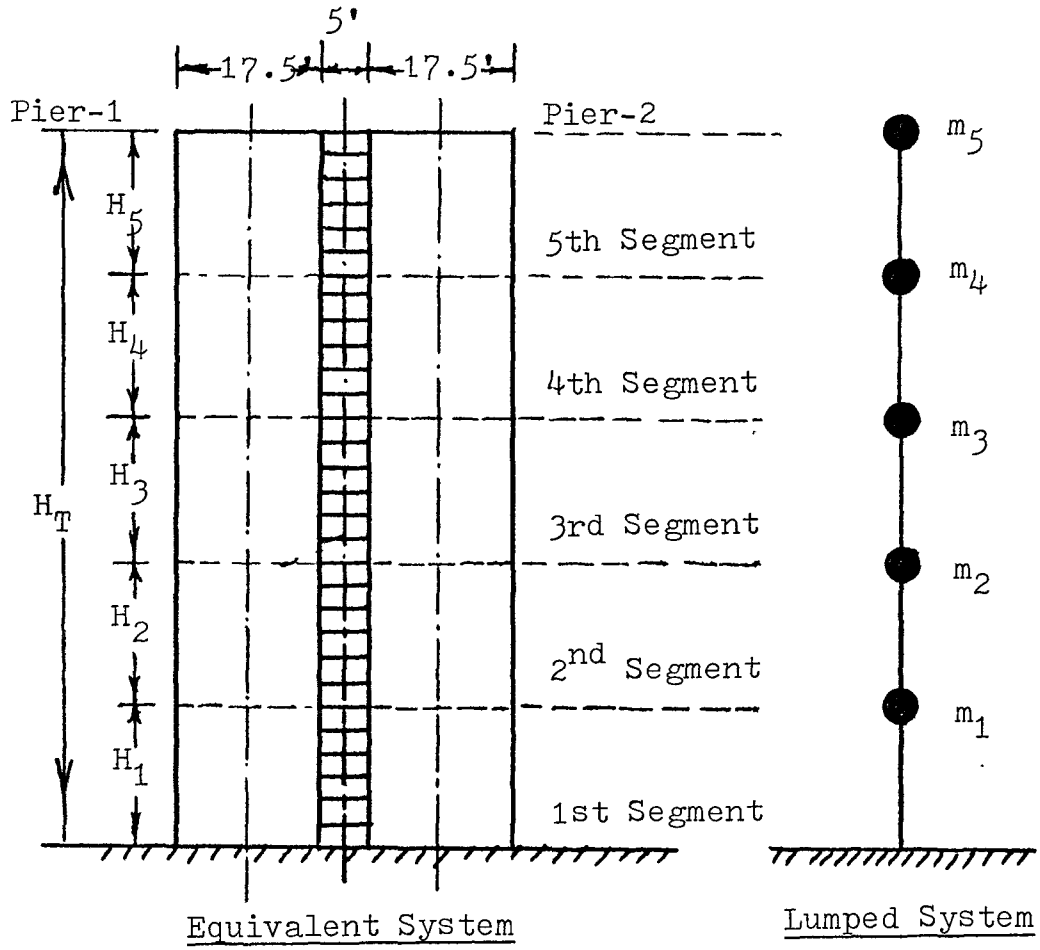

$H_1=H_2=H_3=H_4=H_5=$ 35.0'

$H_T=175'$

Walls	$m_1=m_2=m_3=m_4=m_5$;Mass (Kips-sec^2/ft)	
	For Mass Matrix	For p-Δ Effect
Exterior Wall	40.148	17.884
Interior Wall	16.985	24.412

FIGURE 4-20 DYNAMIC MODEL OF EXTERIOR AND INTERIOR SHEAR WALL

MODE	1	2	3	4	5
(1) Exterior wall	1.48 sec	0.290 sec	0.121 sec	0.072 sec	0.053 sec
(2) Interior wall	1.48 sec	0.305 sec	0.114 sec	0.060 sec	0.041 sec
$\frac{(2)}{(1)}$ X100	100%	105%	94.2%	83.3%	77.4%

Table 4.9 Corresponding Periods of the Walls of Twenty Storey Building

From the table above, it is seen that the fundamental periods of the two walls are the same. However, the periods of the other modes are different. The difference between the corresponding periods increases as the mode number increases. This is because the end walls with the stiffer connecting beams behave differently from the interior walls for higher modes of vibration. To obtain the identical periods for all modes in the two walls, it would become necessary to distribute the masses nonuniformly along the height of each wall. For simplicity the masses are taken to be distributed uniformly along the height of the walls in proportion to their stiffness in this chapter.

4.4.2 Seismic Response

In this section the seismic responses of an exterior and an interior coupled shear wall of the twenty storey building are presented.

The parameters of the interest are:

(i) Top Displacement

The study of the top displacement is essential for understanding the overall behaviour of the structure. The flexibility of the structure is proportional to the top displacement and the overall

ductility of the structure can be calculated from the top displacement.

(ii) Base Moment of the Piers

The most critical section for the piers is at the base. The base moments in the left and right piers in combination with the couple arised from the axial force in the piers are responsible for resisting the external overturning moment at the base caused by the seismic loads. The piers of both shear walls are identical, so that the bending moment of the left pier will be same as the bending moment of the right pier. Hence only the bending moment at the base of one pier is presented in the present work. As the base moment in each pier is affected by the axial force in the piers, this moment is sensitive to the condition of the connecting beams.

(iii) Axial Force at the Base of Piers

As the axial force is the integration of the shearing force intensity in the laminae, it is directly affected by the changing of the connecting beams state. When the dead load is included in the axial force, the resultant net axial force at the base of each pier can be obtained.

These parameters are used to evaluate the performance of the structure under seismic excitation. The shearing force intensity in the connecting laminae is also presented in some cases to clarify the behaviour, especially when large inelastic deformations occurred in the connecting laminae.

The El-Centro (1940) N.S component earthquake record is used in the present analysis. This record is normalized to the maximum horizontal acceleration of 16% g and 32% g. In the present work these two normalized records will be called as "moderate" and "severe" earthquake, i.e.,

	Maximum Acceleration	Duration
Moderate Earthquake	16% g	15.0 sec
Severe Earthquake	32% g	15.0 sec

The typical waveform is shown in Fig. (4.21).

The modal critical damping ratios are taken as: $\xi_1 = 4\%$, $\xi_2 = 5\%$, $\xi_3 = 6\%$, $\xi_4 = 7\%$, $\xi_5 = 8\%$.

Realistic values to account for the limited rotational ductility of the connecting beams of the two walls are considered. A very large ductility factor $\bar{\mu} = 500$ is also included to study the effect of ductility on the response.

Table 4.10 shows the details of the cases of different earthquake excitation studied for the elasto-plastic dynamic analysis of coupled shear walls.

WALL	Run No.	Earthquake Excitation	Rotational Ductility factor for the Connecting Beams ($\bar{\mu}$)
Exterior	1	moderate	500
	2	moderate	15
	3	severe	15
Interior	4	moderate	500
	5	moderate	5
	6	severe	5

Table 4.10 Summary of Assumed Conditions for Dynamic Runs

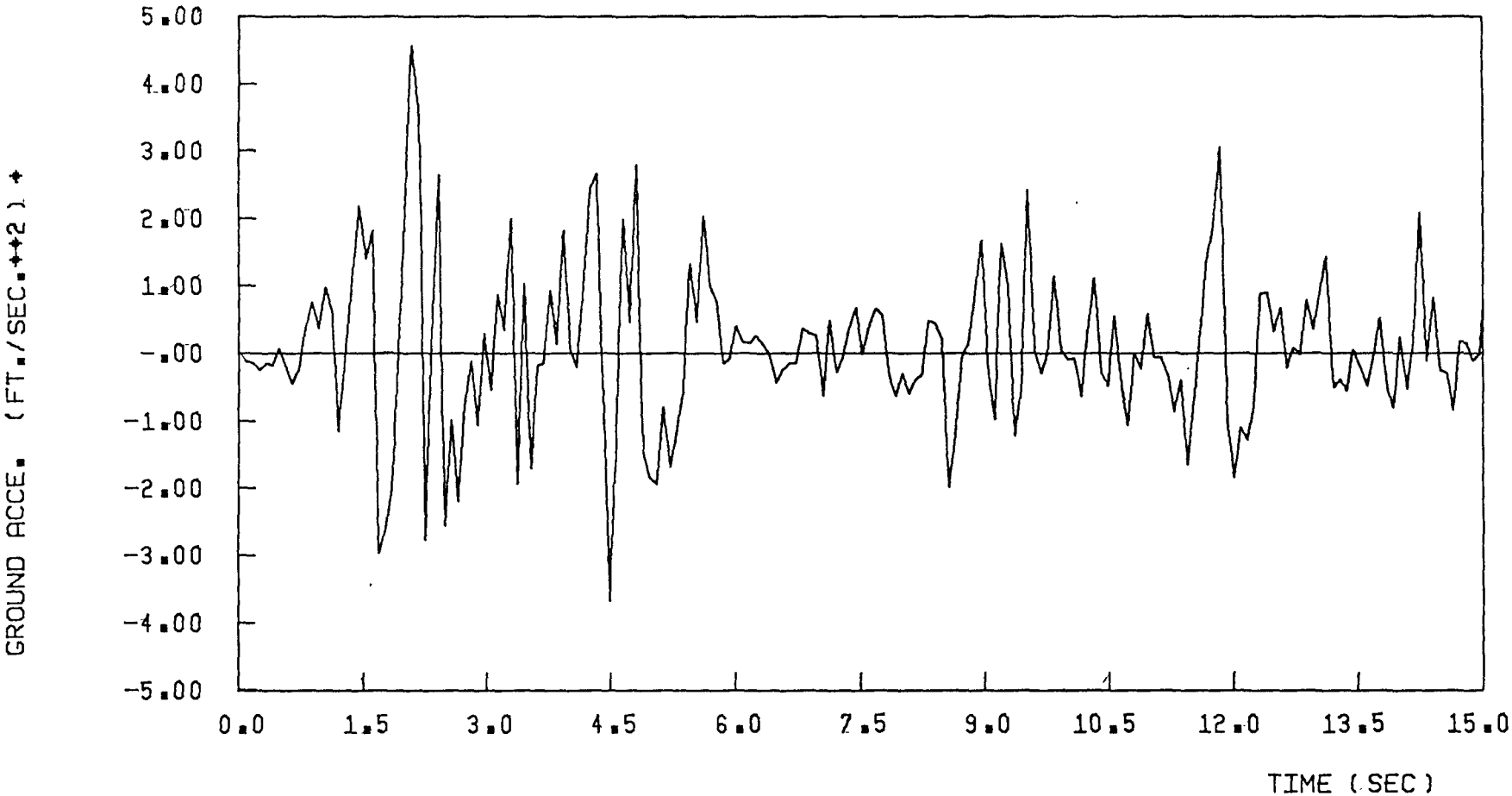

FIGURE 4-21 ELCENTRO COMP.NORTH 16 PERC. g

The responses of an interior and an exterior coupled shear walls in these different cases are compared by considering each parameter separately.

a) Top Displacement

Figure (4.22) shows the superimposed responses of an interior coupled shear wall and an exterior coupled shear wall under the moderate earthquake. This clearly shows that the top displacement responses of an exterior wall and an interior wall, under the same excitation, are identical.

Figure (4.23) compares the response of the interior coupled shear wall under moderate and severe earthquake. The intensity of the severe earthquake is twice of the moderate earthquake and this figure shows clearly that the response under severe earthquake is also twice of the response under moderate earthquake.

All these responses indicate that the top displacement is mainly due to the first mode of vibration.

b) Axial Force at the Base

Figure (4.24) shows the responses of an exterior wall under moderate earthquake excitation with the rotational ductility factor for the connecting beams as $\bar{\mu}$ = 500 and 15. The maximum axial force and overall pattern is almost similar up to 2.0 seconds. The response decreases in case of limited ductility after 2.0 seconds due to the formation of the real hinges along 40% of height of the wall. Therefore, the tensile force is reduced considerably. Figure (4.25)

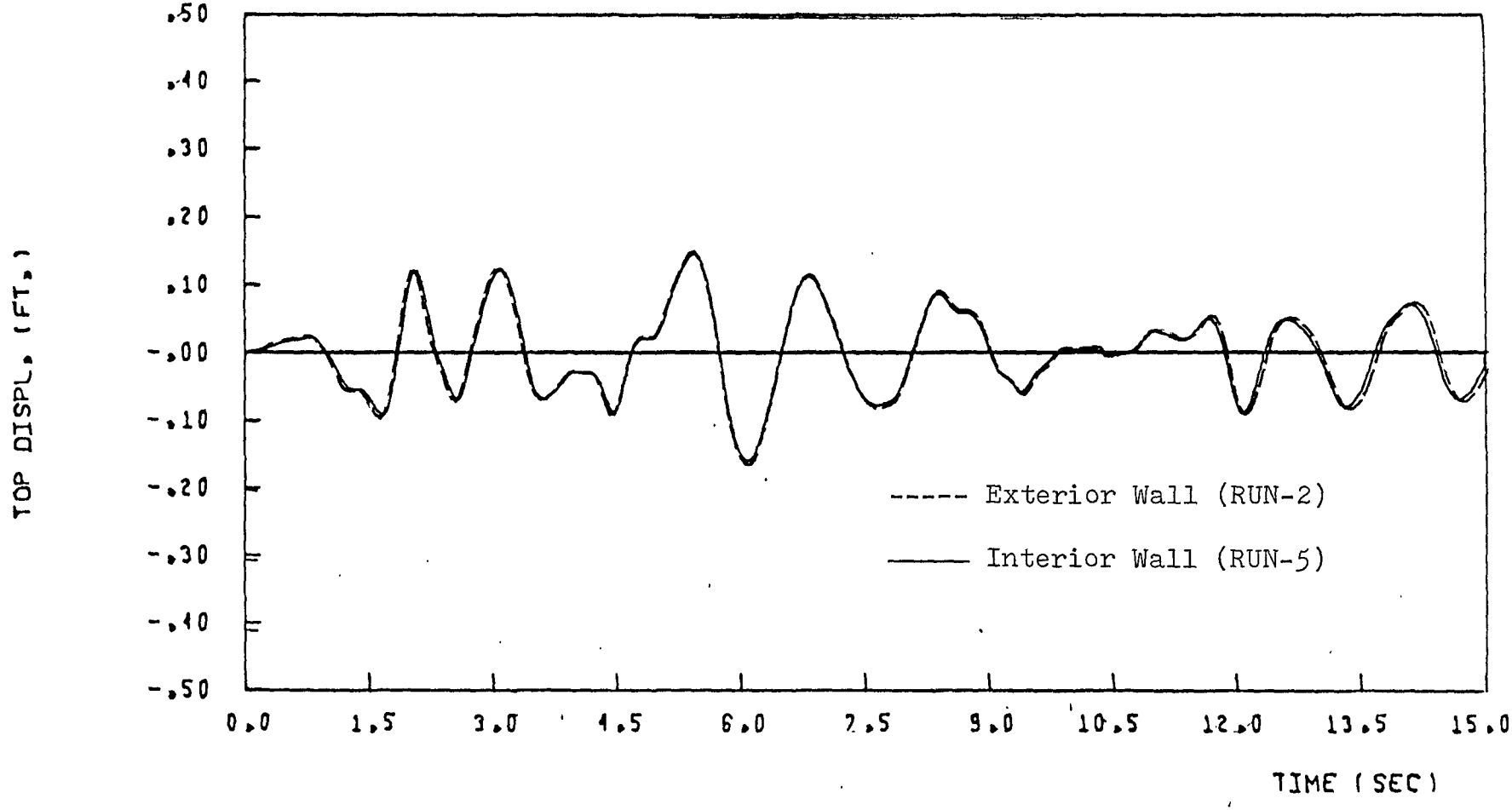

FIGURE 4-22 TOP DISPL., ELCENTRO COMP.NORTH 16 PERC. g

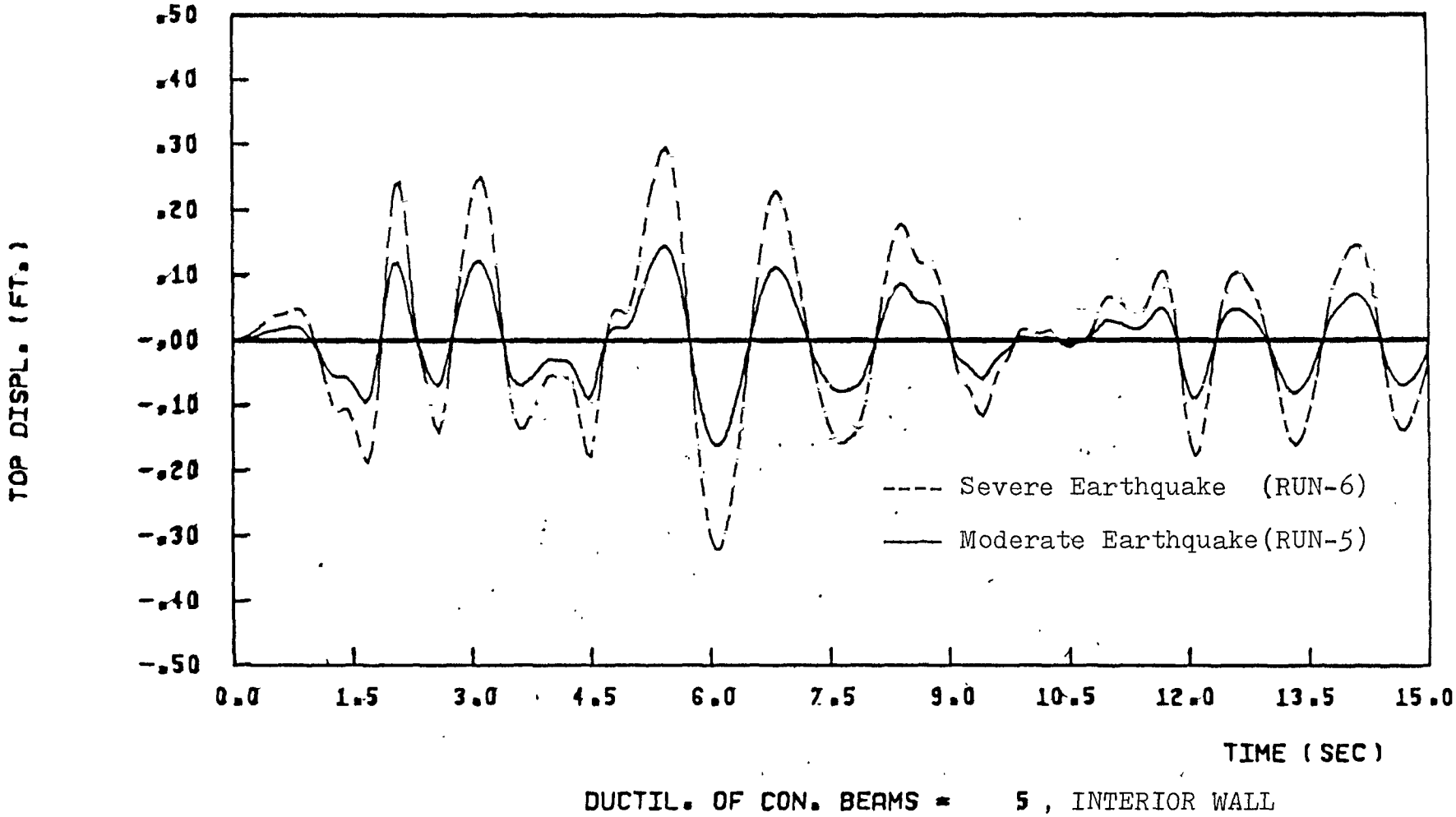

FIGURE 4-23 TOP DISPL., ELCENTRO COMP.NORTH. 16. PERC. AND 32 PERC. g

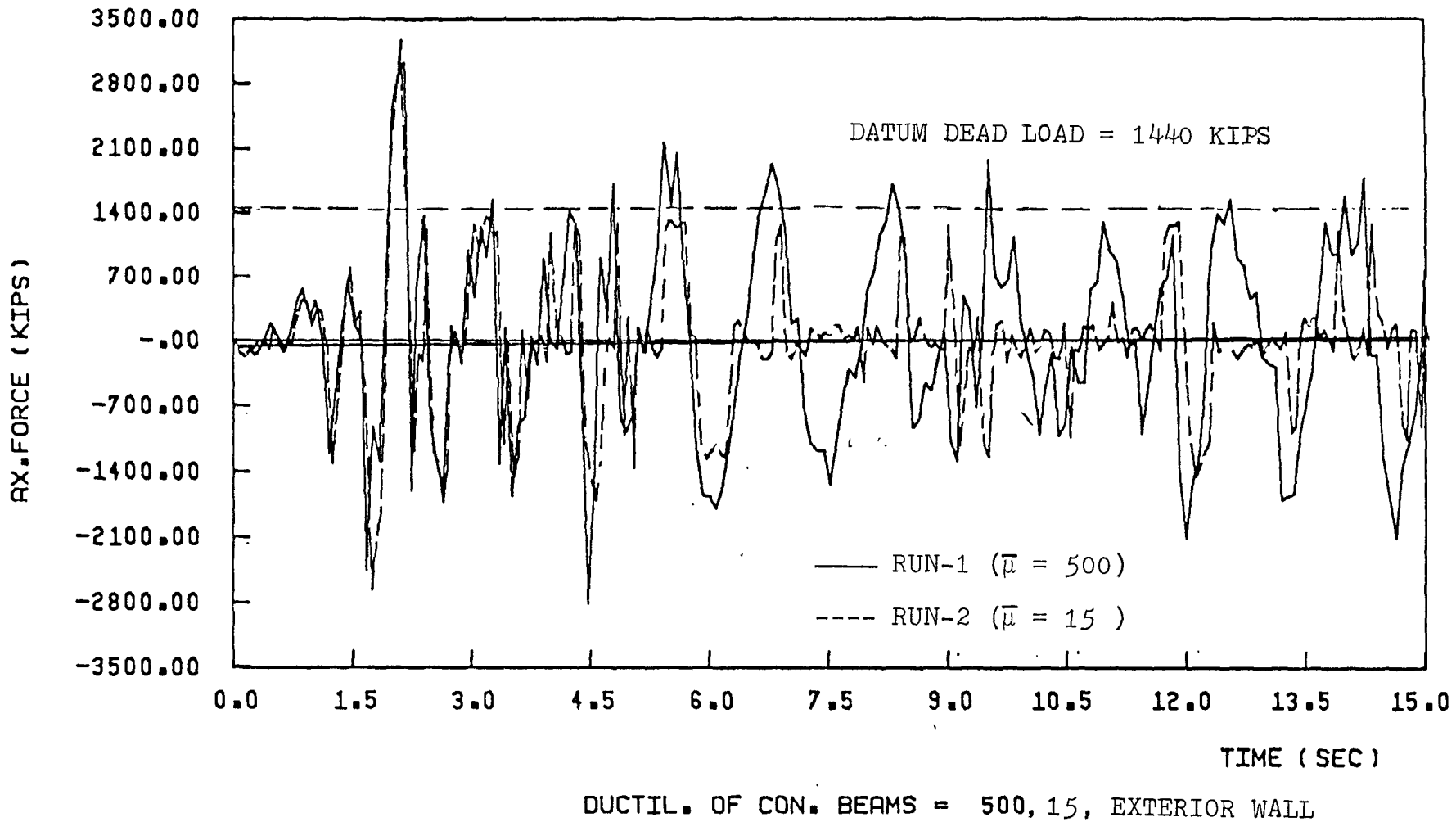

FIGURE 4-24 BASE A.F., ELCENTRO COMP.NORTH 16 PERC. g

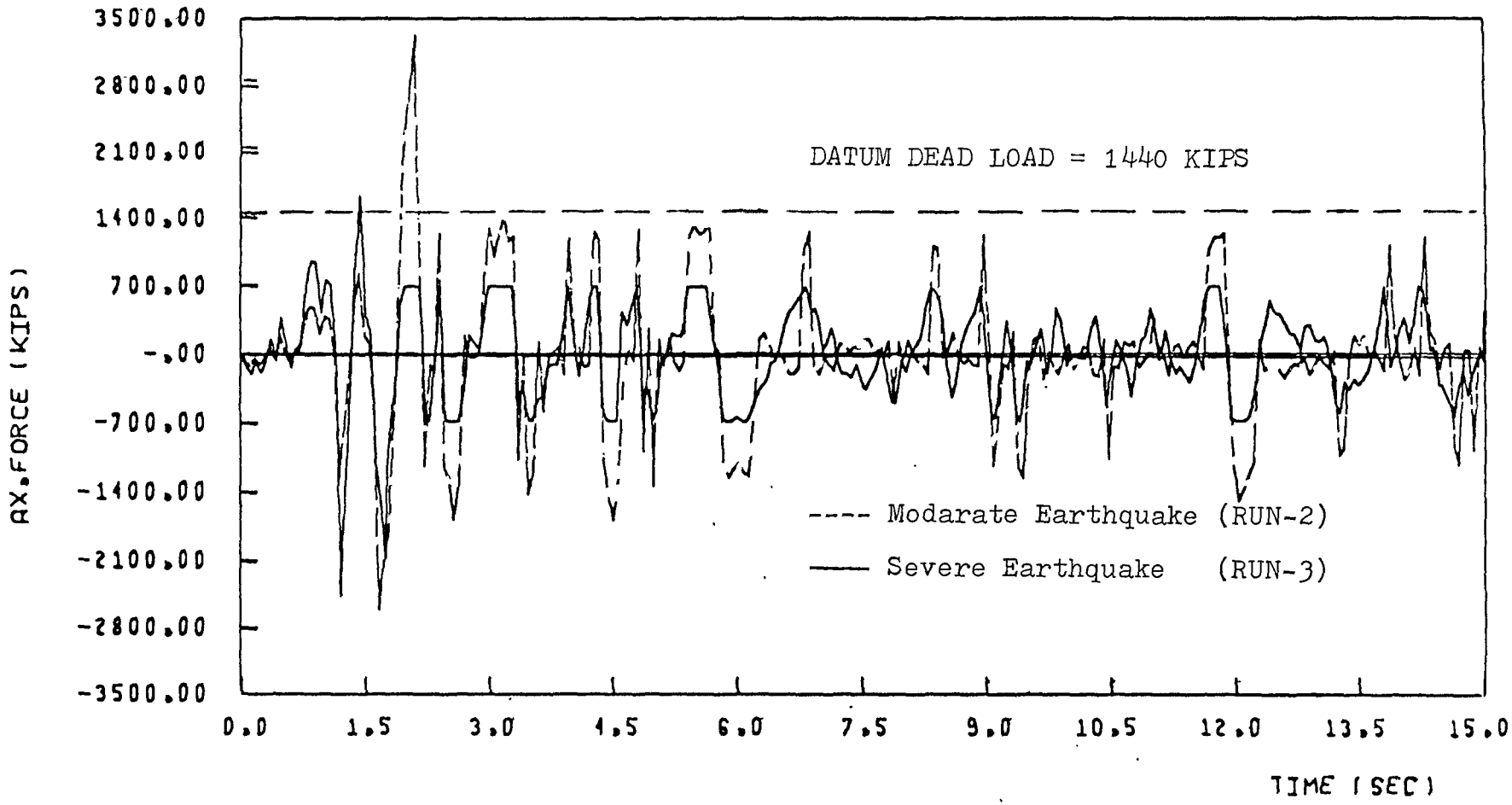

FIGURE 4-25 BASE A.F., ELCENTRO COMP.NORTH 32 PERC. AND 16 PERC. g

compares the responses of an exterior wall under moderate and severe earthquake. The waveforms in both cases are similar with higher response under the severe earthquake up to 2.0 seconds. The response under severe earthquake excitation on the other hand is less due to immediate formation of real hinges in 60% of the lintels. Figure (4.26) compares the responses of an interior wall under moderate and severe earthquake. The response under severe earthquake after 2.0 second is not exactly two fold of the response under moderate earthquake excitation. This is due to the difference in the order of plastification.

All these responses show clearly that, the axial force response contains contribution from higher modes.

c) Wall Moment at the Base of Left Pier

Figure (4.27) compares the responses of the interior wall under moderate and severe earthquake excitation. Both responses are similar in nature with the increase in magnitude of the response under severe earthquake excitation. Figure (4.28) gives the comparison between the responses of the exterior and interior wall under moderate earthquake excitation. The exterior wall response is larger than the interior wall response. This is because the forces are proportional to the inertial masses and the exterior wall is assumed to take a mass 2.4 times that of the mass ascribed to the interior wall. Figure (4.29) shows the comparison of the responses of the exterior and interior wall under severe earthquake condition. In both Figs. (4.28) and (4.29) the responses of the exterior wall are not exactly 2.4 times that of the

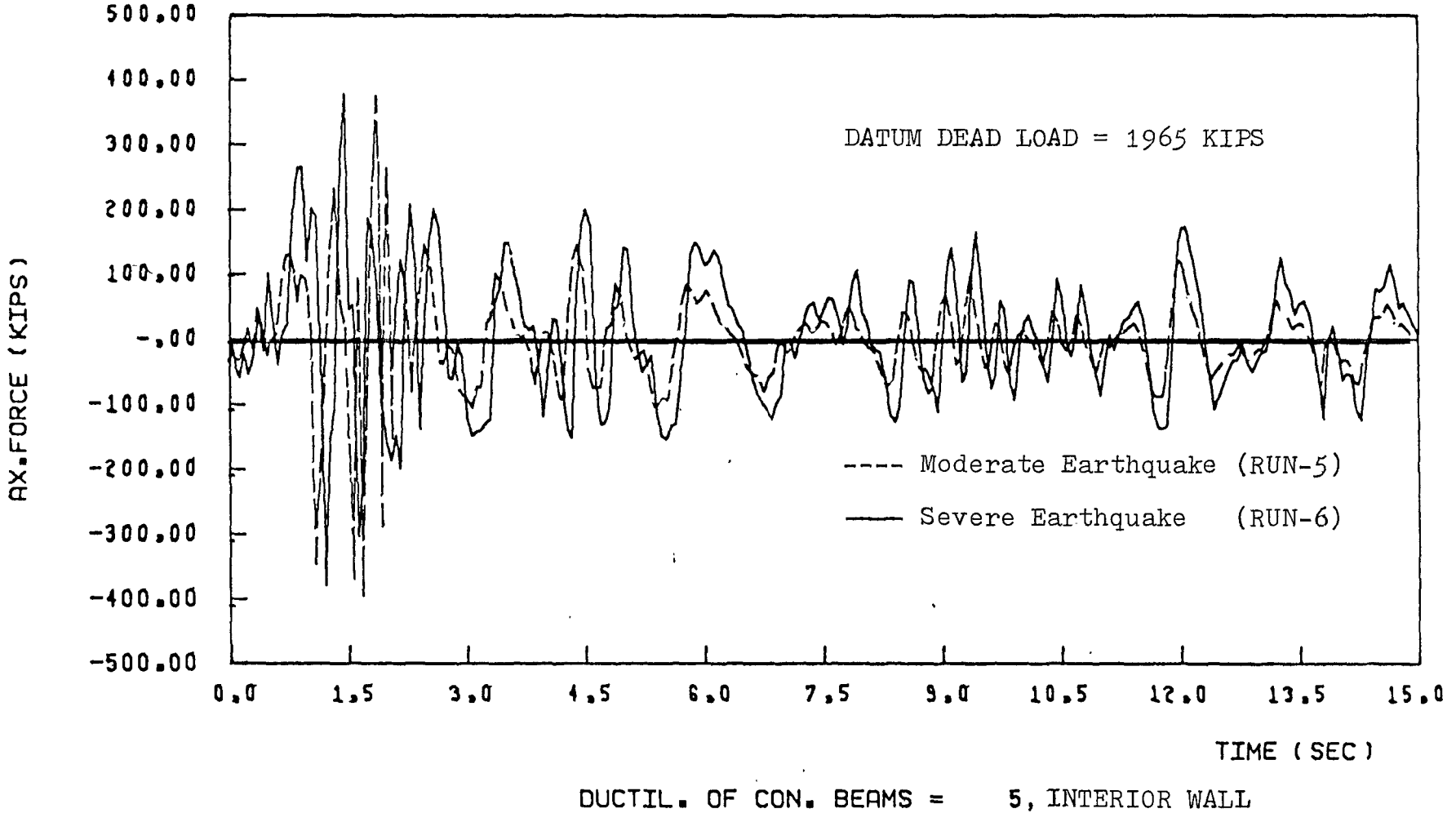

FIGURE 4-26 BASE A.F., ELCENTRO COMP.NORTH 32 PERC. AND 16 PERC. g

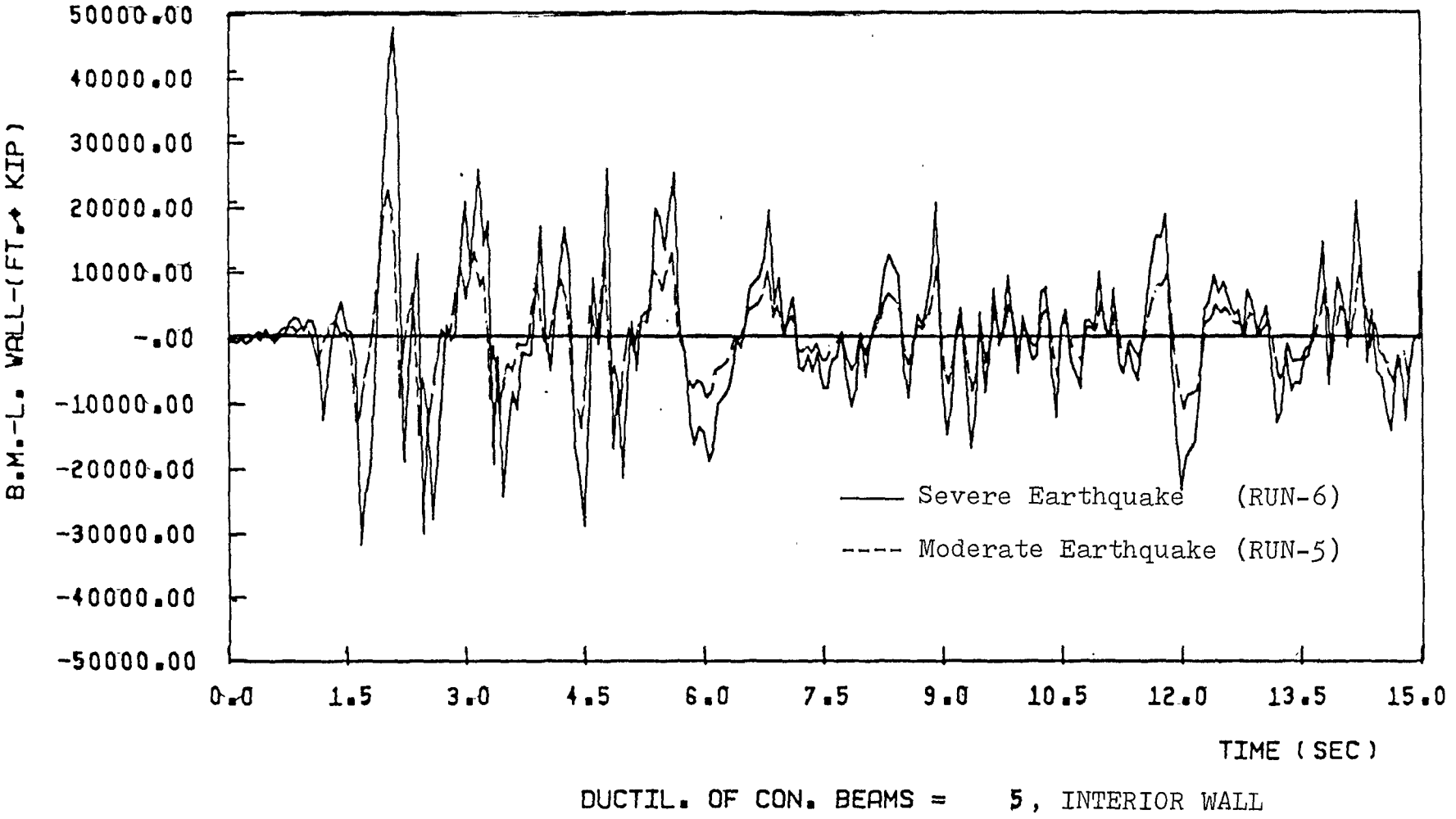

FIGURE 4-27 B.M.L. WALL, ELCENTRO COMP.NORTH. 32 PERC. AND 16 PERC. g

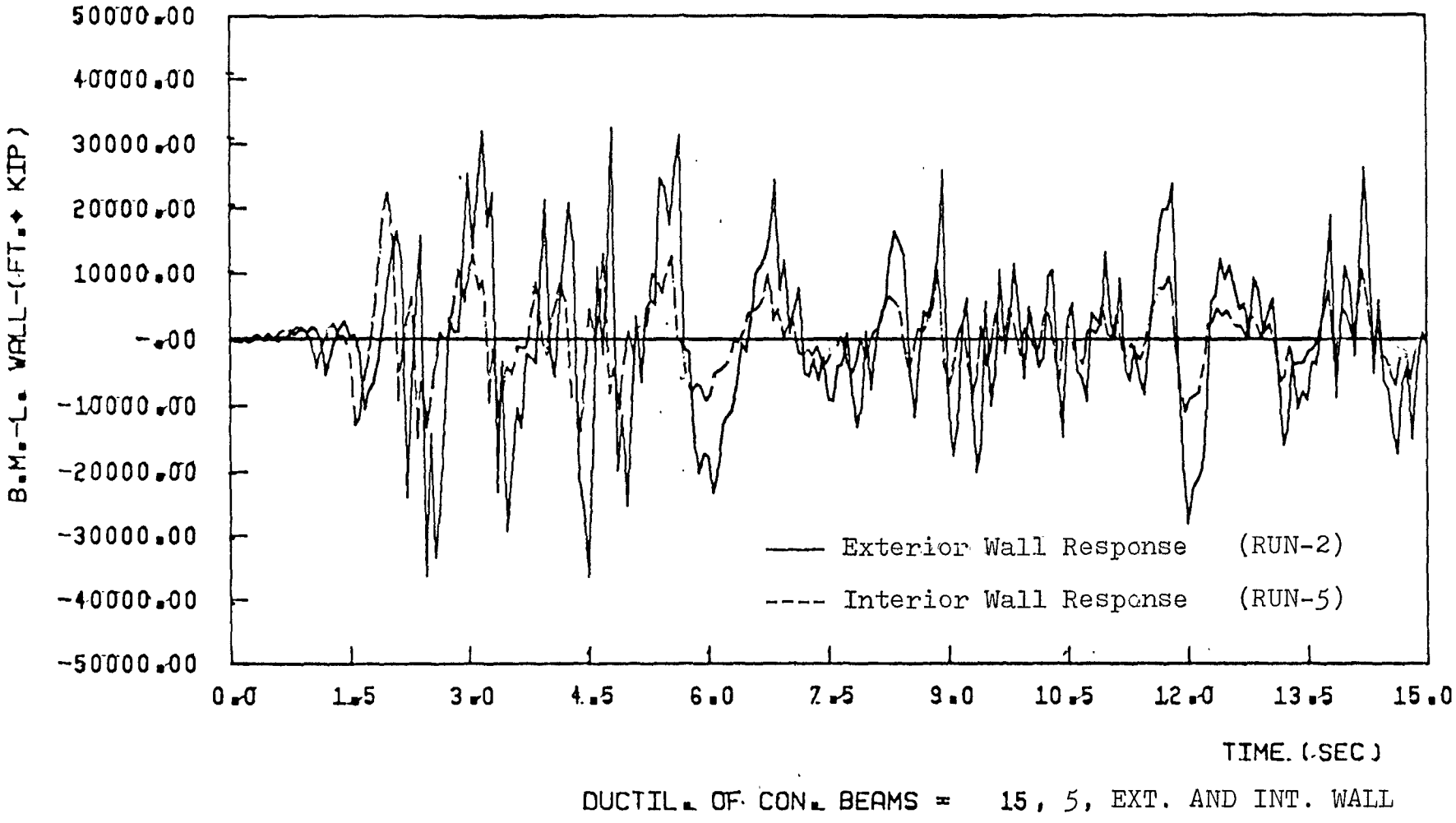

FIGURE 4.28 B.M,L.-WALL, ELCENTRO COMP.NORTH. 16 PERC. g

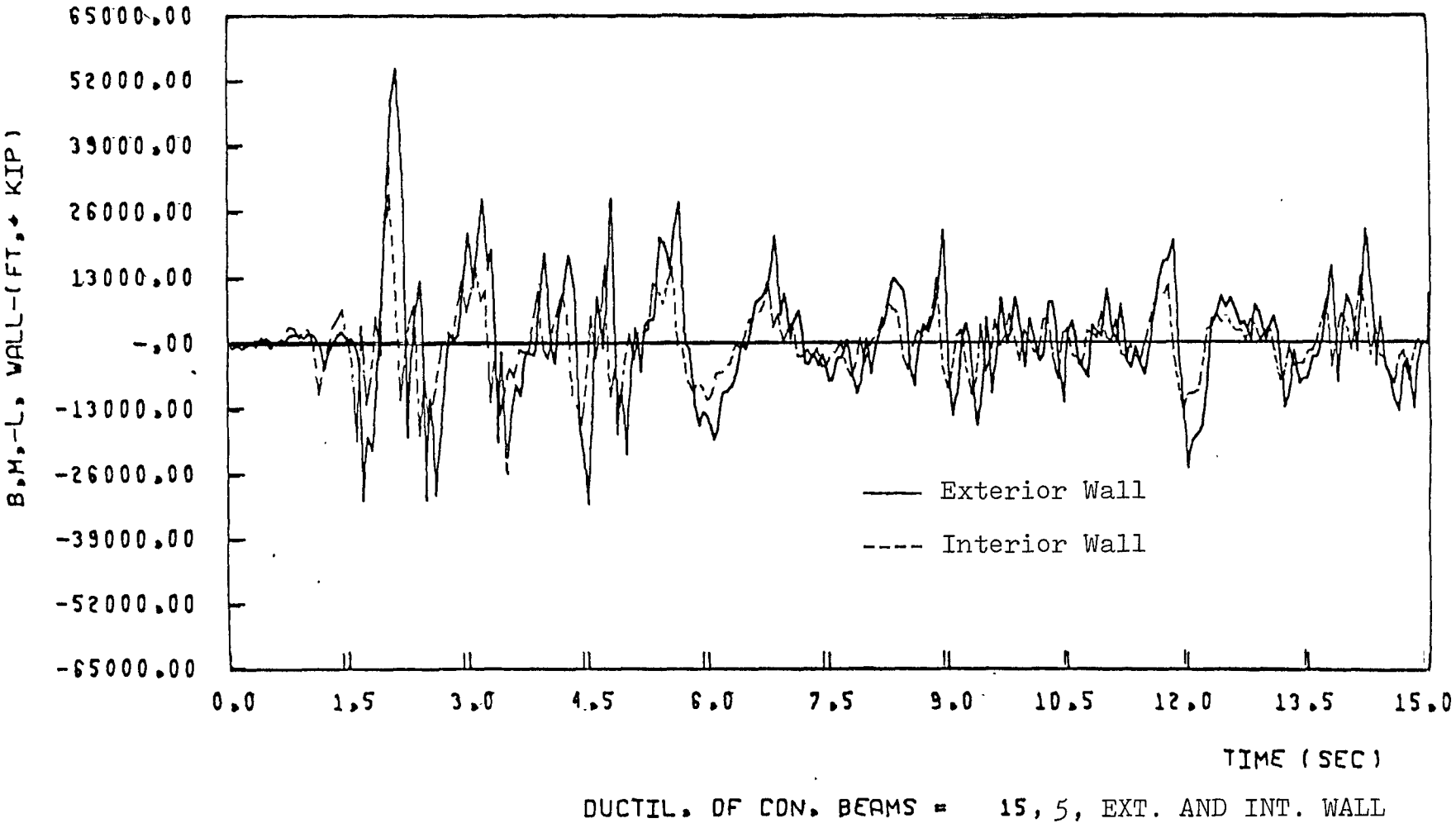

FIGURE 4-29 B.M.L.-WALL, ELCENTRO COMP.NORTH 32 PERC. g

interior wall. The difference in the order of plastification and real hinges formation may account for the difference. It is seen that the accelerations at the mass levels of the exterior wall are sometimes less than those at corresponding mass levels of the interior wall.

It should be noted from Figs. (4.27) through (4.29) that there is a sudden increase in the magnitude of moments around 2.0 seconds. This is because of the formation of the real hinges at that time, affecting the ability of the couple due to the interaction of the walls to resist the overturning moment.

d) Shear Force Intensity

Figures (4.30) through (4.34) show the shear force intensity responses of the interior wall subjected to the moderate earthquake (Run-5). These responses are limited up to the shear force intensity capacity of the connecting beams. In Figs. (4.33) and (4.34) the shearing force intensity drops to zero when the end rotation of the laminae exceeds the ultimate rotation value and the segments change to real hinged segments. The contribution of higher modes is clear in the shearing force intensity responses.

Listed below are the maximum values of the parameters of interest discussed above for the interior wall.

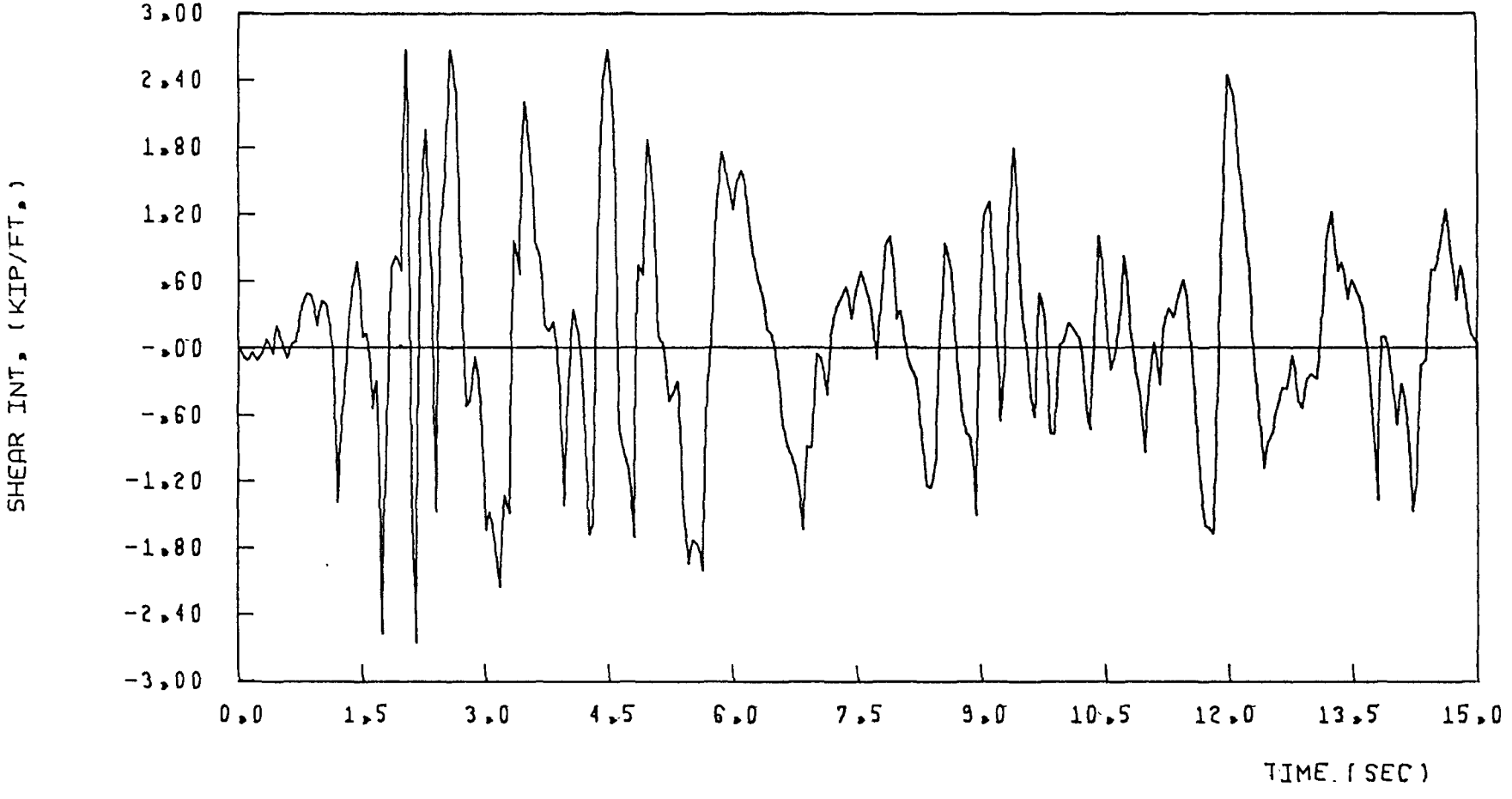

FIGURE 4-30 SHEAR INT., ELCENTRO COMP.NORTH 16 PERC. g

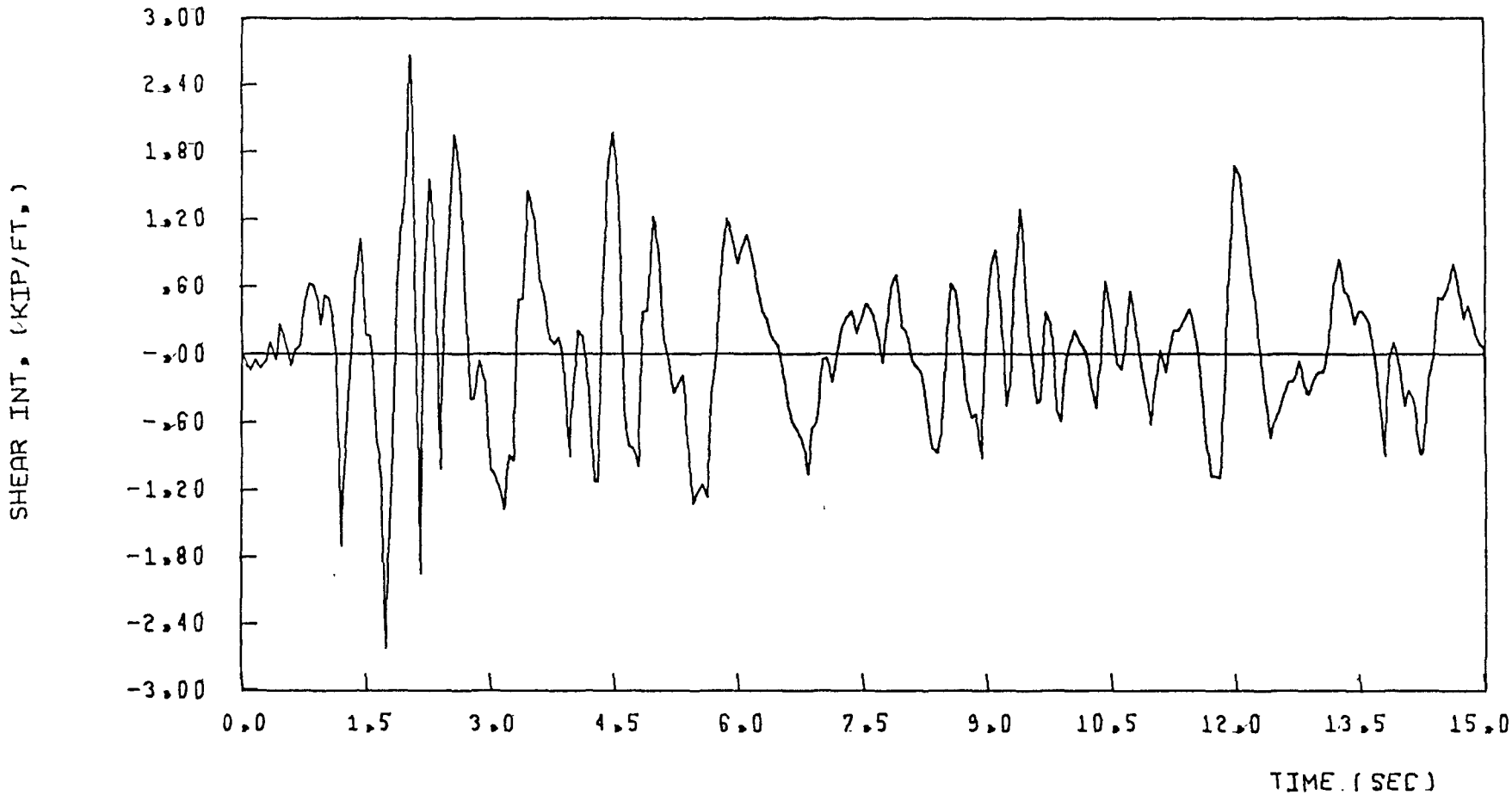

FIGURE 4.31 SHEAR INT., ELCENTRO COMP.NORTH 16 PERC. g

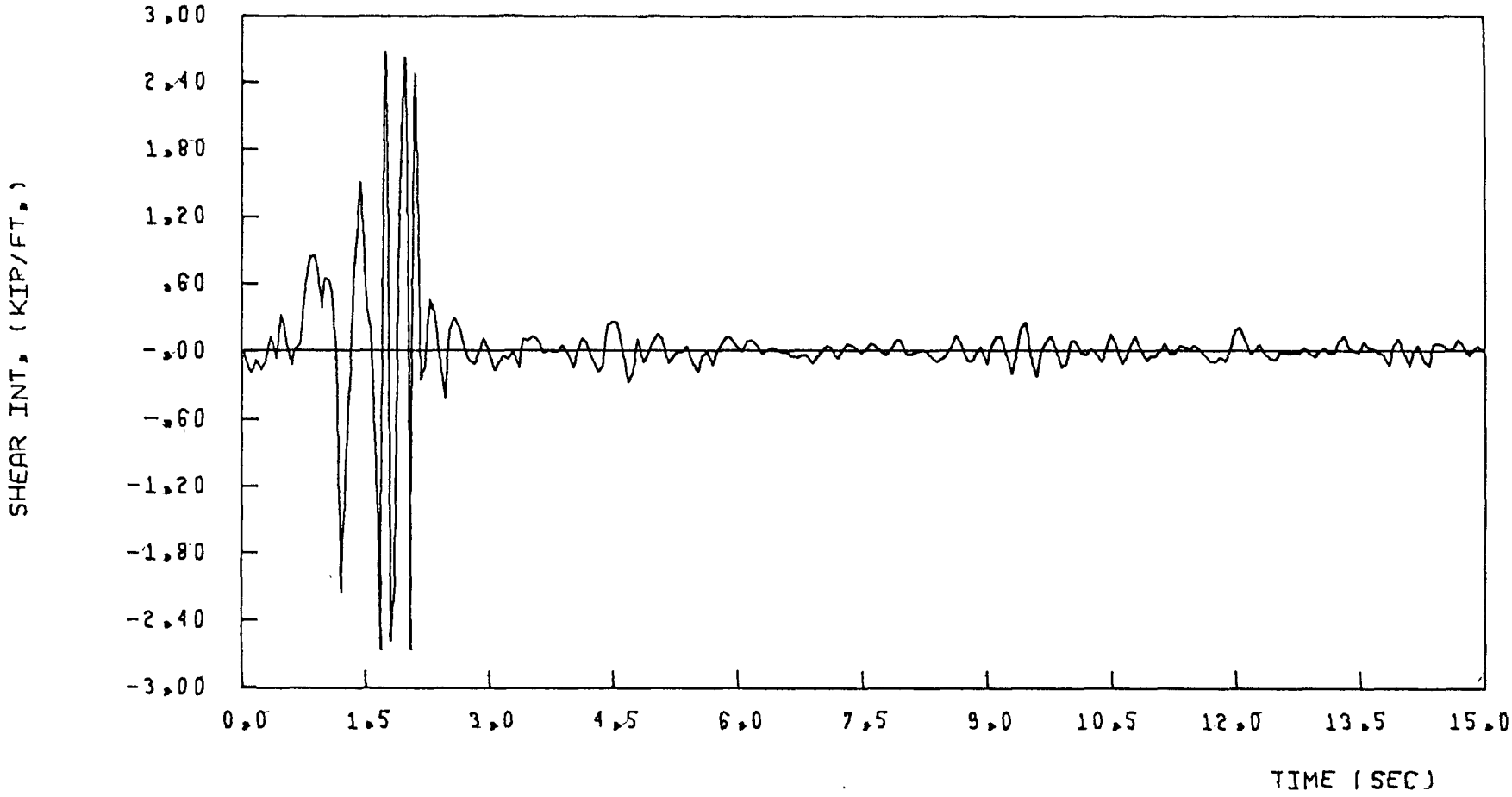

FIGURE 4-32 SHEAR INT., ELCENTRO COMP.NORTH 16 PERC. g

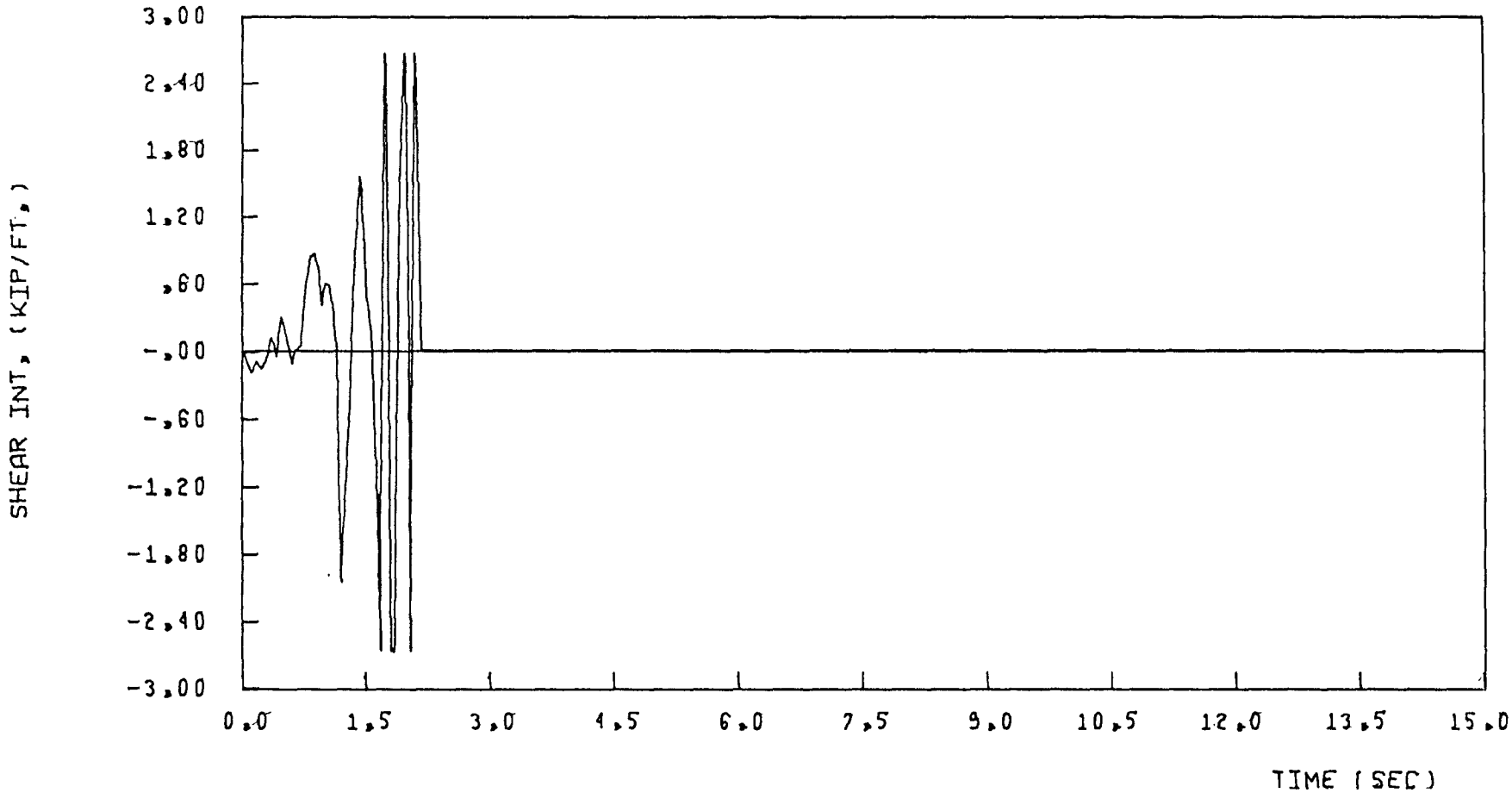

FIGURE 4.33 SHEAR INT., ELCENTRO COMP.NORTH 16 PERC. g

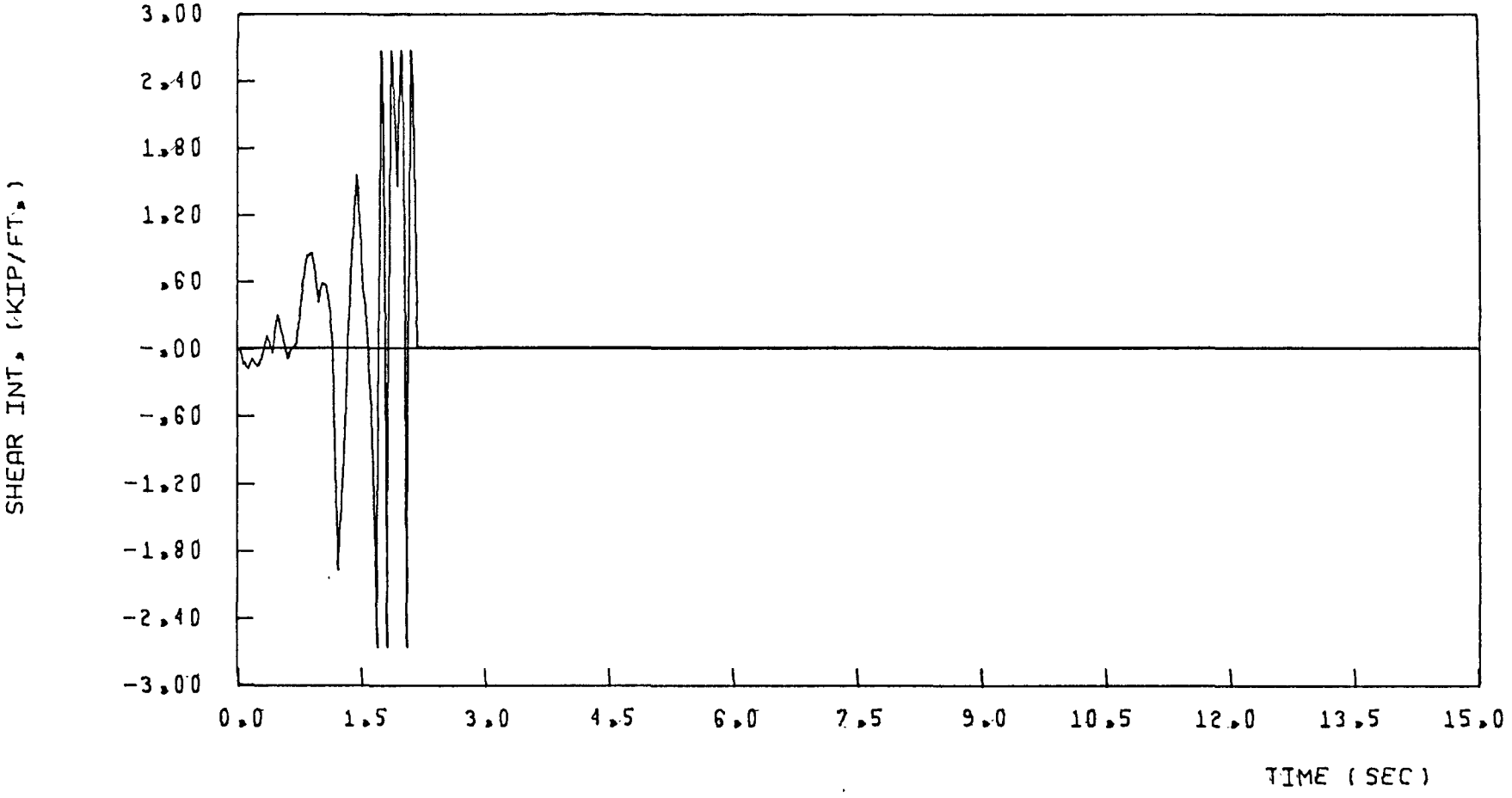

FIGURE 4.34 SHEAR INT., ELCENTRO COMP.NORTH 16 PERC. g

Maximum intensity of El-Centro earth-quake	Ductility of Conn. Beams $\frac{-}{\mu}$	Base moment (kips-ft)	Base A.F. (kips)	top deflec-tion (ft)	Np* Segment Number					NP	NR
					1	2	3	4	5		
16% g	500	14000	425	0.18	0	2	2	5	3	4	0
16% g	5	22000	390	0.18	0	3	2	2 Δ	2 Δ	3	2
32% g	5	48200	380	0.32	0	4	4	2 Δ	1 Δ	3	2

Δ: indicates the formation of real hinge

Np*: No. of plastifications of each segment during the course of the earthquake

NP: maximum number of plstic hinged segments at any instant

NR: maximum number of real hinged segments at any instant

Table 4.11 Maximum Responses of the Interior wall

It should be noted from the above table that, when the dead load (1965 kips) is included in the axial force, the piers remain under compressive forces all the time. This can be seen in the responses shown in Fig. (4.26). This is because of the relatively low shear force intensity capacity of the connecting beams and the high dead load carried by the interior walls. The high dead load arises from the large tributary area of the interior wall as shown in Fig. (4.17).

Listed below are maximum values of the parameters of interest discussed above for the exterior wall.

Maximum intensity of El-Centro earthquake	Ductility of Conn. Beams $\bar{\mu}$	Base moment (kips-ft)	Base A.F. (kips)	top deflection (ft)	Np* Segment Number					NP	NR
					1	2	3	4	5		
16% g	500	26700	2950	0.18	0	3	1	0	0	2	0
16% g	15	32500	3270	0.18	0	2 Δ	1 Δ	1	0	3	2
32% g	15	56500	2510	0.33	0	2 Δ	1 Δ	1 Δ	3	2	3

Δ: indicates the formation of real hinge

N_P^*: No. of plastifications of each segment during the course of the earthquake

NP: maximum number of plastic hinged segments at any instant

NR: maximum number of real hinged segments at any instant

Table 4.12 Maximum Responses of the Exterior Wall

It should be noted from above table and Figs. (4.24) and (4.25) that the piers may be subjected to tensile forces even after including the dead load (1440 kips). This is because the connecting beams have a high capacity to transmit shear forces between the two walls, while the tributary area carried by the end shear wall is small compared to the interior shear wall.

4.4.3 Overall Behaviour

In this section the relation between the overall ductility demand of the coupled shear walls $\bar{\mu}_{overall}$ and the connecting beam rotational ductility factor $\bar{\mu}$ is studied. The pattern of the formation of the real and plastic hinges at the connecting beams during the earthquake is also

presented in this section.

The overall ductility demand, which will be referred as "Top Deflection Ratio" (T.D.R.), is defined by

$$T.D.R. = \bar{\mu}_{overall} = \frac{\Delta u}{\Delta y} \qquad (4.1)$$

where Δu: maximum top displacement response

Δy: top displacement at the time when the segments first change from elastic to inelastic state, due to a triangularly distributed static load.

Table 4.13 indicates that the connecting beams ductility factor $\bar{\mu}$ is of minor influence when we use the definition of Δu as the maximum top displacement. It should be noted that the maximum value may occur after the formation of the real hinges in the connecting beams when the structure becomes more flexible.

Ground Acceleration	WALL	Ductility of Connecting Beams	
		Limited (=5 for int =15 for ext)	High (= 500)
16% g El-Centro	Exterior Wall	1.55	1.45
	Interior Wall	1.67	1.67
32% g El-Centro	Exterior Wall	2.97	
	Interior Wall	3.33	

Table 4.13 Top Deflection Ratio for the Exterior and Interior Wall

The damage happened in the shear walls due to the earthquake loads is measured qualitatively by the number of segments which are changed to the real hinged state and the maximum number of segments changed to the plastic hinged state at any instant of time.

This is tabulated in Tables 4.11 and 4.12 of the previous section. It can be seen that the interior walls will suffer more damage than the exterior walls, although the latter share more than the former in resisting the lateral seismic loads. This is due to the lower bending capacity of the connecting slabs in the interior walls.

It should also be noted that the shear walls carry much higher bending moments at the base when the ductility of the connecting beams is limited. Therefore, the rotational ductility factor $\overline{\mu}$ has considerable influence on the inelastic behaviour of the coupled shear wall.

In the exterior shear walls, the occurrence of the tensile forces (with the gravity dead loads included) at the base of the piers is more frequent when the ductility of the connecting beams is high. This shows that the increase in ductility of the connecting beams may not be favourable, especially in case of the exterior shear walls with a higher capacity to trasmit axial forces and a lesser section of tributory area.

The damage pattern of the interior coupled shear wall subjected to 32% El-Centro record will be considered in details. The state of the segments at different times are found out and the segments state time-history is shown in Fig. (4.35). As shown in this figure, the inelastic action started at 1.20 seconds when the plastic hinges start forming at the ends of connecting beams of second and third segment. This inelastic action moved upward up to the top segment and at 1.68 seconds the end rotation of the laminae of fifth segment is exceeded the ultimate rotation value and the segment changed to the real hinged

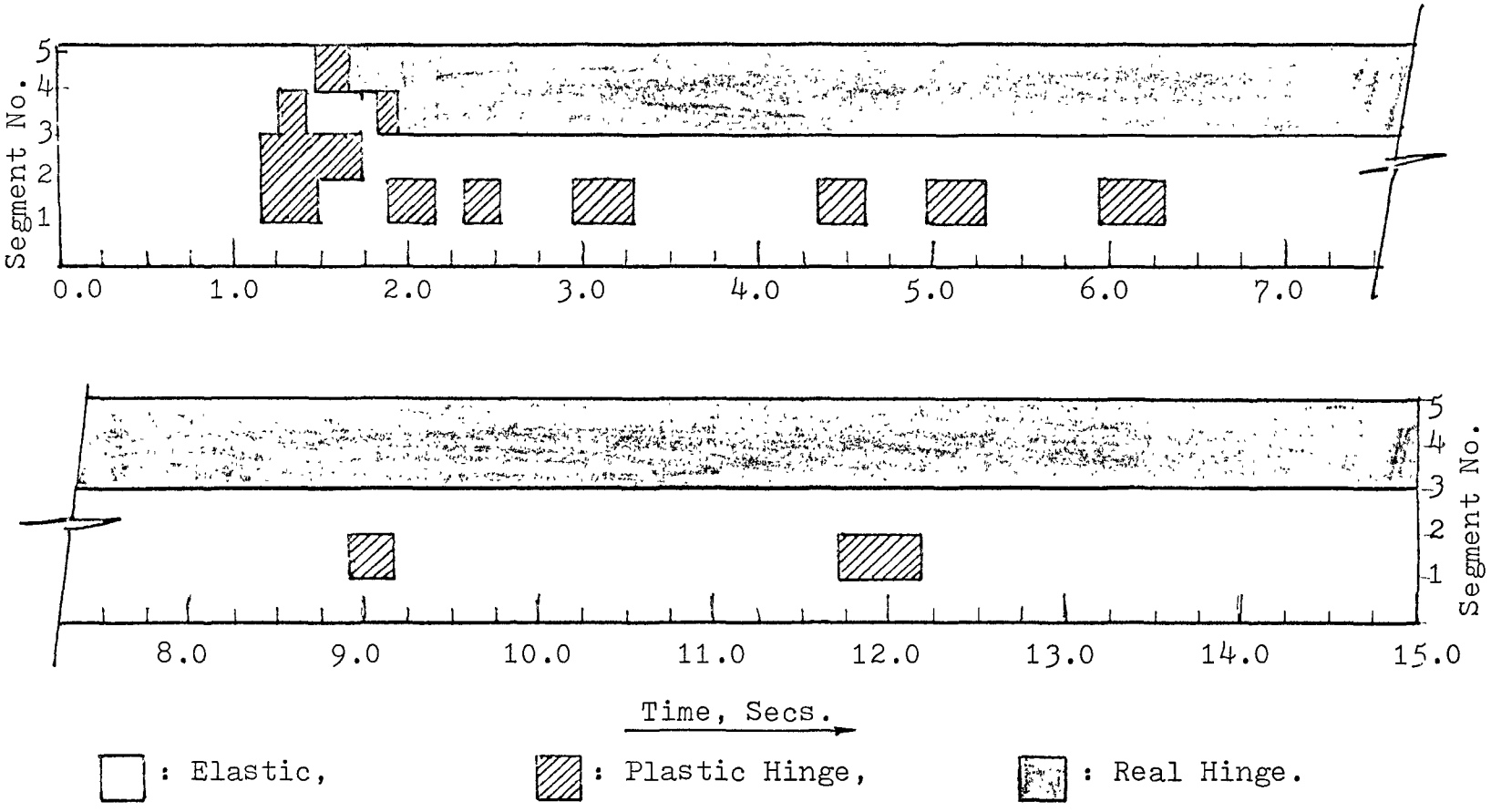

FIGURE 4-35 YIELDING HISTORY OF COUPLING BEAMS, INTERIOR WALL [RUN-6]

segment. At 1.92 seconds the fourth segment also became a real hinged segment and these two segments remained in real hinged state throughout the earthquake excitation. The plastic hinges are formed in second segment, occasionally, for some time. This clearly shows that major inelastic action has occurred from 1.20 secs to 2.1 secs of the excitation where the earthquake record has most of the significant peaks.

4.5 DYNAMIC BEHAVIOUR CONSIDERING WALL HINGE FORMATION AT THE BASE

In the previous sections, the formulation of the plastic hinges at both ends of the connecting beams was the only source of inelastic action considered. In reality, when the wall moment at the base of each pier reaches its ultimate value, plastic hinges may form at its base. The final collapse mechanism of a typical coupled shear wall under the action of strong earthquake is the full plastification of the connecting beams and the formation of the hinges at the base of both piers. The behaviour of the exterior and the interior coupled shear wall subjected to moderate and severe earthquake excitations with the consideration of possible formulation of plastic hinges at the base is presented in this section. The following table gives the details of the cases considered.

WALL	Case No.	Earthquake Excitation	Rotational Ductility Factor for the Connecting Beams ($\bar{\mu}$)
Interior	1	moderate	5
	2	severe	5
Exterior	3	moderate	15
	4	severe	15

Table 4.14 Summary of Assumed Conditions for Different Case Studies Considering the Wall Hinge Formation at the Base

Case-1

The interior wall is safe under moderate earthquake and no hinge is formed at the base of the piers. This is because, the base moment always falls within the interaction curve throughout the time history of the record. Hence the time history responses of the top displacement, base moment, axial force at the base and shear force intensities in the segment are the same as given in Figs. (4.22), (4.27), (4.26) and (4.30) through (4.34).

Case-2

Figures (4.36) through (4.44) show the top displacement, bending moments at the base of left and right pier, axial force at the wall base and shear force intensities in five segments. This coupled shear wall fails by formation of the plastic hinges at the base of both piers at 2.10 seconds. It should be noted that the piers of the coupled shear wall are subjected to different axial forces (considering the dead loads). Therefore, the bending moment response at the base of both piers has to be considered separately in deciding whether a hinge has been formed or not.

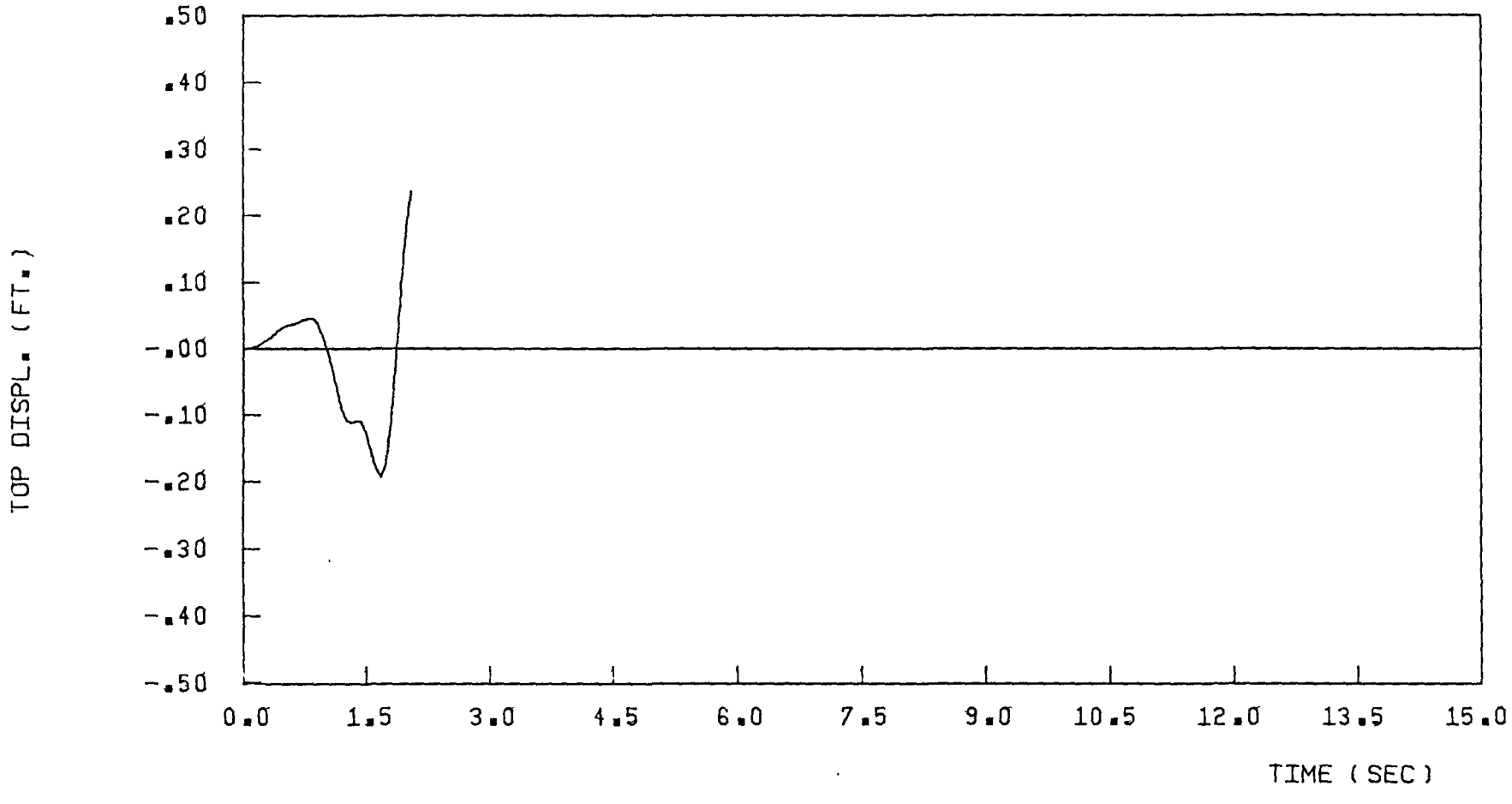

FIGURE 4-36 TOP DISPL., ELCENTRO COMP.NORTH 32 PERC. g

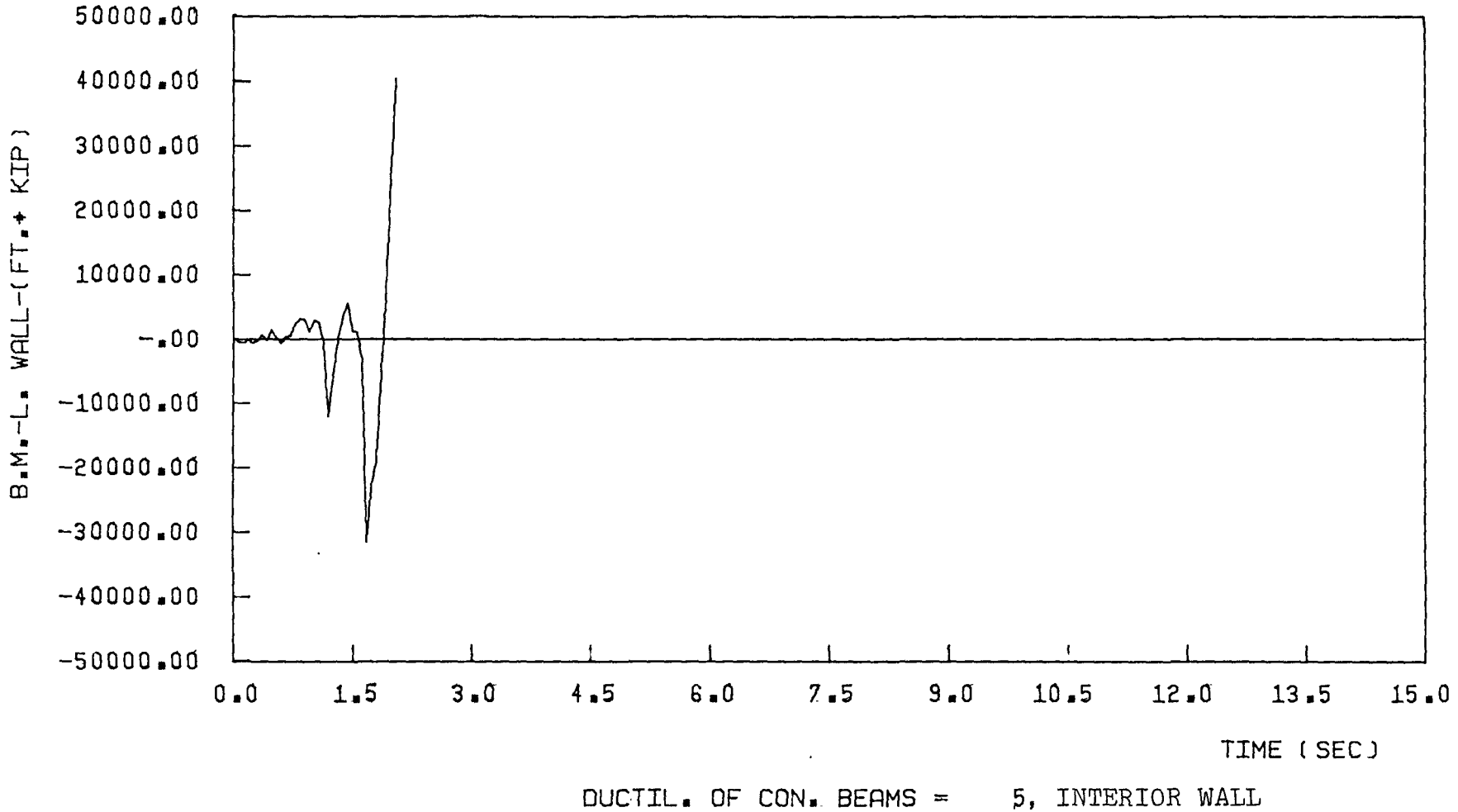

FIGURE 4.37 B.M.L. WALL, ELCENTRO COMP.NORTH 32 PERC. g

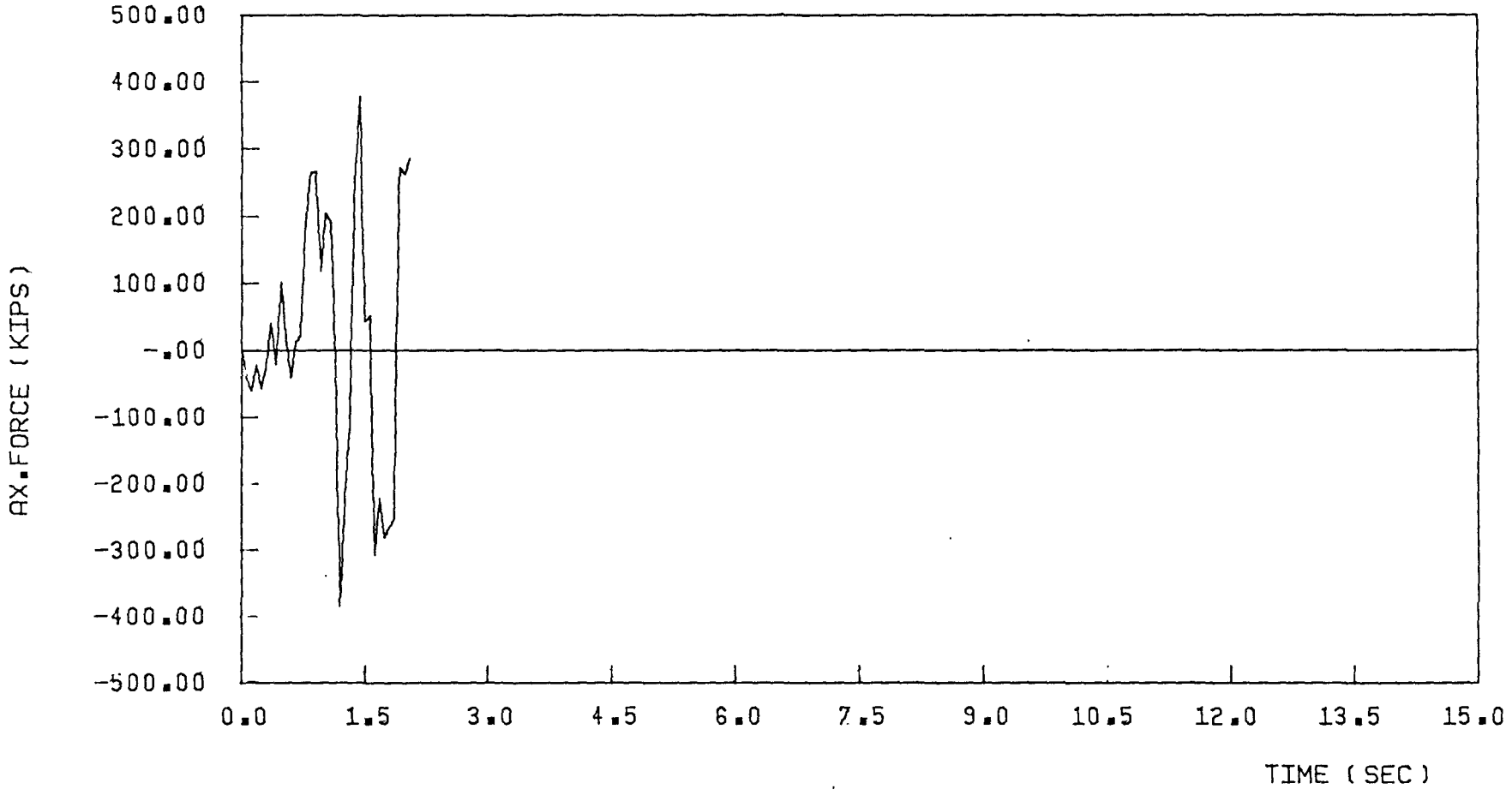

FIGURE 4-39 AX. FORCE, ELCENTRO COMP.NORTH 32 PERC. g

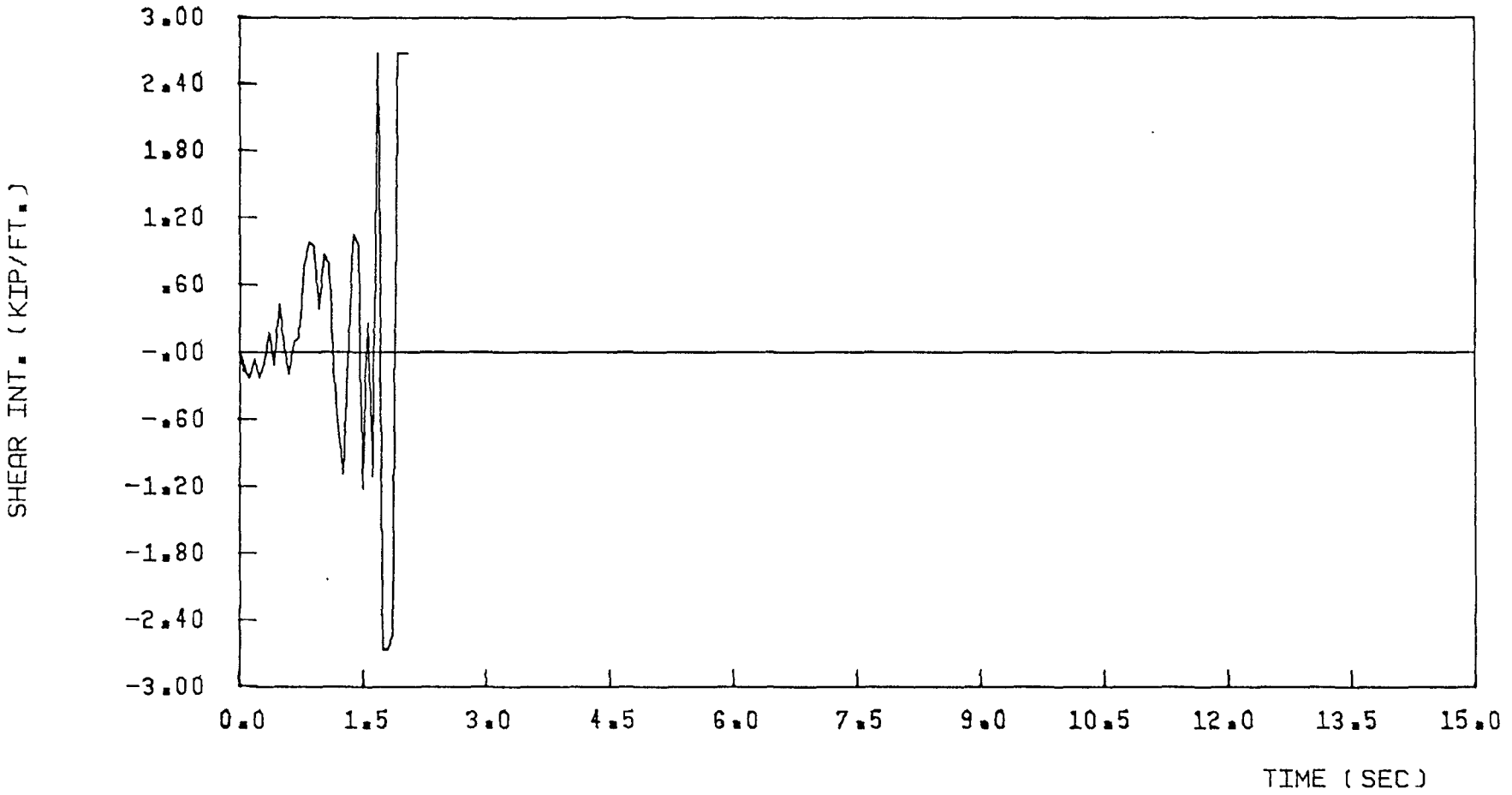

FIGURE 4-40 SHEAR INT.,ELCENTRO COMP.NORTH 32 PERC. g

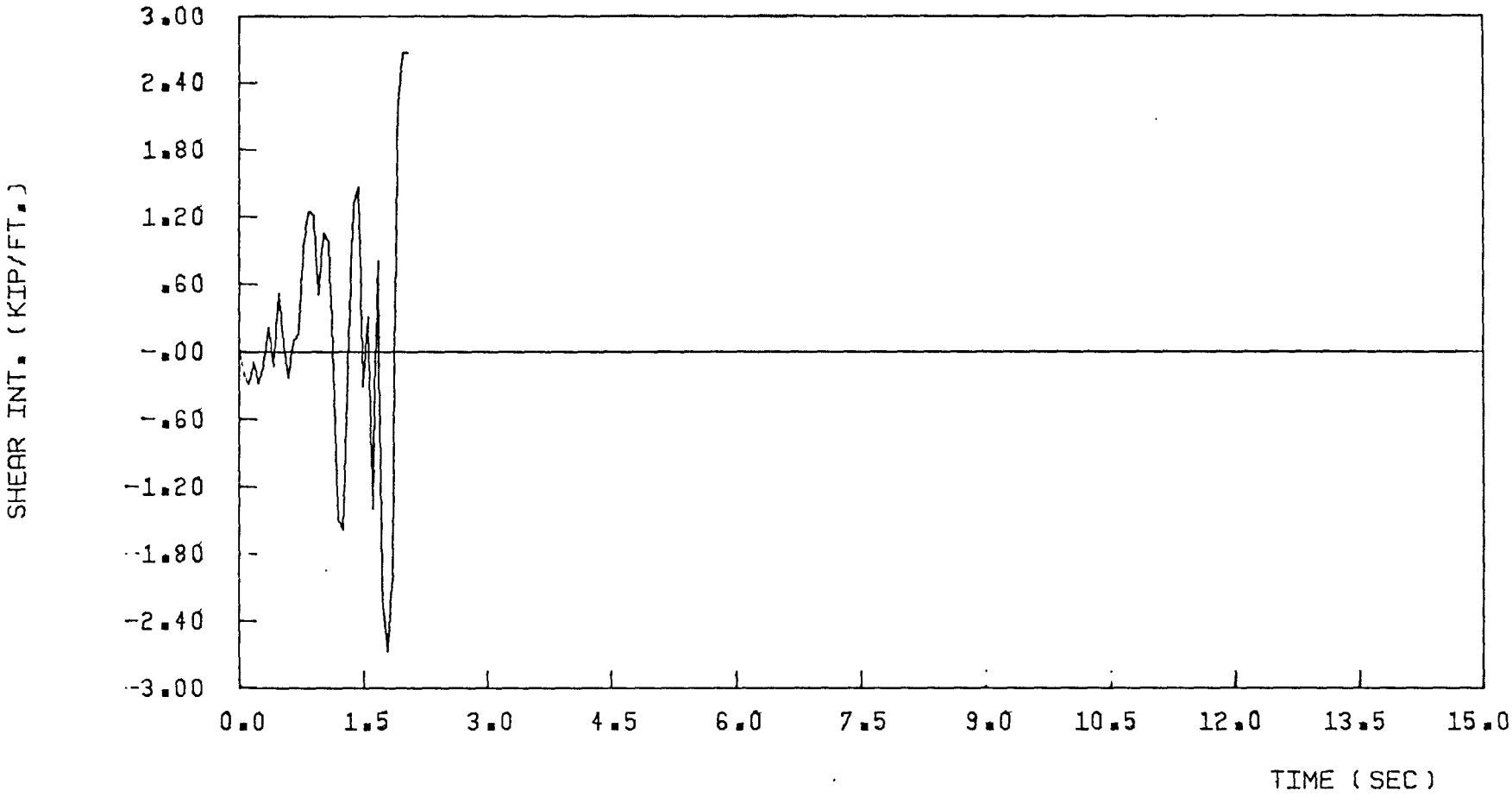

FIGURE 4-41 SHEAR INT., ELCENTRO COMP.NORTH 32 PERC. g

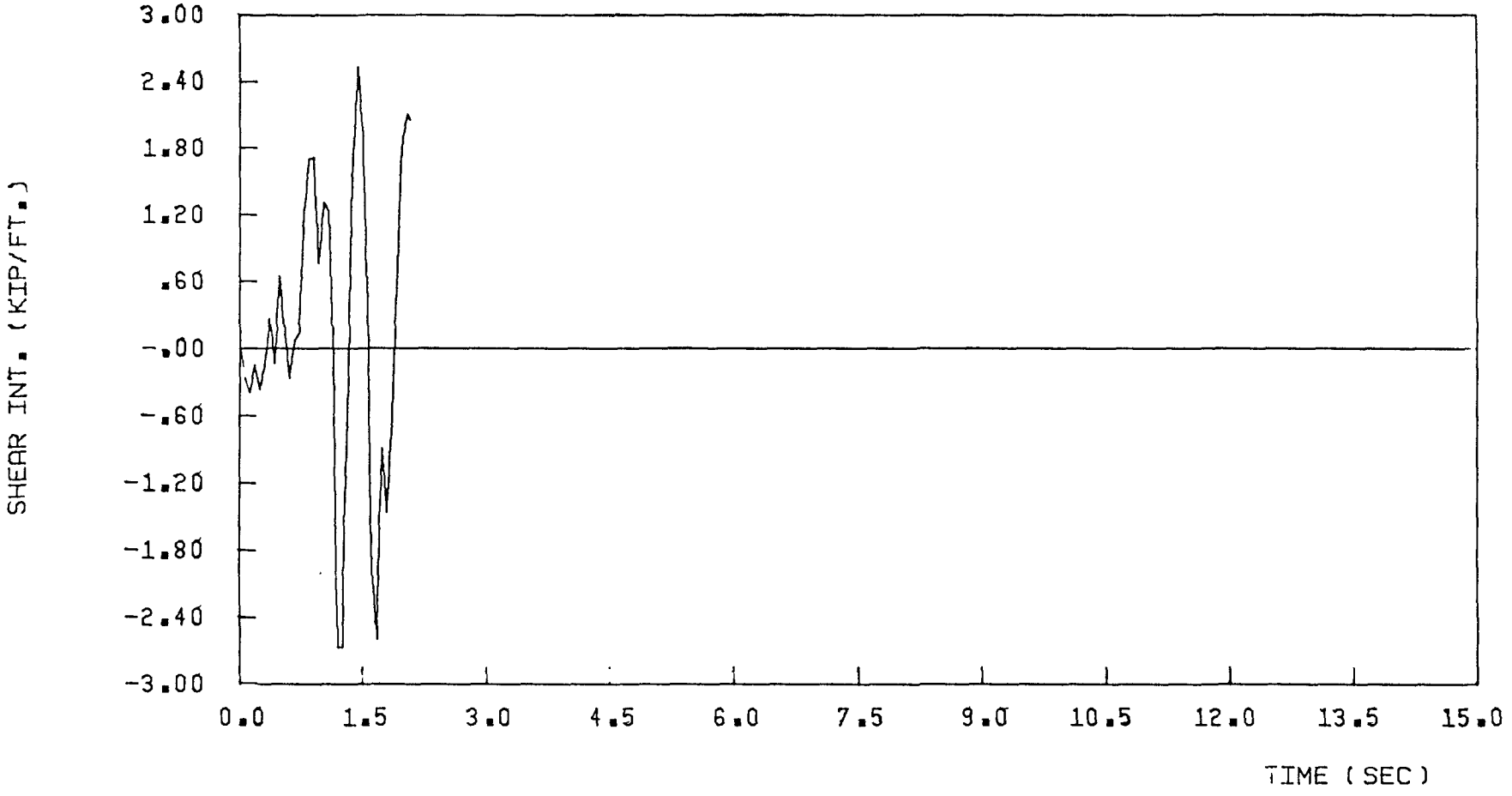

(SEGMENT NO. 3) DUCTIL. OF CON. BEAMS = 5, INTERIOR WALL

FIGURE 4-42 SHEAR INT., ELCENTRO COMP.NORTH 32 PERC. g

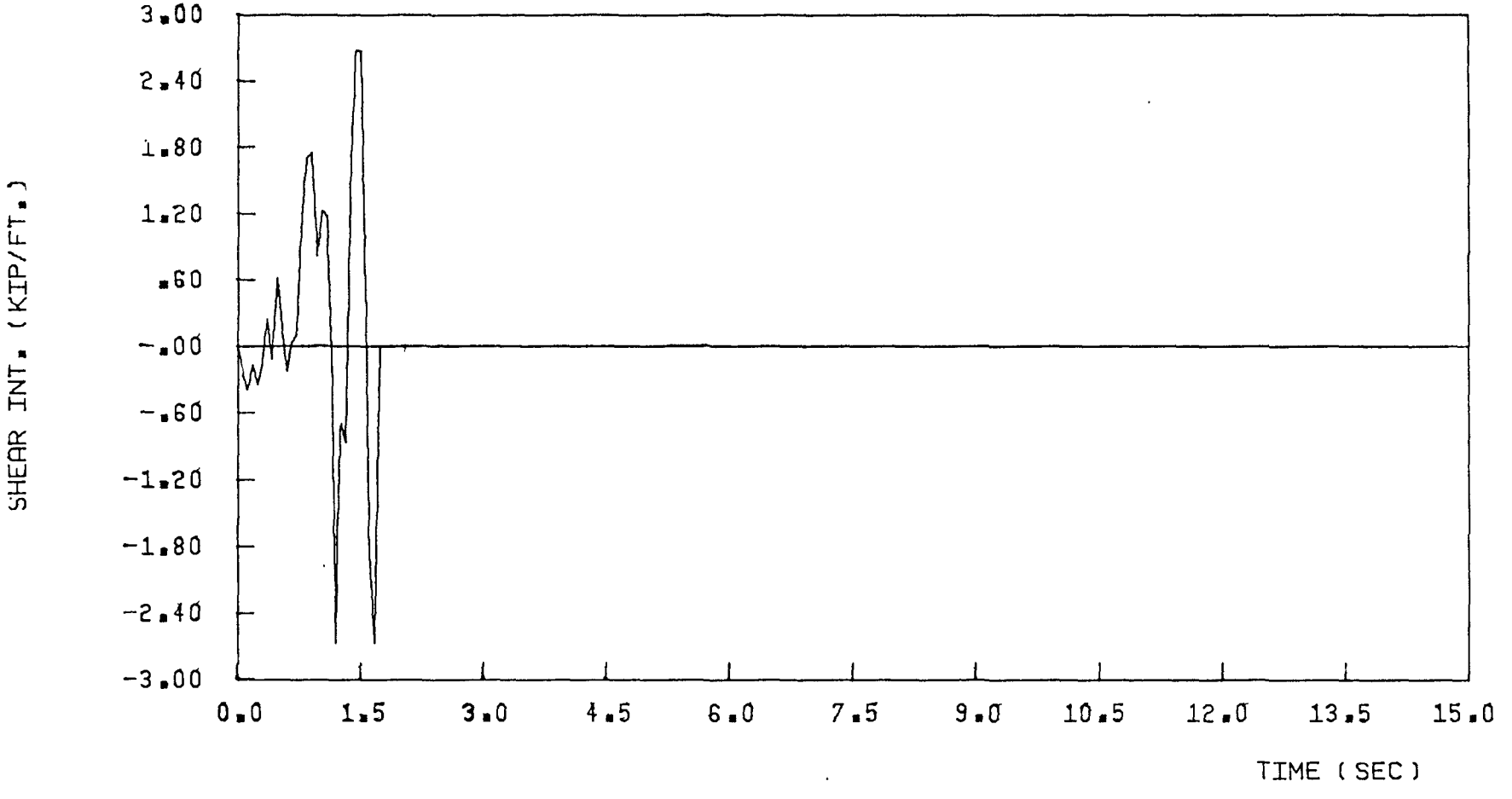

FIGURE 4-43 SHEAR INT., ELCENTRO COMP.NORTH 32 PERC. g

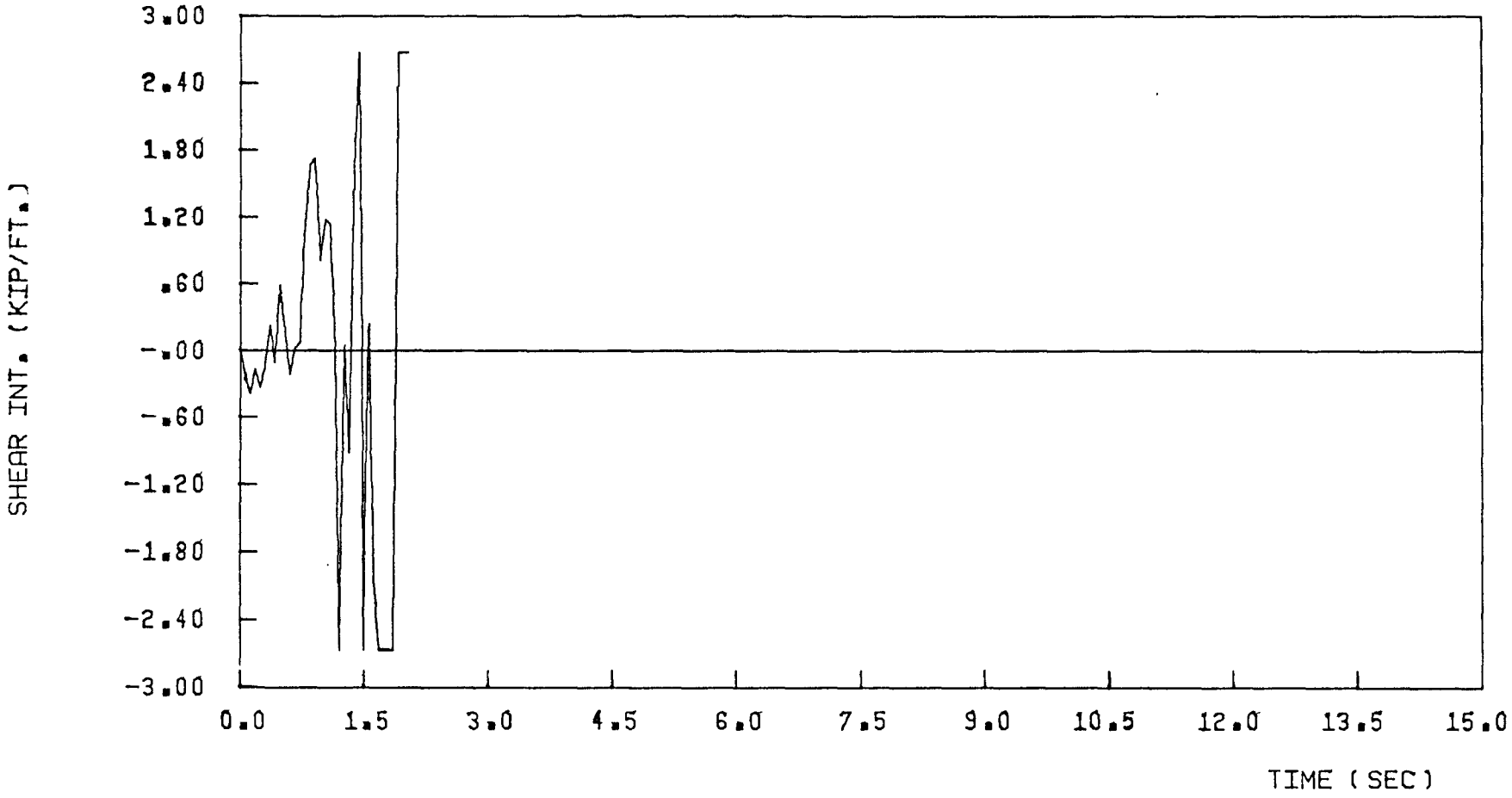

(SEGMENT NO. 5) DUCTIL. OF CON. BEAMS = 5, INTERIOR WALL

FIGURE 4-44 SHEAR INT., ELCENTRO COMP.NORTH 32 PERC. g

The step-by-step formation of the hinges at the bases is shown in the Fig. (4.45). As shown in that figure, up to 2.04 seconds the bending at the base of each piers falls within the interaction curve and fixed-fixed condition is maintained at the base (stage "I"). At the next time step at 2.10 seconds both base moments fall beyond the interaction curve (stage "II") and both hinges are formed at the same time (stage "III"). Hence the state of collapse is achieved at time 2.10 seconds.

Case-3

Figures (4.46) through (4.49) show the top displacement, bending moments at the base of both piers and axial force at the wall base. In this case the exterior coupled shear wall almost reaches the state of collapse. Figure (4.50) shows the behaviour at the critical time. At 2.10 seconds the bending moment at the base of first pier is greater than the ultimate value (stage "II"). Therefore, the remaining moment has to be taken by the other pier. At the end of the iteration, the moment at the base of second pier is found to be still within the interaction curve (stage "III"). At the next time step, the bending moments at the base of both piers become less than the ultimate value and the same is true for the remaining portion of the response. Therefore, no collapse occurs although the wall is close to the collapse state.

Case-4

Figures (4.51) through (4.54) give the responses of the top displacement, bending moments at the base of both piers and axial force

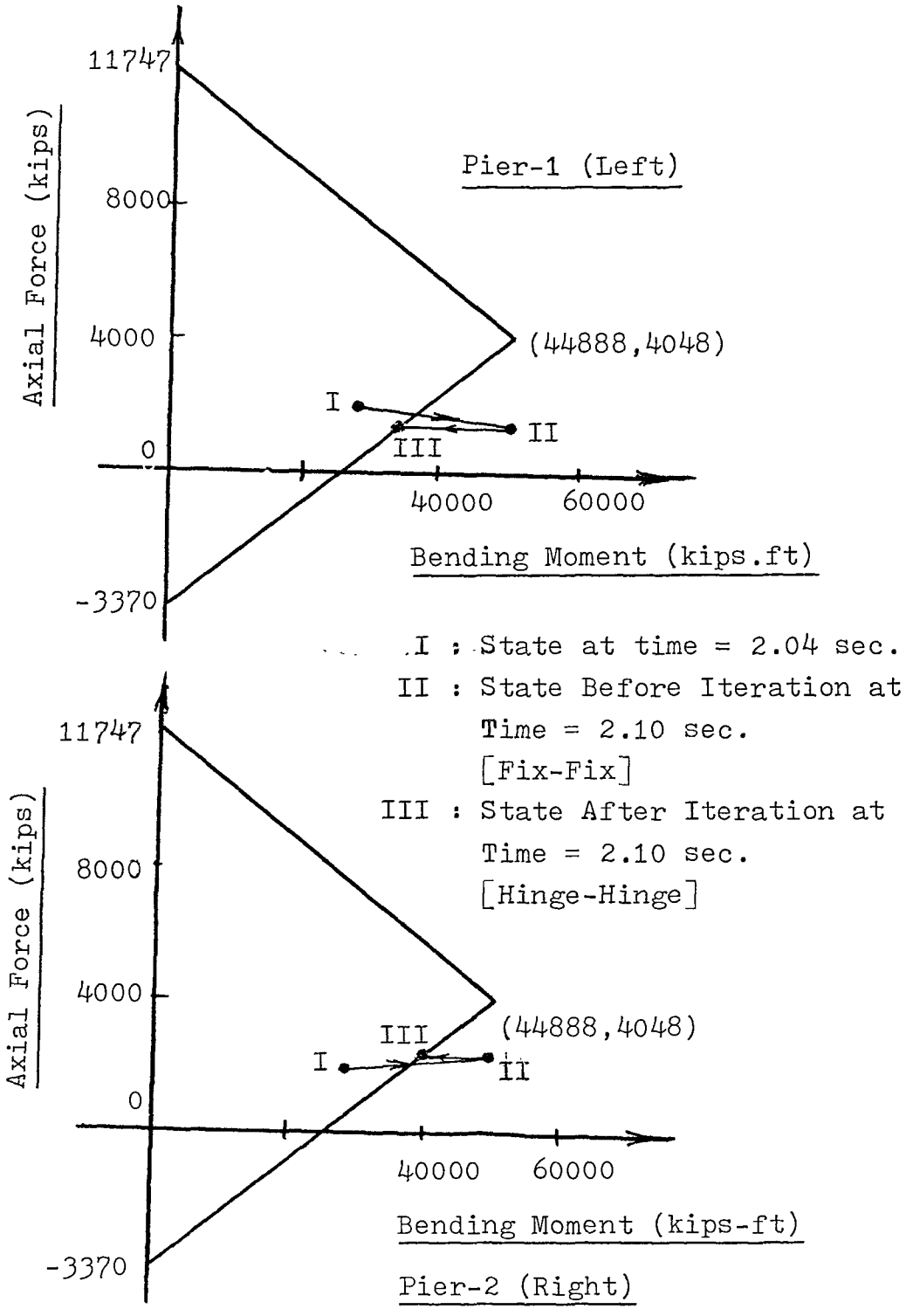

FIGURE 4-45 WALL HINGE FORMATION AT THE BASE OF PIERS OF INTERIOR WALL UNDER SEVERE EARTHQUAKE

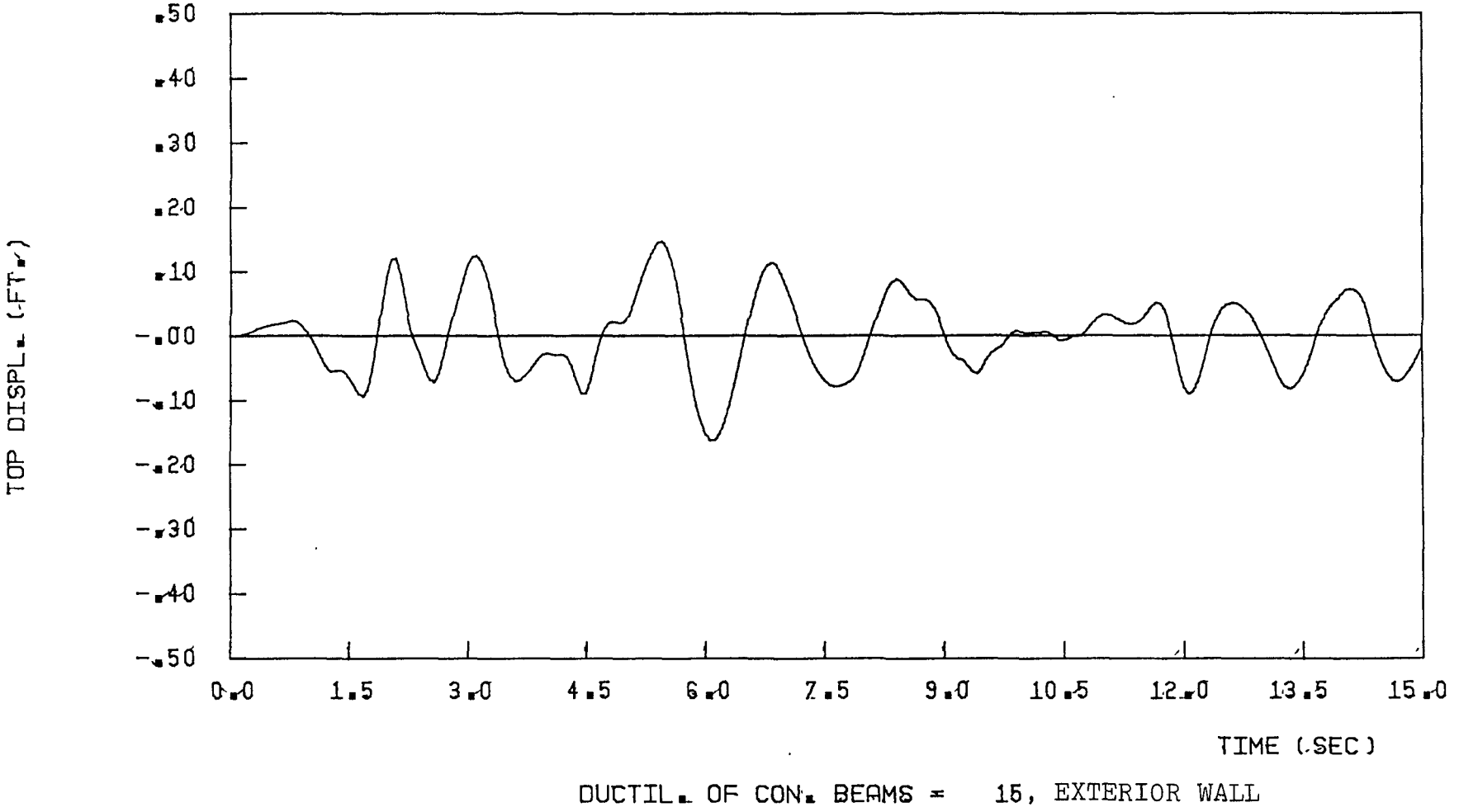

FIGURE 4-46 TOP DISPL., ELCENTRO COMP. NORTH. 16 PERC. g

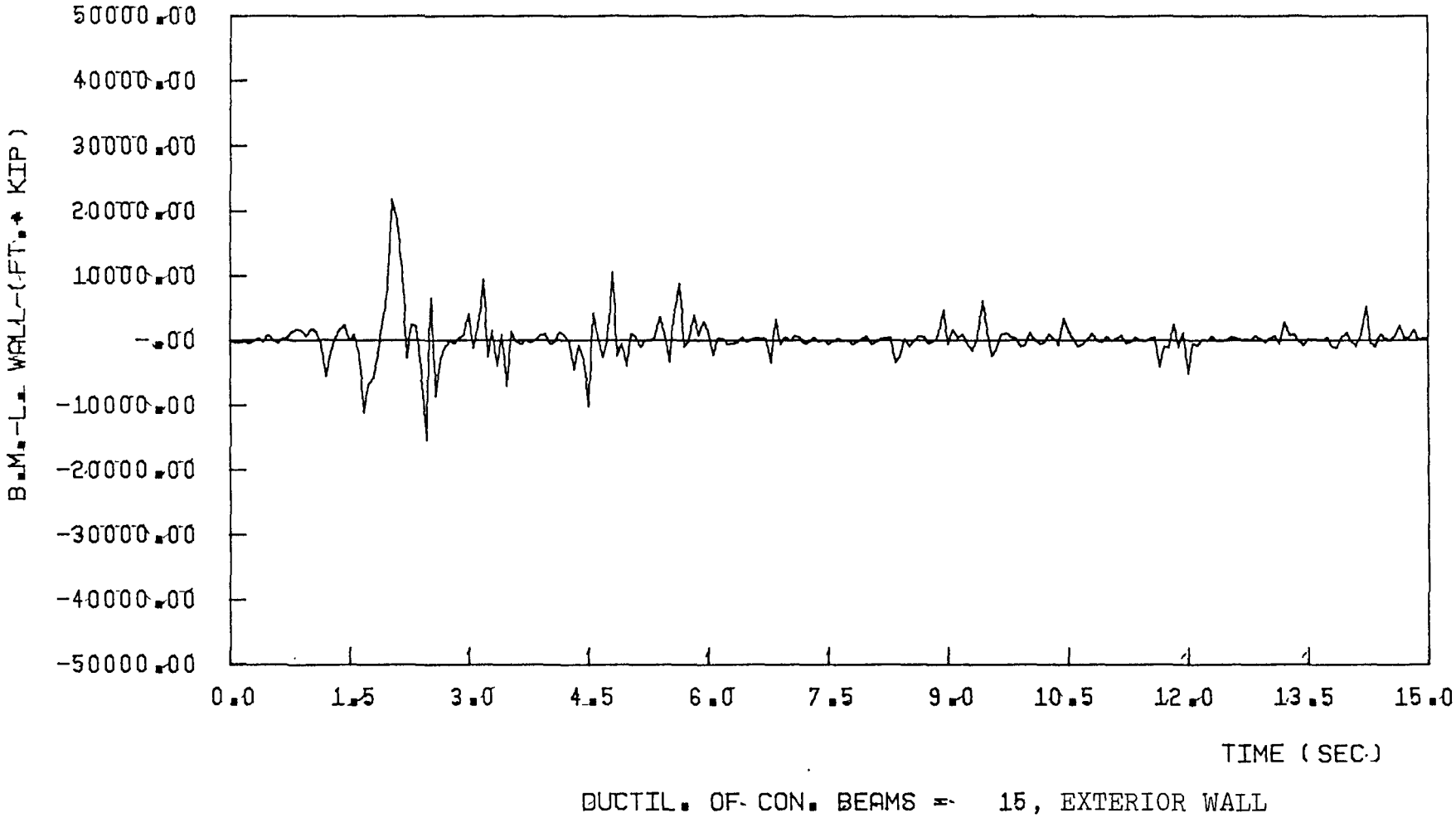

FIGURE 4-47 B.M.L.-WALL, ELCENTRO COMP.NORTH. 16 PERC. g

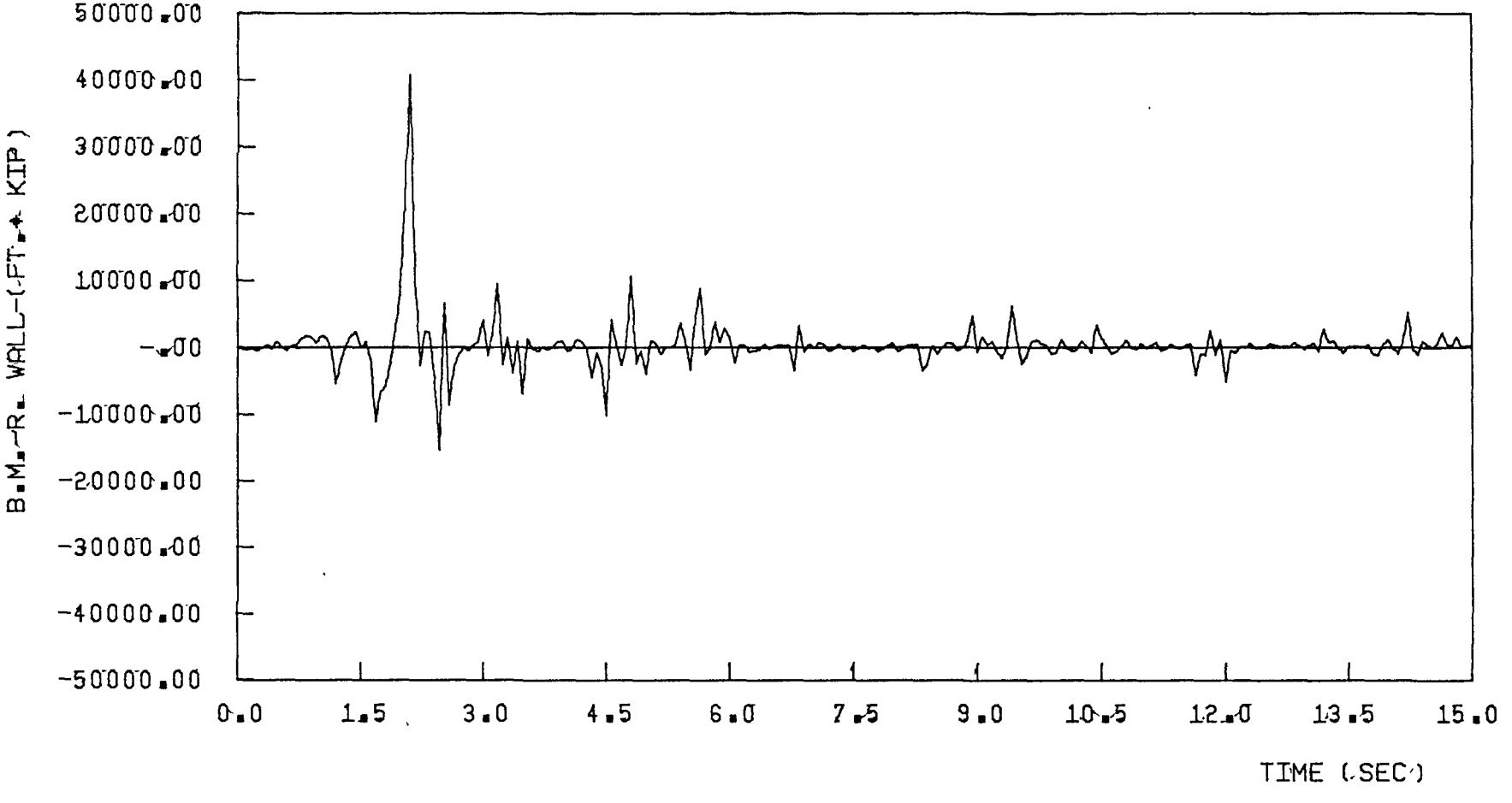

FIGURE 4-48 B.M.R.WALL, ELCENTRO COMP.NORTH 16 PERC. g

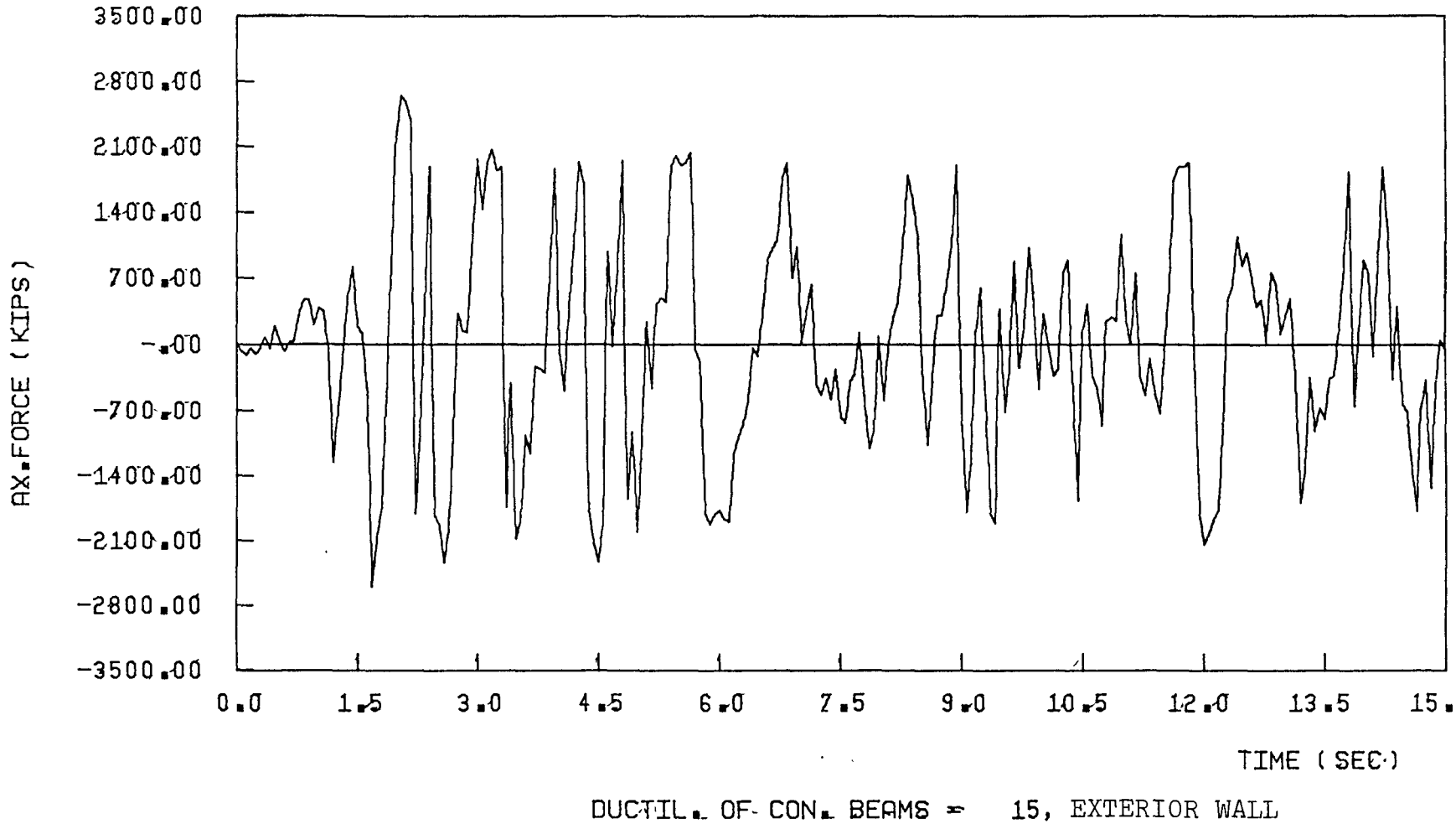

FIGURE 4-49 AX. FORCE, ELCENTRO COMP.NORTH. 16 PERC. g

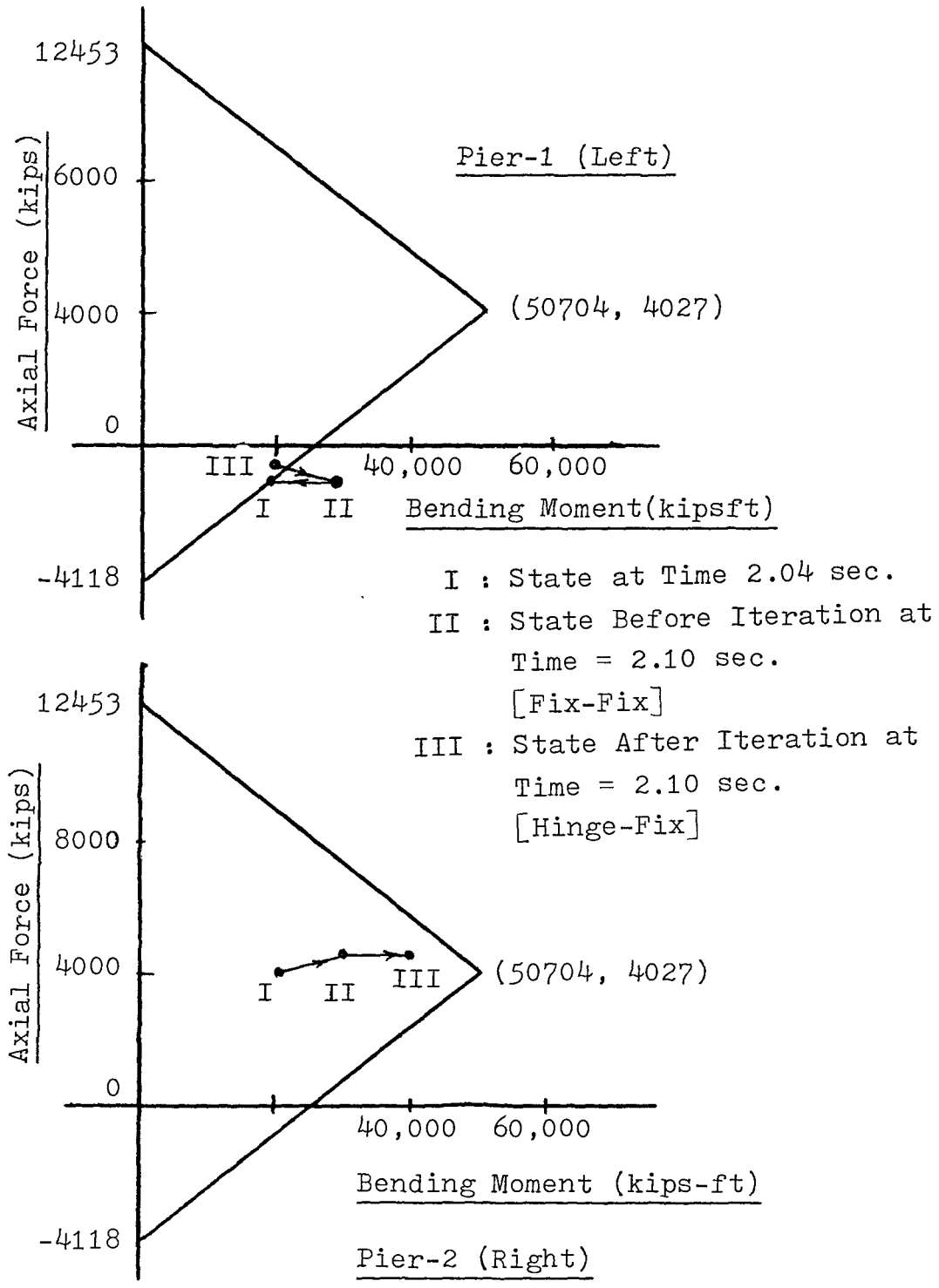

FIGURE 4.50 WALL HINGE FORMATION AT THE BASE OF PIERS OF EXTERIOR WALL UNDER MODERATE EARTHQUAKE

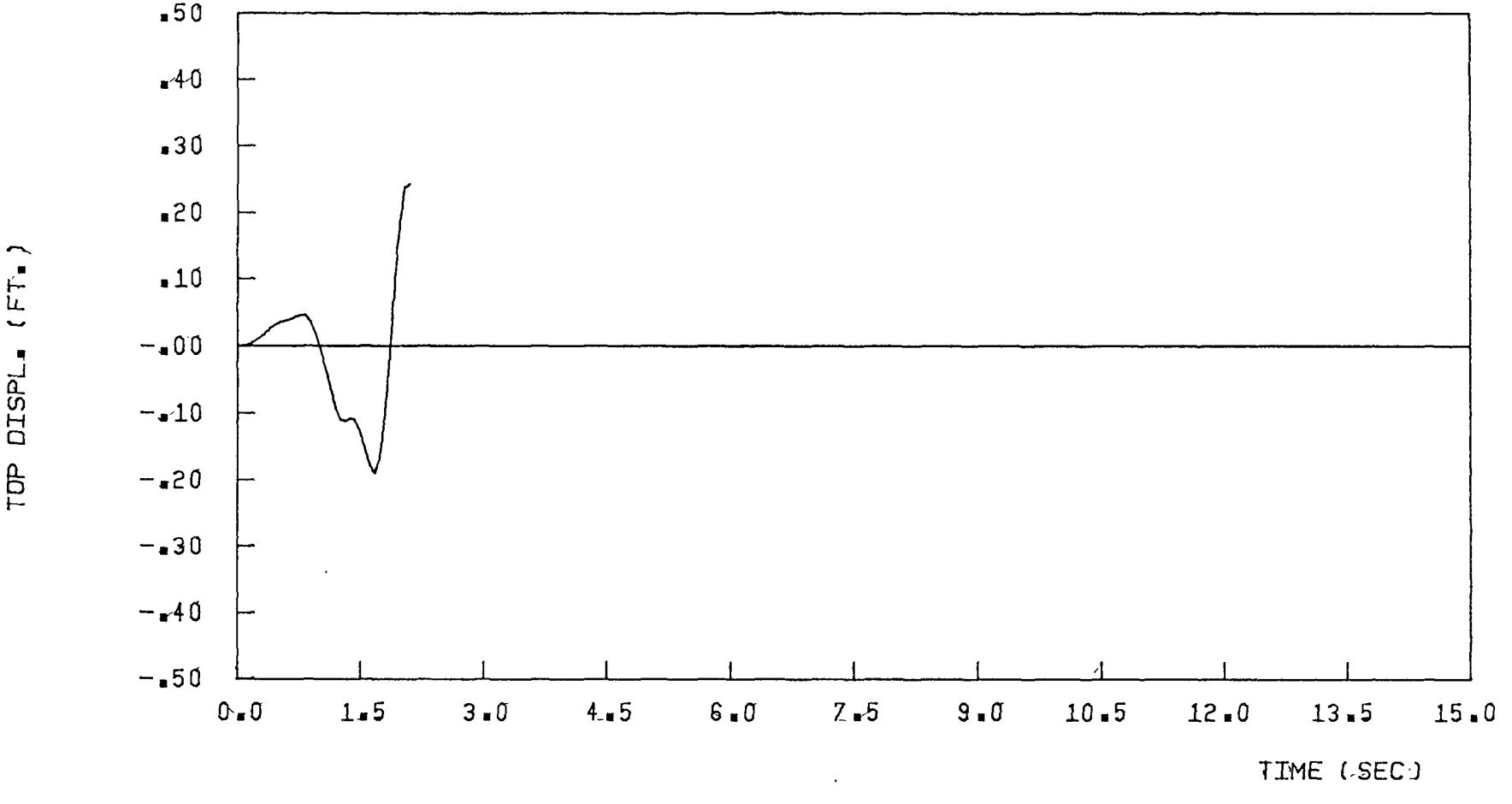

FIGURE 4-51 TOP DISPL., ELCENTRO COMP.NORTH 32 PERC. g

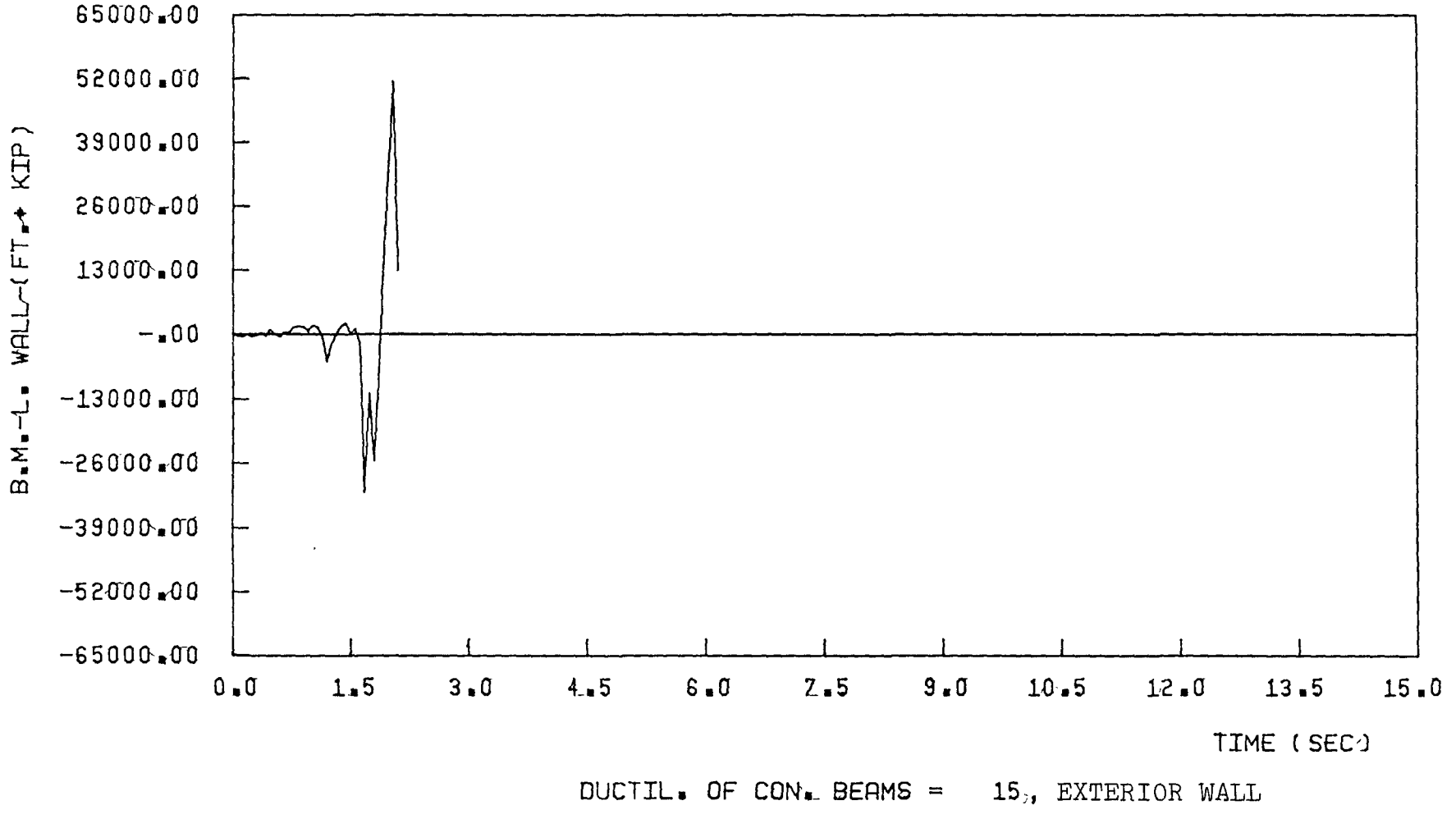

FIGURE 4.52 B.M.L.-WALL, ELCENTRO COMP.NORTH 32 PERC. g

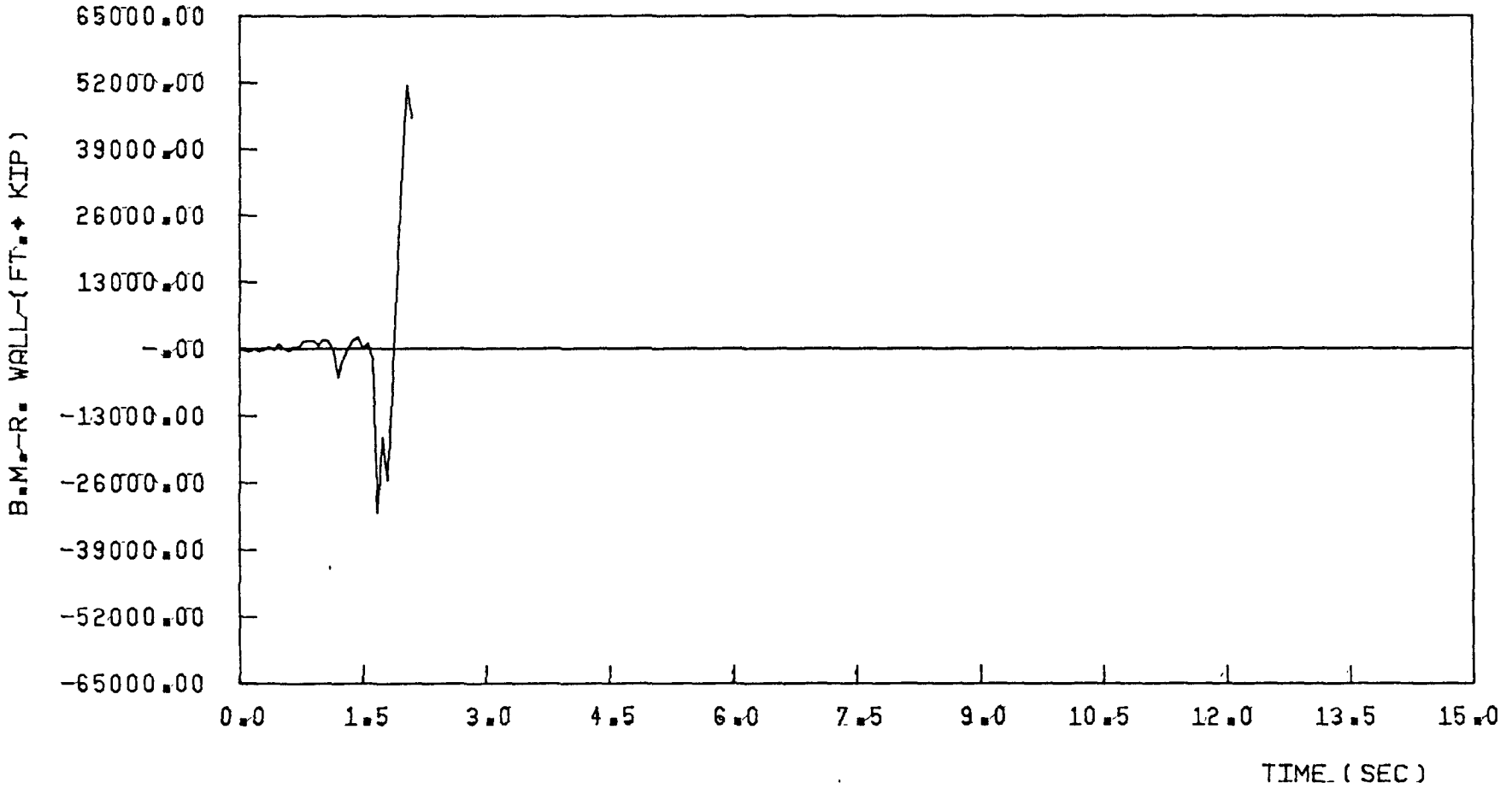

FIGURE 4.53 B.M.R-WALL, ELCENTRO COMP.NORTH 32 PERC. g

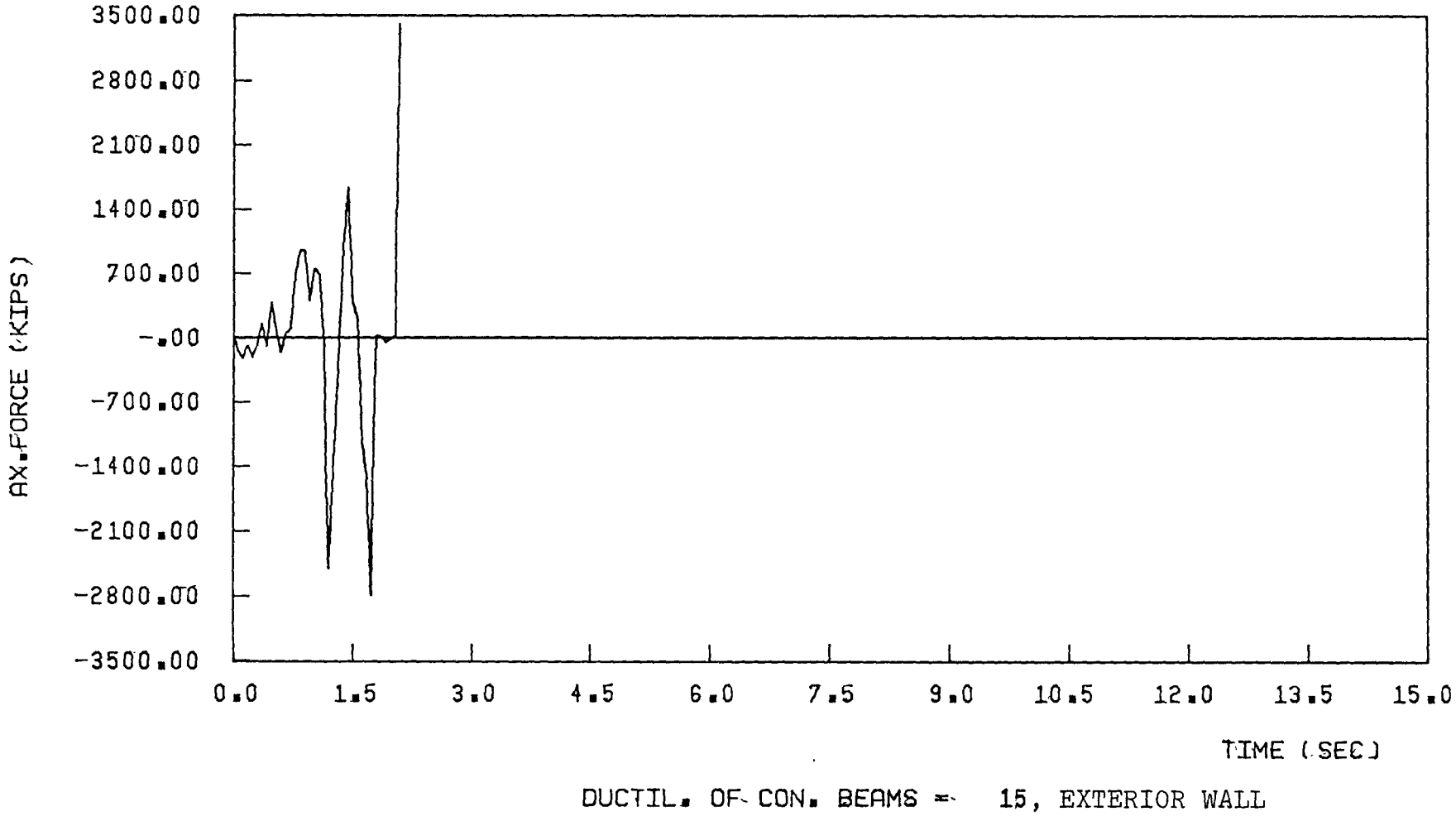

FIGURE 4-54 AX. FORCE, ELCENTRO COMP.NORTH 32 PERC. g

at the wall base. In this case, the exterior wall fails by formation of the plastic hinges at the base of both piers. The formation of the plastic hinges is explained in different stages by Fig. (4.55). As shown in this figure the wall moments at the base of both piers are greater than the ultimate values (stage "II"). After the balance of moments at the end of the iteration, it is concluded that both hinges have formed at the base of the piers. This formation of collapse mechanism occurs at 2.10 seconds (stage "III").

From the behaviour of these coupled shear walls, it may be concluded that the collapse mechanism is most likely under the severe earthquake loading and the coupled shear wall may survive under moderate earthquake excitation. Specially the interior coupled shear wall, in spite of its flexible connecting beams, has more chances of survival than the exterior wall of the same capacity if it is shaken by the moderate earthquake. This is primarily because of its smaller overall stiffness and it shows that the increase in the stiffness of the connecting beams may not necessarily give an improvement in the behaviour of the coupled shear wall.

4.6 DESIGN CONSIDERATIONS FOR COUPLED SHEAR WALLS

In the coupled shear walls, the bending moments are reduced considerably by the higher magnitudes of induced axial forces developed due to the higher shear force carrying capacity of the deep connecting beams. But high axial forces reduce the flexural ductility capacity of the wall and may cause more cracks and fractures.

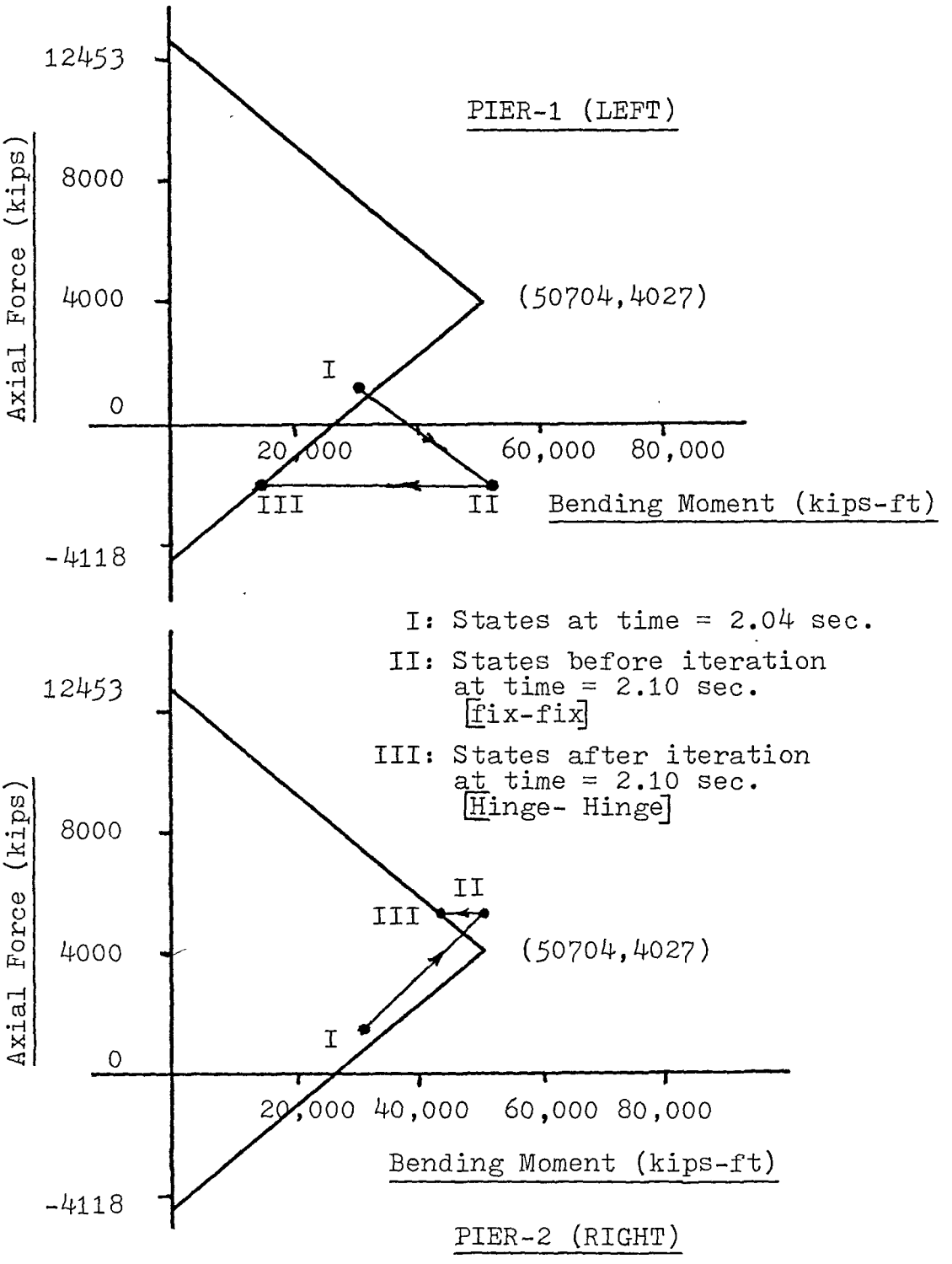

FIGURE 4.55 WALL HINGE FORMATION AT THE BASE OF PIERS OF EXTERIOR WALL UNDER SEVERE EARTHQUAKE

It is seen in the present work that the connecting beams undergo numerous cycles of large yielding reversal under high shear. Consequently, deep coupling beams which cannot normally sustain very large ductility under high reversal shear should be avoided. If these deep beams fail, high moment couples will be redistributed back, increasing wall moment possibly beyond the yielding capacity. Therefore, it is preferable and more practical to have a coupling system with moderately stiff connecting beams with maximum ductility that can be achieved by proper arrangement of the flexural reinforcement.

In addition, specially detailed and sufficient shear reinforcement should be provided to ensure that full flexural capacity can be developed in all connecting beams. Also the openings in the connecting beams should not be permitted as they can be detrimental to the shear strength of the beam section.

In a coupled shear wall system, the walls provide a major part of the lateral stiffness, thereby controlling lateral storey drift and limiting the nonstructural damages during an earthquake. The elastic walls maintain structural stability, while the coupling beams dissipate earthquake energy through an inelastic action. It is seen that if the inelastic action occurs at the base of the walls, it will most likely lead to the collapse of the entire system. Therefore, the walls in a coupling system should be designed not to undergo an inelastic yielding during an earthquake excitation.

For a planar wall with rectangular section, a strong wall can be achieved by concentrating the flexural reinforcement and confining

enclosed concrete at the ends of the wall sections. In addition to reinforcing the walls for elastic behaviour, some ductility capacity should also be provided as a second line of defense.

CHAPTER 5

ELASTO-PLASTIC ANALYSIS OF TWO INTERCONNECTED COUPLED SHEAR WALLS

5.1 INTRODUCTION

In the previous chapters, the behaviour of a flat-slab coupled shear wall building is studied by considering the behaviour of a typical coupled shear wall. It is assumed that the building considered is symmetrical in plan and consists of a series of planar coupled shear walls such that all interior coupled shear walls are the same with two identical end coupled shear walls that are different from the interior walls. Hence, while studying the behaviour of these interior and exterior coupled shear walls, it was assumed that these walls take the lateral load in proportion of their elastic stiffnesses. This proportion of load is assumed to be constant throughout the elasto-plastic analysis of the wall. This assumption is true as long as the shear wall is in the elastic state, but when the plastic hinges start forming at the ends of the connecting beams, the distribution of the lateral loads between the interior and the exterior walls will be different. A transfer of lateral load takes place between these two types of walls. The part of the wall which is in the plastic hinged state will pass some load to its counterpart. This phenomenon of the transfer of loading may lead to different behaviour of the coupled shear

walls of the building. This behaviour is studied in this and the next chapter by considering a mathematical model consisting of two coupled shear walls joined together.

5.1.1 Modeling of the Building

Normally, a typical apartment multistorey building of shear-wall flat slab construction contains sets of parallel coupled shear walls as shown in Figure (5.1) to resist the lateral loads in the short direction. To study the response of a shear wall building under lateral loadings, this original system of coupled shear walls, the exterior and interior walls, can be modelled as two coupled shear walls, one representative of the exterior walls and the other representing the interior walls, connected by a pin-pin rigid member at each floor level. This pin-pin rigid member can transfer only horizontal force from one coupled shear wall to the other coupled shear wall, thereby to ensure the deflection of the two coupled shear walls at the floor levels be the same. As shown in Figure (5.2), this equivalent system will then have one coupled shear wall which has the sum of the stiffness and strength of all the interior coupled shear walls, and the other coupled shear wall which represents the exterior coupled shear walls having the total stiffness and strength of the two external shear walls.

To study the problem, this equivalent system of two coupled shear walls can be divided into the segments of one or more storey heights. A typical segment of this equivalent system with the internal forces acting on it is shown in Figure (5.3).

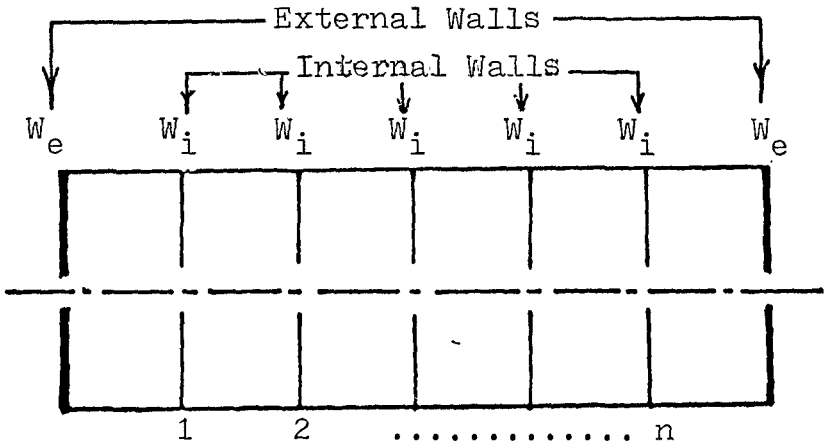

FIGURE 5-1 ORIGINAL SYSTEM OF SHEAR WALLS

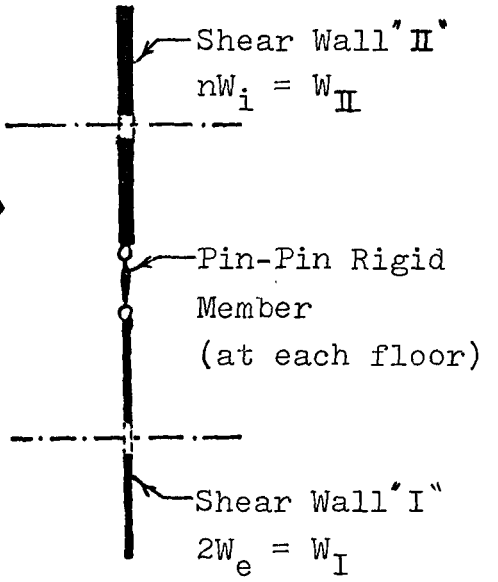

FIGURE 5-2 EQUIVALENT SYSTEM OF TWO INTERCONNECTED COUPLED SHEAR WALLS

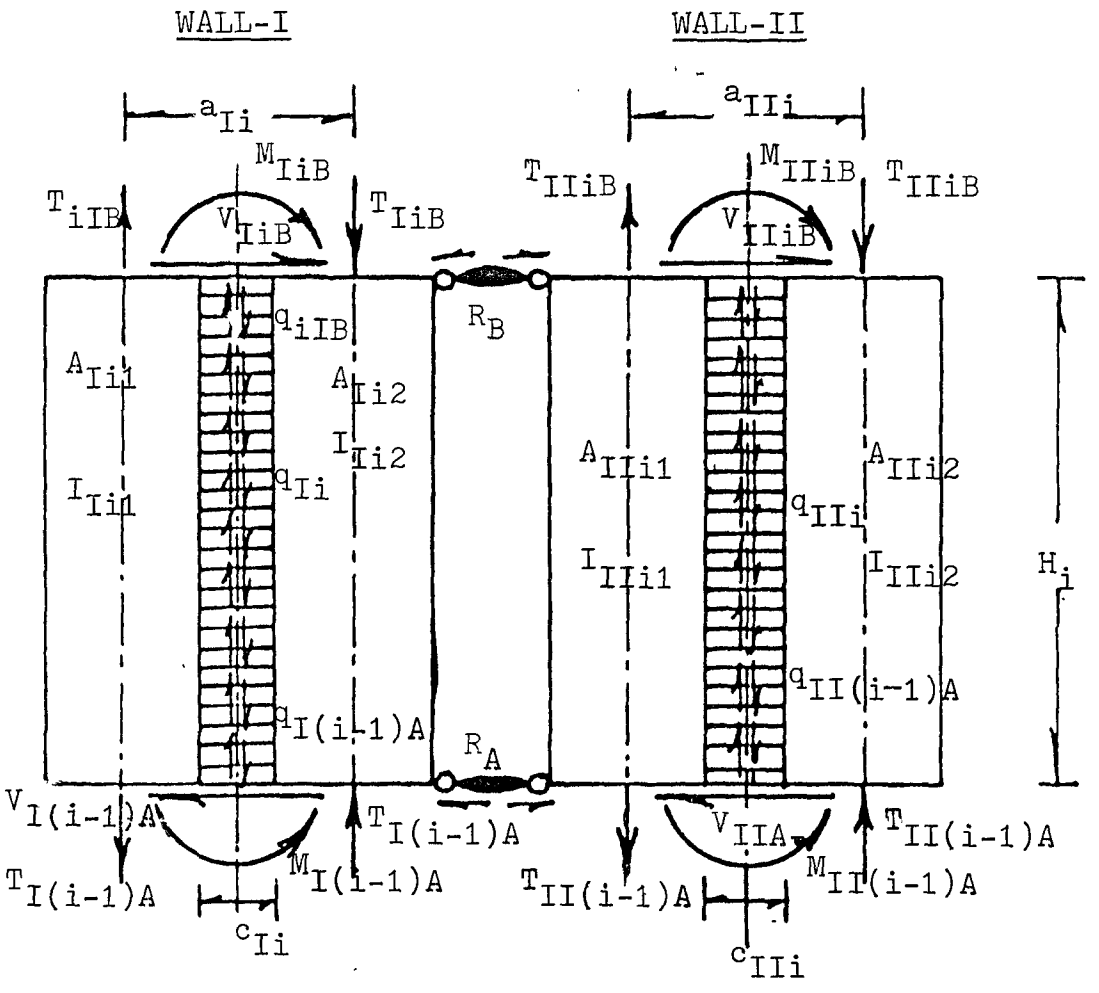

FIGURE 5-3 FORCES ACTING ON THE SEGMENT OF ith EQUIVALENT SYSTEM

5.1.2 Segment States

Depending on the shear intensity $q_i(x,t)$ {i = I, II} of each coupled shear wall, as explained for the one coupled shear wall analysis in the beginning of the second chapter, the segment of each coupled shear wall may be in one of the three states, namely, Elastic, Plastic-hinged or Real-hinged state. Hence it is necessary to develop nine field transfer matrices to cover all the combinations of segment variations as shown in Figure (5.4).

Furthermore, to connect these segments, each station will have four segments (two segments at the top and two at the bottom of the station) and each of these segments may be in one of the three states, namely, Elastic, Plastic-hinnged or Real-hinged state. Hence to cover all the combinations of segment-state variations, it is necessary to develop eighty-one (3x3x3x3 = 81) station-transfer matrices as shown in Figure (5.5). For simplicity, the station is identified by the state of segments with top-left segment at first. For example if the top segment of first shear wall is in Plastic-hinged state, the top segment of second shear wall in Elastic state, the bottom segment of first shear wall in Plastic hinged state and the bottom segment of second shear wall is in Real-hinged state, then that station is named as "Plastic-Elastic-Plastic-Real" station. [See 67 of Figure (5.5)].

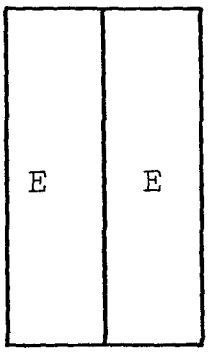

a. Elastic-Elastic Segment

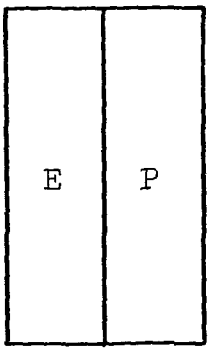

b. Elastic-Plastic Segment

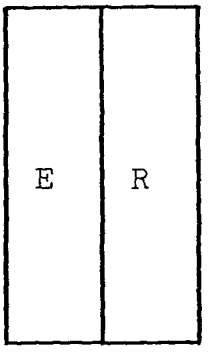

c. Elastic-Real Segment

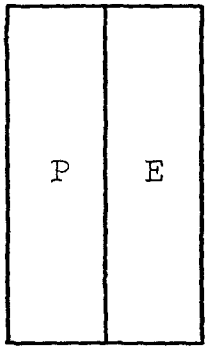

d. Plastic-Elastic Segment

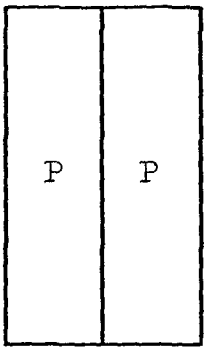

e. Plastic-Plastic Segment

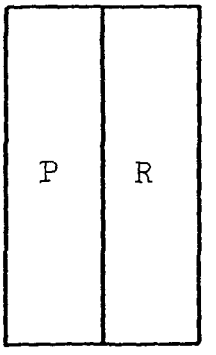

f. Plastic-Real Segment

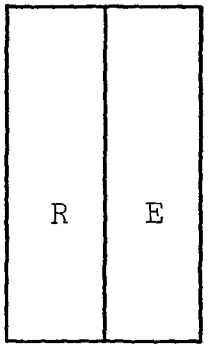

g. Real-Elastic Segment

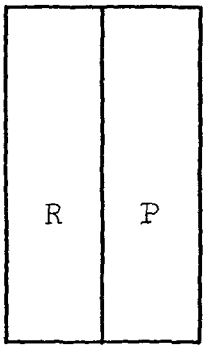

h. Real-Plastic Segment

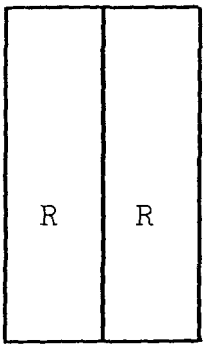

i. Real-Real Segment

FIGURE 5.4 SEGMENT STATES

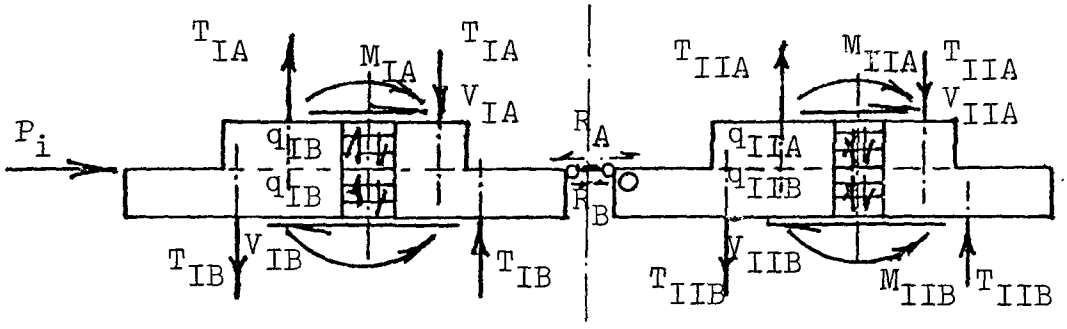

1. ELASTIC ELASTIC-ELASTIC ELASTIC STATION

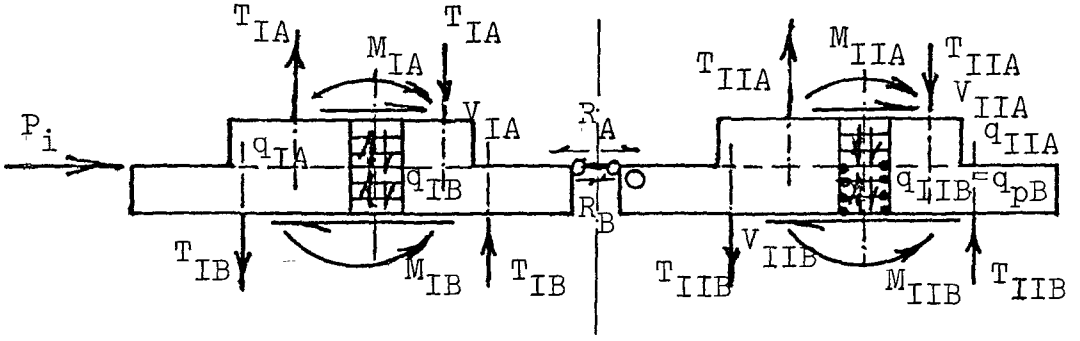

2. ELASTIC ELASTIC - ELASTIC PLASTIC STATION

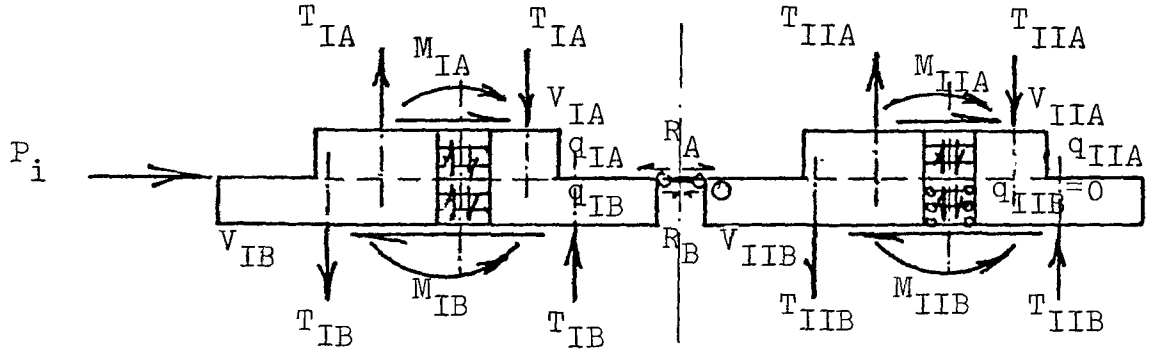

3. ELASTIC ELASTIC - ELASTIC REAL STATION

FIGURE 5-5 STATION COMBINATIONS

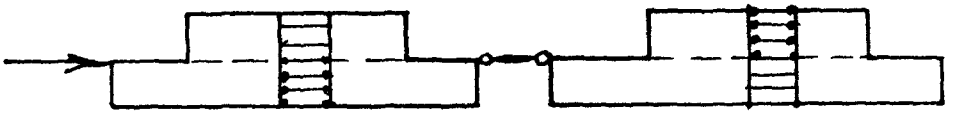

4. E1-P1 - E1-E1 Station

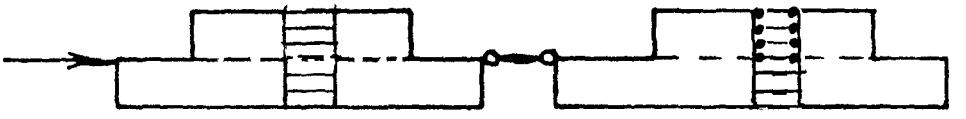

5. E1-E1 - P1-E1 Station

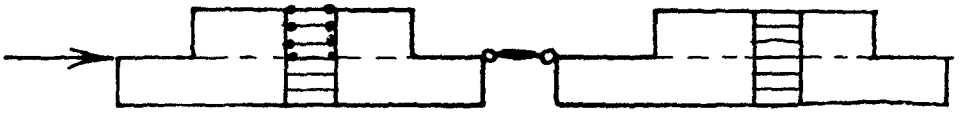

6. P1-E1 - E1-E1 Station

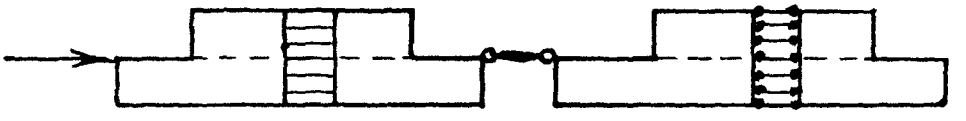

7. E1-P1 - E1-P1 Station

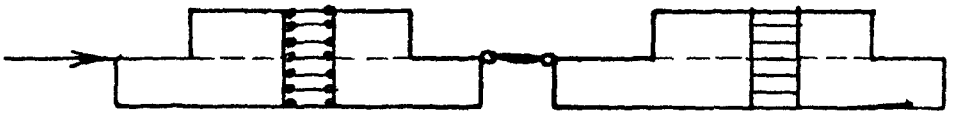

8. P1-E1 - P1-E1 Station

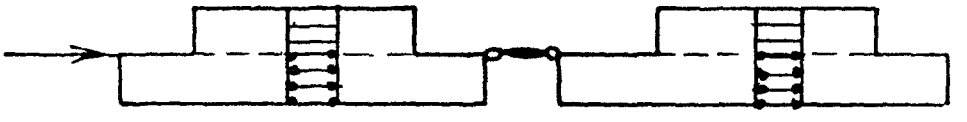

9. E1-E1 - P1-P1 Station

FIGURE 5.5 STATION COMBINATIONS

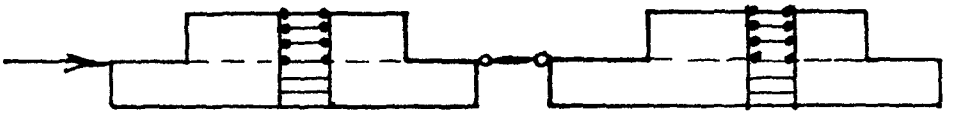

10. P1-P1 - E1-E1 Station

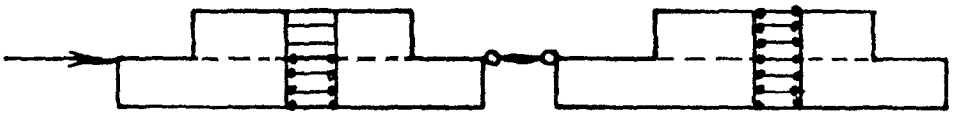

11. E1-P1 - P1-P1 Station

12. P1-P1 -E1-P1 Station

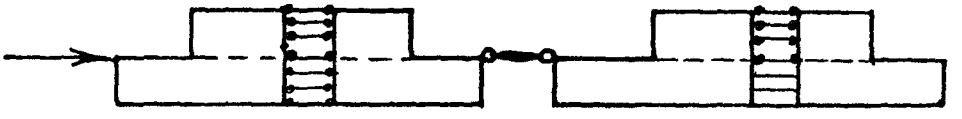

13. P1-P1 - P1-E1 Station

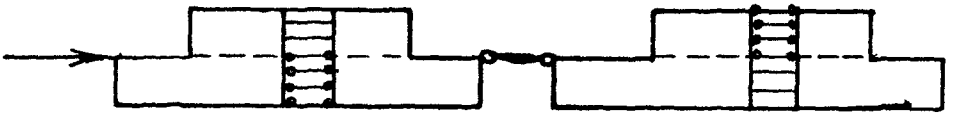

14. E1-P1 - P1-E1 Station

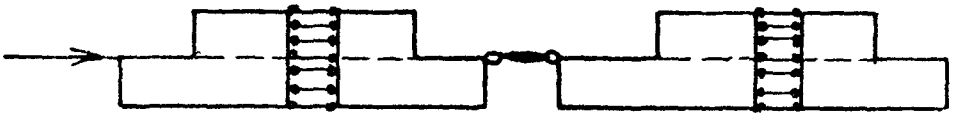

15. P1-P1 - P1-P1 Station

FIGURE 5.5 STATION COMBINATIONS

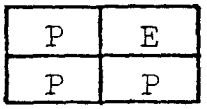

16. Pl. El. - Pl. Pl. Station

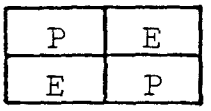

17. Pl. El. - El. Pl. Station

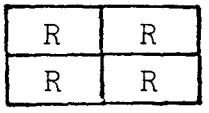

18. Real Real-Real Real Station

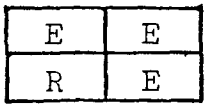

19. El. El. - Real El. Station

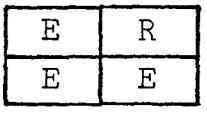

20. El. Real-El. El. Station

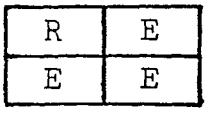

21. Real El. - El. El. Station

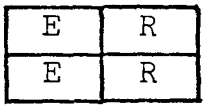

22. El. Real-El. Real Station

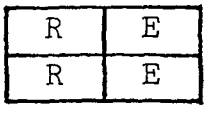

23. Real El. - Real El. Station

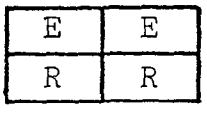

24. El. El. - Real Real Station

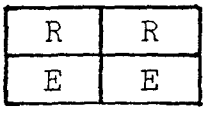

25. Real Real - El. El. Station

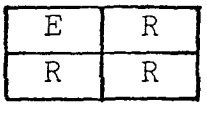

26. El. Real-Real Real Station

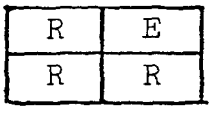

27. Real El. - Real Real Station

FIGURE 5-5 STATION COMBINATIONS

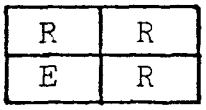

28. Real Real-El. Real Station

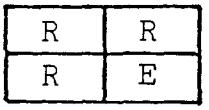

29. Real Real-Real El. Station

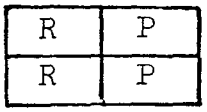

30. Real Pl. - Real Pl. Station

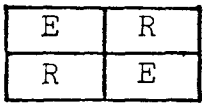

31. El. Real-Real El. Station

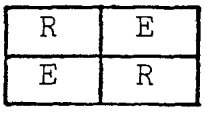

32. Real El. - El. Real Station

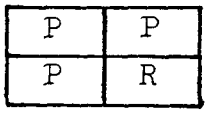

33. Pl. Pl. - Pl. Real Station

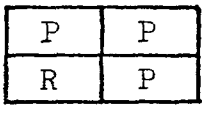

34. Pl. Pl. - Real Pl. Station

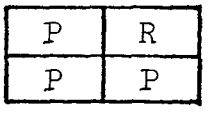

35. Pl. Real - Pl. Pl. Station

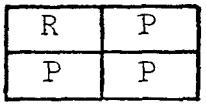

36. Real Pl. - Pl. Pl. Station

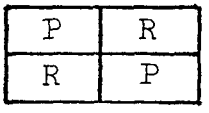

37. Pl. Real-Real Pl. Station

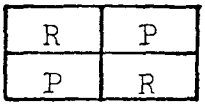

38. Real Pl. - Pl. Real Station

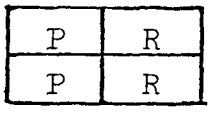

39. Pl. Real-Pl. Real Station

FIGURE 5-5 STATION COMBINATIONS

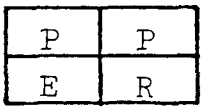

40. Pl. Pl. - El. Real Station

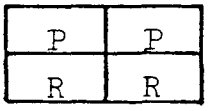

41. Pl. Pl. - Real Real Station

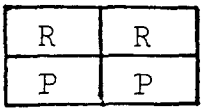

42. Real-Real - Pl. Pl. Station

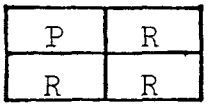

42. Pl. Real-Real Real Station

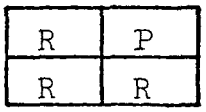

44. Real Pl. - Real Real Station

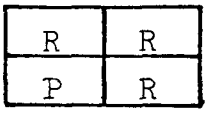

45. Real Real- Pl. Real Station

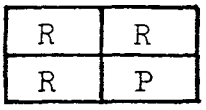

46. Real Real - Real Pl. Station

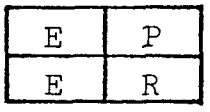

47. El. Pl. - El. Real Station

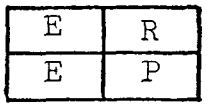

48. El. Real - El. Plastic Station

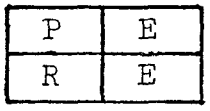

49. Pl. El. - Real El Station

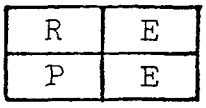

50. Real El. - Pl. El. Station

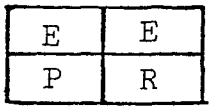

51. El. El. - Pl. Real Station

FIGURE 5-5 STATION COMBINATIONS

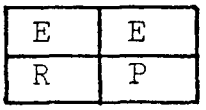

52. El. El. - Real Pl. Station

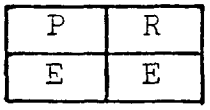

53. Pl. Real-El. El. Station

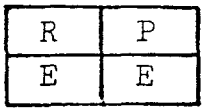

54. Real Pl. - El. El. Station

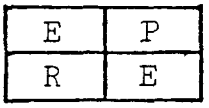

55. El. Pl. - Real El. Station

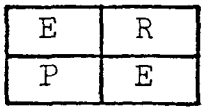

56. El. Real-Pl. El. Station

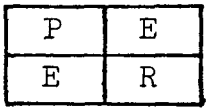

57. Pl. El. - El. Real Station

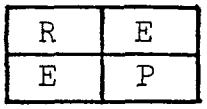

58. Real El. - El. Pl. Station

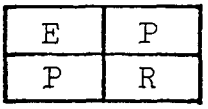

59. El. Pl. - Pl. Real Station

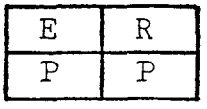

60. El. Real-Pl. Pl. Station

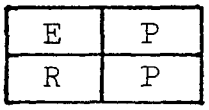

61. El. Pl. - Real Pl. Station

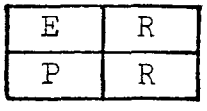

62. El. Real-Pl. Real Station

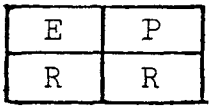

63. El. Pl. - Real Real Station

FIGURE 5.5 STATION COMBINATIONS

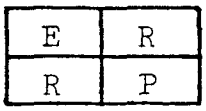

64. El. Real - Real Pl. Station

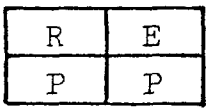

65. Real El. - Pl. Pl. Station

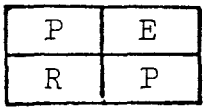

66. Pl. El. - Real Pl. Station

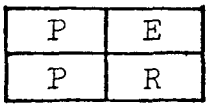

67. Pl. El. - Pl. Real Station

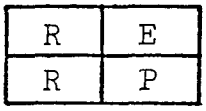

68. Real El. - Real Pl. Station

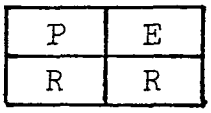

69. Pl. El. - Real Real Station

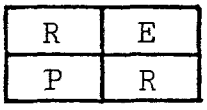

70. Real El. - Pl. Real Station

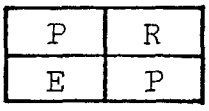

71. Pl. Real - El. Pl. Station

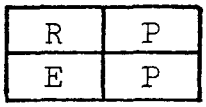

72. Real Pl. - El. Pl. Station

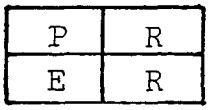

73. Pl. Real - El. Real Station

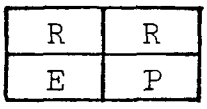

74. Real Real - El. Pl. Station

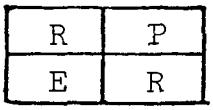

75. Real Pl. - El. Real Station

FIGURE 5-5 STATION COMBINATIONS

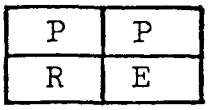

76. Pl. Pl. - Real El. Station

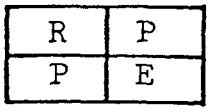

77. Real Pl. - Pl. El. Station

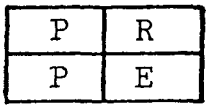

78. Pl. Real - Pl. El. Station

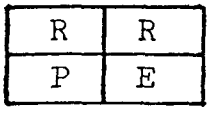

79. Real Real - Pl. El. Station

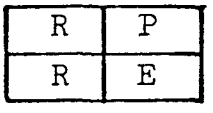

80. Real Pl. - Real El. Station

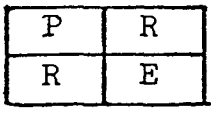

81. Pl. Real - Real El. Station

FIGURE 5-5 STATION COMBINATIONS

5.2 DEVELOPMENT OF TRANSFER MATRICES

In this section, nine field transfer matrices are developed to cover all combinations of the states of the segments for both walls. In addition, eighty-one station transfer matrices are presented which cover all the combinations of segment-state-variations.

5.2.1 Field Transfer Matrices

The field transfer matrix will relate the states at the base of the segment to the states at the top of the segment [Figure (5.3)] in the following form

$$\underset{8x1}{\{\phi\}_A} = \underset{8x8}{[F]_i}\ \underset{8x1}{\{\phi\}_B} \tag{5.1}$$

where $\{\phi\}_A$: the states at the base of ith segment.

: column $\{y\ y'\ y''\ y'''\ T_I\ T_{II}\ q_I\ q_{II}\}_{(i-1)_A}$.

$\{\phi\}_B$: the states at the top of ith segment.

: column $\{y\ y'\ y''\ y'''\ T_I\ T_{II}\ q_I\ q_{II}\}_{i_B}$.

$[F]_i$: the field transfer matrix for ith segment relating above two states

As the two shear walls are connected at each station, as shown in Fig. (5.6). The deflection of each wall at the station level should be the same as that of the center line, i.e. that of the two shear wall system. Hence

$$y_{I_A} = y_{II_A} = y_A$$
$$\text{and}\quad y_{I_B} = y_{II_B} = y_B \tag{5.2a}$$

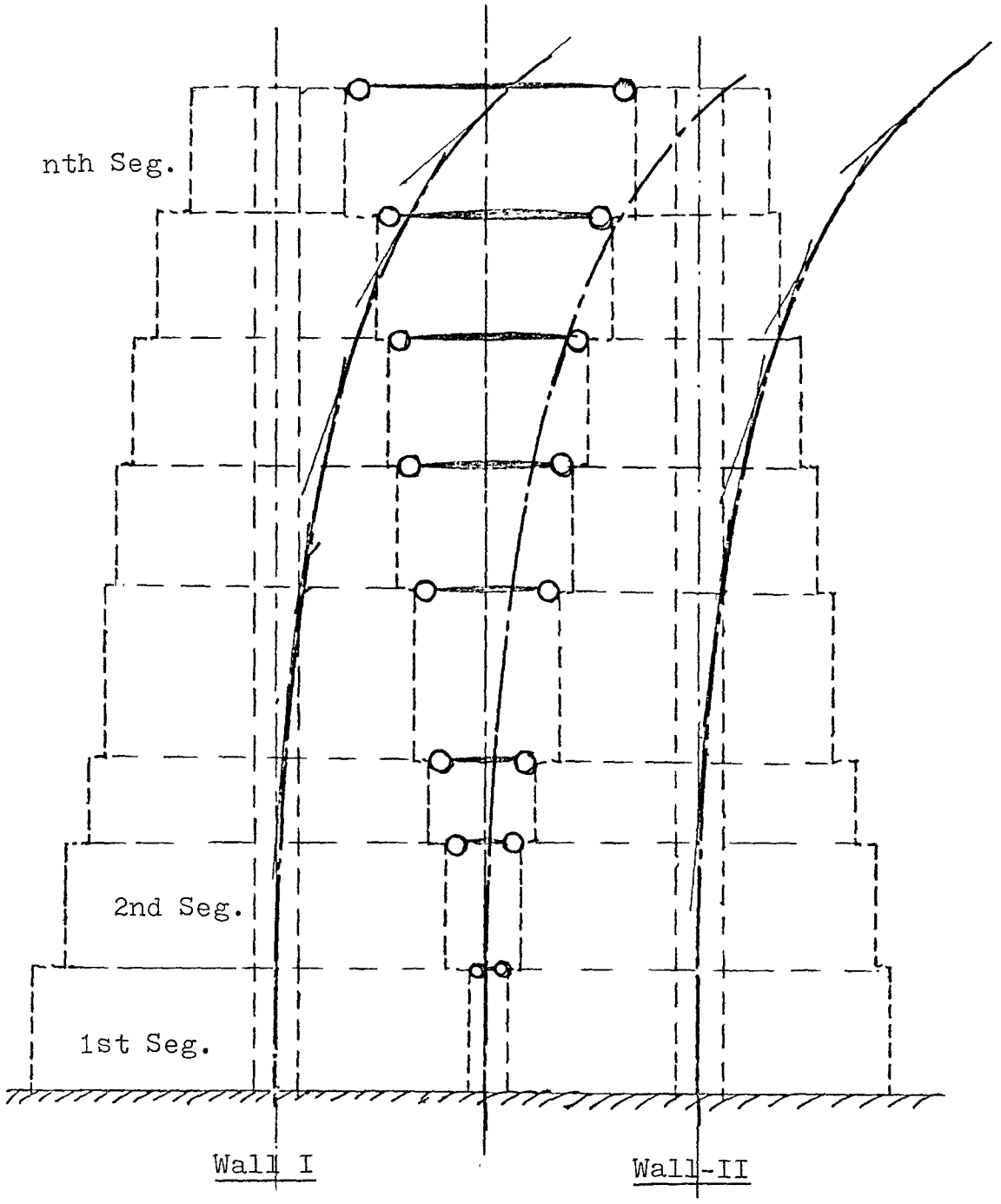

FIGURE 5.6 DEFLECTION PATTERN OF TWO INTERCONNECTED COUPLED SHEAR WALLS

As shown in Figure (5.6), the deflection pattern of each shear wall should be similar. Hence it is assumed that the slope, curvature and variation of curvature of each wall is the same at station levels. Writing in mathematical form, they become

At the bottom of the segment, and at the top of the segment,

$$y'_{IA} = y'_{IIA} = y'_{A} \qquad y'_{IB} = y'_{IIB} = y'_{B} \tag{5.2b}$$

$$y''_{IA} = y''_{IIA} = y''_{A} \qquad y''_{IB} = y''_{IIB} = y''_{B} \tag{5.2c}$$

$$y'''_{IA} = y'''_{IIA} = y'''_{A} \qquad y'''_{IB} = y'''_{IIB} = y'''_{B} \tag{5.2d}$$

Now the field transfer matrix for each coupled shear wall is individually given by a (6x6) matrix and can be written as

$$\begin{Bmatrix} y \\ y' \\ y'' \\ y''' \\ T \\ q \end{Bmatrix}_{\substack{A \\ I \\ II}} = \begin{bmatrix} F_{11} & F_{12} & F_{13} & F_{14} & F_{15} & F_{16} \\ F_{21} & F_{22} & F_{23} & F_{24} & F_{25} & F_{26} \\ F_{31} & F_{32} & F_{33} & F_{34} & F_{35} & F_{36} \\ F_{41} & F_{42} & F_{43} & F_{44} & F_{45} & F_{46} \\ F_{51} & F_{52} & F_{53} & F_{54} & F_{55} & F_{56} \\ F_{61} & F_{62} & F_{63} & F_{64} & F_{65} & F_{66} \end{bmatrix}_{\substack{I \\ II}} \begin{Bmatrix} y \\ y' \\ y'' \\ y''' \\ T \\ q \end{Bmatrix}_{\substack{B \\ I \\ II}} \tag{5.3}$$

or $\{\phi\}_{\substack{A \\ I,II}} = [F]_{I,II} \{\phi\}_{\substack{B \\ I,II}}$

where I : corresponds to first shear wall
II : corresponds to second shear wall

Using eqn. (5.3) and also the compatibility conditions given by eqns. (5.2), we get

$$y_A = \frac{y_{I_A}+y_{II_A}}{2} = \frac{F^I_{11}+F^{II}_{11}}{2} y_B + \frac{F^I_{12}+F^{II}_{12}}{2} y'_B + \frac{F^I_{13}+F^{II}_{13}}{2} y''_B + \frac{F^I_{14}+F^{II}_{14}}{2} y'''_B$$

$$+ \frac{F^I_{15}}{2} T_{I_B} + \frac{F^{II}_{15}}{2} T_{II_B} + \frac{F^I_{16}}{2} q_{I_B} + \frac{F^{II}_{16}}{2} q_{II_B}$$

$$y'_A = \frac{y'_{I_A}+y'_{II_A}}{2} = \frac{F^I_{21}+F^{II}_{21}}{2} y_B + \frac{F^I_{22}+F^{II}_{22}}{2} y'_B + \frac{F^I_{23}+F^{II}_{23}}{2} y''_B + \frac{F^I_{24}+F^{II}_{24}}{2} y'''_B$$

$$+ \frac{F^I_{25}}{2} T_{I_B} + \frac{F^{II}_{25}}{2} T_{II_B} + \frac{F^I_{26}}{2} q_{I_B} + \frac{F^{II}_{26}}{2} q_{II_B}$$

$$y''_A = \frac{y''_{I_A}+y''_{II_A}}{2} = \frac{F^I_{31}+F^{II}_{31}}{2} y_B + \frac{F^I_{32}+F^{II}_{32}}{2} y'_B + \frac{F^I_{33}+F^{II}_{33}}{2} y''_B + \frac{F^I_{34}+F^{II}_{34}}{2} y'''_B$$

$$+ \frac{F^I_{35}}{2} T_{I_B} + \frac{F^{II}_{35}}{2} T_{II_B} + \frac{F^I_{36}}{2} q_{I_B} + \frac{F^{II}_{36}}{2} q_{II_B}$$

$$y'''_A = \frac{y'''_{I_A}+y'''_{II_A}}{2} = \frac{F^I_{41}+F^{II}_{41}}{2} y_B + \frac{F^I_{42}+F^{II}_{42}}{2} y'_B + \frac{F^I_{43}+F^{II}_{43}}{2} y''_B + \frac{F^I_{44}+F^{II}_{44}}{2} y'''_B$$

$$+ \frac{F^I_{45}}{2} T_{I_B} + \frac{F^{II}_{45}}{2} T_{II_B} + \frac{F^I_{46}}{2} q_{I_B} + \frac{F^{II}_{46}}{2} q_{II_B}$$

The axial force T and lintel shear q for each of the coupled shear walls at the bottom and at the top of the segment are related by

$$T_{I_A} = F^I_{51}y_B + F^I_{52}y'_B + F^I_{53}y''_B + F^I_{54}y'''_B + F^I_{55}T_{I_B} + 0 + F^I_{56}q_{I_B} + 0$$

$$T_{II_A} = F^{II}_{51}y_B + F^{II}_{52}y'_B + F^{II}_{53}y''_B + F^{II}_{54}y'''_B + 0 + F^{II}_{55}T_{II_B} + 0 + F^{II}_{56}q_{II_B}$$

$$q_{I_A} = F^I_{61}y_B + F^I_{62}y'_B + F^I_{63}y''_B + F^I_{64}y'''_B + F^I_{65}T_{I_B} + 0 + F^I_{66}q_{I_B} + 0$$

$$q_{II_A} = F^{II}_{61}y_B + F^{II}_{62}y'_B + F^{II}_{63}y''_B + F^{II}_{64}y'''_B + 0 + F^{II}_{65}T_{II_B} + 0 + F^{II}_{66}q_{II_B}$$

Writing this in matrix form, we get the field transfer matrix for two coupled shear walls system as,

$$\begin{Bmatrix} y \\ y' \\ y'' \\ y''' \\ T_I \\ T_{II} \\ q_I \\ q_{II} \end{Bmatrix}_{A}^{(i-1)} = \begin{bmatrix} \overrightarrow{F}_{11} & \overrightarrow{F}_{12} & \overrightarrow{F}_{13} & \overrightarrow{F}_{14} & F^I_{15}/2 & F^{II}_{15}/2 & F^I_{16}/2 & F^{II}_{16}/2 \\ \overrightarrow{F}_{21} & \overrightarrow{F}_{22} & \overrightarrow{F}_{23} & \overrightarrow{F}_{24} & F^I_{25}/2 & F^{II}_{25}/2 & F^I_{26}/2 & F^{II}_{26}/2 \\ \overrightarrow{F}_{31} & \overrightarrow{F}_{32} & \overrightarrow{F}_{33} & \overrightarrow{F}_{34} & F^I_{35}/2 & F^{II}_{35}/2 & F^I_{36}/2 & F^{II}_{36}/2 \\ \overrightarrow{F}_{41} & \overrightarrow{F}_{42} & \overrightarrow{F}_{43} & \overrightarrow{F}_{44} & F^I_{45}/2 & F^{II}_{45}/2 & F^I_{46}/2 & F^{II}_{46}/2 \\ F^I_{51} & F^I_{52} & F^I_{53} & F^I_{54} & F^I_{55} & 0 & F^I_{56} & 0 \\ F^{II}_{51} & F^{II}_{52} & F^{II}_{53} & F^{II}_{54} & 0 & F^{II}_{55} & 0 & F^{II}_{56} \\ F^I_{61} & F^I_{62} & F^I_{63} & F^I_{64} & F^I_{65} & 0 & F^I_{66} & 0 \\ F^{II}_{61} & F^{II}_{62} & F^{II}_{63} & F^{II}_{64} & 0 & F^{II}_{65} & 0 & F^{II}_{66} \end{bmatrix}_{i} \begin{Bmatrix} y \\ y' \\ y'' \\ y''' \\ T_I \\ T_{II} \\ q_I \\ q_{II} \end{Bmatrix}_{B}^{i} \tag{5.4a}$$

that is,

$$\{\phi\}_A = [F]_i \{\phi\}_B \tag{5.4b}$$

where: FI_{ij} : element in ith row, jth column in FTM for first shear wall

F^{II}_{ij} : element in ith row, jth column in FTM for second shear wall

$$\tilde{F}_{k\ell} = \frac{F^{I}_{k\ell} + F^{II}_{k\ell}}{2}$$

$i,j = 1, 6$

$k,\ell = 1, 4$

It should be noted that depending on the states of the connecting beams in the segment of the first and the second wall, the corresponding field transfer matrices (of order 6x6) should be used to get the appropriate field transfer matrix (of order 8x8) to relate the states y, y', y", y"', T_I, T_{II}, q_I and q_{II} in the two interconnected coupled shear wall problem.

5.2.2 Station Transfer Matrices

Listed below are sixteen basic station transfer matrices with their derivations. The remaining sixty-five matrices may be derived from combination of these basic matrices as mentioned below.

5.2.2.1 Station Transfer Matrix Relating a State Vector in an Elastic Segment of First Wall and an Elastic Segment of the Second Wall to State Vector in an Elastic Segment of First Wall and an Elastic Segment of Second Wall Respectively [Elastic Elastic-Elastic Elastic S.T.M.;] $\begin{bmatrix} E & E \\ E & E \end{bmatrix}$

From the continuity conditions of the walls at the station as deflecton and slope should be the same at bottom and top of the station.

$$y_B = y_A \tag{5.5}$$

$$y'_B = y'_A \tag{5.6}$$

from the equilibrium of vertical forces at the top and bottom of station

$$T_{I_B} = T_{I_A} \tag{5.7}$$

$$T_{II_B} = T_{II_A} \tag{5.8}$$

Equilibrium of moment about the central point "0" [Ref. Figure 5.5(1)] gives

$$M_{IA} + T_{IA}\, a_{IA} + M_{IIA} + T_{IIA}\, a_{IIA} = M_{IB} + T_{IB}\, a_{IB} + M_{IIB} + T_{IIB}\, a_{IIB}$$

Substituting for moment and axial force from eqns. (2.13), (5.7) and (5.8) gives

$$EI_{I_A} y''_A + T_{I_A} a_{I_A} + EI_{II_A} y''_A + T_{II_A} a_{II_A} = EI_{I_B} y''_B + T_{I_A} a_{I_B} + EI_{II_B} y''_B + T_{II_A} a_{II_B}$$

therefore

$$y_B'' = \frac{I_A}{I_B} y_A'' + \frac{a_{I_A} - a_{I_B}}{EI_B} T_{I_A} + \frac{a_{II_A} - a_{II_B}}{EI_B} T_{II_A} \tag{5.9}$$

where $I_A = I_{I_A} + I_{II_A}$; $I_B \quad I_{I_B} + I_{II_B}$

Equilibrium of lateral forces gives

$$V_{I_A} + V_{II_A} + P_i = V_{I_B} + V_{II_B}$$

therefore from eqn. (2.6)

$$-EI_{I_A} y_A''' + q_{I_A} a_{I_A} - EI_{II_A} y_A''' - q_{II_A} a_{II_A} + P_i$$

$$= EI_{I_B} y_B''' + q_{I_B} a_{I_B} - EI_{II_B} y_B''' + q_{II_B} a_{II_B} \tag{5.10}$$

as from equation (2.33), shear intensity at the bottom and top of station "i" are related by

$$q_{I_B} = \left(\frac{a_A \mu_B^2}{a_B \mu_A^2} \right)_I q_{I_A} \tag{5.11}$$

$$q_{II_B} = \left(\frac{a_A \mu_B^2}{a_B \mu_A^2} \right)_{II} q_{II_A} \tag{5.12}$$

Hence equation (5.10) will be

$$y_B''' = \frac{I_A}{I_B} y_A''' + \left(\frac{\mu_B^2 - \mu_A^2}{\mu_A^2} \right)_I \frac{a_{I_A}}{EI_B} q_{I_A} + \left(\frac{\mu_B^2 - \mu_A^2}{\mu_A^2} \right)_{II} \frac{a_{II_A}}{EI_B} q_{II_A} - \frac{P_i}{EI_B} \tag{5.13}$$

The station transfer matrix then becomes

$$\begin{Bmatrix} y \\ y' \\ y'' \\ y''' \\ T_I \\ T_{II} \\ q_I \\ q_{II} \end{Bmatrix}_{iB} = \begin{bmatrix} 1 & 0 & 0 & 0 & 0 & 0 & 0 & 0 \\ 0 & 1 & 0 & 0 & 0 & 0 & 0 & 0 \\ 0 & 0 & \frac{I_A}{I_B} & 0 & \frac{(a_A-a_B)_I}{EI_B} & \frac{(a_A-a_B)_{II}}{EI_B} & 0 & 0 \\ 0 & 0 & 0 & \frac{I_A}{I_B} & 0 & 0 & \frac{-a_{I_A}}{EI_B}(1-\frac{\mu_B^2}{\mu_A^2})_I & \frac{-a_{II_A}}{EI_B}(1-\frac{\mu_B^2}{\mu_A^2})_{II} \\ 0 & 0 & 0 & 0 & 1 & 0 & 0 & 0 \\ 0 & 0 & 0 & 0 & 0 & 1 & 0 & 0 \\ 0 & 0 & 0 & 0 & 0 & 0 & (\frac{a_A\mu_B^2}{a_B\mu_A^2})_I & 0 \\ 0 & 0 & 0 & 0 & 0 & 0 & 0 & (\frac{a_A\mu_B^2}{a_A\mu_B^2})_{II} \end{bmatrix} \begin{Bmatrix} y \\ y' \\ y'' \\ y''' \\ T_I \\ T_{II} \\ q_I \\ q_{II} \end{Bmatrix}_{iA} + \begin{Bmatrix} 0 \\ 0 \\ 0 \\ \frac{-P_i}{EI_B} \\ 0 \\ 0 \\ 0 \\ 0 \end{Bmatrix} \tag{5.14}$$

5.2.2.2 Elastic Elastic-Elastic Plastic Station Transfer Matrix $\left[\begin{array}{c|c} E & E \\ \hline E & P \end{array}\right]$

From the continuity and equilibrium conditions at the bottom and top of the station, equations (5.5), (5.6), (5.7), (5.8) and (5.9)) hold good.

Equilibrium of lateral forces gives the same equation no. (5.10). But as the segment of the second wall at the bottom of station is in a plastic state [Fig. 5.5(2).]

$$q_{II_B} = q_{II_{PB}} \tag{5.15}$$

Hence from equation (5.11) and (5.15), eqn. (5.10) becomes

$$y_B''' = \frac{I_A}{I_B} y_A''' + \frac{a_{I_A}}{EI_B}\left(\frac{\mu_B^2}{\mu_A^2} - 1\right)_I q_{I_A} - \frac{a_{II_A}}{EI_B} q_{II_A} - \frac{(P_i - q_{II_{PB}} a_{II_B})}{EI_B}$$

Hence the station transfer matrix becomes

$$\begin{Bmatrix} y \\ y' \\ y'' \\ y''' \\ T_I \\ T_{II} \\ q_I \\ q_{II}=q_{PII} \end{Bmatrix}_{iB} = \begin{bmatrix} 1 & 0 & 0 & 0 & 0 & 0 & 0 & 0 \\ 0 & 1 & 0 & 0 & 0 & 0 & 0 & 0 \\ 0 & 0 & \frac{I_A}{I_B} & 0 & \frac{(a_A-a_B)_I}{EI_B} & \frac{(a_A-a_B)_{II}}{EI_B} & 0 & 0 \\ 0 & 0 & 0 & \frac{I_A}{I_B} & 0 & 0 & \frac{-a_{I_A}}{EI_B}\left(1 - \frac{\mu_B^2}{\mu_A^2}\right)_I & \frac{-a_{II_A}}{EI_B} \\ 0 & 0 & 0 & 0 & 1 & 0 & 0 & 0 \\ 0 & 0 & 0 & 0 & 0 & 1 & 0 & 0 \\ 0 & 0 & 0 & 0 & 0 & 0 & \left(\frac{a_A \mu_B^2}{a_B \mu_A^2}\right)_I & 0 \\ 0 & 0 & 0 & 0 & 0 & 0 & 0 & \left(\frac{a_A \mu_B^2}{a_B \mu_A^2}\right)_{II} \end{bmatrix}$$

$$\begin{Bmatrix} y \\ y' \\ y'' \\ y''' \\ T_I \\ T_{II} \\ q_I \\ q_{II} \end{Bmatrix}_{iA} + \begin{Bmatrix} 0 \\ 0 \\ 0 \\ \frac{-(P_i - q_{II_{PB}} a_{II_B})}{EI_B} \\ 0 \\ 0 \\ 0 \\ 0 \end{Bmatrix} \tag{5.17}$$

5.2.2.3 Elastic Elastic-Plastic Elastic Station Transfer Matrix $\left[\begin{array}{c|c} E & E \\ \hline P & E \end{array}\right]$

Equations (5.5) to (5.9) and (5.12) hold good, and with segment of the first wall at the base of the station in the plastic state, we have

$$q_{I_B} = q_{I_{PB}} \tag{5.18}$$

Equation (5.10) becomes

$$y_B''' = \frac{I_A}{I_B} y_A''' - \frac{a_{I_A}}{EI_B} q_{I_A} + \frac{a_{II_A}}{EI_B} \left(\frac{\mu_B^2}{\mu_A^2} - 1 \right)_{II} q_{II_A} - \frac{(P_i - q_{II_{PB}} a_{II_B})}{EI_B} \tag{5.19}$$

Hence the station transfer matrix becomes

$$\begin{Bmatrix} y \\ y' \\ y'' \\ y''' \\ T_I \\ T_{II} \\ q_I = q_{I_P} \\ q_{II} \end{Bmatrix}_{iB} = \begin{bmatrix} 1 & 0 & 0 & 0 & 0 & 0 & 0 & 0 \\ 0 & 1 & 0 & 0 & 0 & 0 & 0 & 0 \\ 0 & 0 & \frac{I_A}{I_B} & 0 & \frac{(a_A - a_B)_I}{EI_B} & \frac{(a_A - a_B)_{II}}{EI_B} & 0 & 0 \\ 0 & 0 & 0 & \frac{I_A}{I_B} & 0 & 0 & \frac{-a_{I_A}}{EI_B} & \frac{-a_{II_A}}{EI_B}\left(1 - \frac{\mu_B^2}{\mu_A^2}\right)_{II} \\ 0 & 0 & 0 & 0 & 1 & 0 & 0 & 0 \\ 0 & 0 & 0 & 0 & 0 & 1 & 0 & 0 \\ 0 & 0 & 0 & 0 & 0 & 0 & \left(\frac{a_A \mu_B^2}{a_B \mu_A^2}\right)_I & 0 \\ 0 & 0 & 0 & 0 & 0 & 0 & 0 & \left(\frac{a_A \mu_B^2}{a_B \mu_A^2}\right)_{II} \end{bmatrix}$$

$$\begin{Bmatrix} \begin{bmatrix} y \\ y' \\ y'' \\ y''' \\ T_I \\ T_{II} \\ q_I \\ q_{II} \end{bmatrix}_{iA} + \begin{bmatrix} 0 \\ 0 \\ 0 \\ \frac{-(P_i - q_{I_{PB}} a_{I_B})}{EI_B} \\ 0 \\ 0 \\ 0 \\ 0 \end{bmatrix} \end{Bmatrix} \tag{5.20}$$

5.2.2.4 Elastic Plastic-Elastic Elastic Station Transfer Matrix

$$\left[\begin{array}{c|c} E & P \\ \hline E & E \end{array}\right]$$

Equations (5.5) to (5.9) and (5.12) remain valid, and with the second wall segment at the top of station in the plastic state

$$q_{II_B} = \left(\frac{a_A \mu_B^2}{a_B \mu_A^2} \right)_{II} q_{II_{PA}} \tag{5.21}$$

from eqns. (5.11) and (5.21), eqn. (5.10) becomes

$$y_B''' = \frac{I_A}{I_B} y_A''' + \frac{a_{I_A}}{EI_B} \left(\frac{\mu_B^2}{\mu_A^2} - 1 \right)_I q_{I_A} - \frac{[P_i - a_{II_A} (\frac{\mu_B^2}{\mu_A^2} - 1)_{II} q_{II_{PA}}}{EI_B} \tag{5.22}$$

Hence the station transfer matrix becomes

$$\begin{Bmatrix} y \\ y' \\ y'' \\ y''' \\ T_I \\ T_{II} \\ q_I \\ q_{II} \end{Bmatrix}_{iB} = \begin{bmatrix} 1 & 0 & 0 & 0 & 0 & 0 & 0 & 0 \\ 0 & 1 & 0 & 0 & 0 & 0 & 0 & 0 \\ 0 & 0 & \frac{I_A}{I_B} & 0 & \frac{(a_A-a_B)_I}{EI_B} & \frac{(a_A-a_B)_{II}}{EI_B} & 0 & 0 \\ 0 & 0 & 0 & \frac{I_A}{I_B} & 0 & 0 & \frac{-a_{I_A}}{EI_B}\left(1-\frac{\mu_B^2}{\mu_A^2}\right)_I & 0 \\ 0 & 0 & 0 & 0 & 1 & 0 & 0 & 0 \\ 0 & 0 & 0 & 0 & 0 & 1 & 0 & 0 \\ 0 & 0 & 0 & 0 & 0 & 0 & \left(\frac{a_A\,\mu_B^2}{a_B\,\mu_A^2}\right)_I & 0 \\ 0 & 0 & 0 & 0 & 0 & 0 & 0 & 0 \end{bmatrix} \begin{Bmatrix} y \\ y' \\ y'' \\ y''' \\ T_I \\ T_{II} \\ q_I \\ q_{II}=q_{II_P} \end{Bmatrix}_{iA} + \begin{Bmatrix} 0 \\ 0 \\ 0 \\ -\left[\frac{P_i-a_{II_A}\left(\frac{\mu_B^2}{\mu_A^2}-1\right)_{II}q_{II_{PA}}}{EI_B}\right] \\ 0 \\ 0 \\ 0 \\ \left(\frac{a_A\,\mu_B^2}{a_B\,\mu_A^2}\right)_{II} q_{II_{PA}} \end{Bmatrix} \tag{5.23}$$

5.2.2.5 Plastic Elastic-Elastic Elastic Station Transfer Matrix

$$\left[\begin{array}{c|c} P & E \\ \hline E & E \end{array}\right]$$

Equations (5.5) to (5.9) and (5.12) remain valid, and with the first wall segment at the top of the station in the plastic state

$$q_{I_B} = \left(\frac{a_A \mu_B^2}{a_B \mu_A^2}\right) q_{I_{PA}} \tag{5.24}$$

From equations (5.24) and (5.12), equation (5.10) becomes

$$y_B''' = \frac{I_A}{I_B} y_A''' + \frac{a_{II_A}}{EI_B}\left(\frac{\mu_B^2}{\mu_A^2} - 1\right) q_{II_A} - \frac{[P_i - a_{I_A}\left(\frac{\mu_B^2}{\mu_A^2} - 1\right)_I q_{I_{PA}}}{EI_B} \tag{5.25}$$

Hence the station transfer matrix becomes

$$\left\{\begin{array}{c} y \\ y' \\ y'' \\ y''' \\ T_I \\ T_{II} \\ q_I \\ q_{II} \end{array}\right\}_{iB} = \left[\begin{array}{cccccccc} 1 & 0 & 0 & 0 & 0 & 0 & 0 & 0 \\ 0 & 1 & 0 & 0 & 0 & 0 & 0 & 0 \\ 0 & 0 & \frac{I_A}{I_B} & 0 & \frac{(a_A - a_B)_I}{EI_B} & \frac{(a_A - a_B)_{II}}{EI_B} & 0 & 0 \\ 0 & 0 & 0 & \frac{I_A}{I_B} & 0 & 0 & 0 & \frac{-a_{II_A}}{EI_B}\left(1 - \frac{\mu_B^2}{\mu_A^2}\right)_{II} \\ 0 & 0 & 0 & 0 & 1 & 0 & 0 & 0 \\ 0 & 0 & 0 & 0 & 0 & 1 & 0 & 0 \\ 0 & 0 & 0 & 0 & 0 & 0 & 0 & 0 \\ 0 & 0 & 0 & 0 & 0 & 0 & 0 & \left(\frac{a_A \mu_B^2}{a_B \mu_A^2}\right)_{II} \end{array}\right]$$

$$\begin{Bmatrix} y \\ y' \\ y'' \\ y''' \\ T_I \\ T_{II} \\ q_I = q_{I_P} \\ q_{II} \end{Bmatrix}_{iA} + \begin{Bmatrix} 0 \\ 0 \\ 0 \\ \dfrac{-[P_i - a_{I_A}\left(\dfrac{\mu_B^2}{\mu_A^2} - 1\right)_I q_{I_{PA}}]}{EI_B} \\ 0 \\ 0 \\ \left(\dfrac{a_A \mu_B^2}{a_B \mu_A^2}\right)_I q_{I_{PA}} \\ 0 \end{Bmatrix} \tag{5.26}$$

5.2.2.6 Plastic Plastic-Elastic Plastic Station Transfer Matrix

$$\left[\begin{array}{c|c} E & P \\ \hline E & P \end{array}\right]$$

Equations (5.5) to (5.9) and (5.12) hold good, and with the second wall segment at the top and bottom of staton in the plastic state

$$q_{II_B} = q_{II_{PB}} \tag{5.27}$$

Eqn. (5.10) becomes

$$y_B''' = \frac{I_A}{I_B} y_A''' + \frac{q_{I_A}}{EI_B}\left(\frac{\mu_B^2}{\mu_A^2} - 1\right)_I q_{I_A} - \frac{(P_i + q_{II_{PA}} a_{II_A} - q_{II_{PB}} a_{II_B})}{EI_B} \tag{5.28}$$

Hence the station transfer matrix becomes

$$
\begin{Bmatrix} y \\ y' \\ y'' \\ y''' \\ T_I \\ T_{II} \\ q_I \\ q_{II}=q_{II_P} \end{Bmatrix}_{iB} =
\begin{bmatrix}
1 & 0 & 0 & 0 & 0 & 0 & 0 & 0 \\
0 & 1 & 0 & 0 & 0 & 0 & 0 & 0 \\
0 & 0 & \frac{I_A}{I_B} & 0 & \frac{(a_A-a_B)_I}{EI_B} & \frac{(a_A-a_B)_{II}}{EI_B} & 0 & 0 \\
0 & 0 & 0 & \frac{I_A}{I_B} & 0 & 0 & \frac{-a_{I_A}}{EI_B}\left(1-\frac{\mu_B^2}{\mu_A^2}\right)_I & 0 \\
0 & 0 & 0 & 0 & 1 & 0 & 0 & 0 \\
0 & 0 & 0 & 0 & 0 & 1 & 0 & 0 \\
0 & 0 & 0 & 0 & 0 & 0 & \left(\frac{a_A}{a_B}\frac{\mu_B^2}{\mu_A^2}\right)_I & 0 \\
0 & 0 & 0 & 0 & 0 & 0 & 0 & 0
\end{bmatrix}
\begin{Bmatrix} y \\ y' \\ y'' \\ y''' \\ T_I \\ T_{II} \\ q_I \\ q_{II}=q_{II_P} \end{Bmatrix}_{iA}
+
\begin{Bmatrix} 0 \\ 0 \\ 0 \\ \frac{-[P_i-(q_{PB}a_B-q_{PA}a_A)]_{II}}{EI_B} \\ 0 \\ 0 \\ 0 \\ q_{II_{PB}} \end{Bmatrix}
$$

(5.29)

5.2.2.7 Plastic Elastic-Plastic Elastic Station Transfer Matrix

$$\left[\begin{array}{c|c} P & E \\ \hline P & E \end{array}\right]$$

Equations (5.5) to (5.9) and (5.12) remain valid, and with the first wall segments at the top and bottom of the station in the plastic state

$$q_{I_B} = q_{I_{PB}} \tag{5.30}$$

Equation (5.10) becomes

$$y'''_B = \frac{I_A}{I_B} y'''_A + \frac{a_{II_A}}{EI_B} \left(\frac{\mu_B^2}{\mu_A^2} - 1 \right)_{II} q_{II_A} - \frac{(P_i - q_{I_{PB}} a_{I_B} + q_{I_{PA}} a_{I_A})}{EI_B} \tag{5.31}$$

Hence the station transfer matrix becomes

$$\begin{Bmatrix} y \\ y' \\ y'' \\ y''' \\ T_I \\ T_{II} \\ q_I = q_{I_P} \\ q_{II} \end{Bmatrix} = \begin{bmatrix} 1 & 0 & 0 & 0 & 0 & 0 & 0 & 0 \\ 0 & 1 & 0 & 0 & 0 & 0 & 0 & 0 \\ 0 & 0 & \frac{I_A}{I_B} & 0 & \frac{(a_A - a_B)_I}{EI_B} & \frac{(a_A - a_B)_{II}}{EI_B} & 0 & 0 \\ 0 & 0 & 0 & \frac{I_A}{I_B} & 0 & 0 & 0 & \frac{-a_{II_A}}{EI_B} \left(1 - \frac{\mu_B^2}{\mu_A^2}\right)_{II} \\ 0 & 0 & 0 & 0 & 1 & 0 & 0 & 0 \\ 0 & 0 & 0 & 0 & 0 & 1 & 0 & 0 \\ 0 & 0 & 0 & 0 & 0 & 0 & 0 & 0 \\ 0 & 0 & 0 & 0 & 0 & 0 & 0 & \left(\frac{a_A \mu_B^2}{a_B \mu_A^2}\right)_{II} \end{bmatrix}$$

iB

$$\begin{Bmatrix} y \\ y' \\ y'' \\ y''' \\ T_I \\ T_{II} \\ q_I = q_{I_P} \\ q_{II} \end{Bmatrix}_{iA} + \begin{bmatrix} 0 \\ 0 \\ 0 \\ \dfrac{-[P_i-(q_{PB}a_B-q_{PA}a_A)_I}{EI_B} \\ 0 \\ 0 \\ q_{I_{PB}} \\ 0 \end{bmatrix} \tag{5.32}$$

5.2.2.8 Elastic Elastic-Plastic Plastic Station Transfer Matrix

$$\left[\begin{array}{c|c} E & E \\ \hline P & P \end{array}\right]$$

Equations (5.5) to (5.9) and (5.12) remain valid, and with the segments of both walls at the bottom of the station in the plastic state

$$q_{I_B} = \left(\frac{a_A \mu_B^2}{a_B \mu_A^2}\right)_I q_{I_A} = q_{I_{PB}} \tag{5.33}$$

$$q_{II_B} = \left(\frac{a_A \mu_B^2}{a_B \mu_A^2}\right)_{II} q_{II_A} = q_{II_{PB}} \tag{5.34}$$

Therefore eqn. (5.10) becomes

$$y_B''' = \frac{I_A}{I_B} y_A''' - \frac{a_{I_A}}{EI_B} q_{I_A} - \frac{a_{II_A}}{EI_B} q_{II_A} - \frac{(P_i - q_{I_{PB}} a_{I_B} - q_{II_{PB}} a_{II_B})}{EI_B} \tag{5.35}$$

Hence the station transfer matrix becomes

$$
\begin{Bmatrix} y \\ y' \\ y'' \\ y''' \\ T_I \\ T_{II} \\ q_I = q_{I_P} \\ q_{II} = q_{II_P} \end{Bmatrix}_{iB} =
\begin{bmatrix}
1 & 0 & 0 & 0 & 0 & 0 & 0 & 0 \\
0 & 1 & 0 & 0 & 0 & 0 & 0 & 0 \\
0 & 0 & \frac{I_A}{I_B} & 0 & \frac{(a_A - a_B)_I}{EI_B} & \frac{(a_A - a_B)_{II}}{EI_B} & 0 & 0 \\
0 & 0 & 0 & \frac{I_A}{I_B} & 0 & 0 & \frac{-a_{I_A}}{EI_B} & \frac{-a_{I_A}}{EI_B} \\
0 & 0 & 0 & 0 & 1 & 0 & 0 & 0 \\
0 & 0 & 0 & 0 & 0 & 1 & 0 & 0 \\
0 & 0 & 0 & 0 & 0 & 0 & \left(\frac{a_A \mu_B^2}{a_B \mu_A^2}\right)_I & 0 \\
0 & 0 & 0 & 0 & 0 & 0 & 0 & \left(\frac{a_A \mu_B^2}{a_B \mu_A^2}\right)_{II}
\end{bmatrix}
\begin{Bmatrix} y \\ y' \\ y'' \\ y''' \\ T_I \\ T_{II} \\ q_I \\ q_{II} \end{Bmatrix}_{iA}
+
\begin{Bmatrix} 0 \\ 0 \\ 0 \\ \frac{-(P_i - q_{I_{PB}} a_{I_B} - q_{II_{PB}} a_{II_B})}{EI_B} \\ 0 \\ 0 \\ 0 \\ 0 \end{Bmatrix}
\tag{5.36}
$$

5.2.2.9 Plastic Plastic-Elastic Elastic Station Transfer Matrix

$$\left[\begin{array}{c|c} P & P \\ \hline E & E \end{array}\right]$$

Equations (5.5) to (5.9) and (5.12) remain valid, and with the segments of both walls at the top of the station in the plastic state

$$q_{I_B} = \left(\frac{a_A \mu_B^2}{a_B \mu_A^2}\right)_I q_{I_{PA}} \tag{5.37}$$

$$q_{I_B} = \left(\frac{a_A \mu_B^2}{a_B \mu_A^2}\right)_{II} q_{II_{PA}} \tag{5.38}$$

Equation (5.10) becomes

$$y_B''' = \frac{I_A}{I_B} y_A''' - \{P_i - [a_A(\frac{\mu_B^2}{\mu_A^2} - 1)q_{PA}]_I - [a_A(\frac{\mu_B^2}{\mu_A^2} - 1)q_{PA}]_{II}\}/EI_B \tag{5.39}$$

Hence the station transfer matrix becomes

$$\begin{Bmatrix} y \\ y' \\ y'' \\ y''' \\ \\ T_I \\ T_{II} \\ q_I \\ q_{II} \end{Bmatrix}_{i_B} = \begin{bmatrix} 1 & 0 & 0 & 0 & 0 & 0 & 0 & 0 \\ 0 & 1 & 0 & 0 & 0 & 0 & 0 & 0 \\ 0 & 0 & \frac{I_A}{I_B} & 0 & \frac{(a_A-a_B)_I}{EI_B} & \frac{(a_A-a_B)_{II}}{EI_B} & 0 & 0 \\ 0 & 0 & & \frac{I_A}{I_B} & 0 & 0 & 0 & 0 \\ & & & & & & & \\ 0 & 0 & 0 & 0 & 1 & 0 & 0 & 0 \\ 0 & 0 & 0 & 0 & 0 & 1 & 0 & 0 \\ 0 & 0 & 0 & 0 & 0 & 0 & 0 & 0 \\ 0 & 0 & 0 & 0 & 0 & 0 & 0 & 0 \end{bmatrix}$$

$$\begin{Bmatrix} y \\ y' \\ y'' \\ y''' \\ T_I \\ T_{II} \\ q_I = q_{I_P} \\ q_{II} = q_{II_P} \end{Bmatrix}_{iA} + \begin{bmatrix} 0 \\ 0 \\ 0 \\ \dfrac{-[P_i - a_{I_A}\left(\dfrac{\mu_B^2}{\mu_A^2} - 1\right)_I q_{I_{PA}} - a_{II_A}\left(\dfrac{\mu_B^2}{\mu_A^2} - 1\right)_{II} q_{II_{PA}}]}{EI_B} \\ 0 \\ 0 \\ \left(\dfrac{a_A}{a_B}\dfrac{\mu_B^2}{\mu_A^2}\right)_I q_{I_{PA}} \\ \left(\dfrac{a_A}{a_B}\dfrac{\mu_B^2}{\mu_A^2}\right)_{II} q_{II_{PA}} \end{bmatrix} \tag{5.40}$$

5.2.2.10 Elastic Plastic-Plastic Plastic Station Transfer Matrix

$$\left[\begin{array}{c|c} E & P \\ \hline P & P \end{array}\right]$$

Equations (5.5) to (5.9) and (5.12) remain valid, and the first wall segment at the bottom and the second wall segments at the top and bottom of the station are in the plastic state

$$q_{I_B} = q_{I_{PB}} \tag{5.41}$$

$$q_{II_B} = q_{II_{PB}} \tag{5.42}$$

Equation (5.10) becomes

$$y_B''' = \frac{I_A}{I_B} y_A''' - \frac{a_{I_A}}{EI_B} q_{I_A} - \frac{(P_i - a_{I_B} q_{I_{PB}} - a_{II_B} q_{II_{PB}} + a_{II_A} q_{II_{PA}})}{EI_B} \tag{5.43}$$

Hence the station transfer matrix becomes

$$\begin{Bmatrix} y \\ y' \\ y'' \\ y''' \\ T_I \\ T_{II} \\ q_I = q_{I_P} \\ q_{II} = q_{II_P} \end{Bmatrix}_{iB} = \begin{bmatrix} 1 & 0 & 0 & 0 & 0 & 0 & 0 & 0 \\ 0 & 1 & 0 & 0 & 0 & 0 & 0 & 0 \\ 0 & 0 & \frac{I_A}{I_B} & 0 & \frac{(a_A - a_B)_I}{EI_B} & \frac{(a_A - a_B)_{II}}{EI_B} & 0 & 0 \\ 0 & 0 & 0 & \frac{I_A}{I_B} & 0 & 0 & \frac{-a_{IA}}{EI_B} & 0 \\ 0 & 0 & 0 & 0 & 1 & 0 & 0 & 0 \\ 0 & 0 & 0 & 0 & 0 & 1 & 0 & 0 \\ 0 & 0 & 0 & 0 & 0 & 0 & \left(\frac{a_A \mu_B^2}{a_B \mu_A^2}\right)_I & 0 \\ 0 & 0 & 0 & 0 & 0 & 0 & 0 & 0 \end{bmatrix}$$

$$\begin{Bmatrix} y \\ y' \\ y'' \\ y''' \\ T_I \\ T_{II} \\ q_I \\ q_{II} = q_{II_P} \end{Bmatrix}_{iA} + \begin{bmatrix} 0 \\ 0 \\ 0 \\ \frac{-[P_i - a_{I_B} q_{I_{PB}} - (q_{PB} a_B - q_{PA} a_A)_{II}]}{EI_B} \\ 0 \\ 0 \\ 0 \\ q_{II_{PB}} \end{bmatrix} \qquad (5.44)$$

5.2.2.11 Plastic Elastic-Plastic Plastic Station Transfer Matrix

$$\begin{bmatrix} P & E \\ P & P \end{bmatrix}$$

Equations (5.5) to (5.9) and (5.12) remain valid. The first wall segments at the top and bottom and the second wall segment at the bottom of the station are in the plastic state and equations (5.41) and (5.42) are also valid with

$$q_{II_B} = \left(\frac{a_A \mu_B^2}{a_B \mu_A^2} \right)_{II} q_{II_A} \tag{5.45}$$

Therefore equation (5.10) becomes

$$y_B''' = \frac{I_A}{I_B} y_A''' - \frac{a_{II_A}}{EI_B} q_{II_A} - \frac{(P_i + q_{I_{PA}} a_{I_A} - q_{I_{PB}} a_{I_B} - q_{II_{PB}} a_{II_B})}{EI_B} \tag{5.46}$$

Hence the station transfer matrix becomes

$$\begin{Bmatrix} y \\ y' \\ y'' \\ y''' \\ T_I \\ T_{II} \\ q_I = q_{I_P} \\ q_{II} = q_{II_P} \end{Bmatrix}_{iB} = \begin{bmatrix} 1 & 0 & 0 & 0 & 0 & 0 & 0 & 0 \\ 0 & 1 & 0 & 0 & 0 & 0 & 0 & 0 \\ 0 & 0 & \frac{I_A}{I_B} & 0 & \frac{(a_A - a_B)_I}{EI_B} & \frac{(a_A - a_B)_{II}}{EI_B} & 0 & 0 \\ 0 & 0 & 0 & \frac{I_A}{I_B} & 0 & 0 & 0 & \frac{-a_{IIA}}{EI_B} \\ 0 & 0 & 0 & 0 & 1 & 0 & 0 & 0 \\ 0 & 0 & 0 & 0 & 0 & 1 & 0 & 0 \\ 0 & 0 & 0 & 0 & 0 & 0 & 0 & 0 \\ 0 & 0 & 0 & 0 & 0 & 0 & 0 & \left(\frac{a_A \mu_B^2}{a_B \mu_A^2} \right)_{II} \end{bmatrix}$$

$$\begin{Bmatrix} y \\ y' \\ y'' \\ y''' \\ T_I \\ T_{II} \\ q_I = q_{I_P} \\ q_{II} = q_{II_P} \end{Bmatrix}_{iA} + \begin{bmatrix} 0 \\ 0 \\ 0 \\ \dfrac{-[P_i - (q_{PB}a_B - q_{PA}a_A)_I - q_{II_{PB}} a_{II_B}]}{EI_B} \\ 0 \\ 0 \\ q_{I_{PB}} \\ 0 \end{bmatrix} \tag{5.47}$$

5.2.2.12 Plastic Plastic-Elastic Plastic Station Transfer Matrix

$$\left[\begin{array}{c|c} P & P \\ \hline E & P \end{array}\right]$$

Equations (5.5) to (5.9) and (5.12) remain valid, as the first wall segment at the top and the second wall segments at the top and bottom of the station are in the plastic state, equation (5.42) remains valid and

$$q_{I_B} = \left(\frac{a_A \mu_B^2}{a_A \mu_B^2} \right)_I q_{I_{PA}} \tag{5.48}$$

Therefore equation (5.10) becomes

$$y_B''' = \frac{I_A}{I_B} y_A''' - \frac{[P_i + q_{II_{PA}} a_{II_A} - q_{II_{PB}} a_{II_B} - q_{I_{PA}} a_{I_A} \left(\frac{\mu_B^2}{\mu_A^2} - 1 \right)_I]}{EI_B} \tag{5.49}$$

Hence the station transfer matrix becomes

$$\begin{Bmatrix} y \\ y' \\ y'' \\ y''' \\ T_I \\ T_{II} \\ q_I \\ q_{II}=q_{II_P} \end{Bmatrix}_{iB} = \begin{bmatrix} 1 & 0 & 0 & 0 & 0 & 0 & 0 & 0 \\ 0 & 1 & 0 & 0 & 0 & 0 & 0 & 0 \\ 0 & 0 & \frac{I_A}{I_B} & 0 & \frac{(a_A-a_B)_I}{EI_B} & \frac{(a_A-a_B)_{II}}{EI_B} & 0 & 0 \\ 0 & 0 & 0 & \frac{I_A}{I_B} & 0 & 0 & 0 & 0 \\ 0 & 0 & 0 & 0 & 1 & 0 & 0 & 0 \\ 0 & 0 & 0 & 0 & 0 & 1 & 0 & 0 \\ 0 & 0 & 0 & 0 & 0 & 0 & 0 & 0 \\ 0 & 0 & 0 & 0 & 0 & 0 & 0 & 0 \end{bmatrix} \begin{Bmatrix} y \\ y' \\ y'' \\ y''' \\ T_I \\ T_{II} \\ q_I=q_{I_P} \\ q_{II}=q_{II_P} \end{Bmatrix}_{iA} + \begin{bmatrix} 0 \\ 0 \\ 0 \\ \frac{-[P_i+(q_{PA}a_A-q_{PB}a_B)_{II}-q_{I_{PA}}a_{I_A}(\frac{\mu_B^2}{\mu_A^2}-1)_I]}{EI_B} \\ 0 \\ 0 \\ (\frac{a_A}{a_B}\frac{\mu_B^2}{\mu_A^2})_I q_{I_{PA}} \\ q_{II_{PB}} \end{bmatrix} \tag{5.50}$$

5.2.2.13 Plastic Plastic-Plastic Elastic Station Transfer Matrix

$$\left[\begin{array}{c|c} P & P \\ \hline P & E \end{array}\right]$$

Equations (5.5) to (5.9) and (5.12) remain valid, and as the first wall segments at the top and bottom and the second wall segment at the top of the station are in the plastic state, eqn. (5.41) remains valid

$$q_{II_B} = \left(\frac{a_A \mu_B^2}{a_B \mu_A^2}\right)_{II} q_{II_{PA}} \tag{5.51}$$

Therefore equation (5.10) becomes

$$y_B''' = \frac{I_A}{I_B} y_A''' - \frac{\left[P_i - q_{I_{PB}} a_{I_B} + q_{I_{PA}} a_{I_A} - q_{II_{PA}} a_{II_A} \left(\frac{\mu_B^2}{\mu_A^2} - 1\right)_{II}\right]}{EI_B} \tag{5.52}$$

Hence the station transfer matrix becomes

$$\begin{Bmatrix} y \\ y' \\ y'' \\ y''' \\ T_I \\ T_{II} \\ q_I = q_{I_P} \\ q_{II} \end{Bmatrix} = \begin{bmatrix} 1 & 0 & 0 & 0 & 0 & 0 & 0 & 0 \\ 0 & 1 & 0 & 0 & 0 & 0 & 0 & 0 \\ 0 & 0 & \frac{I_A}{I_B} & 0 & \frac{(a_A - a_B)_I}{EI_B} & \frac{(a_A - a_B)_{II}}{EI_B} & 0 & 0 \\ 0 & 0 & 0 & \frac{I_A}{I_B} & 0 & 0 & 0 & 0 \\ 0 & 0 & 0 & 0 & 1 & 0 & 0 & 0 \\ 0 & 0 & 0 & 0 & 0 & 1 & 0 & 0 \\ 0 & 0 & 0 & 0 & 0 & 0 & 0 & 0 \\ 0 & 0 & 0 & 0 & 0 & 0 & 0 & 0 \end{bmatrix}_{iB}$$

$$\begin{Bmatrix} y \\ y' \\ y'' \\ y''' \\ T_I \\ T_{II} \\ q_I = q_{I_P} \\ q_{II} = q_{II_P} \end{Bmatrix}_{iA} + \begin{Bmatrix} 0 \\ 0 \\ 0 \\ \dfrac{-[P_i + (q_{PA}a_A - q_{PB}a_B)_I - q_{II_{PA}} a_{II_A} (\frac{\mu_B^2}{\mu_A^2} - 1)_{II}]}{EI_B} \\ 0 \\ 0 \\ q_{I_{PB}} \\ (\frac{a_A}{a_B}\frac{\mu_B^2}{\mu_A^2})_{II} q_{II_{PA}} \end{Bmatrix} \tag{5.53}$$

5.2.2.14 Plastic Plastic-Plastic Plastic Station Transfer Matrix

$$\begin{bmatrix} P & P \\ P & P \end{bmatrix}$$

Equations (5.5) to (5.9) remain valid and as all the segments at the top and bottom of staiton are in the plastic state, the eqns. (5.41) and (5.42) remain valid.

Equation (5.10) becomes

$$y_B''' = \frac{I_A}{I_B} y_A''' - \frac{(P_i + a_{I_A} q_{I_{PA}} - a_{I_B} q_{I_{PB}} + a_{II_A} q_{II_{PA}} - a_{II_B} q_{II_{PB}})}{EI_B} \tag{5.54}$$

Hence the station transfer matrix becomes

$$\begin{Bmatrix} y \\ y' \\ y'' \\ y''' \\ T_I \\ T_{II} \\ q_I = q_{I_P} \\ q_I = q_{II_P} \end{Bmatrix}_{iB} = \begin{bmatrix} 1 & 0 & 0 & 0 & 0 & 0 & 0 & 0 \\ 0 & 1 & 0 & 0 & 0 & 0 & 0 & 0 \\ 0 & 0 & \frac{I_A}{I_B} & 0 & \frac{(a_A - a_B)_I}{EI_B} & \frac{(a_A - a_B)_{II}}{EI_B} & 0 & 0 \\ 0 & 0 & 0 & \frac{I_A}{I_B} & 0 & 0 & 0 & 0 \\ 0 & 0 & 0 & 0 & 1 & 0 & 0 & 0 \\ 0 & 0 & 0 & 0 & 0 & 1 & 0 & 0 \\ 0 & 0 & 0 & 0 & 0 & 0 & 0 & 0 \\ 0 & 0 & 0 & 0 & 0 & 0 & 0 & 0 \end{bmatrix} \begin{Bmatrix} y \\ y' \\ y'' \\ y''' \\ T_I \\ T_{II} \\ q_I = q_{I_P} \\ q_{II} = q_{II_P} \end{Bmatrix}_{iA} + \begin{Bmatrix} 0 \\ 0 \\ 0 \\ \frac{-[P_i + (q_{PA}a_A - q_{PB}a_B)_I + (q_{PA}a_A - q_{PB}a_B)_{II}]}{EI_B} \\ 0 \\ 0 \\ q_{I_{PB}} \\ q_{II_{PB}} \end{Bmatrix} \tag{5.55}$$

5.2.2.15 Elastic Plastic-Plastic Elastic Station Transfer Matrix

$$\begin{bmatrix} E & P \\ P & E \end{bmatrix}$$

Equations (5.5) to (5.9) remain valid, and as the first wall segment at the bottom and the second wall segment at the top of station are in the plastic state eqn. (5.11) remains valid

$$q_{II_B} = \left(\frac{a_A \mu_B^2}{a_B \mu_A^2} \right)_{II} q_{II_{PA}} \tag{5.56}$$

Therefore equation (5.10) becomes

$$y_B''' = \frac{I_A}{I_B} y_A''' - \frac{a_{I_A}}{EI_B} q_{I_A} - \frac{[P_i - q_{I_{PB}} a_{I_B} - q_{II_{PA}} a_{II_A} \left(\frac{\mu_B^2}{\mu_A^2} - 1 \right)_{II}]}{EI_B} \tag{5.57}$$

Hence the station transfer matrix becomes

$$\begin{Bmatrix} y \\ y' \\ y'' \\ y''' \\ T_I \\ T_{II} \\ q_I = q_{I_P} \\ q_{II} \end{Bmatrix} = \begin{bmatrix} 1 & 0 & 0 & 0 & 0 & 0 & 0 & 0 \\ 0 & 1 & 0 & 0 & 0 & 0 & 0 & 0 \\ 0 & 0 & \frac{I_A}{I_B} & 0 & \frac{(a_A - a_B)_I}{EI_B} & \frac{(a_A - a_B)_{II}}{EI_B} & 0 & 0 \\ 0 & 0 & 0 & \frac{I_A}{I_B} & 0 & 0 & \frac{-a_{IA}}{EI_B} & 0 \\ 0 & 0 & 0 & 0 & 1 & 0 & 0 & 0 \\ 0 & 0 & 0 & 0 & 0 & 1 & 0 & 0 \\ 0 & 0 & 0 & 0 & 0 & 0 & \left(\frac{a_A \mu_B^2}{a_B \mu_A^2} \right)_I & 0 \\ 0 & 0 & 0 & 0 & 0 & 0 & 0 & 0 \end{bmatrix}_{iB}$$

$$\begin{Bmatrix} y \\ y' \\ y'' \\ y''' \\ T_I \\ T_{II} \\ q_I \\ q_{II}=q_{II_P} \end{Bmatrix}_{iA} + \begin{bmatrix} 0 \\ 0 \\ 0 \\ \dfrac{-[P_i - q_{I_{PB}} a_{I_B} - q_{II_{PA}} a_{II_A} (\frac{\mu_B^2}{\mu_A^2} - 1)_{II}]}{EI_B} \\ 0 \\ 0 \\ 0 \\ (\dfrac{a_A}{a_B} \dfrac{\mu_B^2}{\mu_A^2})_{II} \, q_{II_{PA}} \end{bmatrix} \tag{5.58}$$

5.2.2.16 Plastic Elastic-Elastic Plastic Station Transfer Matrix

$$\left[\begin{array}{c|c} P & E \\ \hline E & P \end{array}\right]$$

Equations (5.5) to (5.9) remain valid, and as the first wall segment at the top and the second wall segement at the bottom of the station are in the plastic state, eqn. (5.12) remains valid and

$$q_{I_B} = (\frac{a_A}{a_B} \frac{\mu_B^2}{\mu_A^2})_I \, q_{I_{PA}} \tag{5.59}$$

Therefore eqn. (5.10) becomes

$$y_B''' = \frac{I_A}{I_B} y_A''' - \frac{a_{II_A}}{EI_B} q_{II_A} - \frac{[P_i - a_{II_B} q_{II_{PB}} - a_{I_A} q_{I_{PA}} (\frac{\mu_B^2}{\mu_A^2} - 1)_I]}{EI_B} \tag{5.60}$$

Hence the station transfer matrix becomes

$$
\begin{Bmatrix} y \\ y' \\ y'' \\ y''' \\ T_I \\ T_{II} \\ q_I \\ q_{II}=q_{II_P} \end{Bmatrix}
=
\begin{bmatrix}
1 & 0 & 0 & 0 & 0 & 0 & 0 & 0 \\
0 & 1 & 0 & 0 & 0 & 0 & 0 & 0 \\
0 & 0 & \frac{I_A}{I_B} & 0 & \frac{(a_A-a_B)_I}{EI_B} & \frac{(a_A-a_B)_{II}}{EI_B} & 0 & 0 \\
0 & 0 & 0 & \frac{I_A}{I_B} & 0 & 0 & 0 & \frac{-a_{IIA}}{EI_B} \\
0 & 0 & 0 & 0 & 1 & 0 & 0 & 0 \\
0 & 0 & 0 & 0 & 0 & 1 & 0 & 0 \\
0 & 0 & 0 & 0 & 0 & 0 & 0 & 0 \\
0 & 0 & 0 & 0 & 0 & 0 & 0 & \left(\frac{a_A\,\mu_B^2}{a_B\,\mu_A^2}\right)_{II}
\end{bmatrix}
\begin{Bmatrix} y \\ y' \\ y'' \\ y''' \\ T_I \\ T_{II} \\ q_I=q_{I_P} \\ q_{II} \end{Bmatrix}_{iB}
+
\begin{Bmatrix} 0 \\ 0 \\ 0 \\ \frac{-[P_i-q_{II_{PB}}a_{II_B}-q_{I_{PA}}a_{I_A}(\frac{\mu_B^2}{\mu_A^2}-1)]_I}{EI_B} \\ 0 \\ 0 \\ \left(\frac{a_A\,\mu_B^2}{a_B\,\mu_A^2}\right)_I q_{I_{PA}} \\ 0 \end{Bmatrix}_{iA}
\tag{5.61}
$$

5.2.2.17 Station Transfer Matrices Relating Real Hinged Segment/ Segments with Elastic, Plastic, Real Hinged Segment/Segments

Each of the remaining sixty-five station is a modified form of one of these sixteen stations. Hence the station transfer matrix for the remaining station can be obtained from the station transfer matrix for corresponding station by setting the appropriate shear intensity/ intensities (q_{IA} and/or q_{IB} and/or q_{IIA} and/or q_{IIB}) equal to zero.

5.3 FORMULATION OF MIXED BOUNDARY VALUE PROBLEM

The transfer matrix technique gives the relationship of eight equations between eight states at the base and eight states at the top of structure as

$$\{\phi\}_o = [\bar{F}]\ \{\phi\}_{nB} + \{\bar{L}\} \tag{5.62}$$

There are eight elements in each of the state vectors $\{\phi\}_o$ and $\{\phi\}_{nB}$. Out of these sixteen elements, eight of them are known by the boundary conditions at the top and bottom of the structure i.e.

At the Base: (for fixed base)

$$y_o = 0 \tag{5.63a}$$

$$y_o' = 0 \tag{5.63b}$$

$$q_{I_o} = 0 \tag{5.63c}$$

$$q_{II_o} = 0 \tag{5.63d}$$

At the Top:

$$y_{nB}'' = 0 \tag{5.63e}$$

$$T_{I_{nB}} = 0 \tag{5.63f}$$

$$T_{II_{nB}} = 0 \tag{5.63g}$$

$$q_{II_{nB}} = \frac{EI_{IIn}}{a_{IIn}} y'''_{nB} + \frac{(P_n - V_{InB})}{a_{IIn}} \tag{5.63h}$$

Hence the mixed boundary value problem becomes:

$$\begin{Bmatrix} 0 \\ 0 \\ y''_0 \\ y'''_0 \\ T_{I_o} \\ T_{II_o} \\ 0 \\ 0 \end{Bmatrix} = \begin{bmatrix} \\ \\ \\ \\ \\ \\ \\ \end{bmatrix} \overline{F} \begin{bmatrix} \\ \\ \\ \\ \\ \\ \\ \end{bmatrix} \begin{Bmatrix} y_{nB} \\ y'_{nB} \\ 0 \\ y'''_{nB} \\ 0 \\ 0 \\ \sigma_{InB} y'''_{nB} + V_{InB}/a_{In} \\ \sigma_{IInB} y'''_{nB} + (P_n - V_{InB})/a_{IIn} \end{Bmatrix} + \begin{Bmatrix} \\ \\ \\ \\ \\ \\ \\ \end{Bmatrix} \overline{L} \begin{bmatrix} \\ \\ \\ \\ \\ \\ \\ \end{bmatrix} \tag{5.64}$$

where

$$\sigma_{InB} = \frac{EI_{In}}{a_{In}}$$

$$\sigma_{IInB} = \frac{EI_{IIn}}{a_{IIn}}$$

Expanding the above eight equations and eliminating the four unknowns y_o'', y_o''', T_{Io}, T_{IIo}, at the left hand side by Gauss-Elimination method, we get the four independent equations in terms of four independent unknowns at top y_{nB}, y_{nB}', y_{nB}''', V_{InB} as

$$\begin{bmatrix} \bar{F}_{11} & \bar{F}_{12} & \bar{F}_{14}+\sigma_{In}\bar{F}_{17}+\sigma_{IIn}\bar{F}_{18} & \bar{F}_{17}/a_{In}-\bar{F}_{18}/a_{IIn} \\ \bar{F}_{21} & \bar{F}_{22} & \bar{F}_{24}+\sigma_{In}\bar{F}_{27}+\sigma_{IIn}\bar{F}_{28} & \bar{F}_{27}/a_{In}-\bar{F}_{28}/a_{IIn} \\ \bar{F}_{71} & \bar{F}_{72} & \bar{F}_{74}+\sigma_{In}\bar{F}_{77}+\sigma_{IIn}\bar{F}_{78} & \bar{F}_{77}/a_{In}-\bar{F}_{78}/a_{IIn} \\ \bar{F}_{81} & \bar{F}_{82} & \bar{F}_{84}+\sigma_{In}\bar{F}_{87}+\sigma_{IIn}\bar{F}_{88} & \bar{F}_{87}/a_{In}-\bar{F}_{88}/a_{IIn} \end{bmatrix} \begin{Bmatrix} y_{nB} \\ y_{nB}' \\ y_{nB}'' \\ V_{InB} \end{Bmatrix} = \begin{Bmatrix} -\bar{L}_1-\bar{F}_{18}P_n/a_{IIn} \\ -\bar{L}_2-\bar{F}_{28}P_n/a_{IIn} \\ -\bar{L}_7-\bar{F}_{78}P_n/a_{IIn} \\ -\bar{L}_8-\bar{F}_{88}P_n/a_{IIn} \end{Bmatrix} \tag{5.65}$$

CHAPTER 6

DYNAMIC ANALYSIS OF TWO INTER-CONNECTING COUPLED SHEAR WALLS

6.1 COUPLED SHEAR WALL SYSTEM

In this chapter, the behaviour of two inter-connecting coupled shear walls subjected to earthquake excitations is studied. This analysis is based on the mathematical model which is explained and derived in the previous chapter.

The example building considered here is the same as that considered in Chapter 4, as shown in Fig. (4.17). The behaviour of each coupled shear wall obtained by this formulation is compared with the behaviour obtained in Chapter 4 where each coupled shear wall is treated separately.

In this study of the two interconnecting shear wall problem, one coupled shear wall represents the two exterior coupled shear walls and other coupled shear wall represents all interior coupled shear walls. That is, as shown in Fig. [6.1(a)], the first coupled shear wall has the sum of stiffness and strength of the two exterior coupled shear walls and the second coupled shear wall has the total stiffness and strength of the interior coupled shear walls. These two coupled shear walls are then connected by a pin-pin rigid member at each floor level. In the dynamic model as shown in Fig. [6.1(b)] the mass of the entire building i.e. the mass of these two representative coupled shear wall is lumped together at each station level. In the present approach there is no

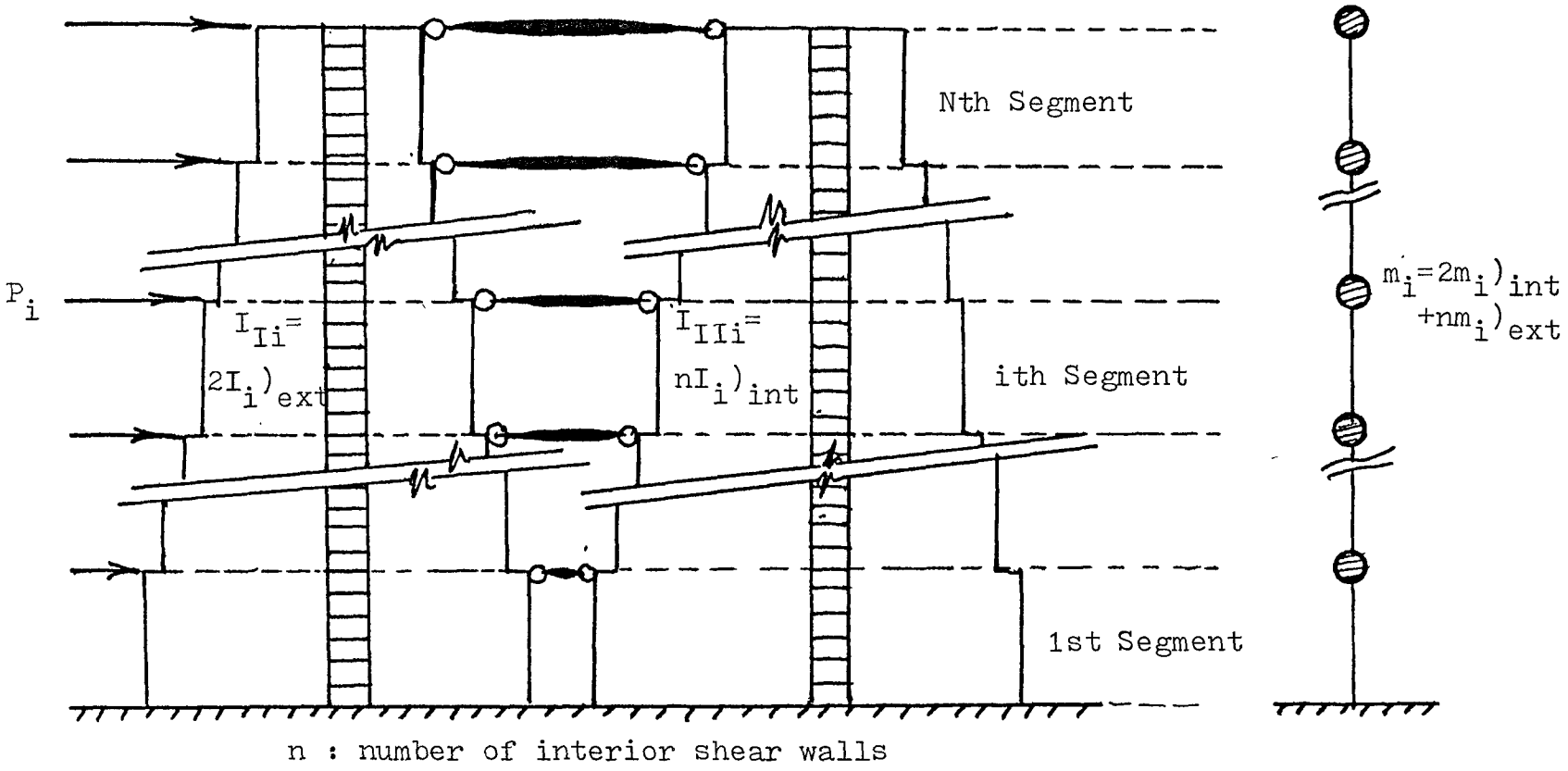

FIGURE 6-1 MODELLING OF TWO INTERCONNECTED COUPLED SHEAR WALL SYSTEM

need to attach a predetermined mass distribution to the shear walls. The transfer matrix technique in the dynamic analysis takes care of the balancing of the loading automatically, based on the requirement that all coupled shear walls shall have same deflection at floor levels.

In the present analysis, the dynamic model of two interconnected coupled shear walls have five lumped masses located at the top of five segments of equal height, as in Fig. (6.2). Table 6.1 gives the summary of the dimensions and capacities of wall-1 and wall-2.

WALL	Wall Thickness (in)	Conn. Beam Depth (in)	Moment of Inertia of Conn. Beams (ft^4)	q_p (kip/ft)
Wall-1	24	24	1.120	40.0
Wall-2	72	6*	0.141	16.08

*Effective connecting slab width = 3.5 ft

Table 6.1 Dimensions and Capacities of Wall-1 and Wall 2

6.2 METHOD OF EXCITATION

The earthquake record of El-Centro (1940) N.S component is used to excite this twenty storey building. This reocrd is normalized to the maximum horizontal accelerations of 16% g and 32% g for analysis purpose and they will be referred to as "moderate" and "severe" earthquake respectively.

The modal critical damping ratios are taken as: $\xi_1 = 4\%$, $\xi_2 = 5\%$, $\xi_3 = 6\%$, $\xi_4 = 7\%$, $\xi_5 = 8\%$.

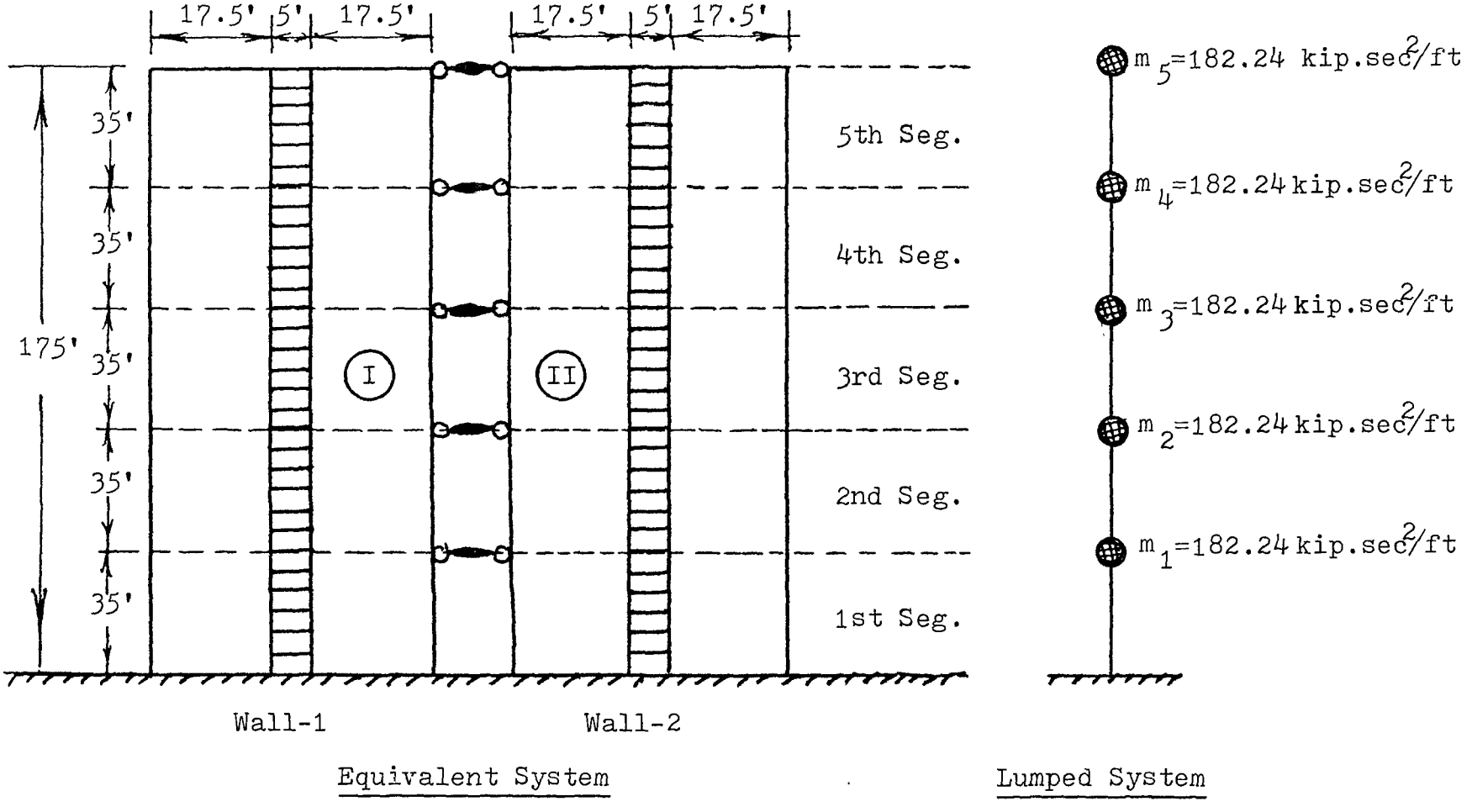

FIGURE 6-2 DYNAMIC MODEL OF 20STOREY BUILDING

Limited rotational ductility factors $\bar{\mu}_I = 15$ and $\bar{\mu}_{II} = 5$ are considered for the connecting beams of wall-1 (exterior) and wall-2 (interior) respectively. Also for moderate excitation very large ductility factors $\bar{\mu}_I = \bar{\mu}_{II} = 500$ are used for both walls. For severe excitation large ductility factors $\bar{\mu}_I = 30$, $\bar{\mu}_{II} = 5$ are also considered to study the effect of ductility on the responses.

The following table summarizes the cases studied.

	Earthquake Excitation	Ductility of the Connecting Beams	
		Wall-1 ($\bar{\mu}_I$)	Wall-2 ($\bar{\mu}_{II}$)
Run-A	moderate	500	500
Run-B	moderate	15	5
Run-C	severe	15	5
Run-D	severe	30	5

Table 6.2 Summary of Cases Studied for Dynamic Analysis

6.3 SEISMIC RESPONSE

In this section the seismic responses of the two coupled shear walls are presented and compared with the corresponding responses of these walls obtained in single coupled shear wall analysis given in Chapter 4.

The parameters of interest are: (i) the top displacement, (ii) the bending moment at the base of one pier and (iii) the axial force at the base. These parameters are used to evaluate the performance of the structure under seismic loads. These are the same parameters considered for the single coupled shear wall response analysis.

Also the phenomenon of the transfer of loading during the earthquake is studied based on the time-history of a "Load Sharing Factor". This is defined as the ratio of the over-turning moment on the exterior wall and the over-turning moment on the interior wall. The Load Sharing Factor is calculated as follows.

The overturning moment in a coupled shear wall is given by

$$M_i^e = M_i + T_i\, a_i \tag{6.1}$$

where

M_i^e: overturning moment at the base of ith segment

M_i: wall moment at the base of ith segment

T_i: axial force at the base of ith segment

a_i: c/c distance between the axes of two piers of the ith segment.

Hence the Load Sharing Factor (L.S.F.) for the exterior coupled shear wall at the base of ith segment is given by

$$\text{L.S.F.} = \frac{M_{i\ ext}^e}{M_{i\ int}^e} = \frac{(M_i + T_i\, a_i)_{ext}}{(M_i + T_i\, a_i)_{int}} \tag{6.2}$$

where the subscript "ext" refers to the parameters of the exterior coupled shear wall and "int" refers to the parameters of the interior coupled shear wall of the building.

As wall-1 consists of two exterior coupled shear walls of the building and wall-2 consists of six interior coupled shear walls of the building, the Load Sharing Factor for the exterior coupled shear wall is given by

$$\text{L.S.F.} = \frac{(M_i + T_i\, a_i)_I}{(M_i + T_i\, a_i)_{II}} \times 3.0 \qquad (6.3)$$

where subscripts I and II are referred to the representative wall-1 and wall-2 respectively in the mathematical model.

This Load Sharing Factor is calculated, at each time step, at the bases of first and third segment and its time history is plotted.

For the single coupled shear wall problem considered in Chapter 4, the time history of the overturning moment is obtained for the exterior and the interior coupled shear wall as a punched deck and time history of Load Sharing Factor is computed for comparison. To facilitate the direct comparison of this factor for the single coupled shear wall problem and the two inter-connected coupled shear wall problem, the time history of L.S.F. of both problems is given in this chapter.

The time-history responses in Run-A are same as those in Run-B i.e. the behaviour of the coupled shear walls under moderate earthquake is not affected by limiting the rotational ductility factors of the connecting beams of wall-1 and wall-2 up to $\overline{\mu}_I = 15$ and $\overline{\mu}_{II} = 5$ respectively. This leads us to consider only last three cases in detail.

For future reference, this present formulation of two inter-connected coupled shear walls will be referred as "Problem-2" and the previous single coupled shear wall formulation as "Problem-1".

6.3.1 Top Displacement Response

Figure (6.3) shows the comparison between the responses of the interior coupled shear wall under moderate earthquake excitation in Problem-1 and Problem-2. Figure (6.4) compares the responses of the interior coupled shear wall under severe earthquake in Problem-1 and Problem-2. As the top deflection of the exterior and interior coupled shear walls are identical under same earthquake, the comparisons of the responses of exterior wall will be the same as that of the interior wall. These figures show that the response of the coupled shear wall analysed as separate single shear wall is almost identical to the response in two inter-connected shear wall problem. Figure (6.5) gives the comparison of the responses in Run-C and Run-D. This shows that the rotational ductility factor of the connecting beams has no effect on the top deflection response.

6.3.2 Base Axial Force Response

Figure (6.6) compares the responses of an exterior coupled shear wall under moderate earthquake in Problem-1 and Problem-2. The responses are almost the same initially. After 2 seconds the response in Problem-2 is slightly higher. This is because of the difference in the order of formation of hinges in the two problems. Real hinges are formed in 40% height of the coupled shear wall in Problem-1. On the other hand no real hinges are formed in Problem-2. The same observation applies for the interior coupled shear wall and this is clearly seen in the Fig. (6.7). Under severe earthquake excitation, real hinges are

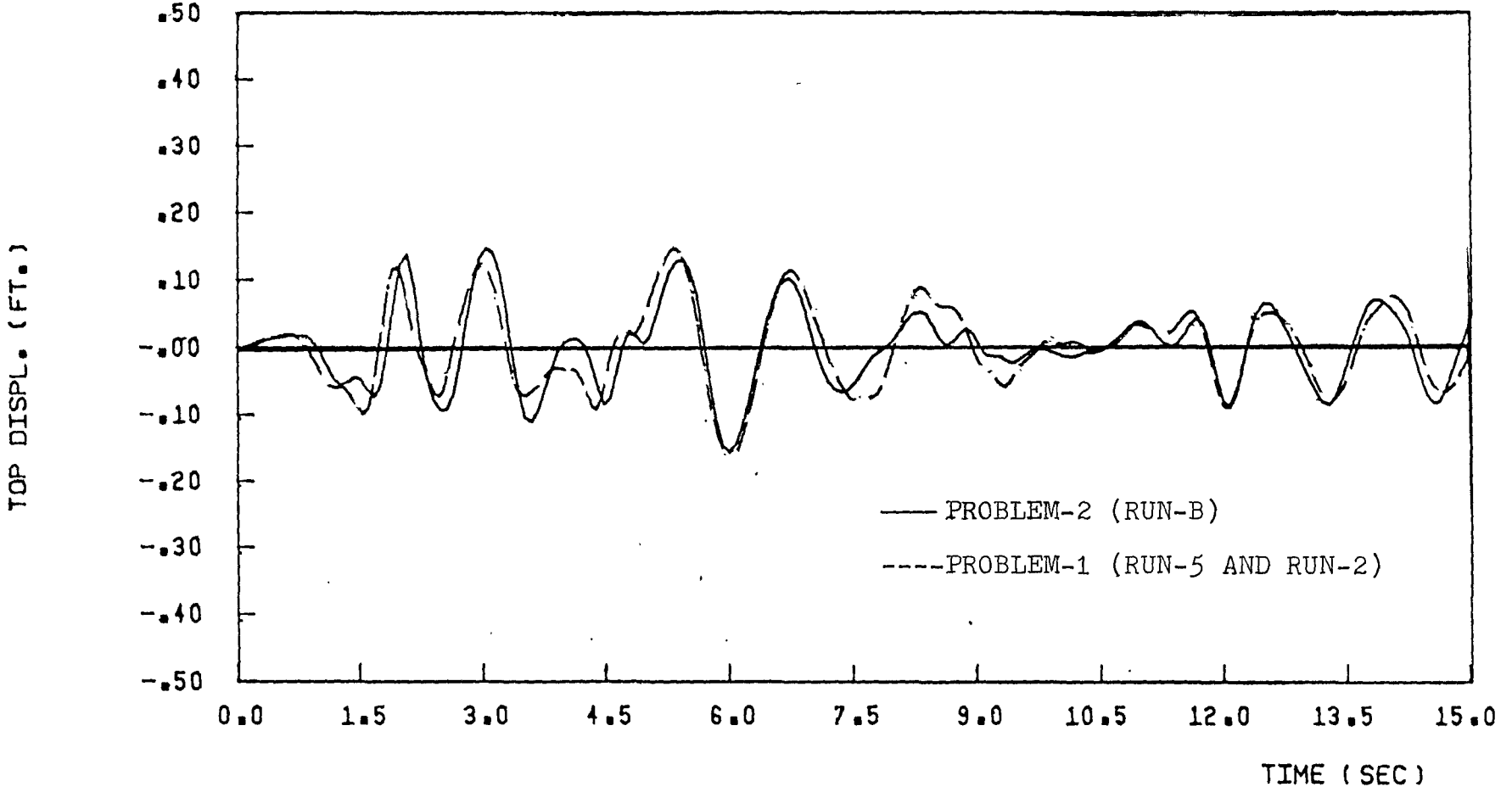

FIGURE 6-3 TOP DISPL., ELCENTRO COMP.NORTH 16 PERC. g

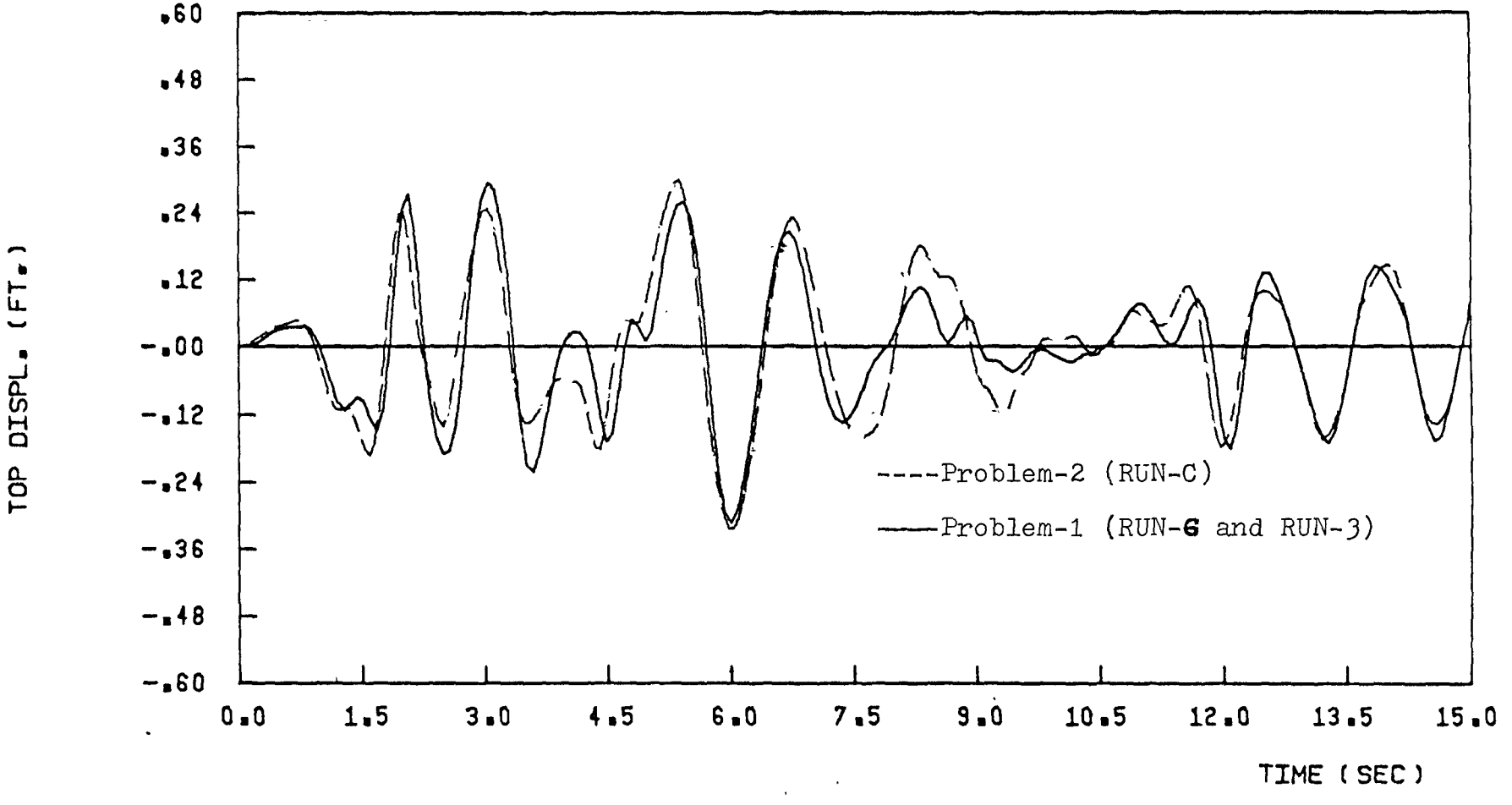

FIGURE 6-4 TOP DISPL., ELCENTRO COMP.NORTH 32 PERC. g

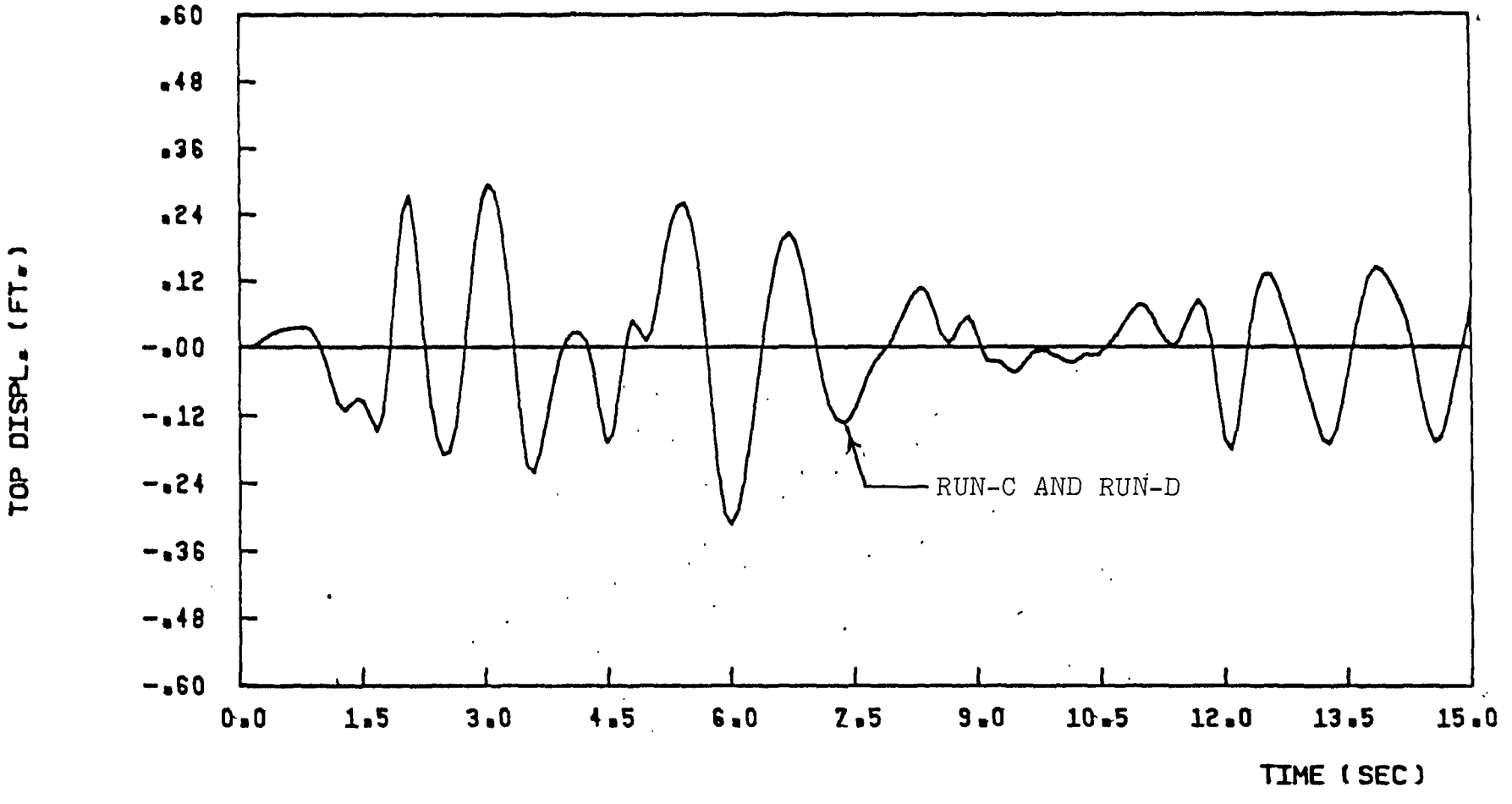

INTERIOR AND EXTERIOR WALL

FIGURE 6-5 TOP DISPL., ELCENTRO COMP.NORTH 32 PERC. g

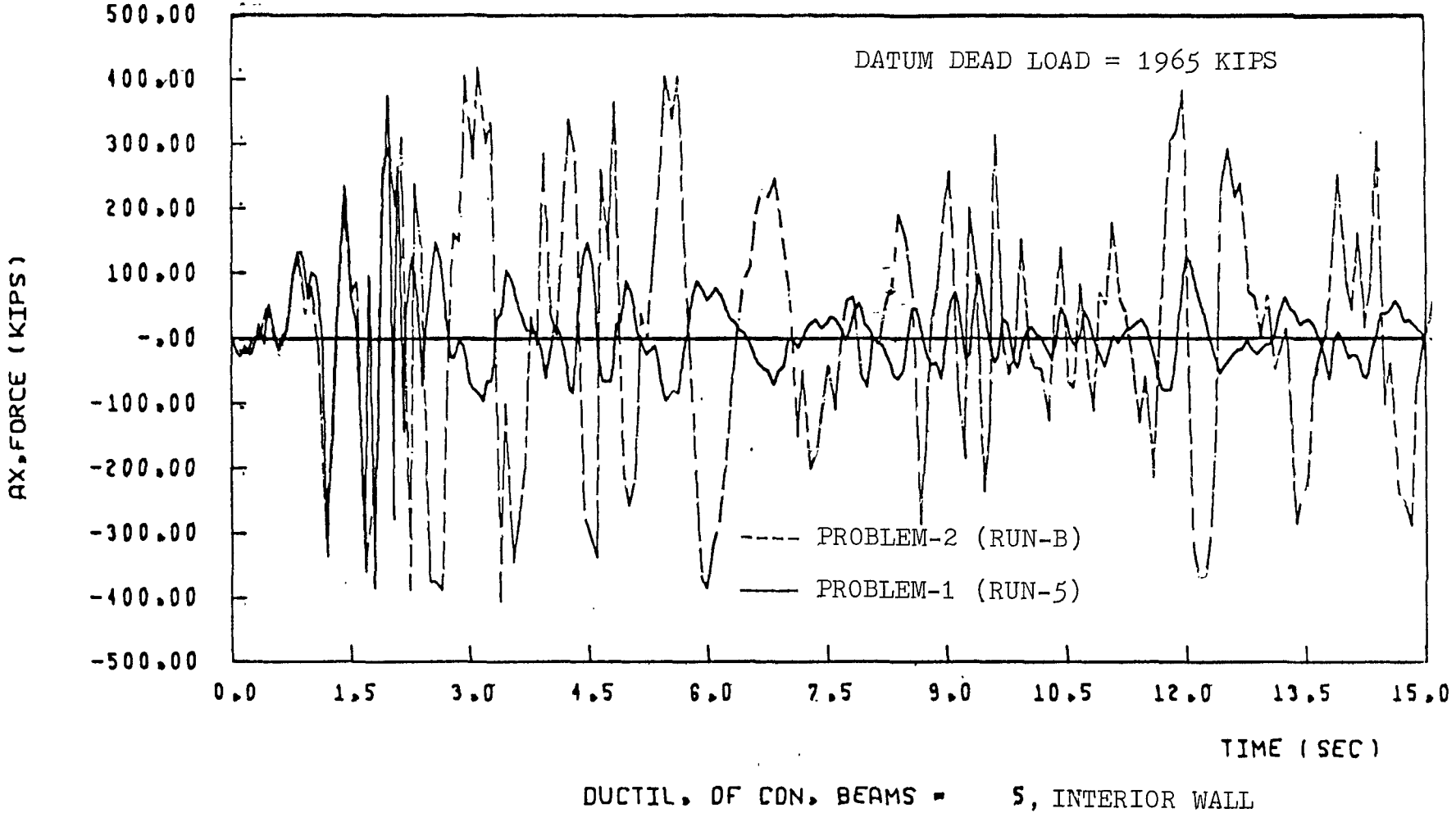

FIGURE 6-7 AX. FORCE, ELCENTRO COMP.NORTH 16 PERC. g

formed in 40% of the connecting beams of the interior shear wall in problem-1 and problem-2; hence, there is little difference in the responses in these two problems. There is some difference between time equals 2.0 sec. and 4.5 sec because of the early plastification and the real hinges are formed at 2 seconds in problem-1 as against at 4.5 sec in Problem-2. This is shown in Fig. (6.8). Figure (6.9) compares the responses of the exterior coupled shear wall under the severe earthquake in Problem-1 (Run-3) and Problem-2 (Run-C). Figure (6.10) compares the same response of the exterior coupled shear wall in Run-3 with that in Problem-2 (Run-D). In both cases the responses in Problem-2 are higher than those in Problem-1. This is because the number of real hinged segments in Problem-2 is less than that in Problem-1.

The difference in the two responses of Fig. (6.10) is more than those of Fig. (6.9). This is because of the difference in the rotational ductility factors of the connecting beams of the exterior coupled shear wall (wall-1). In Run-D the rotational ductility factor of the connecting beams of the exterior wall is 30 while that in Run-C is 15. The higher rotational ductility factor of the connecting beams in Run-D allows higher axial forces because of the higher limitations on the rotation of the ends of the connecting beams and hence preventing the formation of the real hinges. This effect of rotational ductility factor is compared directly in Fig. (6.11) by considering the responses of the exterior coupled sheaer wall in Problem-2 (Run C and Run-D). Figure (6.12) compares the responses of the interior coupled shear walls in these two cases. There is a very little difference in these two

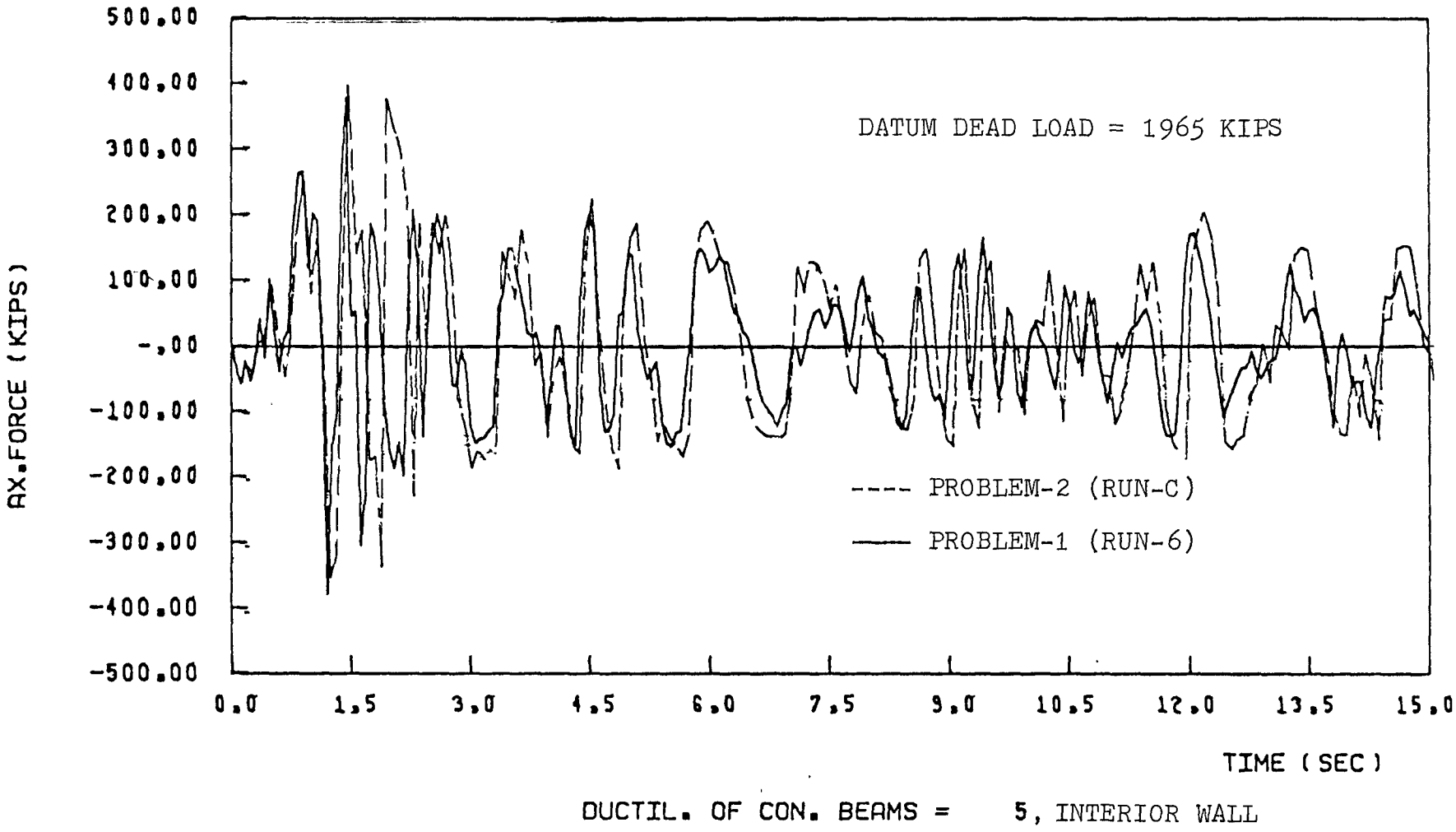

FIGURE 6-8 AX. FORCE, ELCENTRO COMP.NORTH 32 PERC. g

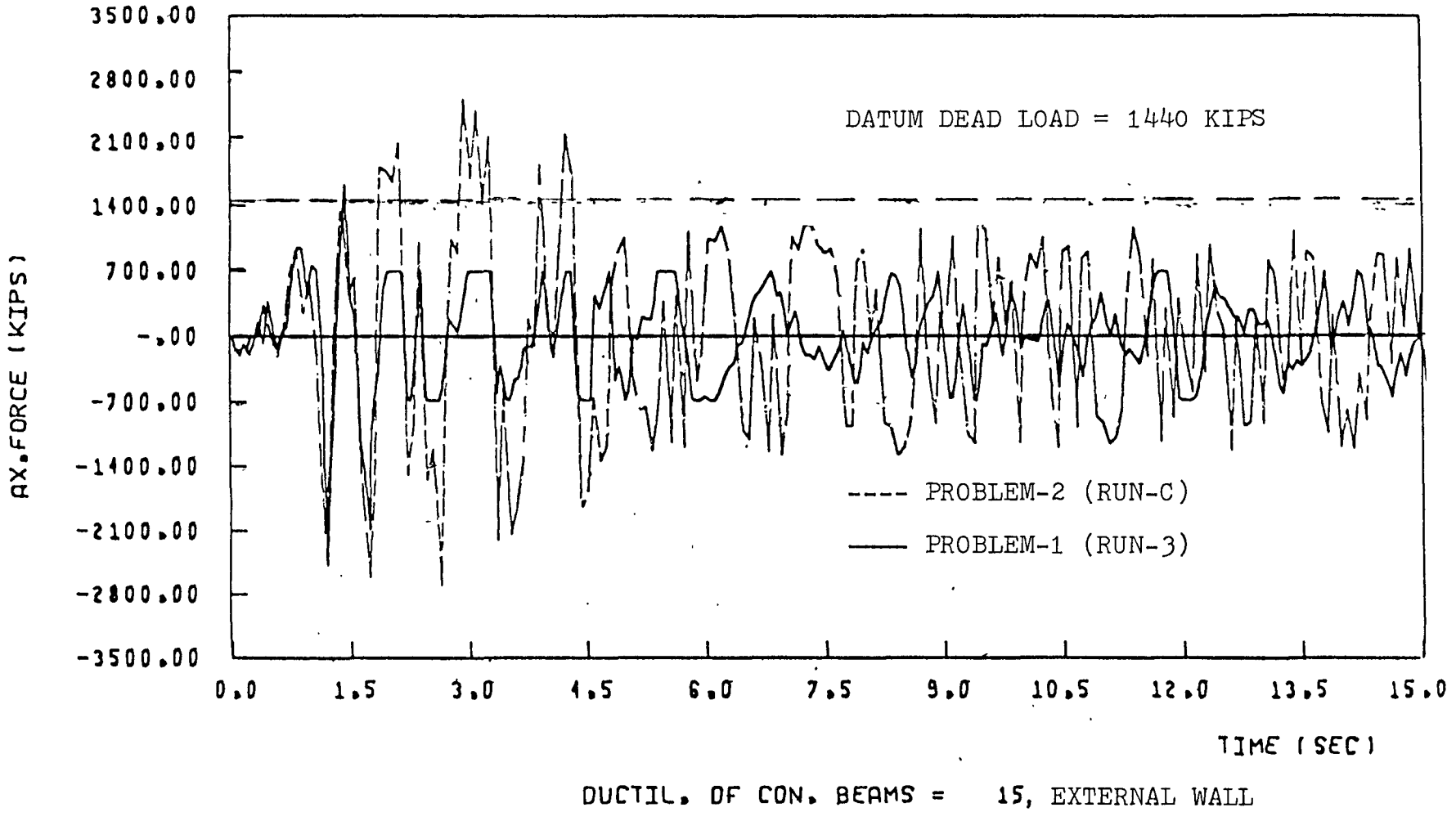

FIGURE 6.9 AX. FORCE, ELCENTRO COMP.NORTH 32 PERC. g

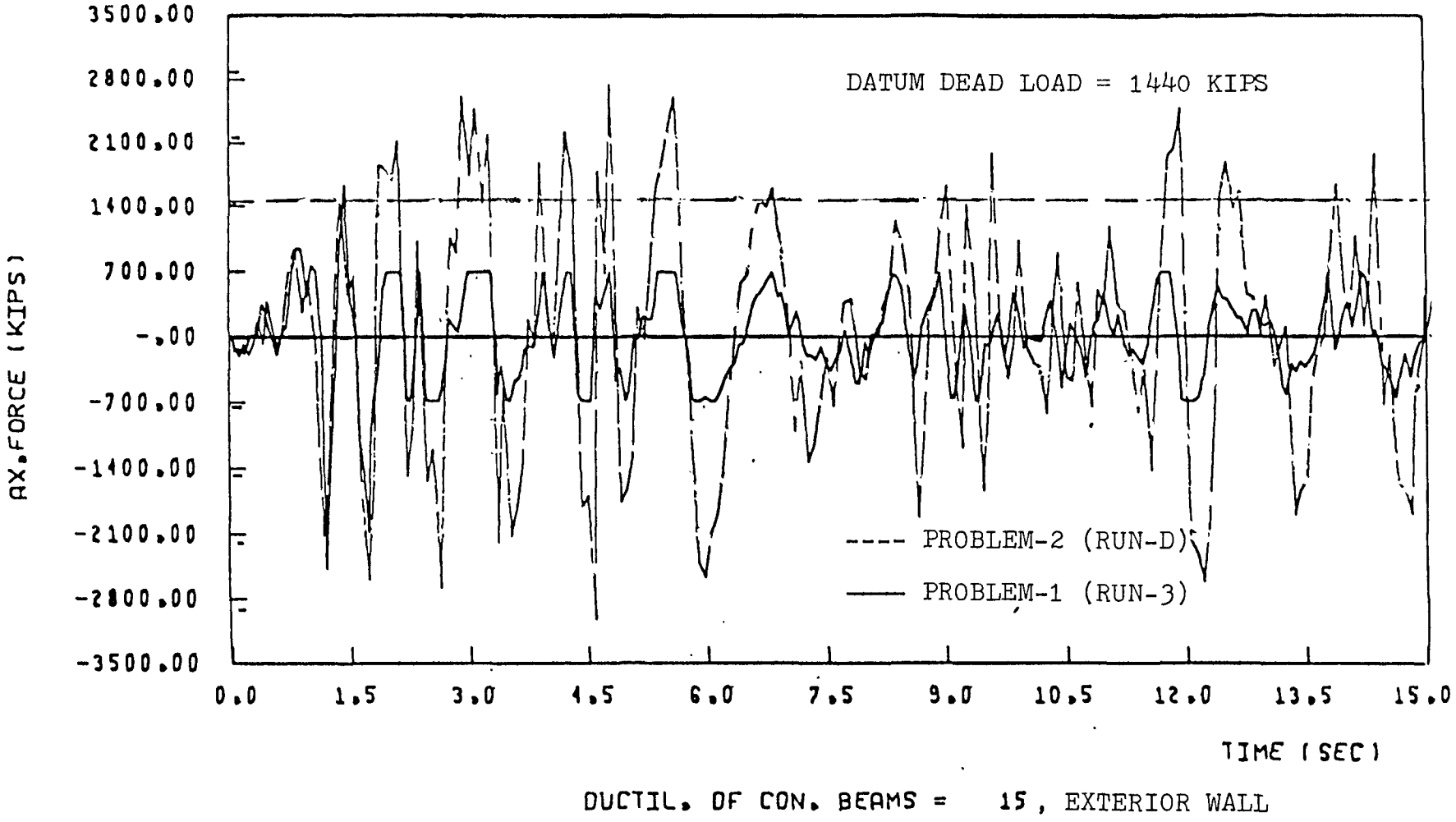

FIGURE 6-10 AX. FORCE, ELCENTRO COMP.NORTH 32 PERC. g

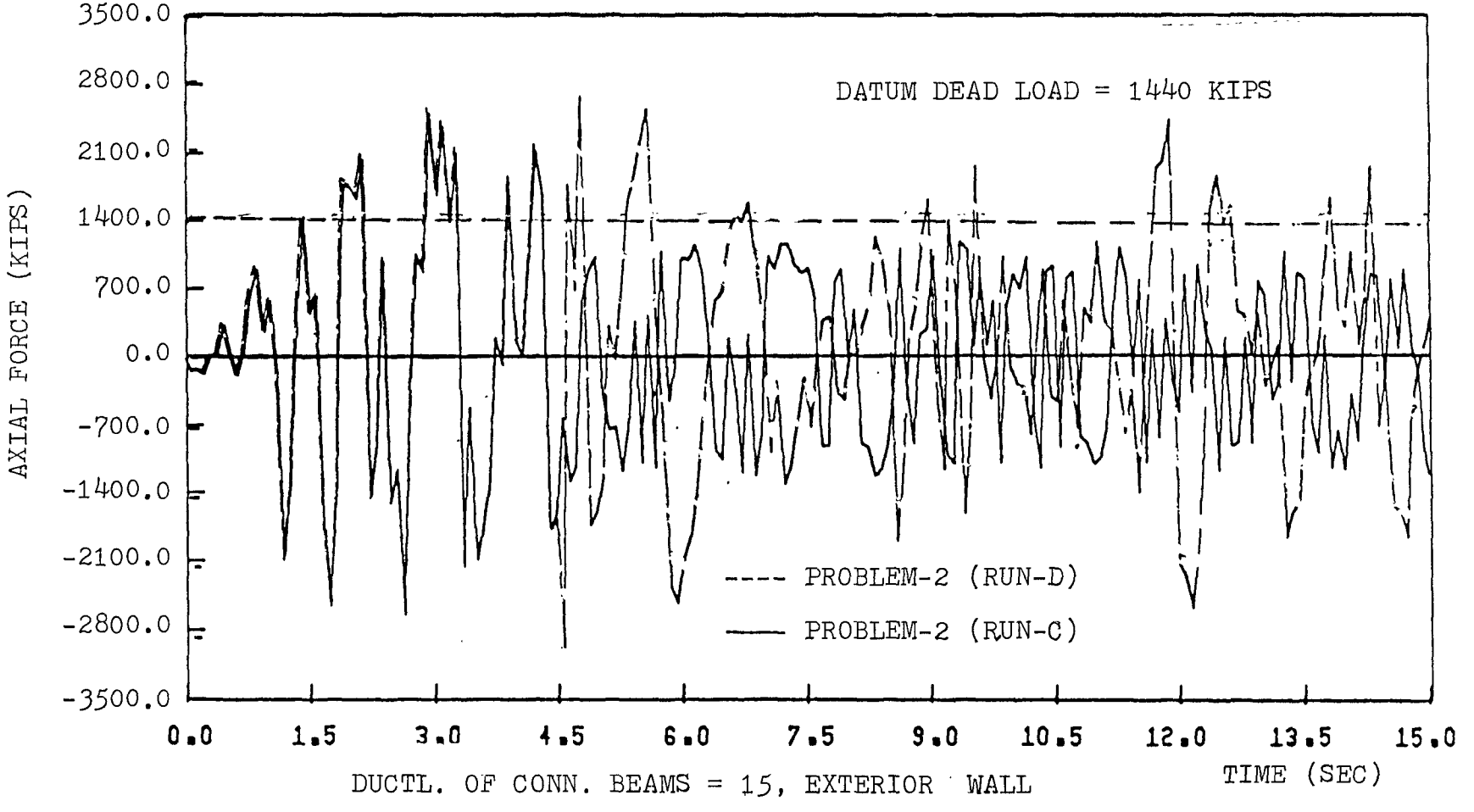

FIGURE 6-11 AX. FORCE, EL-CENTRO COMP. NORTH. 32 PER. g

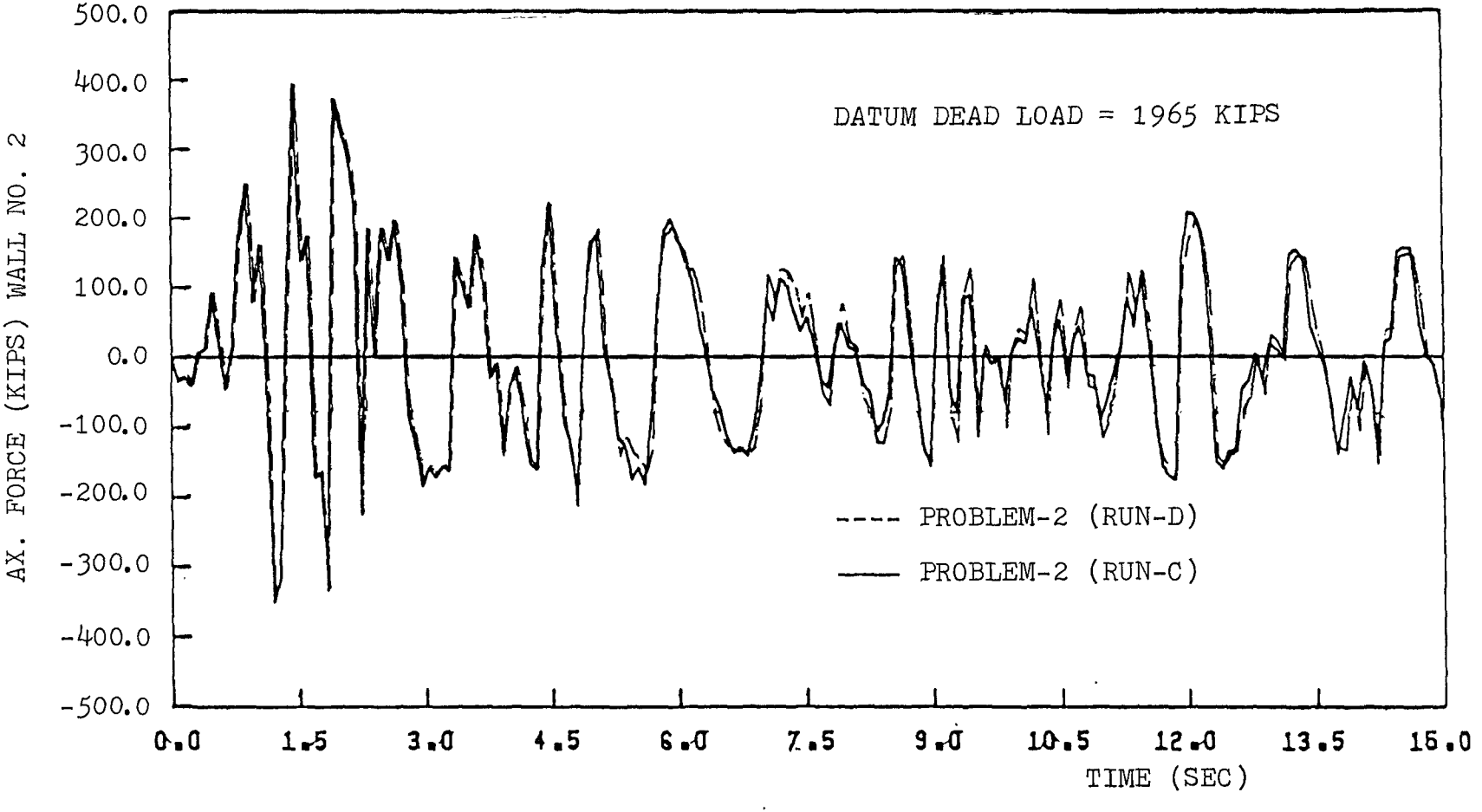

DUCTL. OF CONN. BEAMS OF WALL NO. 2 = 5, INTERIOR WALL

FIGURE 6-12 AX. FORCE, ELCENTRO COMP. NORTH 32 PERC. g

responses. It is to be noted that in these two cases (Run-C and Run-D) the rotational ductility factor of the connecting beams of the interior coupled shear wall is the same.

This shows that there is a considerable effect of the rotational ductility factor of the connecting beams of the coupled shear wall on its behaviour, but a very little effect on the other coupled shear wall which is interconnected to it. Hence the improvement in the member ductility of only one or some of the coupled shear walls may not be of much advantageous for the behaviour of the other coupled shear walls of the same system.

6.3.3 Base Moment Response

Figures (6.13) and Fig. (6.14) gives the comparison between the response of the interior coupled shear wall under moderate and severe earthquake excitation respectively. In both figures it is seen that the responses in Problem-1 are underestimated, with peak response by 7% to 12%. This is because the interior coupled shear wall is assumed to take less load (mass) in Problem-1. For the same reason, the responses of the exterior coupled shear wall in Problem-1 are overestimated. This is seen in Figs. (6.15) and (6.16) which compares the responses of the exterior coupled shear wall under moderate and severe earthquake excitation respectively. The difference between the responses under moderate earthquake is increased [Fig. (6.15)], because of the formation of real hinges over 40% height of the wall in Problem-1 (Run-2). This formation of real hinges reduces the axial forces at the base of the

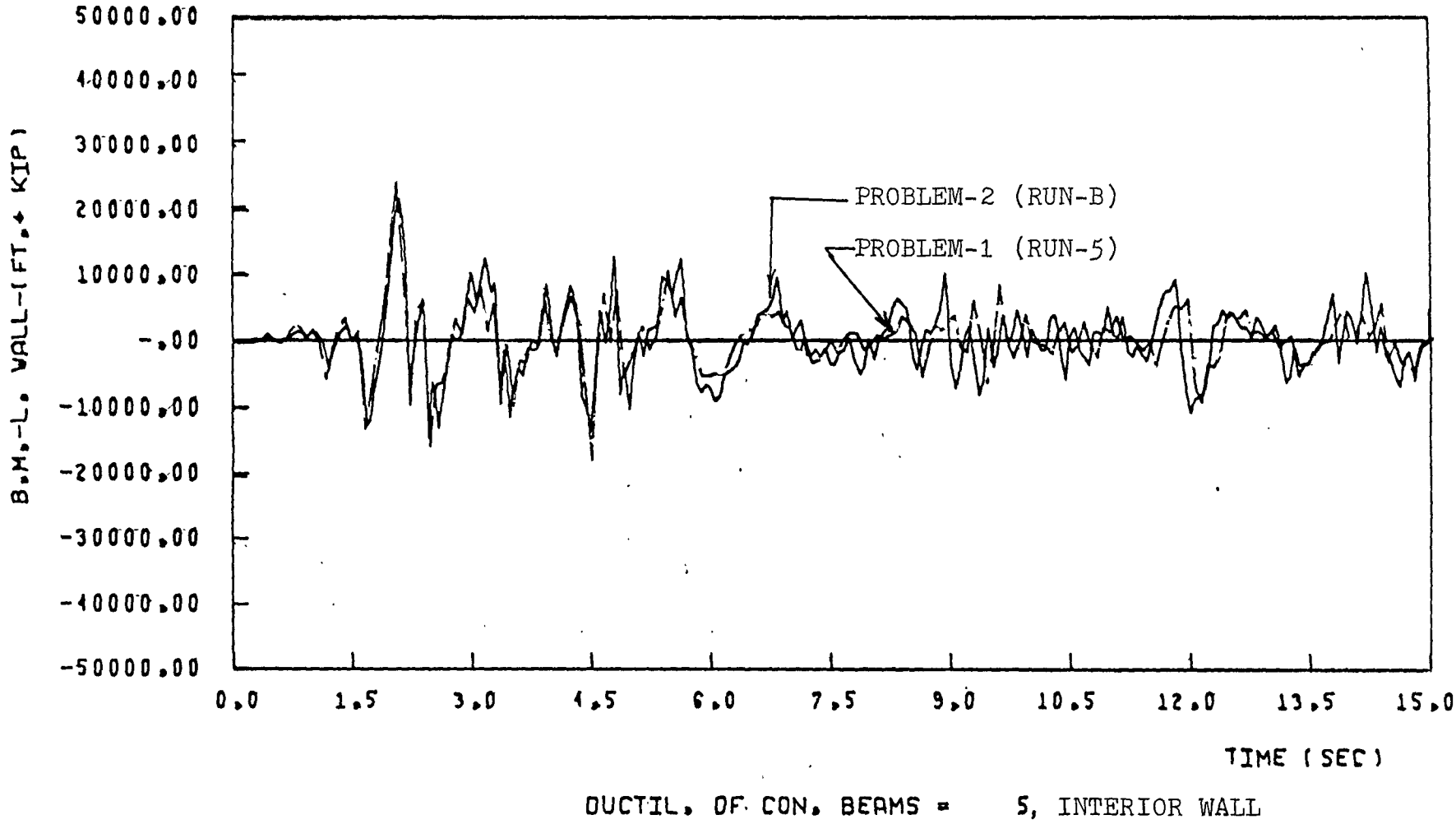

FIGURE 6-13 B.M.L. WALL, ELCENTRO COMP.NORTH. 16 PERC. g

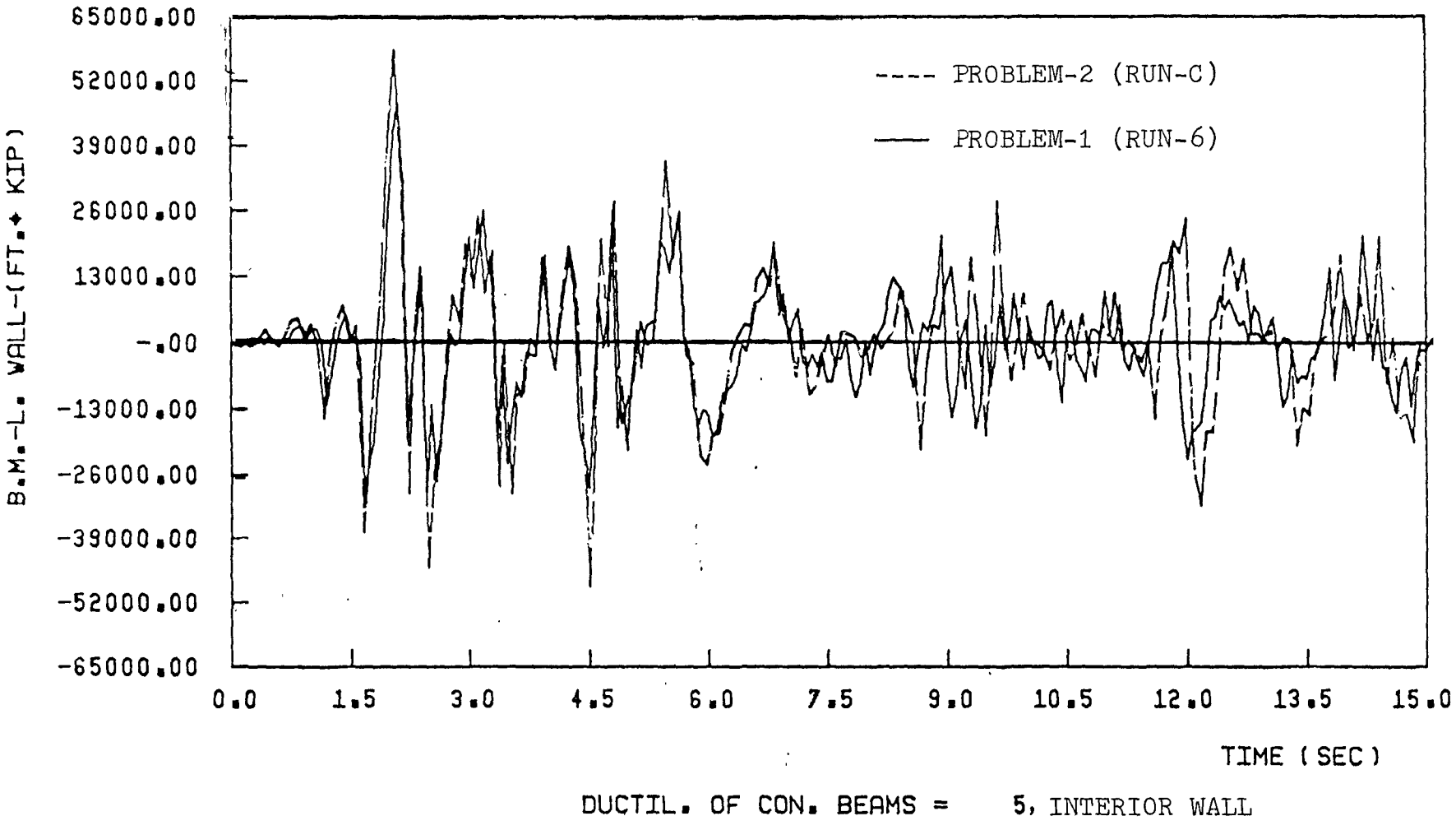

FIGURE 6-14 B.M.L.-WALL, ELCENTRO COMP.NORTH 32 PERC. g

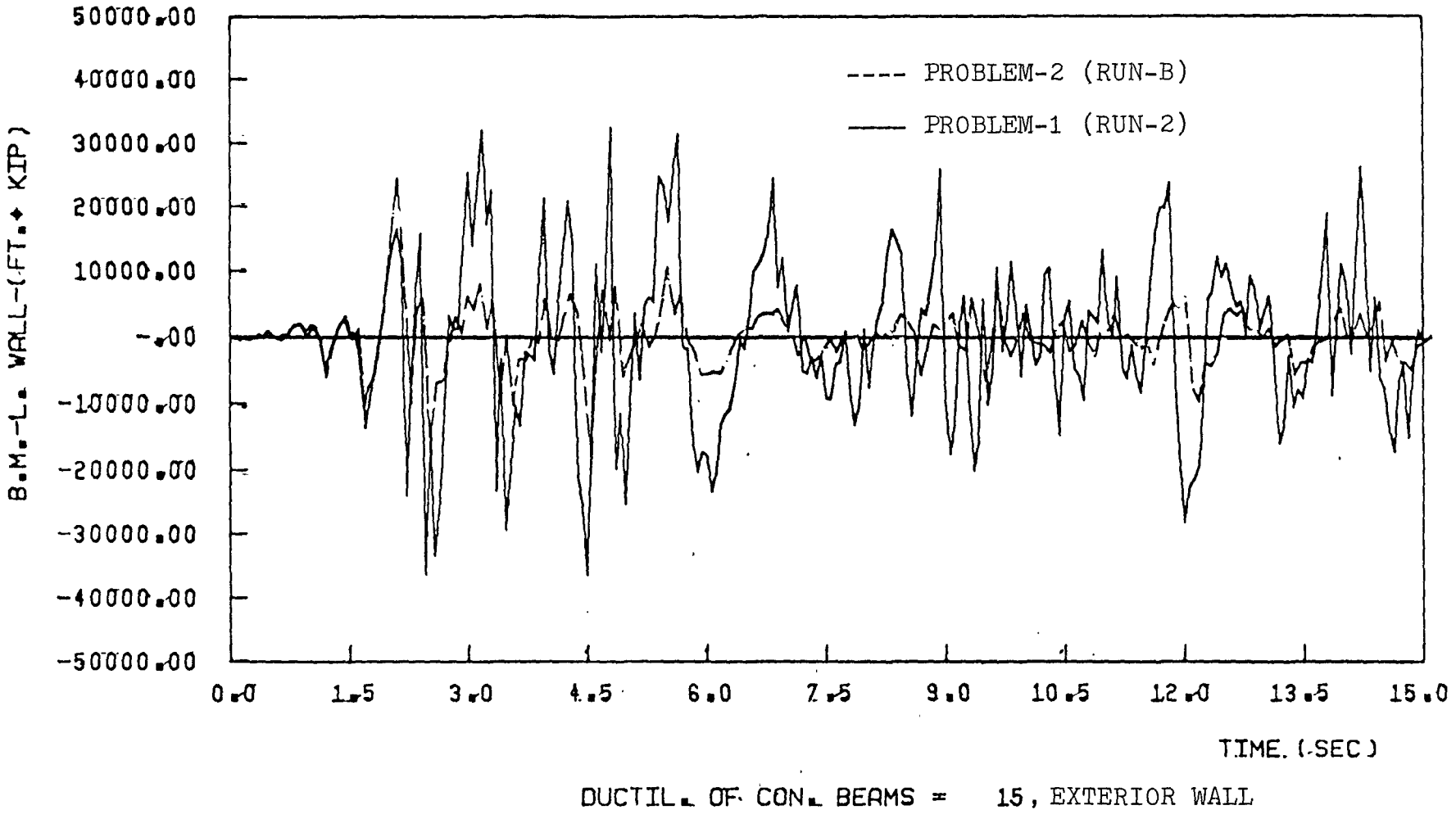

FIGURE 6-15 B.M.L.-WALL, ELCENTRO COMP. NORTH. 16 PERC. g

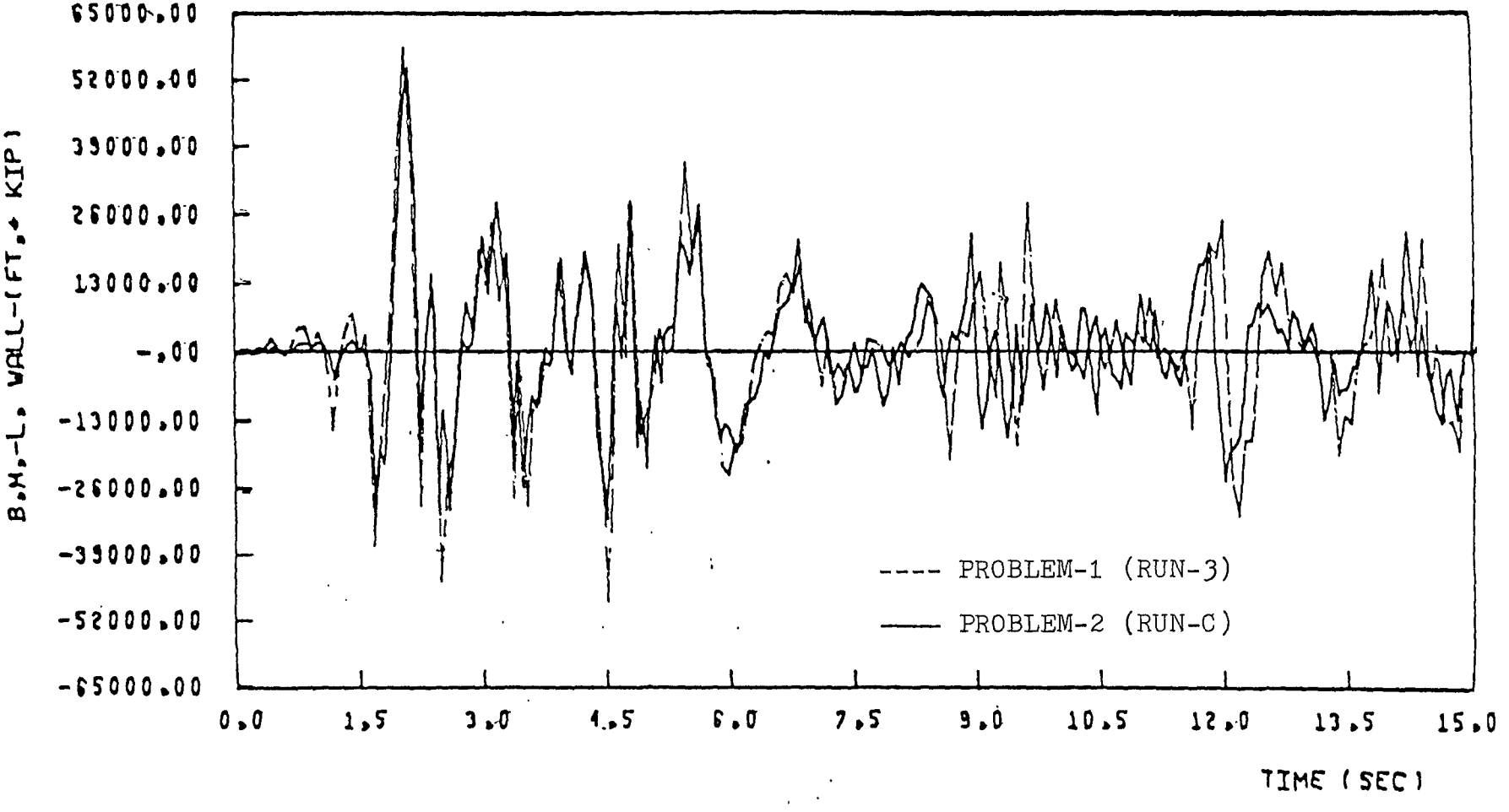

FIGURE 6-16 B.M.L. WALL, ELCENTRO COMP. NORTH 32 PERC. g

coupled shear wall and hence leads to a larger base moment.

Figure (6.17) compares the responses of the interior coupled shear walls under severe earthquakes in Run-C and Run-D. They are almost identical and this shows that there is very little effect of the rotational ductility factors of the connecting beams on the base moment response. Figure (6.18) shows the comparison between these response of the exterior coupled shear wall and this also shows the same trend. In fact both figures are almost identical. This shows that the base moments in the exterior and interior wall in the two inter-connected coupled shear wall formation are the same, a direct consequence of the assumption of constant curvature at the station levels and also at the base of shear walls.

6.3.4 Load Sharing Factor for Exterior Wall

Figures (6.19) and (6.20) give the responses, under moderate earthquake, at the base of first and third segment respectively. Figures (6.21) and (6.22) give the same responses for the single coupled shear wall paroblem. These figures show that the phenomenon of load sharing is different in the two interconnected coupled shear wall problem from that in the single shear wall problem. For the single coupled shear wall problem it fluctuates around 2.4. The reason is that the exterior wall takes a mass in proportion to its stiffness and it is 2.4 times stiffer than the interior wall. These fluctuations are due to the different order of formation of plastic hinges in the exterior wall and the interior wall. The response in the two interconnected

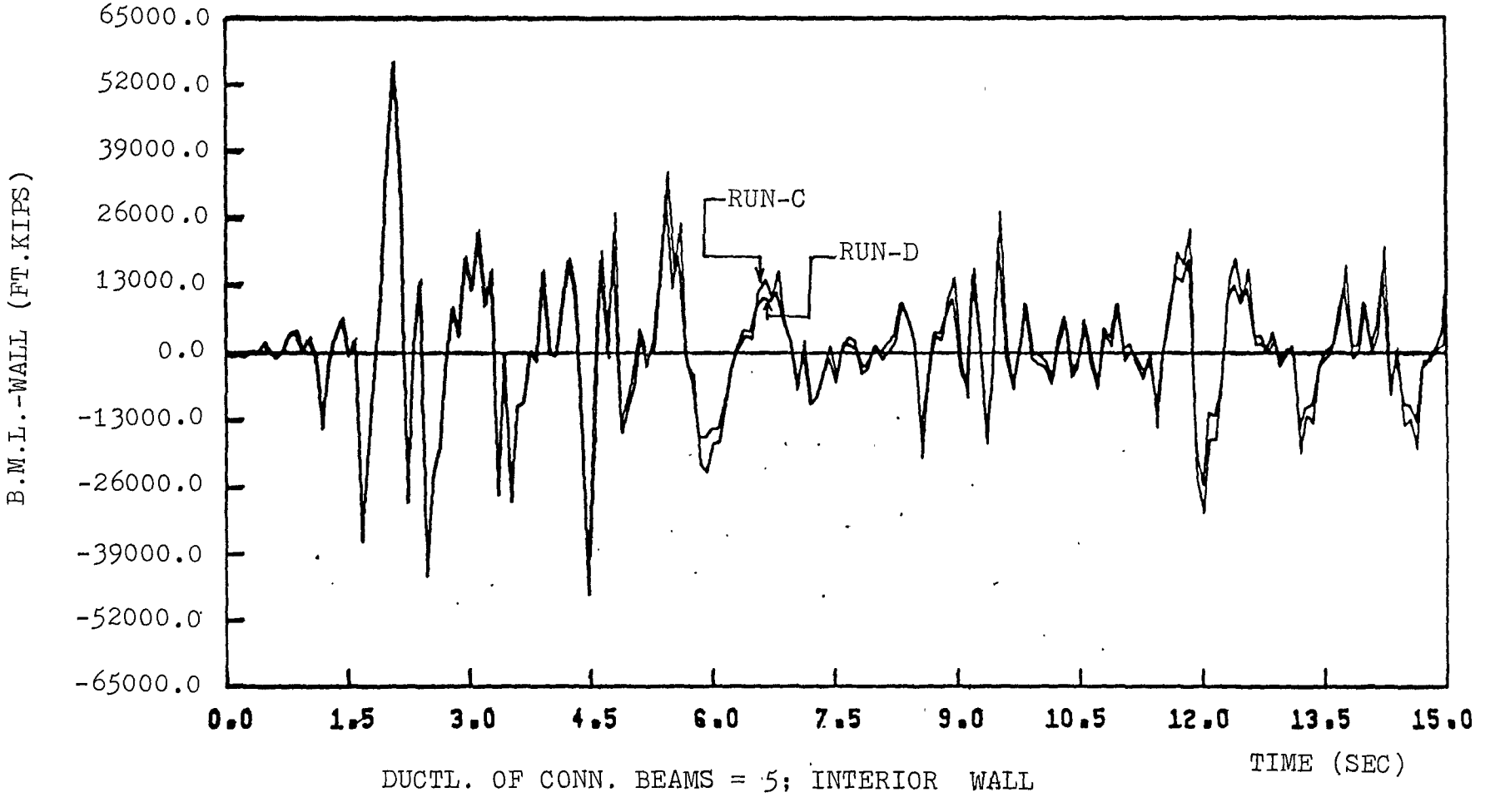

FIGURE 6-17 B.M.L.-WALL, ELCENTRO COMP. NORTH 32 PERC. g

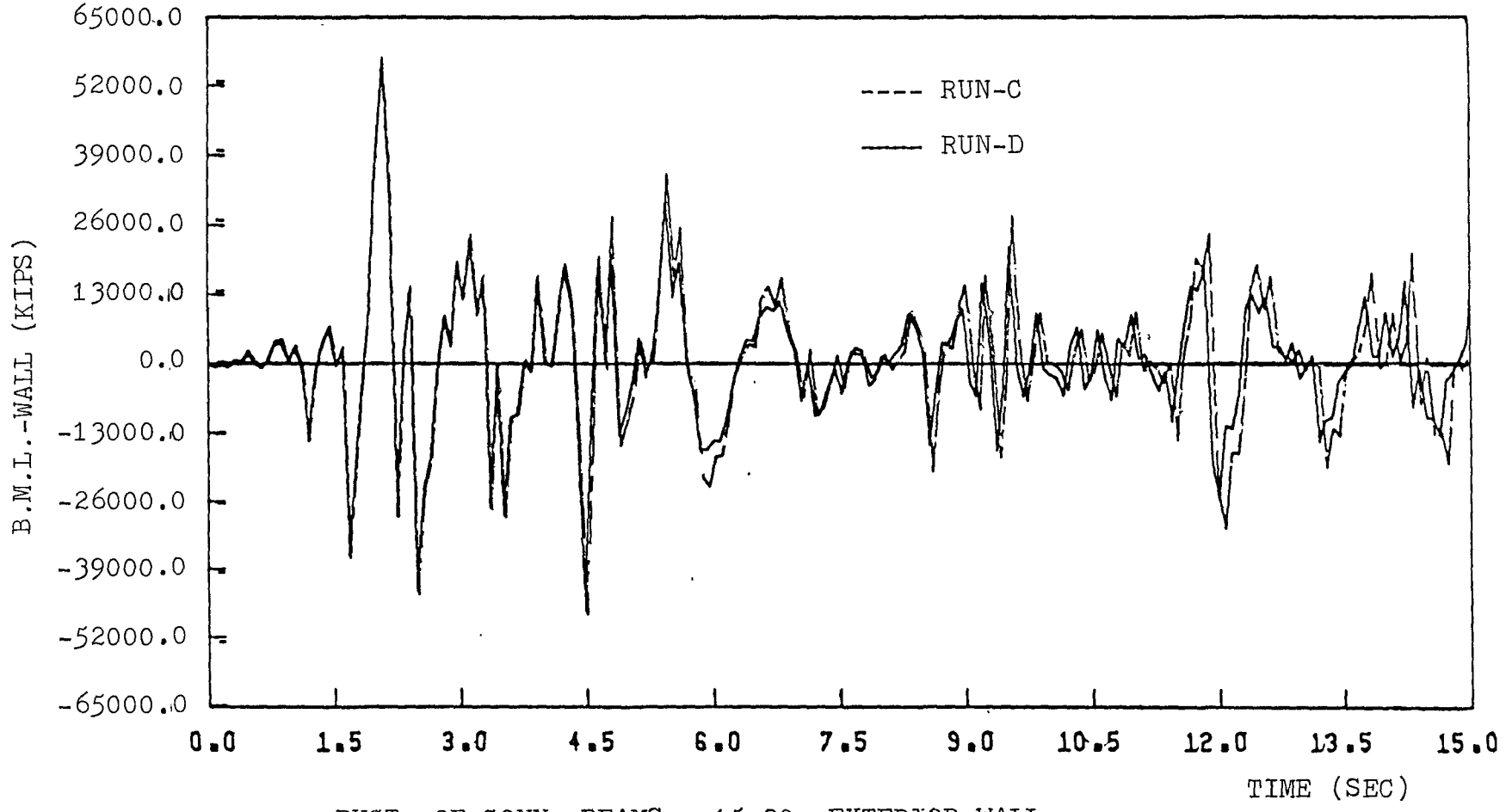

DUCT. OF CONN. BEAMS = 15,30; EXTERIOR WALL

FIGURE 6-18 B.M.L.-WALL, ELCENTRO COMP. NORTH 32 PERC. g

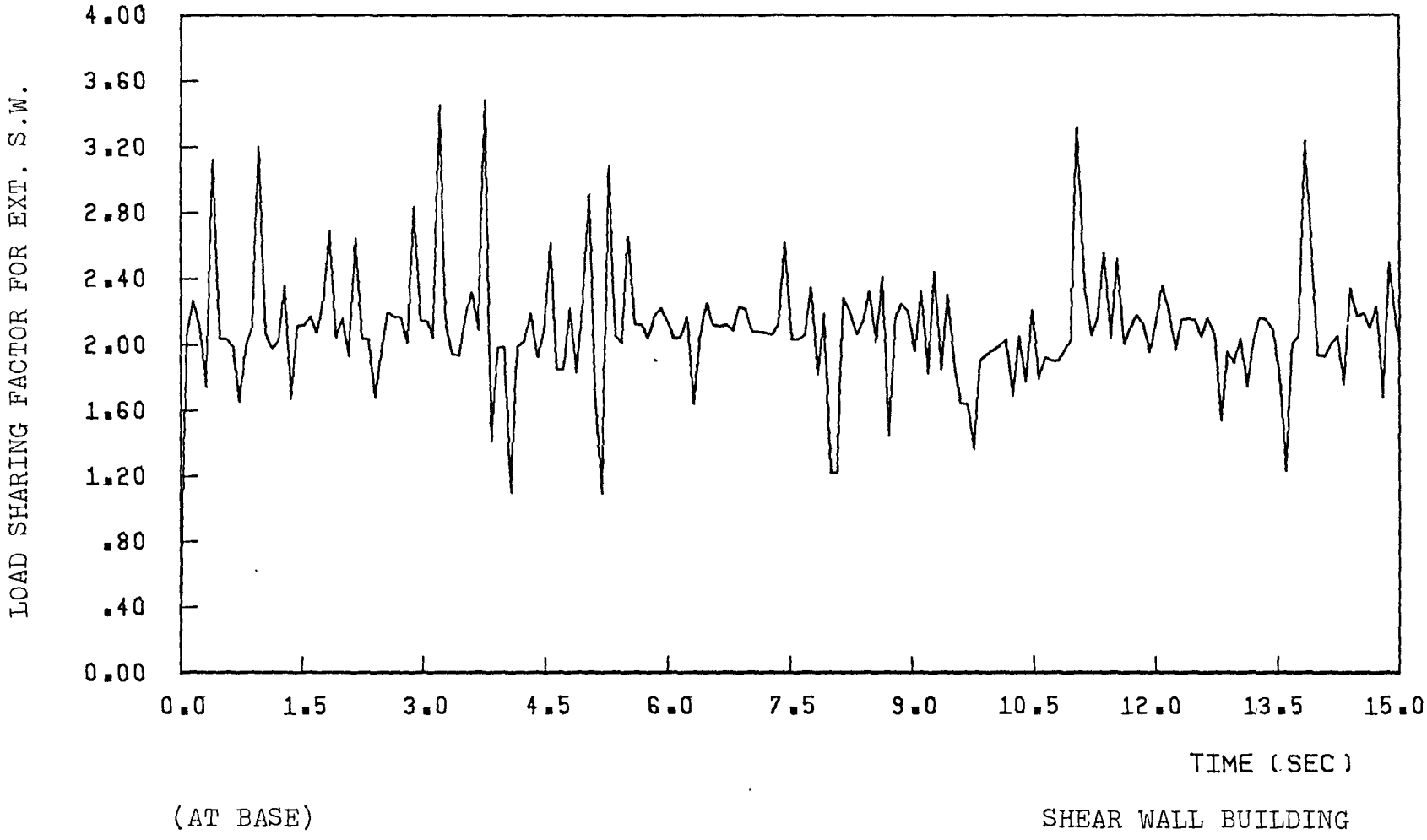

FIGURE 6-19 LOAD SHARING FACTOR, ELCENTRO COMP. NORTH 16 PERC. g

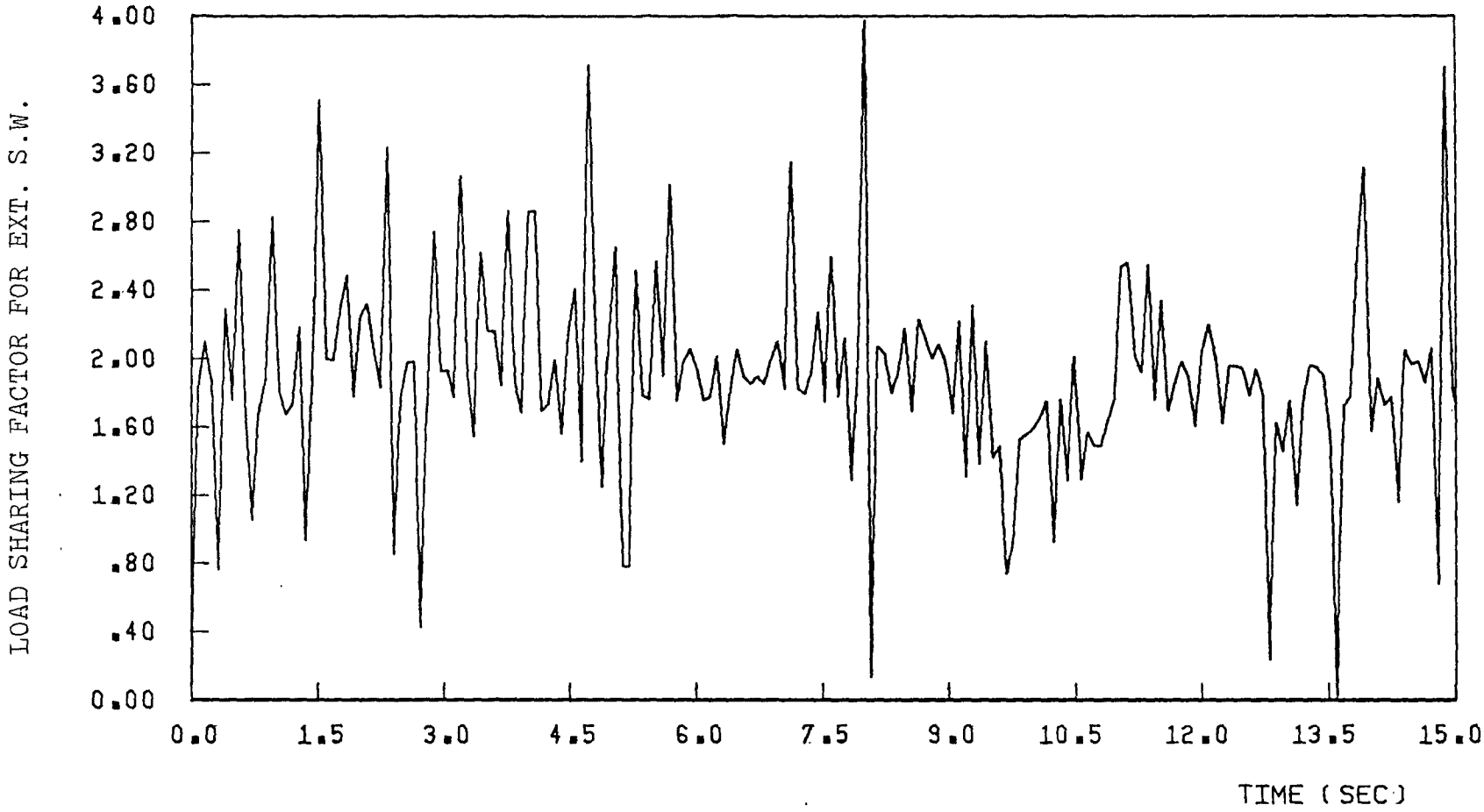

FIGURE 6-20 LOAD SHARING FACTOR, ELCENTRO COMP. NORTH 16 PERC. g

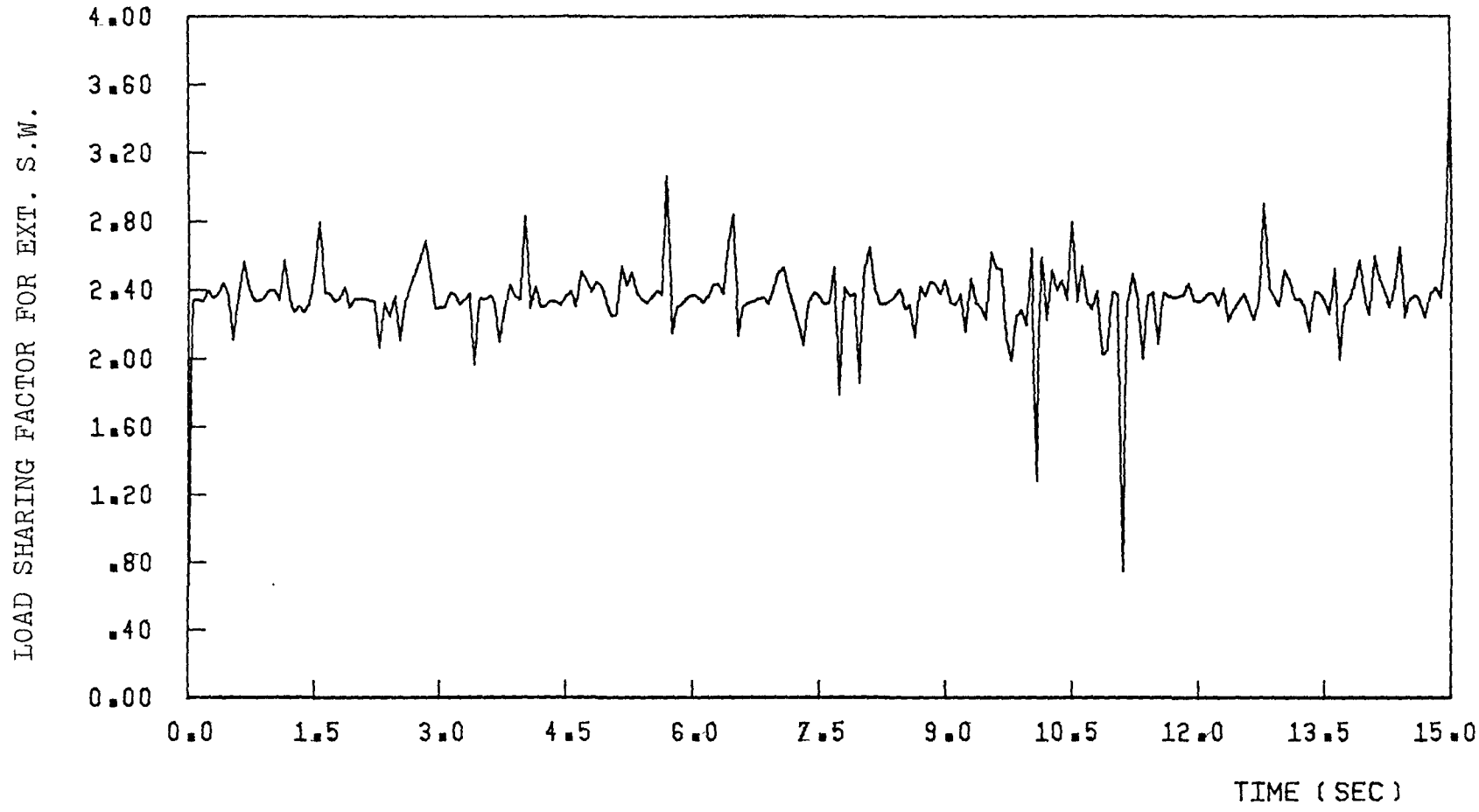

FIGURE 6-21 LOAD SHARING FACTOR, ELCENTRO COMP. NORTH 16 PERC. g

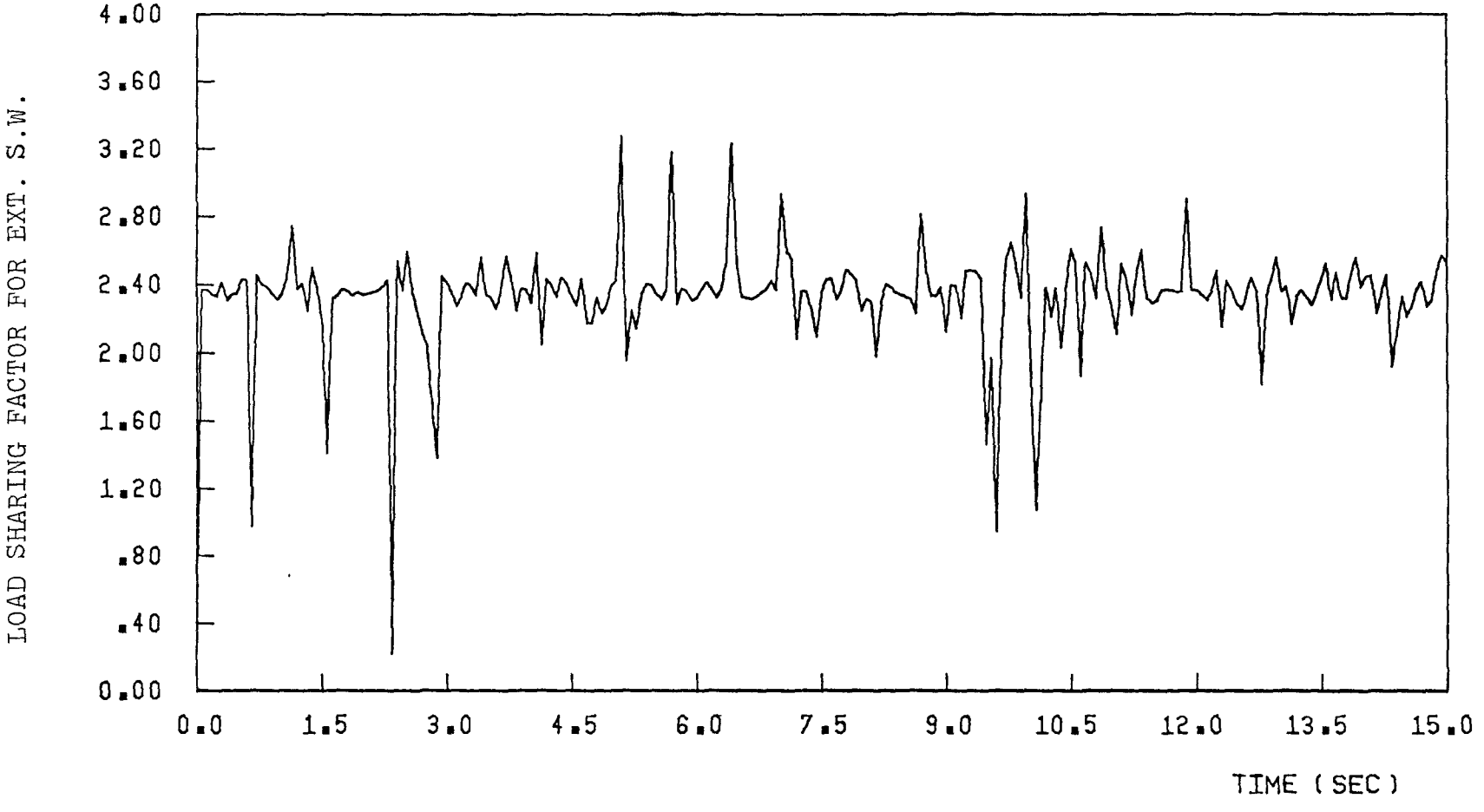

FIGURE 6-22 LOAD SHARING FACTOR, ELCENTRO COMP. NORTH 16 PERC. g

coupled shear wall problem fluctuates more and the fluctuations are not about the value of 2.4. This is because the transfer of loading between the two walls is not fixed, but depends on the instantaneous stiffnesses of the two coupled shear walls. The same observation applies to the shear walls which are shaken by a severe earthquake as shown in Figs. (6.23) through (6.26).

6.4 COMPARISON BETWEEN SINGLE COUPLED SHEAR WALL PROBLEM AND TWO INTERCONNECTED COUPLED SHEAR WALLS PROBLEM

After studying the behaviour of the exterior and the interior shear wall, by analysis as single individual coupled shear walls in Chpater 4 and in the two interconnected coupled shear wall problem in the previous section, it is worthwhile to compare the responses of these two walls in both problems under same loading and geometrical conditions.

Table 6.3 gives the maximum values of the parameters of interest discussed above for the interior and exterior wall under 16% g El-Centro N.S record excitation. It also includes the number of plastifications in the segments during the entire time-history of the earthquake loading considered. These numbers and the maximum number of plastic and real hinged segments give some indication to the nature of plastification along the entire height of the structure. Also the number of occurrence of the tensile force at the base of the wall gives the idea of the nature of severity at the base during the entire loading history.

Table 6.4 gives the same parameters for the interior and exterior wall when subjected to 32% g El-Centro earthquake loading.

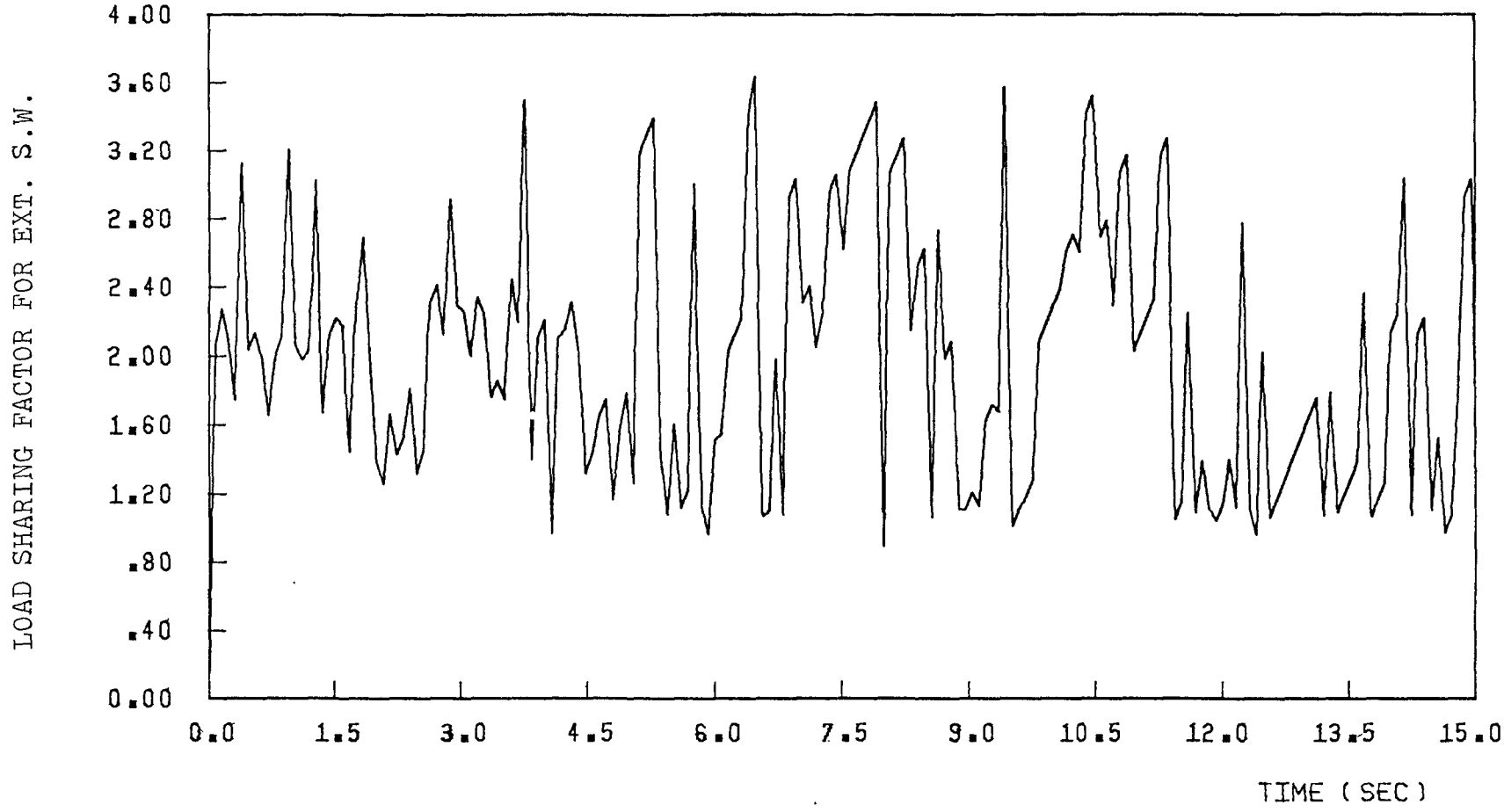

FIGURE 6-23 LOAD SHARING FACTOR, ELCENTRO COMP. NORTH 32 PERC. g

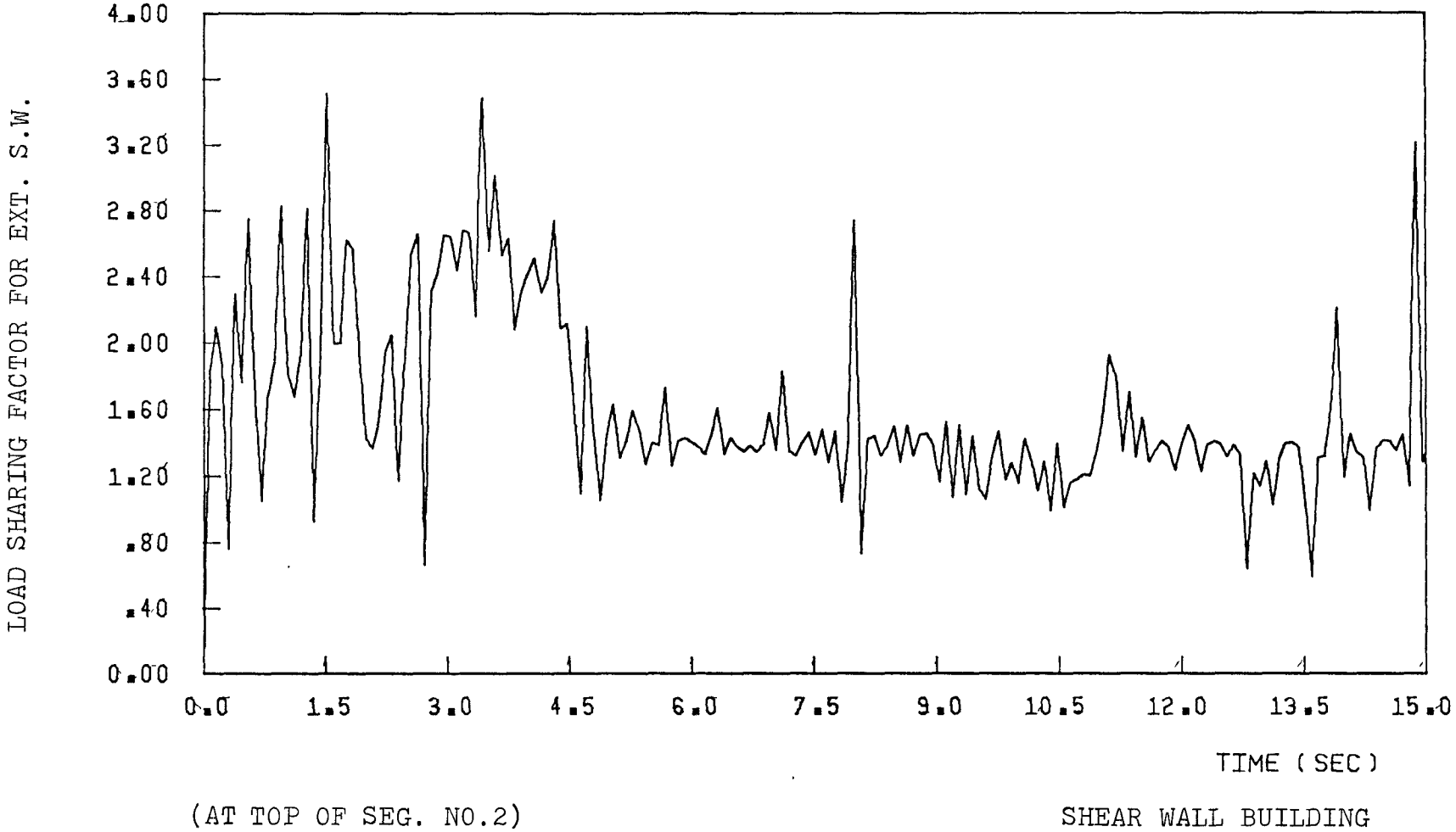

FIGURE 6-24 LOAD SHARING FACTOR, ELCENTRO COMP. NORTH 32 PERC. g

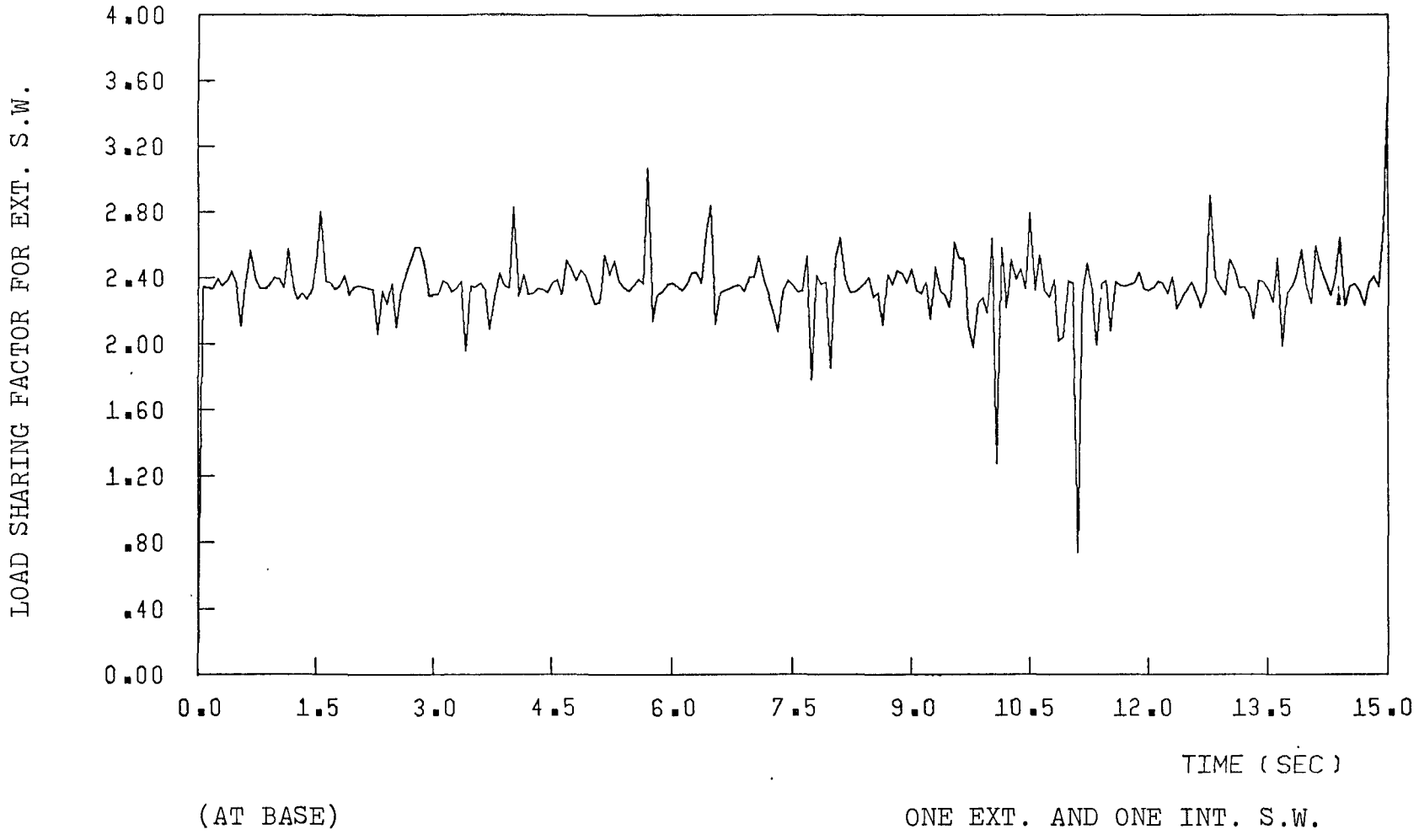

FIGURE 6-25 LOAD SHARING FACTOR, ELCENTRO COMP. NORTH 32 PERC. g

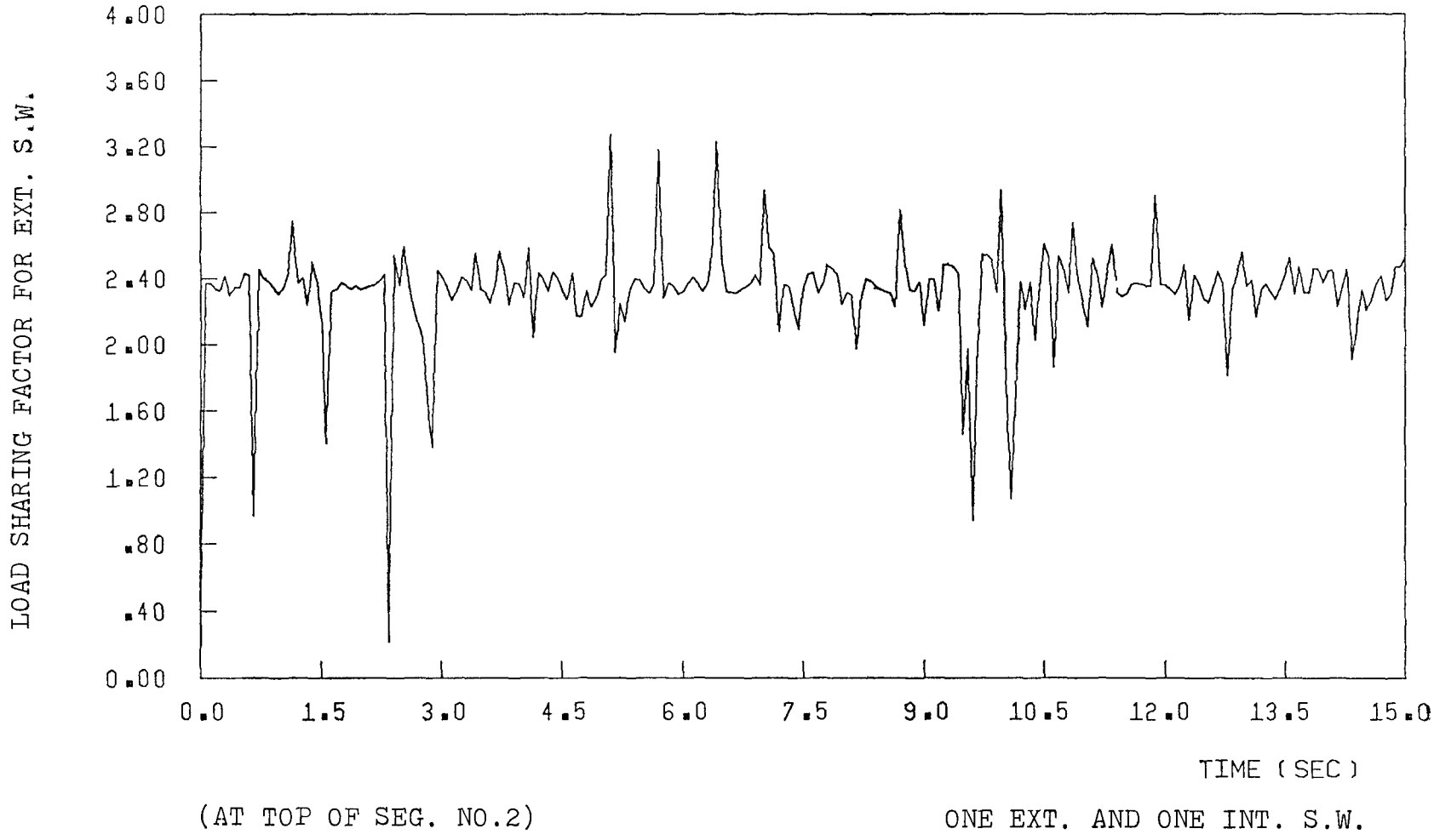

FIGURE 6-26 LOAD SHARING FACTOR, ELCENTRO COMP. NORTH 32 PERC. g

WALL		Ductility $\overline{\mu}$	Maximum Base Moment (kips.ft)	Maximum Base Axial Force (kips)	No. of Occurrences of Tensile Axial Force at Base	Maximum Top Deflection (ft)	No. of Plastification in the Segment Number					Maximum No. of segments Plastified at one time	Maximum No. of Real Hinged Segments
							1	2	3	4	5		
Exterior Shear Wall	Problem-1	500	26700	2950	8	0.18	0	3	1	0	0	2	0
	Problem-2		23700	2350	6	0.18	0	2	1	0	0	2	0
	Problem-1	15	32500	3270	2	0.18	0	2 Δ	1 Δ	1	0	3	2
	Problem-2		23700	2350	6	0.18	0	2	1	0	0	2	0
Interior Shear Wall	Problem-1	500	14000	425	0	0.18	0	2	2	5	3	4	0
	Problem-2		23700	410	0	0.18	0	2	2	4	3	4	0
	Problem-1	5	22000	390	0	0.18	0	3	2	2 Δ	2 Δ	3	2
	Problem-2		23700	410	0	0.18	0	2	2	4	2	3	0

Problem-1: Single S.W. Problem Problem-2: Two S.W. Problem Δ: Real Hinge

Table 6.3 Comparison of Maximum Responses of an Exterior and an Interior Wall, 16%g El Centro

WALL		Ductility $\overline{\mu}$	Maximum Base Moment (kips.ft)	Maximum Base Axial Force (kips)	No. of Occurrences of Tensile Axial Force at Base	Maximum Top Deflection (ft)	No. of Plastification in the Segment Number					Maximum No. of Plastic Hinged Segments at one time	Maximum No. of Real Hinged Segments at one time
							1	2	3	4	5		
Exterior Shear Wall	Problem-1	15	56500	2510	4	0.33	0	2 Δ	1 Δ	1 Δ	3	2	3
	Problem-2		53500	2590	8	0.32	0	8	4 Δ	2 Δ	0	3	2
	Problem-2	30	53300	2925	16	0.32	0	6	4	1	1	4	0
Interior Shear Wall	Problem-1	5	48200	380	0	0.32	0	4	4	2 Δ	1 Δ	3	2
	Problem-2		53500	395	0	0.32	0	3	2	2 Δ	2 Δ	4	2
	Problem-2	5	53300	395	0	0.32	0	6	2	2 Δ	2 Δ	4	2

Problem-1: Single S.W. Problem Problem-2: Two S.W. Problem Δ: Real Hinge

Table 6.4 Comparison of Maximum Responses of an Exterior and an Interior Wall; 32%g El Centro

The overall "Top Deflection Ratio" (T.D.R.) is also calculated in these cases by equation (4.1) and is given in Table 6.5.

Ground Acceleration	WALL	Ductility of the connecting Beams ($\bar{\mu}$) Limited (=5 for int; = 15 for ext)	High (=500)
16% g El-Centro	Exterior	1.45	1.45
	Interior	1.45	1.45
32% g El-Centro	Exterior	2.91	
	Interior	2.91	
	Exterior (μ = 30)	2.91	

Table 6.5 Top Deflection Ratio for an Exterior and an Interior Wall

From the comparison of the parameters in Tables 4.3 and 4.4 it can be seen that the order of formation of plastic hinges and real hinges is different for problem-1 and problem-2. This may be because of the difference in the percentage loading shared by each wall. In problem-1, as initially the exterior wall is 2.4 times stiffer than the interior wall, the exterior wall is assumed to have the mass as 2.4 times that of the interior wall. While in problem-2, the exterior wall seems to take a load around 1.5 to 2.0 times that of the interior wall.

The bending moments at the base of the interior wall are under-estimated in problem-1. The base moment in the exterior wall on the other hand are over-estimated in problem-1.

The extent of formation of the real hinges is over-estimated in problem-1.

For limited ductilities the occurrence of tensile axial force at the base of the exterior shear wall is less frequent in problem-1.

From the Tables 4.12 and 6.2, it can be seen that the overall "Top Deflection Ratio", i.e. the overall ductility demand is slightly over estimated in problem-1 for the limited member ductilities.

From the tables 6.3 and 4.4, considering the effect of rotational member ductilities, it may be concluded that, the occurrence of tensile axial force at the base of the exterior shear wall increases by increasing the member ductility. The limited member ductility increases the maximum values of base moments and axial forces.

CHAPTER 7

CONCLUSIONS, DESIGN RECOMMENDATIONS AND FURTHER INVESTIGATIONS

7.1 CONCLUSIONS

The following conclusions are drawn based on the work presented in the previous chapters.

(1) The continuum approach in combination with the transfer matrix technique can provide an efficient means to obtain a full time history response of single and two interconnected coupled shear walls subjected to ground motions. The proposed method is capable of handling plane non-uniform coupled shear wall structures subjected to any ground accelerations. The effect of flexible foundation can be incorporated in the analysis. Complexity in the structural configuration and/or the inelastic regions are conveniently handled by dividing the structure into a series of segments where each segment has uniform structural properties within itself. To save computer time the number of lumped masses need not be equal to the number of segments. A large number of segments can be used to achieve the necessary accuracy. The number of segments here can be taken an integer multiple of the number of masses. Independent of the number of stories of the structure or the number of the segments into which the walls are to be divided, the resulting transfer matrices are

six by six matrices in single coupled shear wall problem and eight by eight matrices in two interconnected coupled shear walls problem. Therefore, computer with limited memory capcity can be used to analyze high rise building using the proposed method.

(2) The present simplified modeling technique of coupled shear walls gives a fairly realistic inelastic behaviour of the coupled shear walls.

(3) The P-Δ Effect appears to have a minor influence. This is due to the piers are assumed to remain elastic throughout the analysis. But when the formation of the plastic hinges at the base of the piers is considered, the P-Δ Effect is likely to become important.

(4) Due to the high shearing force transmitting capacity of the connecting beams, the axial force in the piers due to the lateral load may exceed the dead load carried by each pier. In such a case the tensile force will occur at the base of the pier. This situation is observed in case of end walls where deep coupling beam is used and yet the tributary area for gravity load is small. To decrease the tensile forces in the piers, it is useful to arrange the shear walls in such a way to keep the tributary areas proportional to the wall stiffness.

(5) For the coupled shear wall of practical dimensions, it may be concluded that when the monotonously increasing load is applied, the second plastic hinge at the base forms almost immediately after the first hinge has been formed.

(6) Based on the present limited study, it may be concluded that the model structure will suffer light damage and may survive against collapse if it is exposed to moderate earthquake shaking. On the other hand, if it is exposed to severe earthquake, then heavy damage may occur and the walls may even fail as collapse mechanism with the formation of hinges at the bases.

(7) The behaviour of the coupled shear wall will be improved if the ductility of the connecting beams is increased. This improvement is more important for the survival against severe earthquakes and hence increase in the ductility of the moderately stiff connecting beams will lead to better performance.

(8) The improvement in the member ductility of only one or some of the coupled shear walls is not advantageous to the behaviour of the other coupled shear walls of the same system.

The following conclusions are drawn to compare the conventional method of single coupled shear wall analysis with the present method of two interconnected coupled shear walls analysis.

(1) The order of formation of plastic and real hinges at the ends of the connecting beams in single coupled shear wall problem is different from that observed in the two interconnected coupled shear walls problem.

(2) The bending moments at the base of the interior coupled shear walls are underestimated by 7% to 12% in single coupled shear wall problem. The bending moments at the base of the exterior

shear wall are overestimated by 12% to 20% in single coupled shear wall problem.

(3) The occurrence of the tensile axial force at the base of the piers is less in single coupled shear wall problem when the rotational ductility factor of the connecting beams is limited.

(4) The overall "Top Deflection Ratio" i.e. the overall ductility demand is slightly overestimated in single coupled shear wall problem.

7.2 DESIGN RECOMMENDATIONS

Based on the behaviour of the coupled shear walls observed in the present study, the following recommendations can be made for the design of coupled shear walls.

(1) It is desirable to design the walls to maintain an elastic behaviour throughout an earthquake response for minimum nonstructural damage, and to ensure the moderate ductility capacity as a second line of defense. A strong and ductile wall can be designed by concentrating the flexural reinforcement at the two extreme ends of the section and detailing the transverse reinformcement to confine the concrete effectively.

(2) The coupling beams should be designed so as to be moderately stiff enough in order to render an effective coupling system.

(3) These beams should be carefully detailed with the diagonal, transverse reinforcement for ductile behaviour without brittle shear failure under a large number of reversals so as to reduce

the possibility of significant yielding in the walls.

7.3 FURTHER INVESTIGATIONS

The following points require further investigations:

(1) The formulation of plastic hinges at the base of the piers should be included in two interconnected coupled shear walls problem, to understand the complete behaviour of the building when exposed to the moderate and strong earthquakes.

(2) The variation in the behaviour of the coupled shear walls can be studied in detail by considering the walls of different flexibilities and by arranging the walls to give different tributary areas for each of them.

APPENDIX A

CALCULATION FOR THE INTERACTION CURVES FOR THE COUPLED SHEAR WALLS CONSIDERED IN EXAMPLES

This appendix presents the calculation for determination of interaction curves for the walls considered in the example building.

A.1 EXTERIOR WALL

The dimensions and stress, strain distribution at the base the pier of 20 storey exterior coupled shear wall is shown in Fig. (A.1). Taking the material properties as

$$Es = 2.9 \times 10^3 \text{ ksi}$$

$$Ec = 3.5 \times 10^3 \text{ ksi}$$

$$f'_c = 4 \text{ ksi}$$

$$fy = 60 \text{ ksi}$$

the distance of then eutral axis "x_b" is given by

$$\frac{x_b}{d} = \frac{0.003}{(fy/Es)+0.003}$$

therefore

$$x_b = \frac{87000\ d}{fy+87000}$$

$$= \frac{87000 \times 201.9}{60000 + 87000}$$

$$= 119.49 \text{ in.}$$

therefore

$$a = 0.85\ x_b = 101.57 \text{ in}$$

therefore $C_c = 0.85\ f'_c\ a\ b$

$= 0.84 \times 4 \times 101.56 \times 12$

$= 4143.98$ kips

$C_s = fy\ A_{st_1} = 0.85\ f'_c\ A_{st_1}$

$= 60 \times 34.32 - 0.85 \times 4 \times 34.32$

$= 1942.51$ kips

therefore $\epsilon'_s = 0.003\ (119.49 - 9.1)/119.49$

$= 2.77 \times 10^{-3} > \epsilon_y = 2.069 \times 10^{-3}$ $\therefore$ O.K.

$T = f_y\ A_{st_1}$

$= 60 \times 34.32$

$= 2059.2$ kips

therefore $P_b = C_c + C_s - T$

$= 4143.98 + 1942.51 - 2059.2$

$= 4027.29$ kips

$$M_b = P_b\ e_b = C_c\ (d - \frac{a_b}{2} - d'') + C_s\ (d - d' - d'') + T\ d''$$

$$= 4143.98\ (105 - \frac{101.66}{2}) + 1942.5(105 - 9.1) + 2059.2\ (105-9.1)$$

$= 608449.6$ kips in.

$= 50704.14$ kips ft

$P_o = 0.85\ P_c(A_g - Ast) + fy\ Ast$

$= 0.85 \times 4\ (2520-34.32 \times 2) + 60 \times 34.32 \times 2$

$= 12453$ kips

$$P_\ell = fy\ Ast$$

$$= 60 \times 34.32 \times 2$$

$$= 4118.4 \text{ kips}$$

therefore for the part AB of interaction curve

$$x = \frac{M_b}{(P_b - P_o)} y - \frac{M_b}{(P_b - P_o)} P_o$$

$$= \frac{50704}{(4027-12453)} y - \frac{50704}{(4027-12453)} 12453$$

$$= -6.0175647\ y + 74936.7$$

for the curve BC

$$x = \frac{M_b}{(P_o + P_\ell)} y + \frac{M_b\ P_\ell}{(P_b + P_\ell)}$$

$$= \frac{50704}{(4027+4119)} y + \frac{50704 \times 4119}{(4027+4119)}$$

$$= 6.2244046\ y + 25638$$

The interaction curve for this exterior wall is shown in Fig. (A.2).

A.2 INTERIOR WALL

The dimensions and stress strain distribution at the base of the pier of 20 storey interior coupled shear wall is shown in Fig. (A.3). Taking the same material properties as exterior wall.

$$x_b = \frac{87000\ d}{87000 + f_y}$$

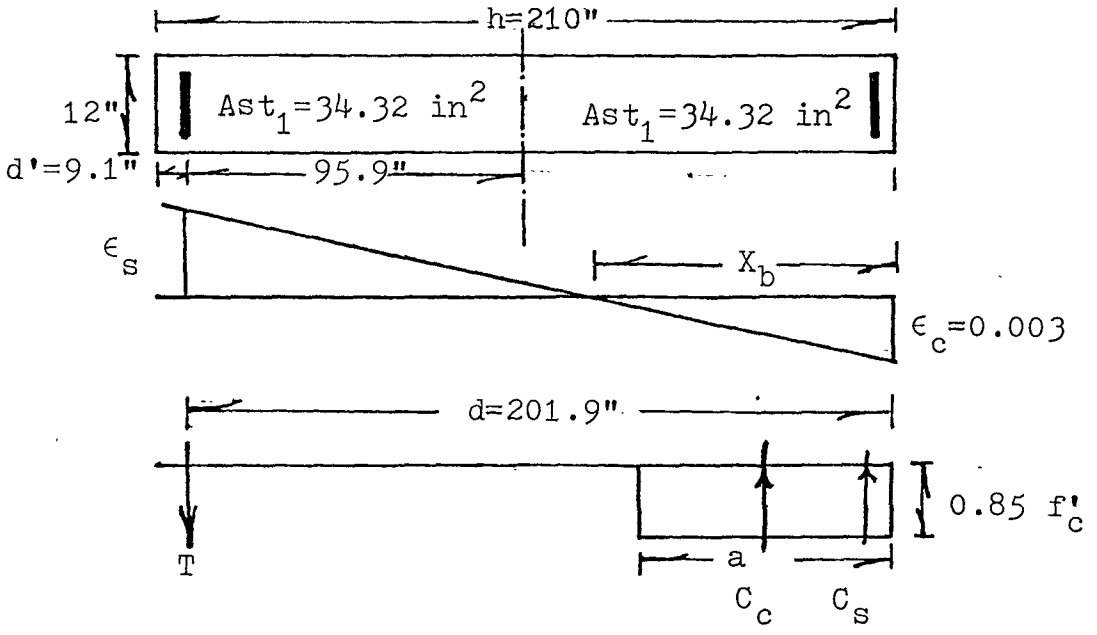

FIGURE A-1 DIMENSIONS AND STRESS-STRAIN DISTRIBUTION AT THE PIER OF EXTERIOR WALL

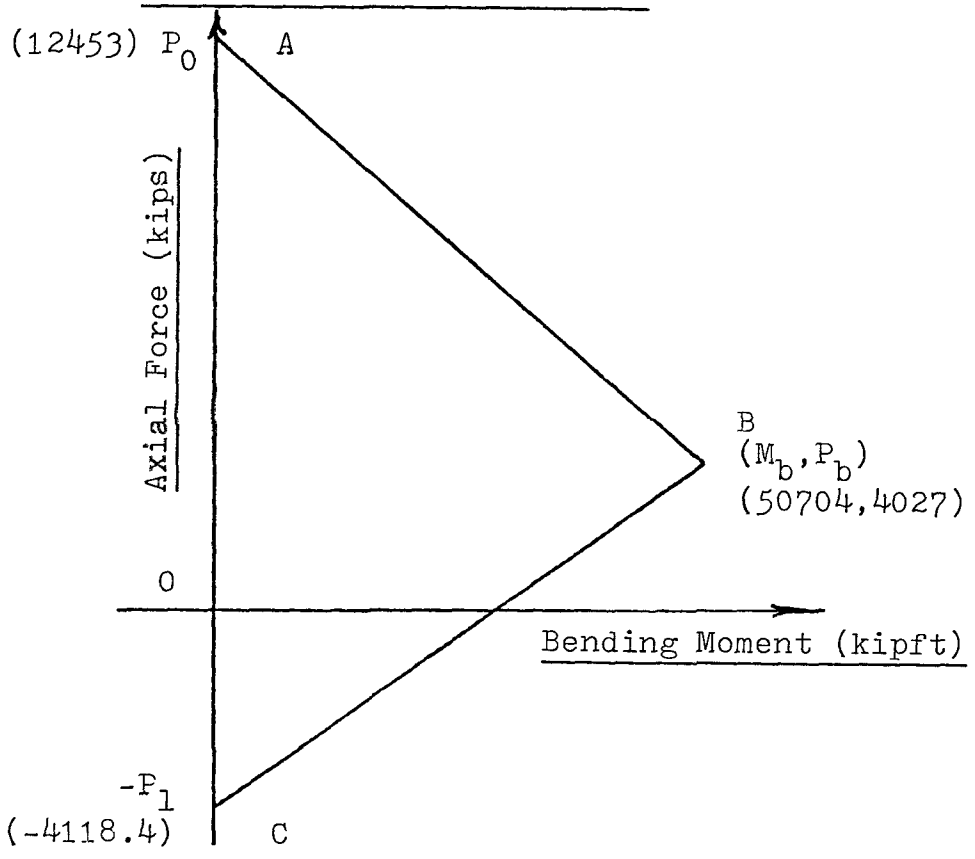

FIGURE A-2 INTERACTION CURVE FOR EXTERIOR WALL

$$= \frac{87000 \times 201.9}{87000+60000}$$

$$= 119.49 \text{ in}$$

therefore $a = 0.85\ x_b$

$$= 101.57 \text{ in}$$

$$C_c = 0.85 \times 4 \times 101.57 \times 12$$

$$= 4143.95 \text{ kips}$$

$$C_s = 60 \times 28.08 - 0.85 \times 4 \times 28.08$$

$$= 1589.33 \text{ kips}$$

$$T = 60 \times 28.08$$

$$= 1684.8 \text{ kips}$$

therefore $P_b = C_s + C_c - T$

$$= 1589.33 + 4143.95 - 1684.8$$

$$= 4048.48 \text{ kips}$$

$$M_b = P_b\ e_b = 4143.95\ (105 - \frac{101.57}{2}) + 1589.33(105-9.1) + 1684.8(105-9.1)$$

$$= 538653.32 \text{ kips in}$$

$$= 44887.78 \text{ kips ft}$$

$$P_o = 0.85 \times 4\ (2520 - 28.08 \times 2) + 60 \times 28.08 \times 2$$

$$= 11746.66 \text{ kips}$$

$$P_\ell = 60 \times 28.08 \times 2$$

$$= 3370 \text{ kips}$$

therefore for part AB of interaction curve

$$x = \frac{44888}{(4048-11747)}\, y - \frac{44888}{(4048-11747)}\, 11747$$

$$= -5.830595\ y + 19626$$

for the part BC

$$x = \frac{44888}{(4048+3370)}\, y + \frac{44888}{(4048+3370)}\, 3370$$

$$= 6.0512267\ y + 20392.6$$

The interaction curve for this interior wall is shown in fig. (A-4).

A.4 STRUCTURE-1

This coupled shear wall is the same as considered by Takayanagi and Schnobrich [30]. The dimension and stress strain distribution at the base of the pier of this coupled shear wall is shown in Fig. (A.5). Taking the material properties as

$$E_s = 29000 \text{ ksi}$$

$$E_c = 3000 \text{ ksi}$$

$$f'_c = 4.5 \text{ ksi}$$

$$f_y = 72 \text{ ksi}$$

therefore $$x_b = \frac{0.003\ d}{f_y/E_s + 0.003}$$

$$= \frac{0.003 \times 6.25}{72/29000 + 0.003}$$

$$= 3.42 \text{ in}$$

therefore $$a = (0.85 - 0.95 \times 1/2)\ 3.42$$

$$= 2.8215 \text{ in}$$

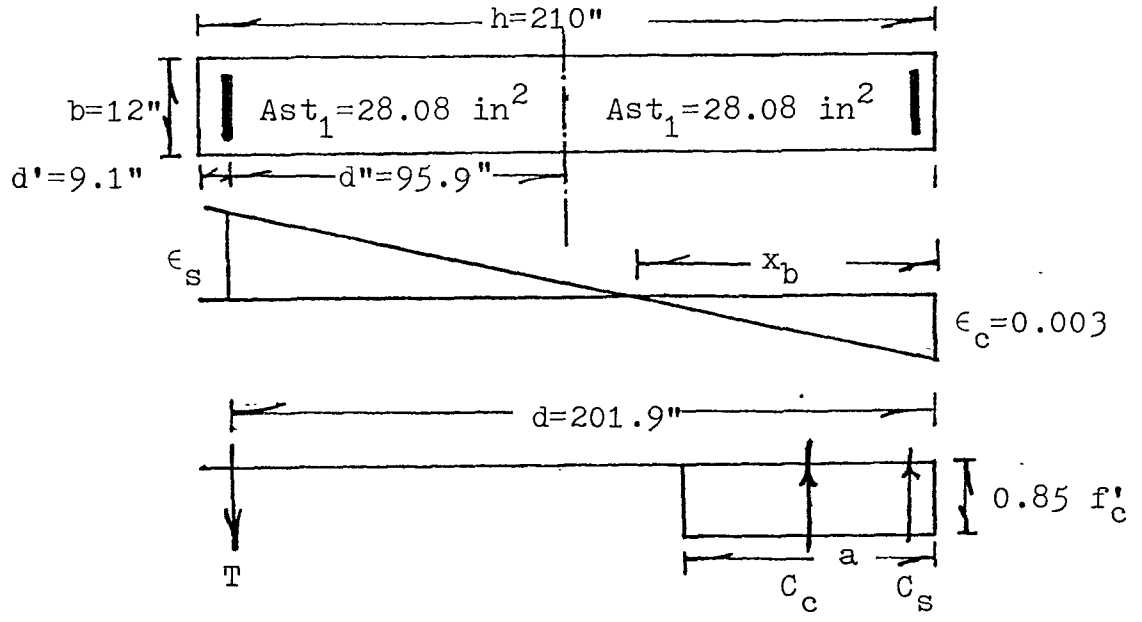

FIGURE A-3 DIMENSIONS AND STRESS-STRAIN DISTRIBUTION AT THE BASE OF THE PIER OF INTERIOR WALL

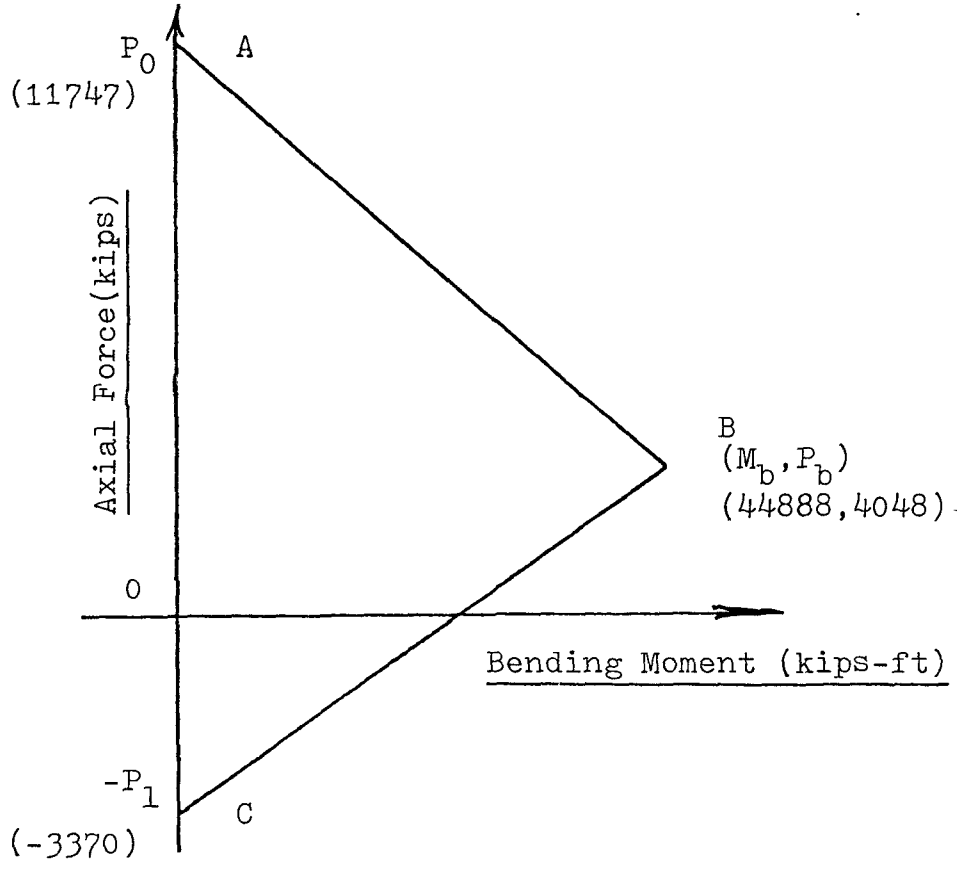

FIGURE A-4 INTERACTION CURVE FOR INTERIOR WALL

therefore $C_c = 0.85 \times 4.5 \times 2.8215 \times 1.0$

$= 10.7923$ kips

$C_s = 72 \times 0.0824 - 0.85 \times 4.5 \times 0.0824$

$= 5.61762$ kips

$T = 72 \times 0.0824$

$= 5.9328$ kips

therefore $P_b = C_c + C_s - T$

$= 10.7923 + 5.61762 - 5.9328$

$= 10.4771$ kips

$$M_b = P_b e_b = 10.7923\left(315 - \frac{2.8215}{2}\right) + 5.6176(3.5-0.75)+5.9328(3.5-0.75)$$

$= 54.311$ kips in

$P_o = 0.85 \times 4.5\ (7 - 0.0824 \times 2) + 72 \times 0.0826 \times 2$

$= 38.01$ kips

$P_\ell = 72 \times 0.0824 \times 2$

$= 11.8656$ kips

therefore for part AB of interaction curve

$$x = \frac{54.311}{10.4771-38.01}\, y - \frac{54.311}{10.4771-38.01}\, 38.01$$

$= -1.9725855\ y + 74.980$

for part BC

$$x = \frac{54.311}{10.4771+11.8656}\, y + \frac{54.311}{10.4771+11.8656}\, 11.8656$$

$= 2.4308163\ y + 28.843$

The interaction curve for this structure-1 is shown in fig. (A-6).

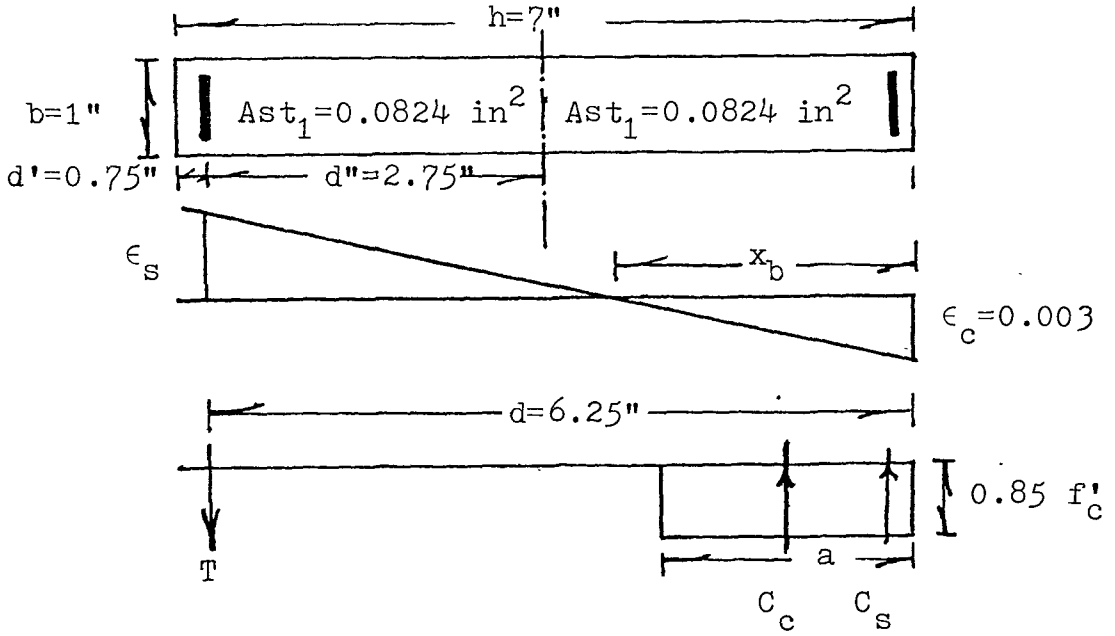

FIGURE A-5 DIMENSIONS AND STRESS-STRAIN DISTRIBUTION AT THE BASE OF THE PIER OF STRUCTURE-1

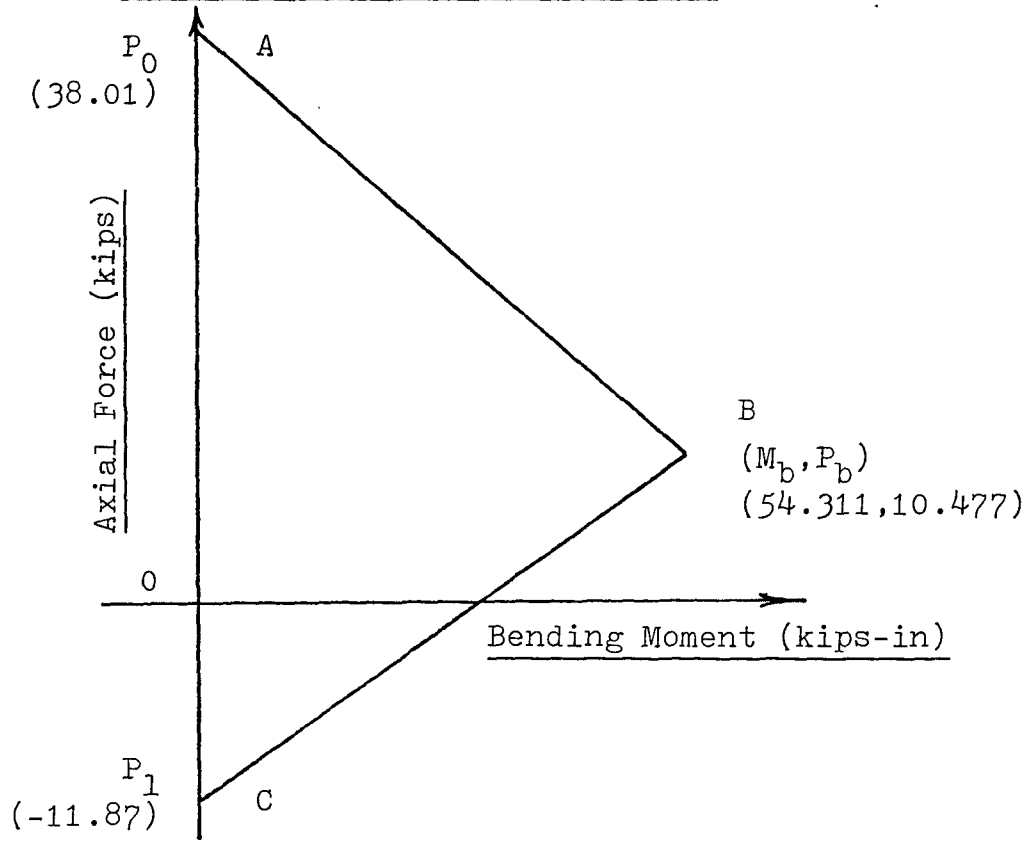

FIGURE A-6 INTERACTION CURVE FOR STRUCTURE-1

REFERENCES

1. ACI Standard 318-71, Building Code Requirements for Reinforced Concrete.

2. Bathe K.J. and Wilson E.L.: "Stability and Accuracy of Direct Integration Methods", Int. J. of Earthquake Engineering and Structural Dynamics, Vol. 1, p. 283-291 (1973).

3. Beck H.: "Contribution to the Analysis of Coupled Shear Walls", J. of American Concrete Institute, Aug. 1962, p. 1055-1068.

4. Biggs J.M.: "Introduction to Structural Dynamics", McGraw-Hill (1964).

5. Clough R.W. and Penzien J.: "Dynamics of Structures", McGraw-Hill (1975).

6. Coull A. and Choudhury J.R.: "Stresses and Deflections in Coupled Shear Walls", ACI Journal Proceedings V. 64, No. 2, Feb. 1967, p. 65-72.

7. Coull A. and Choudhury J.R.: "Analysis of Coupled Shear Walls", ACI Journal, Proceedings, Sept. 1967, p. 587-593.

8. Coull A. and ElHag A.A.: "Effective Coupling of Shear Walls by Floor Slabs", Supplement to Journal of American Concrete Institute, August 1975.

9. El-Shafee O.M.: "Elasto-Plastic Dynamic Analysis of Coupled Shear Walls", M.Engg. Thesis, McMaster University, Hamilton, Ontario, Canada, 1976.

10. Gluck J.: "Elasto-Plastic Analysis of Coupled Shear Walls", J. of Structural Division, ASCE, V. 99, ST8, Aug. 1973, p. 1743-1760.

11. Hart G.L. and Ramaswami Vasudevan: "Earthquake Design of Buildings, Damping", J. of Structural Div., ASCE, ST1, Jan. 1975, p. 11-30.

12. Humar J.L. and Wright E.W.: "Numerical Methods in Structural Dynamics", Canadian J. of Civil Engg., 1, 1974, p. 179-193.

13. Jennings P.C. and Skattum K.S.: "Dynamic Properties of Planar Coupled Shear Walls", J. of Earthquake Engg. and Structural

Dynamics, V. 1, 1973, p. 387-405.

14. MacLeod I.A. and Hosny H: "Frame Analysis of Shear Wall Cores", Paisley College of Technology, Research Report.

15. Mendelson E. and Baruch M.: "Damped Earthquake Response of Non-Symmetric Multistory Structures", The Structural Engineer, Apr. 1975, No. 4, V. 53, p. 165-171.

16. National Building Code of Canada, 1975.

17. Neal B.G.: "The Plastic Method of Structural Analysis", John Wiley and Sons, Inc., NY (1963).

18. Newmark N.M.: "A Method of Computation for Structural Dynamics", Proc. of American Society of Civil Engineers, 85, EM3, 1959, p. 67-94.

19. Newmark N.M. and Hall W.J.: "Procedures and Criteria for Earthquake Resistant Design", Building Practices for Disaster Mitigation, Building Science Series 46, U.S. Dept. of Commerce Publication, 1973.

20 Paulay T.: "Design Aspects of Shear Walls for Seismic Areas", Second Canadian Conference on Earthquake Engg., Paper 15, June 1975.

21. Paulay T.: "An Elasto-Plastic Analysis of Coupled Shear Wall", ACI Journal, Nov. 1970, p. 915-922.

22. Paulay T.: "Simulated Seismic Loading of Spandrel Beams", J. of Structural Div., ASCE, 97, ST9, Sept. 1971, p. 2407-2419.

23. Paulay T. and Santhakumar A.R.: "Ductile Behaviour of Coupled Shear Walls", J. of Structural Div., ASCE, St. 1, Jan. 1976, p. 93-108.

24. Pisanty A. and Traum L.E.: "Simplified Analysis of Coupled Shear Walls of Variable Cross Section", Building Science, V. 5, 1970, p. 11-20.

25. Robinson H. and Elkholy I.A.S.: "An Inelastic Analysis of Coupled Shear Walls", Building Science, V. 9, 1974, p. 1-8.

26. Saul W.E.: "Damping in Structures with Rigid Body Displacement Components", Second Canadian Conference on Earthquake Engg., Paper 10, June 1975.

27. Schwaighofer J. and Singh G.: "A Bibliography on Shear Walls (1928-1976)", U. of Toronto Publication No. 76-02, May 1976.

28. Smith S.: "Modified Beam Method for Analyzing Symmetrical Interconnected Shear Walls", ACI Journal, Nov. 1970, p. 977-980.

29. Sozen M.A. and A. Dario Aristizabal Ochoa: "Behaviour of Ten Story Reinf. Concrete Shear Wall Subjected to Earthquake Motions", University of Illinois Report, Structural Research Series No. 431, Oct. 1976.

29a. Srichatrapimuk T.: "Earthquake Response of Coupled Shear Wall Buildings", Earthquake Engineering Research Center, Berkeley. Report No. EERC 76-27, Nov. 1976.

30. Takayanagi T. and Schnobrich W.C.: "Computed Behaviour of Reinf. Concrete Coupled Shear Walls", U. of Illinois Report, Structural Research Series No. 434, Dec. 1976.

31. Tso W.K. and Chan P.C.K.: "Static Analysis of Stepped Coupled Walls by Transfer Matrix Method", Building Science, V. 8, 1973, p. 167-177.

32. Tso W.K. and Chan H.: "Dynamic Analysis of Plane Coupled Shear Walls", J. Engg. Mech. Div., ASCE, 97, EM1, Jan. 1971, p. 33-48.

33. Tso W.K. and Chan P.C.K.: "Flexible Foundation Effect on Coupled Shear Walls", ACI Journal, Nov. 1972, p. 678-683.

34. Wang C.K. and Salmon C.G.: "Reinforced Concrete Design," Index Educational Publishers, N.Y. (1973).

35. Wiegel R.L.: "Earthquake Engineering," Prentice Hall Inc., N.J., 1970.

36. Wilson E.L., Farhoomand I. and Bathe K.J.: "Non-Linear Dynamic Analysis of Complex Structures", J. of Earthquake Engg. and Structural Dynamics, V. 1, 1973, p. 241-252.

37. Winokur A. and Gluck J.: "Ultimate Strength Analysis of Coupled Shear Walls", ACI Journal, Proceedings, Vol. 65, No. 12, Dec. 1968, p. 1029-1036.